Non-Canonical Functions of the Essential Autophagy Protein ATG5 in Antigen Processing and Presentation

---

Dissertation

zur

Erlangung der naturwissenschaftlichen Doktorwürde
(Dr. sc. nat.)

vorgelegt der

Mathematisch-naturwissenschaftlichen Fakultät

der

Universität Zürich

von

Christian Wolfgang Keller

aus Deutschland

Promotionskomitee

Prof. Dr. med. Jan D. Lünemann (Vorsitz)
Prof. Dr. rer. nat. Christian Münz
Prof. Dr. rer. nat. Burkhard Becher

Zürich, 2017

Disclaimer

This thesis is based on and partly adapted from the following manuscripts:

Keller CW, Loi M, Ewert S, Quast I, Theiler R, Gannagé M, Münz C, De Libero G, Freigang S, Lünemann JD. The autophagy machinery restrains iNKT cell activation through CD1D1 internalization. *Autophagy*, 2017.
doi: org/10.1080/15548627.2017.1297907

Keller CW, Sina C, Ramelli G, Mundt S, Quast I, Weber P, Becher B, Münz C, Lünemann JD. Noncanonical autophagy in DCs drives autoimmune $CD4^+$ T cell pathogenicity.
In review

Keller CW & Lünemann JD. Autophagy and Autophagy-Related Proteins in CNS Autoimmunity. *Front Immunol,* 2017. 8:165.
doi: 10.3389/fimmu.2017.00165

Keller CW, Freigang S, Lünemann JD. Reciprocal Crosstalk between Dendritic Cells and Natural Killer T cells: Mechanisms and Therapeutic Potential.
In review

Acknowledgement

I would like to thank Jan Lünemann for letting me join his laboratory, for giving me the opportunity to pursue several interesting research projects and for his precious and continuous advice and neverending support throughout my studies.

I thank Christian Münz for his valuable scientific guidance during my time at the *Institute*, for his generous sharing of ideas and funding, for letting me participate in his lab meetings and being a member in my PhD committee.

I thank Burkhard Becher for his continuous and helpful feedback and expertise throughout my PhD studies, for providing the impetus of fruitful discussions during my committee meetings and for being a valued member of my PhD committee.

A special thank you goes out to past and present members of the Lünemann lab:

To Isaak Quast who always and very ungrudgingly shared his bag of tricks and from whom I have learned a multitude of techniques and approaches:
Thank you for making the time in (and outside of) the lab not only very instructive and educational but also exceedingly joyful.

To Patrick Weber whose excellent technical support was of utmost importance for the success of numerous experiments:
Thank you for your uplifting demeanor, your motivation to always further optimize processes and your perseverance during several challenging lab days.

To Christina Sina, who introduced me to animal work with an untiring patience:
Thank you for welcoming me very kindly when I joined the lab.

To Giulia Ramelli, who was my first master student and indeed a great one:
Thanks for your support during some very difficult assays, your kindness and your relentless effort and enthusiasm.

Thank you Miguel Maurer, Kristina Kakalacheva, Flavio Cueni, Benjamin Peschke and Monika Kotur for creating a wonderful work atmosphere as well as for your valuable input and feedback.

Thank to Carmen Merki, Elvira Ender and Ines Scholz for your excellent, always fast, uncomplicated and efficient bureaucratic assistance.

To Obinna Chijioke:
Thank you for always having an open ear, discussing science and beyond during running and post-running events.

To Donal McHugh:
Thank you for your challenging thoughts and critical thinking and for countless science-unrelated conversations.

To Monica Loi:
Thank you for your valuable contribution to this study and your kind help and patience throughout.

Thanks to all the past and present members of the *Institute* for making this experience nicely balanced between a joyride and a descent into hell. In particular, thank you Ana Raykova, Vanessa Landtwing, Bithi Chatterjee, Rosa Barreira da Silva, Johannes vom Berg, Sarah Mundt, Olga Antsiferova, Carol Sze Ki Leung, Danusia Vanoaica, Anne Müller, Anita Murer, Cornelia Gurer, Julia Rühl, Laure-Anne Ligeon, Hana Zdimerova, Nicole Caduff, Petra Paul, Yun Deng, Pratiksha Gulati, Kay Hänggi, Monique Gannage, Tom Hartwig, Susana Romao, Heike Nowag, Iva Lelios, Margit Lanzinger, Bettina Schreiner, Paulina Klug, Melissa Vrohlings, Kathrin Nussbaum, Sabine Spath, Melanie Greter, Felix Hartmann, Vinko Tosevski, Andrew Croxford, Florian Mayr, Andreas Müller, Laura Codarri, Lynn Wong and Nicole Joller for your personal and professional contributions.

I thank our collaborators, especially Stefan Freigang for helping with several experiments, for providing essential reagents and for discussing experimental results, Svenja Ewert and Romina Theiler for helping with experiments and Gennaro De Libero for providing essential reagents and for discussion of data.

I thank Fabian Tormin, Karl Frontzek, Johannes Dreyer and Sascha Höfer for always providing refuge.

To my parents and my two brothers Patrick and Daniel:
Thank you for your unconditional support and patience. None of this would have been possible without you.

To Heather, Oskar and Anika:
Thank you for being the most wonderful.

Summary

Autophagy comprises a group of cellular pathways that enables eukaryotic cells to deliver cytoplasmic constituents for lysosomal degradation, to recycle nutrients and to survive during starvation. In addition to these primordial functions, autophagy has emerged as a pivotal mechanism in orchestrating innate and adaptive immune responses. Autophagosomes intersect with MHC class II-containing compartments (MIICs) and autophagy-related proteins are known to support antigen loading for increased $CD4^+$ T cell immunity.

Reactivation and expansion of autoreactive $CD4^+$ T cells within the central nervous system (CNS) are considered to play a key role in the pathogenesis of multiple sclerosis (MS) and its animal model, experimental autoimmune encephalomyelitis (EAE). How encephalitogenic lymphocytes recognize the CNS as their target organ to induce inflammatory demyelination is incompletely understood. Our study shows that CNS dendritic cells (DCs) require expression of the autophagy protein ATG5 for myelin-specific $CD4^+$ T cell reactivation. Mice with conditional deletion of ATG5 in $CD11c^+$ DCs are completely resistant to develop adoptively tranferred EAE and depict substantially reduced $CD4^+$ T cell expansion within the CNS. Endogenous myelin peptide presentation to $CD4^+$ T cells following phagocytosis of injured, phosphatidylserine-exposing oligodendroglial cells is abrogated in the absence of ATG5.

CD1d molecules survey endocytic compartments to bind lipid antigens in MIICs before recycling to the plasma membrane. We show that mice with DC-specific deletion of the essential autophagy gene *Atg5* exhibited better CD1d-restricted glycolipid presentation *in vivo*. These effects led to enhanced invariant Natural Killer T (iNKT) cell cytokine production upon antigen recognition and lower bacterial loads during *Sphingomonas paucimobilis* infection. Enhanced iNKT cell activation was independent of receptor-mediated glycolipid uptake and costimulatory signals. Instead, loss of *Atg5* in DCs impaired clathrin-dependent internalization of CD1d molecules via the adaptor protein complex 2 (AP2) and consequently increased surface expression of stimulatory CD1d-glycolipid complexes. Thus, ATG5 facilitates the recruitment of AP2 to CD1d molecules resulting in attenuated iNKT cell activation, which is in contrast to the supporting role of macroautophagy in $CD4^+$ T cell stimulation.

These results illustrate that the use and function of ATG5 is context-dependent therefore a clear and comprehensive concept of how the autophagy machinery couples to antigen-presentation and lymphocyte activation appears to be required to predict the outcome of therapeutic interventions in this pathway to boost adaptive immunity.

Zusammenfassung

Autophagie umfasst eine Reihe zellulärer Signalwege, welche es eukaryotischen Zellen ermöglichen, zytoplasmatische Bestandteile dem lysosomalen Abbau zuzuführen, Nährstoffkomponenten wiederzuverwerten und trophische Mangelzustände zu überleben. Zusätzlich zu diesen ursprünglichen Funktionen hat sich die Autophagie als zentraler Mechanismus in der Orchestrierung angeborener und adaptiver Immunantworten herauskristallisiert. Autophagosomen fusionieren mit MHC-Klasse-II-haltigen Kompartimenten (*engl. MHC class II-containing compartments*, MIICs) und Autophagie-verwandte Proteine (*engl. autophagy related genes,* ATGs) unterstützen bekanntermaßen Antigenbeladung zur Verstärkung der $CD4^+$ T-Zell-Antwort.

Der Reaktivierung und Expansion autoreaktiver $CD4^+$ T-Zellen innerhalb des zentralen Nervensystems (ZNS) kommt eine Schlüsselrolle in der Pathogenese der Multiplen Sklerose (MS) und ihres Tiermodells Experimentelle autoimmune Enzephalomyelitis (EAE) zu. Wie enzephalitogene Lymphozyten das ZNS als ihr Zielorgan zur Induktion entzündlicher Demyelinisierung erkennen, ist unvollständig verstanden. Unsere Studie zeigt, dass ZNS dendritische Zellen (*engl. dendritic cells*, DCs) die Expression des Autophagie-Proteins ATG5 für die Reaktivierung Myelin-spezifischer $CD4^+$ T-Zellen benötigen. Mäuse mit konditionaler Deletion von ATG5 in $CD11c^+$ DCs sind vollständig resistent gegenüber der Entwicklung adoptiv transferierter EAE und zeigen substanziell reduzierte $CD4^+$ T-Zell-Expansion innerhalb des ZNS. Die Präsentation endogener Myelin-Peptide gegenüber $CD4^+$ T-Zellen nach Phagozytose beschädigter Phosphatidylserin-exponierender oligodendroglialer Zellen ist in Abwesenheit von ATG5 aufgehoben.

CD1d-Moleküle durchlaufen endozytische Kompartimente um Lipid-Antigene in MIICs zu binden bevor sie zur Plasmamembran rezyklieren. Wir zeigen, dass Mäuse mit DC-spezifischer Deletion des essentiellen Autophagie-Gens *Atg5*, eine bessere CD1d-restringierte Glycolipid-Präsentation *in vivo* vorweisen. Dies führte nach Antigen-Erkennung zu erhöhter Produktion von Zytokinen durch invariante natürliche Killer T-(iNKT-) Zellen und einer geringeren bakteriellen Last während *Sphingomonas paucimobilis* Infektion. Die erhöhte iNKT-Zell-Aktivierung war unabhängig von Rezeptor-mediierter Glycolipid-Aufnahme und costimulierenden Signalen. Vielmehr behinderte der Verlust von *Atg5* in DCs die Clathrin-abhängige Internalisierung von CD1d via Adapterprotein-Komplex 2 (AP2) und erhöhte infolgedessen die Oberflächenexpression stimulierender CD1d-Glycolipid-Komplexe. Somit begünstigt ATG5 die Rekrutierung von AP2 zu CD1d Molekülen was, im Gegensatz zu der unterstützenden Rolle der Makroautophagie bei der $CD4^+$ T-Zell-Stimulation, zu einer verminderten iNKT-Zell-Aktivierung führt.

Diese Resultate illustrieren, dass die Verwendung und Funktion von ATG5 kontextabhängig ist und daher ein klares und vollumfängliches Konzept wie die Autophagie-Maschinerie Antigenpräsentation und Lymphozyten-Aktivierung reguliert, notwendig erscheint um den Ausgang therapeutischer Interventionen in diesem Signalweg zur Verstärkung der adaptiven Immunantwort, vorherzusagen.

Table of Contents

Disclaimer II
Acknowledgement III
Summary V
Zusammenfassung VI

1. Introduction 1
1.1 Autophagy Pathways and Autophagy-Related Protein Functions 1
1.2 Macroautophagy 1
1.2.1 ATGs and Autophagosome Formation 3
1.2.2 The ATG Core Machinery 4
1.2.2.1 The ULK-Complex 4
1.2.2.2 The Class III PI3K-Complex 5
1.2.2.3 The ATG12-Conjugation System 5
1.2.2.4 The LC3-Conjugation System 6
1.2.3 Regulation of Macroautophagy 7
1.2.4 Autophagosome Maturation and Fusion with the Endolysosomal System 8
1.3 Non-Canonical Autophagy Pathways 10
1.3.1 LC3-Associated Phagocytosis 10
1.4 Antigen Presentation: Selected Pathways and Mechanisms 13
1.4.1 MHC Class II Antigen Presenting Pathway 14
1.4.1.1 Autophagy-Related Protein Function in Antigen Processing and Presentation With a Focus on the MHC Class II Pathway 16
1.4.1.2 Experimental Autoimmune Encephalomyelitis: *In Vivo* Model for CD4$^+$ T Cell-Mediated Autoimmunity 19
1.4.2 CD1d Antigen Presenting Pathway 20
1.4.2.1 CD1d Assembly and Trafficking 20
1.4.2.2 Lipid Loading on CD1d 22
1.4.2.3 Invariant Natural Killer T Cells 23
1.4.2.4 Invariant Natural Killer T Cell Activation by Dendritic Cells 24
1.4.2.5 Invariant Natural Killer T Cell-Mediated Maturation and Licensing of Dendritic Cells 25
1.4.2.6 Modifications of Invariant Natural Killer T Cell Responses: Implications for Human Health and Disease 26
1.5 Hypothesis 29

2. Results 30
2.1 ATG5 in DCs Drives CD4$^+$ T Cell-Mediated CNS Autoimmunity 30
2.1.1 Phenotypic Analysis of DC-*Atg5*$^{+/+}$ and DC-*Atg5*$^{-/-}$ Mice 30
2.1.2 Absence of ATG5 in CD11c$^+$ Cells Protects Mice from Adoptive Transfer EAE 32
2.1.3 Characterization of CD11c-Expressing DCs in the CNS of DC-*Atg5*$^{-/-}$ and DC-*Atg5*$^{+/+}$ Mice at Steady State 34
2.1.4 Characterization of Microglia in DC-*Atg5*$^{-/-}$ and DC-*Atg5*$^{+/+}$ Mice at Steady State 35
2.1.5 Lack of ATG5 in CD11c$^+$ DCs Limits Expansion of Encephalitogenic CD4$^+$ T Cells Within the CNS 37
2.1.6 Analysis of CNS Regulatory T Cells at AT-EAE Peak of Disease 39
2.1.7 CNS-Infiltrating CD4$^+$ T Cells in DC-*Atg5*$^{-/-}$ Mice Maintain their Capacity to Produce Effector Cytokines 40
2.1.8 Analysis of CNS Myeloid Cells at AT-EAE Peak of Disease 42
2.1.9 Analysis of Microglia at AT-EAE Peak of Disease 42
2.1.10 Endogenous Myelin Presentation by CD11c$^+$ DCs is Abrogated in Absence of ATG5 43
2.2 The Role of DC-Inherent ATG5 During Presentation of Exogenous Lipid Antigens to Invariant Natural Killer T Cells 47
2.2.1 Colocalization Analysis Between CD1d and LC3 in RAW 264.7 Cells and Splenic CD11c$^+$ DCs 47
2.2.2 Absence of ATG5 Increases the NKT Cell Stimulatory Capacity of APCs *In Vitro* 49
2.2.3 Increased Capacity of ATG5-Deficient APCs to Stimulate NKT Cells is Independent of Lipid Uptake Receptor Pathway 53
2.2.4 Analysis of CD1d-Restricted Presentation of αGalCer in Absence of ATG5 in GM-CSF BMDCs 53
2.2.5 Analysis of Costimulatory Properties for NKT:DC Crosstalk in DC-*Atg5*$^{-/-}$- and DC-*Atg5*$^{+/+}$-Derived DCs 55
2.2.6 Analysis of CD1d-Surface Expression on DC-*Atg5*$^{-/-}$- and DC-*Atg5*$^{+/+}$-Derived APCs and on a Macrophage-Like Cell Line 56
2.2.7 Analysis of CD1d Turnover 57
2.2.8 Recruitment of CD1d and its Adaptor Protein AP2 to Endosomal Compartments is Reduced in *Atg5*-Deficient CD11c$^+$ DCs 60
2.2.9 Analysis of Organspecific NKT Cell and Splenic B cell Frequencies at Steady State in DC-*Atg5*$^{-/-}$ and DC-*Atg5*$^{+/+}$ Mice 61
2.2.10 Serum Cytokine Quantification Upon αGalCer *In Vivo* Challenge in DC-*Atg5*$^{-/-}$ and DC-*Atg5*$^{+/+}$ Mice 62
2.2.11 DC Phenotypisation Upon αGalCer *In Vivo* Challenge in DC-*Atg5*$^{-/-}$ and DC-*Atg5*$^{+/+}$ Mice 63

2.2.12 *Sphingomonas paucimobilis In Vivo* Challenge in DC-*Atg5*$^{-/-}$ and DC-*Atg5*$^{+/+}$ Mice 64
3. Discussion 67
3.1 Prelude 67
3.2 ATG5-Dependent Autophagy During Autoimmune CNS Inflammation 67
3.3 ATG5-Mediated Stabilization of Surface CD1d Expression in DCs 77
3.4 Concluding Remarks 83
4. Materials and Methods 84
4.1 Materials 84
4.1.1 Machines 84
4.1.2 Antibodies, Flow Cytometry and Cellular Assays 85
4.1.3 Miscellaneous 88
4.1.4 Primary and Secondary Antibodies for Immunocytochemistry 89
4.1.5 Tetramer 89
4.1.6 MACS Beads 90
4.1.7 General Material 90
4.1.8 NKT Cell Agonists 91
4.1.9 General Reagents 92
4.1.10 Kits 96
4.1.11 MOG Protein and Peptide 97
4.1.12 OVA Peptide 97
4.1.13 Antibodies for T cell Stimulation During Coculture Assays 97
4.1.14 Antibodies (1° and 2°) for Western Blot 98
4.1.15 Plastic Supplies 98
4.1.16 Cell Lines and Bacteria 98
4.1.16.1 NKT Cell Hybridoma Lines 99
4.1.16.2 *Atg5*-Deficient Immortalized Macrophage-Like Cell Line 99
4.1.17 PCR Primers 100
4.1.18 Cell Culture Media 100
4.1.19 General Buffers 101
4.1.20 Buffers Immunocytochemistry 102
4.1.21 Buffer for SDS-PAGE and Western Blot 103
4.1.22 ELISA Buffer 103
4.1.23 Recipes for SDS-PAGE Gels (0.75 mm) 103
4.1.24 Percoll Solutions 104
4.1.24.1 Leukocyte Isolation From Mouse Liver 104
4.1.24.2 Leukocyte Isolation from Mouse CNS 104
4.1.25 Optical Configurations of Flow Cytometers Used 104
4.1.25.1 BD SLR Fortessa 104
4.1.25.2 BD FACSCanto-II 105
4.2 Methods 105
4.2.1 Mice 105
4.2.2 Mouse Organ Processing 106
4.2.2.1 Leukocyte Isolation from Spleen, Thymus and Lymph Nodes 106
4.2.2.2 Leukocyte Isolation from Liver 106
4.2.2.3 Leukocyte Isolation from CNS 107
4.2.3 Bleeding of Mice 108
4.2.4 Generation of BMDCs (General Protocol) 108
4.2.5 Genotyping 109
4.2.5.1 Tissue Digestion and DNA Isolation 109
4.2.5.2 *Atg5*$^{flox/flox}$ Genotyping 110
4.2.5.3 Master Mix Components and PCR Program 110
4.2.5.4 CD11c-Cre genotyping 111
4.2.5.5 Master Mix Components and PCR Program 111
4.2.5.6 2D2/TCR^{MOG} Genotyping 111
4.2.6 Flow Cytometry 112
4.2.7 Magnetic Activated Cell Sorting (MACS) 113
4.2.8 UVB Irradiation 113
4.2.9 Quantification of Ptd-L-Ser^{+} Cells 114
4.2.10 Ptd-L-Ser-Expressing Cell Phagocytosis and Coculture Assay 114
4.2.11 Fluorescent Activated Cell Sorting 115
4.2.12 Immunocytochemistry and Colocalization Assays 115
4.2.13 Coculture Assays with Splenic DCs and NKT Cell Hybridoma 116
4.2.14 CD1d Antigen Presentation Assays 117
4.2.15 NKT Cell Detection 117
4.2.16 Determination of Cytokine Concentration 117
4.2.17 CD1d Internalization Assay 118
4.2.18 CD1d Recycling Assay 118
4.2.19 Lipid *In Vivo* Chase 119
4.2.20 Infection with *S. paucimobilis* 119
4.2.21 Adoptively Transferred EAE 119
4.2.22 Detection of Regulatory T Cells Via Intranuclear FOXP3 Staining 121

4.2.23 Detection of the Intracellular Cytokines IFNγ, IL-17 and GM-CSF 122
4.2.24 Cell Culture 123
4.2.25 Cell Count 123
4.2.26 Freezing Cells 124
4.2.27 Cell Lysis for Protein Quantification 124
4.2.28 BCA/Protein Quantification 125
4.2.29 SDS-PAGE and Western Blot 125
4.2.30 Statistics 126
5. References 127
6. Abbreviations 148
7. Declaration 153
8. Curriculum Vitae 154

1. Introduction

1.1 Autophagy Pathways and Autophagy-Related Protein Functions

Organisms with subcellular compartmentalization and membrane-bound organelles face constant challenges in order to maintain metabolic integrity and homeostasis. Autophagy comprises a set of evolutionary conserved catabolic pathways that converge in the guided direction of assigned cargo to the endolysosomal system (Deter and De Duve, 1967; Deter *et al.*, 1967; Mizushima and Komatsu, 2011). Initially, autophagy was recognized for its contribution in keeping energy homeostasis, and degradation of aberrant protein aggregates (Hara *et al.*, 2006; Komatsu *et al.*, 2006) and as mediator of development-associated forms of cell death (Denton *et al.*, 2012). In recent years, however, autophagy's function has exceeded the originally allotted role as a mere protein degradation system alongside the proteasomal machinery. In addition to regulating cellular proteostasis and cell death, autophagy pathways are increasingly recognized for actively participating in physiological and pathological immune responses. In doing so, autophagy pathways limit intracellular proliferation of pathogens (Thurston *et al.*, 2012), restrict secretion of proinflammatory mediators (Saitoh *et al.*, 2008), and tweak T cell responses by orchestrating both loading and preservation of antigens on and surface-expression of antigen-presenting molecules (Loi *et al.*, 2016; Paludan *et al.*, 2005; Romao *et al.*, 2013; Schmid *et al.*, 2007).

Canonical autophagy implicates at least three distinct pathways: macroautophagy, microautophagy and chaperone-mediated autophagy (Codogno *et al.*, 2011). Although all of the above mentioned pathways coalesce in the lysosome, they considerably differ (albeit showing some overlap), in their means of cargo transportation, triggering events and regulatory factors.

1.2 Macroautophagy

Macroautophagy (MA), the canonical autophagy pathway *sensu strictu*, is evolutionary conserved from yeast to mammalian cells and characterized by highly regulated membrane reorganization processes with the subsequent *de novo* formation of a 0.5–1.5 μm wide double-membraned vesicle termed

autophagosome (Mizushima *et al.*, 2002). Upon sequestering neighboring parts of the cytoplasm, the autophagosome subsequently fuses with lysosomes resulting in enzymatic cargo break down (Deretic, 2016; Feng *et al.*, 2014). The process is partitioned in five sequential steps (1. induction/nucleation, 2. elongation, 3. closing/maturation, 4. fusion, 5. degradation) that are orchestrated by hierarchies of autophagy-related genes/proteins (*Atg*s/ATGs) and other essential components, in a tightly regulated enzymatic cascade (Codogno *et al.*, 2011; Mizushima *et al.*, 2011; Tsukada and Ohsumi, 1993) (**Figure 1.1**). Albeit originally identified in yeast, mammalian counterparts for many *Atg*s have been characterized and some ATGs are so far exclusively reported in mammalian cells and lack yeast orthologs (Mizushima *et al.*, 2011). Among all autophagy pathways, MA is to date the most extensively investigated one and, depending on the target constituent encompasses subentities such as macromitophagy, -pexophagy, -xenophagy, and -lipophagy (Klionsky *et al.*, 2007; Levine *et al.*, 2011; Mizushima *et al.*, 2011; Randow and Youle, 2014; Singh *et al.*, 2009).

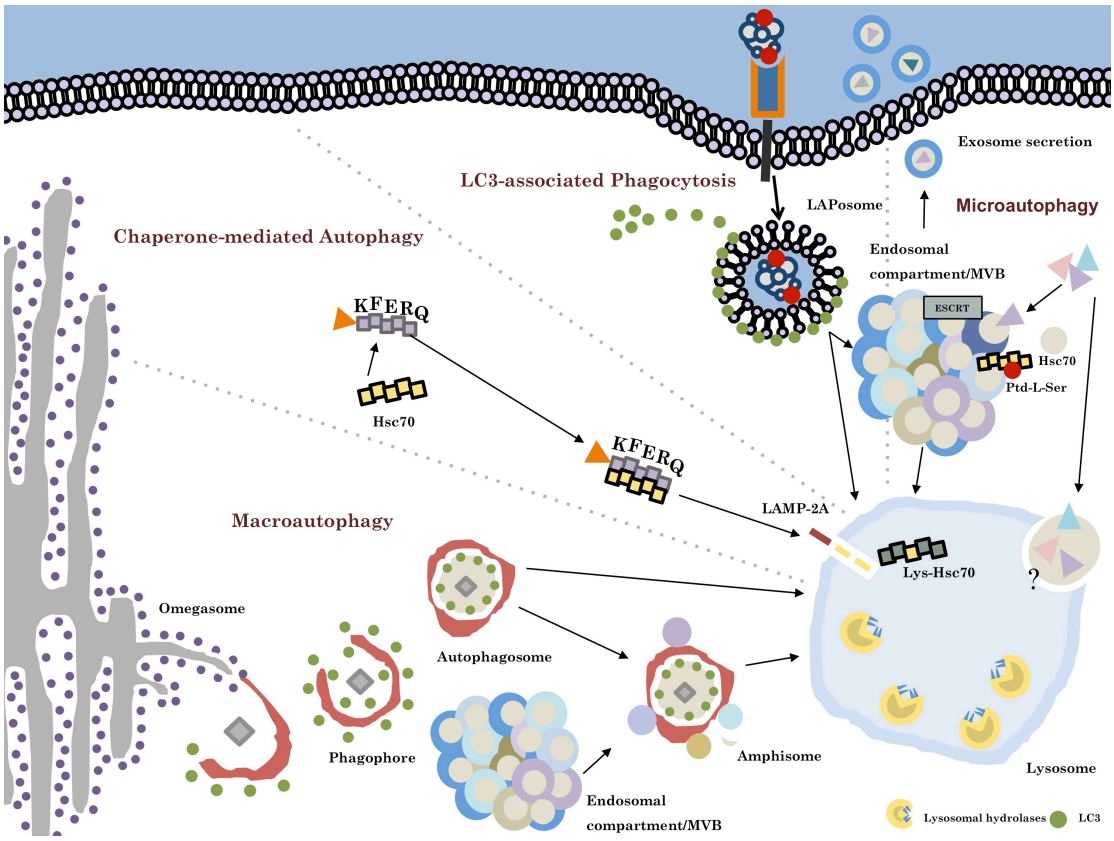

Figure 1.1 Autophagy pathways converge in the lysosomal compartment.

Macroautophagy. The phagophore emanates most likely from ER-derived membrane sources at a PI3P-rich (not depicted) structure called the omegasome. Upon recruitment of LC3 on the outer and inner leaflet of the forming autophagosome, cytoplasmic cargo is engulfed and LC3 removed from the outer membrane as the autophagosome is closed. The

completed vesicles may now be further matured via step-wise fusion with the endocytic compartment resulting in the generation of amphisomes or immediately fuse with hydrolytic enzymes-containing lysosomes. *Chaperone-mediated autophagy*. Target proteins that contain an exposed KFERQ sequence motif are guided in an hsc70-dependent manner towards LAMP-2A, which resides in the lysosomal membrane. Upon unfolding of the target protein, LAMP-2A multimers together with lysosomal hsc70 facilitate the transport into the lysosomal lumen. *LC3-associated phagocytosis.* Ligation of an appropriate receptor (e.g. TLR2, Dectin-1, TIM4, etc.) leads to receptor-mediated phagocytosis recruitment and binding of LC3 to the outer membrane of the LAPosome. By analogy with the MA pathway, completed LAPosomes may either fuse with other endocytic vesicles or directly merge with lysosomes. *Microautophagy.* Cytosplasmic cargo can be directly targeted to endosomal compartments/multivesicular bodies (MVB) in a hsc70-, phosphatidylserine (Ptd-L-Ser)- and ESCRT-dependent manner. Exosomes containing cytoplasmic material may emanate from the MVB and be secreted into the extracellular space. The molecular events and regulatory processes orchestrating the direct invagination of cytoplasmic constituents into lysosomes remains largely unbeknownst.

1.2.1 ATGs and Autophagosome Formation

De novo synthesis and maturation of the autophagosome as well as the trafficking of such vesicles to and fusion with lysosomes are distinctive features of MA in opposition to other autophagy pathways. Formation of this typifying vesicle requires approximately 5-10 min and is under the control of an ever-growing number of ATGs (Feng *et al.*, 2014; Mizushima *et al.*, 2001; 2011; Suzuki *et al.*, 2016). The finalized autophagosome is usually swiftly turned over but may reach a half-life of 10-25 min (Pfeifer, 1978; Schworer *et al.*, 1981). The key proteins that initiate and govern the formation of the autophagosome can be assembled in functionally designated groups: unc-51-like kinase (ULK)-complex (1), the class III phosphatidylinositide 3-kinase (PI3K) complex (2), the ATG2/WD repeat domain phosphoinositide-interacting protein (WIPI)-complex and the ATG9 cycling system (3), the ATG12-conjugation system (4) and the microtubule-associated protein 1 light chain 3 (LC3)-conjugation system (5) (Feng *et al.*, 2014; Mizushima *et al.*, 2011; Shibutani and Yoshimori, 2014).

The autophagosome emanates from the double-membraned phagophore (also called isolation membrane), which sequesters and closes around designated parts of the cytoplasm to form the completed autophagosome. The emergence of said phagophore constitutes the induction/nucleation phase. However, the exact assembly platform and membrane source for the generation of these initial structures are still debated. Similar to the pre-autophagosomal structure (PAS) that is observed adjacent to the vacuole in yeast, an autophagosome formation site, represented by dot-like accumulations of ATGs, has been identified in mammalian cells (Itakura and Mizushima, 2010). Primary suspect organelles to provide membranes include specialized PI3P-enriched endoplasmic reticulum

(ER) domains coined omegasomes (Axe *et al.*, 2008). 3D electron tomography studies corroborated these results by showing that the double-membraned phagophore originates in between two protruding ER flaps. The phagophore then entwines one of the two extensions and finally buds off the ER containing the previously enfolded ER flap. This model is further supported by the fact that >70% of autophagosomes contain ER-derived cargo (Hayashi-Nishino *et al.*, 2009; Ylä-Anttila *et al.*, 2009). Nevertheless, other membrane sources for autophagosome generation have been suggested. Amongst them is the outer mitochondrial membrane (Hailey *et al.*, 2010). These two opposing results might be brought together by a recent study that identified ER-mitochondria contact sites as the originating platform for the autophagosome initiation (Hamasaki *et al.*, 2013). The VAMP3-dependent heterotypic fusion between early endosome-derived ATG9$^+$ vesicles and recycling endosome-derived ATG16L1$^+$ vesicles has also been suggested to contribute to autophagosome precursor generation (Puri *et al.*, 2013). Additionally, ER exit sites (Guo *et al.*, 2012; Zoppino *et al.*, 2010), the ER-Golgi intermediate compartment together with coat protein complex II (COPII) (Ge *et al.*, 2013; 2014), the plasma membrane (Ravikumar *et al.*, 2010) and a novel compartment comprised of ATG9$^+$ vesicles and tubules (Mari *et al.*, 2010) were implicated in providing membrane material. It is conceivable that different subentities of MA preferentially harness distinct membrane sources. Possibly, there is a hierarchy of membrane reservoirs that sequentially may serve as alternative when other sources have been exploited. Furthermore, various tissues with specific composition of subcellular compartments may differ in their means to utilize membranes for autophagosome generation.

1.2.2 The ATG Core Machinery

1.2.2.1 The ULK-Complex

The ULK-complex is an upstream ATG-unit and, by differential phosphorylation of ULK1 (the main mammalian orthologue to yeast ATG1), a direct target of MA regulation via target of rapamycin complex 1 (TORC1) and AMP-activated protein kinase (AMPK) respectively (Egan *et al.*, 2011; J. Kim *et al.*, 2011). ULK1/2 builds a stable complex with FIP200, ATG13 and ATG101 (Ganley *et al.*, 2009; Hara and Mizushima, 2009; Hosokawa, Hara, *et al.*, 2009). Not composition

of the complex itself but rather differential phosphorylation of its members procures promotion or inhibition of MA. In a state of MA inactivation TORC1 restrains the process via coordinate phosphorylation of ULK1/2 and ATG13. During activation, MA-promoting phosphorylation of ULK1/2 via AMPK, ULK1/2 autophosphorylation and ULK1/2-mediated phosphorylation of ATG13 and FIP200 occurs followed by translocation of the entire complex to autophagosomal initiation sites possibly on tubulovesicular areas comprised of ER and $ATG9^+$ vesicles (Chan *et al.*, 2007; Y.-Y. Chang and Neufeld, 2009; Ganley *et al.*, 2009; Hara *et al.*, 2008; Karanasios *et al.*, 2016). ATG101 may facilitate phosphorylation of ATG13 and minimize its proteasomal degradation (Hosokawa, Sasaki, *et al.*, 2009; Mercer *et al.*, 2009).

1.2.2.2 The Class III PI3K-Complex

The tetrameric core of this complex consists of vacuolar protein sorting protein (Vps)34 (a phosphoinositide 3 kinase), Vps15 (a regulatory subunit of Vps34 also called p150), Beclin 1 (orthologue of ATG6) and ATG14L (aka ATG14 and Barkor) (Itakura *et al.*, 2008; Q. Sun *et al.*, 2008; Suzuki *et al.*, 2016). NRBF2 (orthologue of ATG38) is a recently identified additional subunit of the complex that augments the enzymatic activity of the lipid kinase Vps34 (Araki *et al.*, 2013; Ohashi *et al.*, 2016; Young *et al.*, 2016). The lipid kinase complex is recruited to autophagosomal initiation sites in an ULK1-complex/ATG9-dependent manner (Itakura and Mizushima, 2010; Matsunaga *et al.*, 2010).

The key function of the complex is to produce PI3P via Vps34-mediated phosphorylation of phosphatidylinositol. Presence and accumulation of PI3P is essential for MA as PI3P-enriched membrane areas then function as platforms to which downstream PI3P-binding partners can be recruited. Regulation of MA occurs also on the level of the PI3P-complex in that death-associated protein kinase (DAPK) promotes autophagosome formation by unleashing Beclin 1 from the Bcl-2/Bcl-XL complex (Zalckvar *et al.*, 2009).

1.2.2.3 The ATG12-Conjugation System

This first of two ubiquitin-like conjugation systems that orchestrate autophagosome formation consists of the MA-essential molecules ATG12, ATG7, ATG10 ATG5 and ATG16L1 (Mizushima *et al.*, 2011). Constitutively and

independent of cellular nutrient status, ATG12 is activated via E1-like enzyme ATG7, followed by transfer to E2-like enzyme ATG10 which catalyzes the covalent conjugation of ATG12 to ATG5. Via binding to ATG5, the conjugate then forms a complex with ATG16L1 (Geng and Klionsky, 2008). WIPI2 now attracts the ATG5-ATG12-ATG16L1-complex by means of a recently identified binding site in ATG16L1 to the site of autophagosome generation (Dooley *et al.*, 2014). Additionally, it has been suggested that ATG16L1 is also recruited to the phagophore via binding to ULK-complex member FIP200 (Gammoh *et al.*, 2013; Nishimura *et al.*, 2013). On site, the complex then functions as an E3-like enzyme for the second conjugation system. The complex is regularly found on the outer membrane of the phagophore but dissociates from there upon completion of the autophagosome (Mizushima *et al.*, 2001).

1.2.2.4 The LC3-Conjugation System

The second and final conjugation system is comprised of the ubiquitin-like LC3, the hydrolase ATG4, ATG7 and ATG3, which function as E1- and E2-like enzymes, respectively. The pro-form of LC3 is cleaved by ATG4 leading to exposure of a C-terminal glycine residue (Hemelaar *et al.*, 2003; Kabeya *et al.*, 2004). The resulting protein termed LC3-I is then lipidated with phosphatidylethanolamine (PE) at said glycine residue by means of ATG3 and ATG7 (Ichimura *et al.*, 2000; Kabeya *et al.*, 2000; Tanida *et al.*, 2004). This PE-lipidation of LC3 is assisted by the ATG5-ATG12-conjugates via E3-like activity (Fujita, Itoh, *et al.*, 2008; Geng and Klionsky, 2008). Additionally, the ATG5-ATG12-ATG16L1-complex guides and determines LC3 to its subcellular destination (Fujita, Itoh, *et al.*, 2008). This lipidated form of LC3, also called LC3-II is initially found symmetrically distributed on the inner and outer membrane of the phagophore (Kabeya *et al.*, 2000; 2004; Kimura *et al.*, 2007). There it appears to aid in elongation of the phagophore as well as coordinate tethering and hemifusion of its membranes, finally leading to closure of the phagophore to what is now called autophagosome (Fujita, Hayashi-Nishino, *et al.*, 2008; Nakatogawa *et al.*, 2007; Sou *et al.*, 2008; Weidberg *et al.*, 2010). Upon vesicle closure, LC3 on the outer membrane is being cleaved from PE via ATG4 while intraluminal LC3 stays associated with the organelle which makes LC3-II a valuable marker for the detection of autophagosomes (Kimura *et al.*, 2007;

'Guidelines for the use and interpretation of assays for monitoring autophagy (3rd edition).', 2016). In addition to its contribution during membrane reorganization, LC3 mediates MA-cargo selectivity by functioning as an adaptor molecule (Johansen and Lamark, 2011).

1.2.3 Regulation of Macroautophagy

Most mammalian cells carry out MA on a constitutive level at varying degrees. However, depending on the cell type, macroautophagic activity can be induced and modulated in numerous ways. Primarily nutrient deprivation is a potent stimulus of autophagy and starvation-induced autophagy is a common means to investigate MA under experimental conditions (Efeyan *et al.*, 2015; Mizushima and Klionsky, 2007). The process receives regulatory input on both a systemic and a cellular level (Efeyan *et al.*, 2015). Amongst the most upstream regulatory units of the MA machinery is the antagonistic interplay of coordinate phosphorylation by the two serine/threonine protein kinases AMPK and TORC1 (Egan *et al.*, 2011; J. Kim *et al.*, 2011) (**Figure 1.2**).

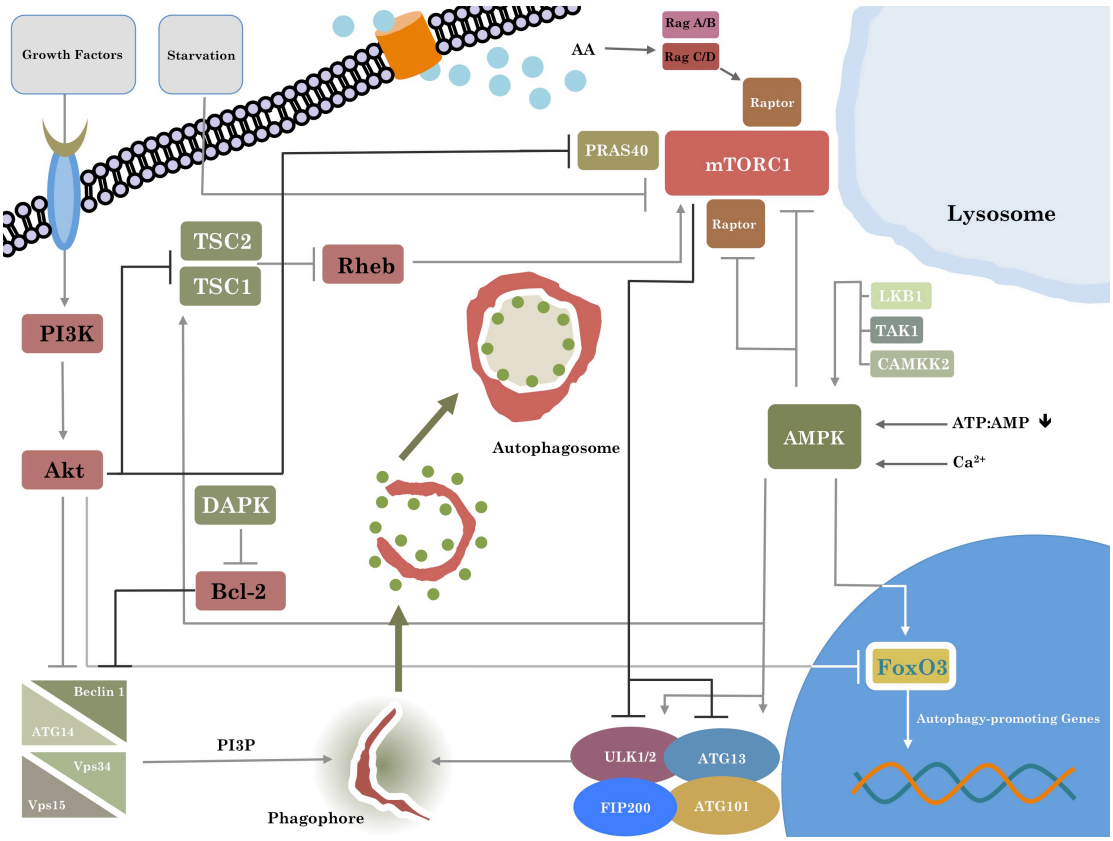

Figure 1.2 Regulatory network of macroautophagy (MA).
This figure illustrates the most important regulatory interplay of molecules that govern MA activity. Growth factors can signal via PI3K to Akt, which in turn inhibits the Beclin

1-containing class III PI3K-complex. Akt may also repress transcription of autophagy-promoting genes via direct inhibition of transcription factor FOXO3. Additionally Akt reduces macroautophagic activity by inhibiting TSC1/TSC2. Akt interaction with PRAS40 promotes mammalian TORC1 (mTORC1) activity thereby further damping MA. The calcium/calmodulin (Ca^{2+}/CaM) serine/threonine kinase DAPK fosters MA via phosphorylation of Beclin 1 at T119 which leads to dissociation of Beclin 1 from Bcl-2. The TSC1/TSC2-complex can promote MA by inhibiting the mTORC1 activator and GTPase Rheb. AMPK and mTORC1 are the two cardinal regulatory units that control MA. mTORC1 may repress the process via phosphorylation of ULK1/2 and/or ATG13. mTORC1 activity is increased by amino acid sensing Rag GTPases via interaction with Raptor. The Rag GTPases also facilitate translocation of mTORC1 to the lysosomal membrane, which serves as a prerequisite for the aforementioned mTORC1-promoting activity of Rheb. AMPK promotes MA by several means: phosphorylation of ULK1/2 and/or ATG13 at different residues than mTORC1, direct interaction with FOXO3 and by directly disinhibiting the inhibitory units mTORC1 and Raptor. AMPK itself can be triggered by increasing levels of AMP relative to ATP, free Ca^{2+} and activity of LKB1, TAK1 and CAMKK2.

1.2.4 Autophagosome Maturation and Fusion with the Endolysosomal System

A hallmark of all autophagic pathways is their convergence into the lysosomal system. During MA, this event requires the coordinated membrane fusion of the autophagosome and endolysosomal vesicles (**Figure 1.1**). Prior to terminal fusion with lysosomes, autophagosomes may (or may not) fuse with vesicles of the endocytic compartments like early or late endosomes. The resulting amphisomes subsequently fuse with lysosomes to form autolysosomes. These partly sequential, partly parallel fusion events underscore the dynamic nature of MA. Hence, observed accumulation of autophagosomes needs to be carefully interpreted, for it can mean both *bona fide* induction of the process and blocked lysosomal fusion.

Autophagosomes are widely distributed throughout the cytoplasm. For these vesicles to fuse with lysosomes and late endosomes (which are predominantly located juxtanuclear) autophagosomes need to be efficiently guided towards this area. Members of the cytoskeleton have been shown to orchestrate the regulated trafficking of autophagosomes from the periphery to sites at which membrane fusion occurs. In fact, microtubules might even aid in autophagosome formation and subsequent fusion with endosomal compartments (Fass *et al.*, 2006; Köchl *et al.*, 2006). In an antagonistic interplay, the members of the motor protein family dynein/dynactin-complex and kinesin were shown to be involved in guiding autophagosomes alongside microtubules towards lysosome-rich areas, a process during which the trafficked vesicles become increasingly acidified as they approach the juxtanuclear area (Kimura *et al.*, 2008; Maday *et al.*, 2012).

Consequently, disruption of the dynein machinery exacerbates aberrant protein aggregation in experimental models of neurodegeneration due to dysfunctional MA (Ravikumar *et al.*, 2005). Interestingly, dynamic distribution of lysosomes within the cytoplasm may actually constitute a mechanism via which autophagic flux is regulated (Korolchuk *et al.*, 2011).

In accordance with general membrane reorganizsation, also the fusion of autophagosomes with endolysosomal vesicles is in large parts orchestrated by members of small GTPases called Rabs, membrane-tethering complexes and SNAREs. Studies in yeast suggest that ATG4-mediated cleavage of the LC3 orthologue ATG8 from the outer membrane constitutes one prerequisite that renders the autophagosome ready for fusion (Nair *et al.*, 2012; Z.-Q. Yu *et al.*, 2012). Possibly, absence of molecules, that are involved in the early phase of autophagosome biogenesis functions as yet another signal (Ganley, 2013).

Our understanding of the precise molecular events during autophagosome biogenesis and fusion has significantly improved during the last decade and enticing models have been proposed as on how the phagophore is initiated. However, one needs to be cautious as of how the aforementioned molecular interplay of ATGs can be generalized since most results were obtained studying starvation-induced MA. There is evidence that autophagosomal biogenesis, subsequent fusion partners, -sites and -mechanisms are highly dependent on induction stimulus and cargo (Ganley, 2013). Furthermore, the degree as to which these processes are actually carried out in sequence remains enigmatic. It is likely that numerous steps occur in parallel and distinct ATGs might not only carry out a single function but take on several tasks within the cascade. The molecular interactions between ATGs and the kinetics of the process may also significantly differ between mammalian species and even on a tissue level there might be specifics to MA that need to be taken into account.

Finally, at least for some ATGs that are essential for MA, an even more promiscuous role has begun to unfold in that these proteins also facilitate MA-independent functions in cellular reprogramming, dynamic membrane re-distribution, pathogen clearance and antigen presentation (Kimmey *et al.*, 2015; Kroemer and Levine, 2008; Loi *et al.*, 2016; Radoshevich *et al.*, 2010; Subramani and Malhotra, 2013; Zhao *et al.*, 2008).

1.3 Non-Canonical Autophagy Pathways

Non-canonical autophagy comprises a set of recently characterized pathways that either result in autophagosome formation but omit the usage of distinct parts of the classical MA-machinery or constitute autophagosome-independent pathways that utilize key components of the MA-network (Codogno *et al.*, 2011; Münz, 2015). One can at least differentiate 5 distinct entities: *LC3-associated phagocytosis*, *Beclin 1-independent autophagy*, *autophagosome-formation from multiple phagophores and pathogen-specific autophagy modification*, *autophagy-associated unconventional protein secretion*, and *defective ribosomal products-containing autophagosome-rich blebs*. Due to its implication in antigen presenting pathways (Cadwell, 2016; Codogno *et al.*, 2011; Münz, 2015) I will focus here on LC3-associated phagocytosis.

1.3.1 LC3-Associated Phagocytosis

During phagocytosis, a specialized way of endocytosis, cells internalize solid extracellular constituents in a receptor-mediated fashion. The resulting phagosome is step-wise matured and subsequently fuses with the lysosomal compartment in order to break down the incorporated material (Gray and Botelho, 2017). Recently, a novel organelle, the single-membraned $LC3^+$ phagosome or LAPosome, has been identified and the process of its generation and fate was coined LC3-associated phagocytosis (LAP) (**Figure 1.3**) (Romao and Münz, 2014; Sanjuan *et al.*, 2007). LAP, that links both phagocytosis of extracellular cargo and members of the autophagy molecular core machinery, is initiated by ligation of a variety of extracellular receptors (Henault *et al.*, 2012; Ma *et al.*, 2012; Martinez *et al.*, 2011; Romao *et al.*, 2013; Sanjuan *et al.*, 2007). Although some components of the MA-machinery are essential for LAP (e.g. ATG5, ATG7, LC3, Beclin 1), the process is independent of others (e.g. the ULK-complex including ULK1/2, FIP200, ATG13, ATG101, WIPI1).

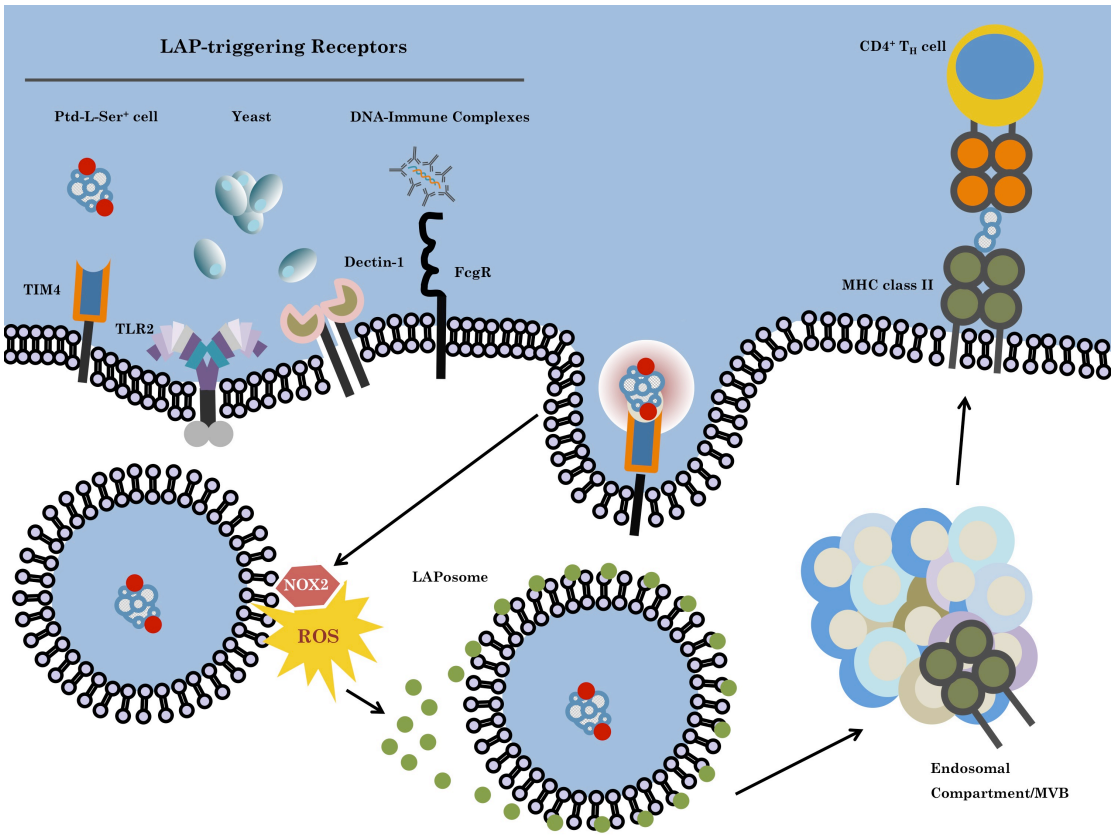

Figure 1.3 LC3-associated phagocytosis.
The ligation of LAP-triggering receptors such as phosphatidylserine (Ptd-L-Ser)-recognizing TIM4, TLR2, Dectin-1 or Fcγ receptors will ensue receptor-mediated phagocytosis and subsequent PI3K-dependent association of the NADPH oxidase NOX2 with the phagosome. The NOX2-derived reactive oxygen species (ROS) and laposomal PI3P (not depicted) mediate the recruitment and binding of LC3 to the outer membrane of the LAPosome. Instead of terminal fusion with the lysosomal compartment, the completed LAPosome may also fuse with endosomal vesicles including MHC class II loading compartments in which after enzymatic digestion, LAPosomal content can be loaded upon MHC class II molecules followed by the presentation of the resulting peptides to $CD4^+$ T_H cells.

LAP-triggering receptors include Toll-like receptors (TLRs), Fc-receptors, C-type lectins and phosphatidylserine (Ptd-L-Ser)-binding receptors (Henault *et al.*, 2012; Ma *et al.*, 2012; Martinez *et al.*, 2011; Romao *et al.*, 2013; Sanjuan *et al.*, 2007). Upon activation of a LAP-triggering surface receptor, a PI3PK complex that differs in its composition from the one involved in MA, is recruited to the cytosolic membrane of the phagosome followed by the recruitment of the NADPH oxidase NOX2. These events are not preceded by involvement of the canonical ULK complex. The LAP-associated PI3PK complex is made up by Beclin 1, Vps34, Vps15 (analogous to MA) but is devoid of ATG14 (Martinez *et al.*, 2015). Instead it includes UVRAG and Rubicon (not members of the canonical PI3PK

complex). Similar to MA, the PI3PK complex is set out to generate PI3P on the LAPosome. The association of the modified PI3PK complex on the LAPosome is potentially liaised via Rubicon which, together with PI3P also appears to be key in recruiting, stabilizing and activating the NADPH oxidase NOX2 to the organelle (Martinez *et al.*, 2015). Rubicon has been suggested to mediate NOX2 stabilization by interaction of its serine-rich domain (AA 567-625) with the NOX2 subunit $p22^{phox}$ whereas PI3P stabilizes the NOX2 subunit $p40^{phox}$ (Martinez *et al.*, 2015; Ueyama *et al.*, 2011). LAPosomal PI3P in concert with NOX2-dependent ROS production then initiates the two canonical MA conjugation systems (see above), which results in efficient deposition of lipidated LC3 on the outer LAPosomal membrane (Martinez *et al.*, 2015). Consequently, LAP is highly dependent on the MA proteins ATG5, ATG12, ATG16L1, ATG7, ATG3 ATG4 and lipidated LC3. Molecules that have been described by one group to be dispensable for canonical MA but are thought to be essential for LAP include NOX2 and Rubicon (Martinez *et al.*, 2015).

Taken together and in contrast to the canonical MA pathway, during which LC3 conjugation to the phagophore allows for recruitment of cytoplasmic substrates into forming autophagosomes via LC3-binding anchor proteins such as p62/sequestosome 1, LAP handles formerly extracellular particles that access the cell through phagocytosis and occurs without the formation of a double-membraned vesicle and in the absence of p62/sequestosome 1 on $LC3^+$ single-membraned phagosomes (Martinez *et al.*, 2015; Münz, 2015; Romao and Münz, 2014). So far LAP has been implicated in efficient clearance of *Saccharomyces cerevisiae* and *Aspergillus fumigatus* (Martinez *et al.*, 2015; Sanjuan *et al.*, 2007). However, in the case of *Listeria monocytogenes* infection, LAPosomes have been described as *Listeria*-containing compartments that promote persistent infection (Lam *et al.*, 2013). In plasmacytoid DCs, LAP, induced upon binding of immune complexes via FcγR, is required to assemble the interferon regulatory factor 7 (IRF7)-signaling compartment which is essential for IRF7 activation and subsequent IFNα secretion downstream of TLR9 ligation (Henault *et al.*, 2012). LysM-Cre^+ conditional knockout mice for LAP-essential proteins mainly target $CD11b^+$/$F4/80^+$ macrophages and $CD11b^+$$Ly\text{-}6G^+$ neutrophils. Aged mice that are

deficient of LAP activity in these myeloid subsets spontaneously acquire a lupus-like phenotype (Martinez *et al.*, 2016).

1.4 Antigen Presentation : Selected Pathways and Mechanisms

Conventional $CD4^+$ and $CD8^+$ T cells constitute a powerful and effective arm of the adaptive immune system. As opposed to a more general immune response of the innate immune system, that is predominantly based on pattern recognition indicating danger and presence of pathogens, adaptive immune responses via $CD4^+$ and $CD8^+$ T cells are highly selective with regard to what they react to. This functional selectivity is morphologically based upon the high variability of existing T cell receptor clones. V(D)J recombination in thymic T lymphocytes, which involves somatic rearrangement of gene segments relevant for distinct T cell receptor expression, is at the basis of this high variability (Janeway, 1996). Unlike B lymphocytes, which are able to recognize native antigen of numerous biochemical make-up via their B cell receptor, $CD4^+$ and $CD8^+$ T cells are imperceptive to native antigen and may only recognize their cognate antigens, which are exclusively peptides, in the context of MHC class I ($CD8^+$ T cells) and MHC class II ($CD4^+$ T cells) presentation of said antigens. This phenomenon in conjuncture with the fact that a given T cell recognizes its cognate antigen only in association with a specific MHC-encoded allelic product is commonly referred to as MHC-restriction (Janeway, 1996; Kazansky, 2008).

The two antigen presenting pathways, the MHC class I and II pathways, not just only activate distinct T lymphocyte subsets but are essentially complementary in their means to survey the organism for relevant cues and protect it from harm. Whereas MHC class I molecules, which are expressed on almost all nucleated cells, predominantly present antigenic peptides that originate from endogenously synthesized cytosolic proteins, MHC class II molecules are constitutively only expressed on professional antigen presenting cells (APCs) such as dendritic cells, macrophages an B cells, and mainly present peptides that emanate from the endocytic compartment. This dichotomy is on the foundation of cell-mediated immunity and allows for an efficient segregation of the T cell effector functions following either the cognate interaction with virus-infected/cancerous host cells or an APC. The former leading to efficient elimination of the antigen-presenting

cell thereby limiting the spread of a pathogen or malignant cell growth, the latter driving $CD4^+$ T helper (T_H) cell responses including B cell help which culminates in the efficient production of plasma cell derived antibodies that can target extracellular pathogens (Janeway, 1996).

Aside from conventional MHC class I and -II-restricted, peptide recognizing T cells also their unconventional counterparts, which recognize small-molecule metabolites, glycolipids or modified peptides, help to shape immune responses in various immunological contexts such as anti-tumor, anti-microbial or autoimmune repsones. CD1d-restricted natural killer T (NKT) cells together with γδ T cells and MR1-restricted mucosal-associated invariant T (MAIT) cells belong to the group of innate-like T lymphocytes (Godfrey *et al.*, 2015; Vermijlen and I. Prinz, 2014). As compared to conventional T cells, much less is known about the modes of interaction between such innate-like T cells with APCs in the context of antigen-presentation. A comprehensive understanding of the underlying mechanisms and detailed molecular pathways that govern and are involved in the effective generation and maintenance of antigen/antigen-presenting molecules in APCs is much needed in order to gain further insight into T cell function, conventional and unconventional alike, in normal and pathological states.

1.4.1 MHC Class II Antigen Presenting Pathway

While upregulated on facultative APCs such as endothelial cells and myoblasts following specific inflammatory signals (e.g. IFNγ) (Hohlfeld and Engel, 1990) (Hohlfeld and Engel, 1991; Shiao *et al.*, 2007; Wiendl *et al.*, 2000), in steady state MHC class II molecules are almost exclusively expressed on professional APCs such as DCs (Kambayashi and Laufer, 2014). Antigenic peptides that are presented to $CD4^+$ T cells via MHC class II, result from proteolysis of self- and non-self proteins in the endosomal/lysosomal compartment (Trombetta and Mellman, 2005). Polymorphic MHC class II molecules are being synthesized in the ER, where αβ dimers of MHC class II associate with the non-polymorphic pseudopeptide invariant chain (Ii). Ii aids MHC class II molecules in passing the ER quality control system and, by means of a specific targeting sequence motif, promotes efficient egress of MHC class II molecules on their way from the ER to

the Golgi apparatus (**Figure 1.4**). Upon traversing the *trans* Golgi network on their way to the plasma membrane, another targeting motif facilitates the αβ-Ii complex to undergo clathrin-mediated endocytosis and therefore grants the complex access to the endocytic pathway, where eventually MHC class II can encounter antigenic peptides (Dugast *et al.*, 2005; McCormick *et al.*, 2005). In its capacity as a pseudopeptide, Ii prevents antigenic peptides to bind until proteolytically processed (Roche and Cresswell, 1990). The αβ-Ii complex passes from early endosomal to late endosomal/lysosomal compartments, where both abundance of proteolytic enzymes and sufficiently low pH, fulfill the requirements for efficient antigen processing and loading on MHC class II molecules (Blum *et al.*, 2013). Sequential proteolysis of Ii by enzymes such as cathepsins L and S, during passage along the endocytic pathway, leaves a small remnant peptide called class II-associated invariant chain peptide (CLIP) within the MHC class II peptide binding groove (Ghosh *et al.*, 1995). Presence of the place holder peptide CLIP precludes binding of antigenic peptides to MHC class II (Trombetta and Mellman, 2005). The molecular chaperones and MHC class II-like proteins H2-DM and HLA-DM in mice and humans respectively, facilitate antigenic peptide loading via catalyzing the dissociation of CLIP from its complex with MHC class II (Denzin and Cresswell, 1995). HLA-DM/H2-DM, both display a much more limited polymorphism as compared to MHC class II and are under the control of another set of non-peptide binding MHC class II-like chaperones, namely HLA-DO (humans) and H2-O (mice) respectively (Denzin *et al.*, 1997; Liljedahl *et al.*, 1996; van Ham *et al.*, 1997). These two chaperones most likely assure that CLIP is only removed in an adequaetely acidic environment, where efficient antigen processing can occur. Once CLIP is dissociated from MHC class II, antigenic peptides may bind to the molecule and antigenic peptide:MHC class II complexes are being transported by endosomal/lysosomal tubules to and inserted in the plasma membrane. Absence of the targeting sequence in Ii now warrants a certain stability of the complex in the plasma membrane and therefore ensures efficient cognate $CD4^+$ T cell interaction, however, MHC class II molecules may still be internalized and recycle back through the endocytic compartment (Hiltbold and Roche, 2002).

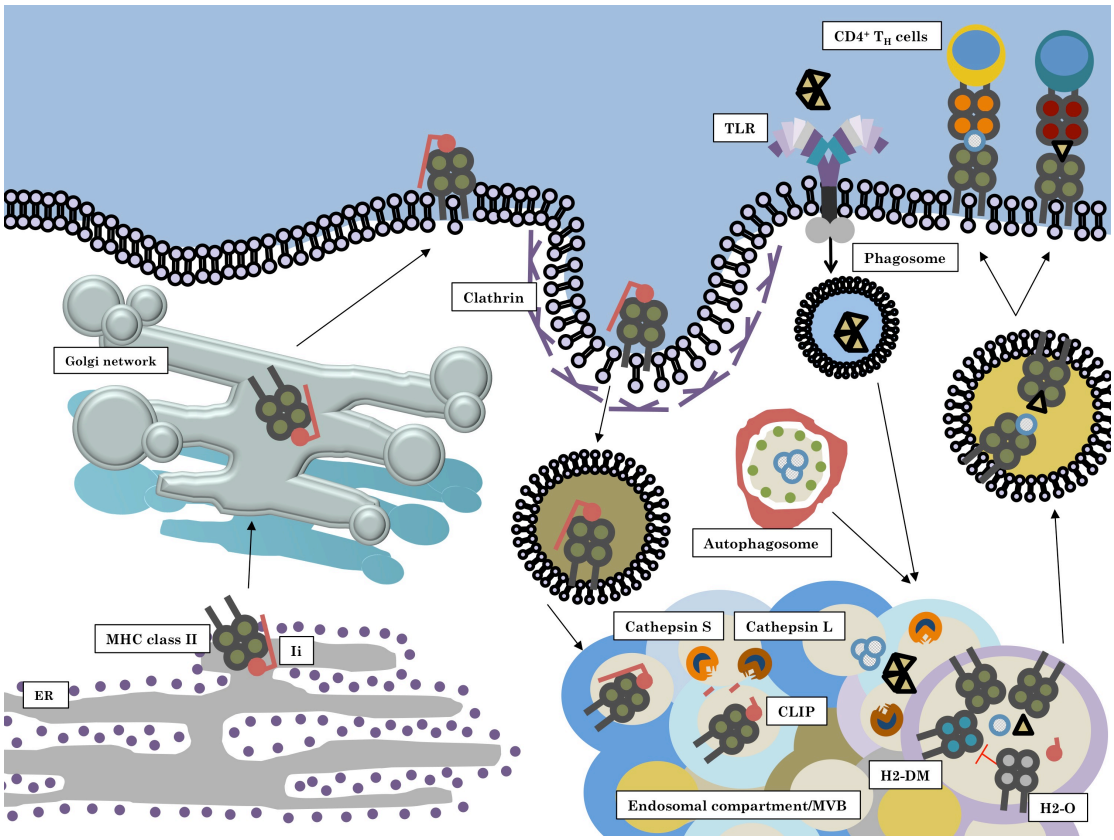

Figure 1.4. MHC class II antigen presentation.
MHC class II molecules are synthesized in the ER where they associate with the invariant chain (Ii) followed by transport via the secretory pathway through the *trans*-Golgi network to the plasma membrane. From there, MHC class II/Ii-complexes are internalized by clathrin-mediated endocytosis and guided towards endosomal compartments. Ii is proteolytically cleaved, and class-II-associated invariant chain peptide (CLIP) remains in the antigen binding groove. Antigenic material may reach the endosomal compartment through phagocytosis or macroautophagy. Within the endosomal system proteolytic processing generates antigenic peptides that can subsequently be loaded onto MHC class II. CLIP is eventually exchanged with antigenic peptides via the non-polymorphic H2-DM, which is negatively regulated by H2-O. MHC class II molecules loaded with antigenic peptides are transported via endosomal tubules and/or vesicles to the plasma membrane where they can interact with $CD4^+$ T_H cells.

1.4.1.1 Autophagy-Related Protein Function in Antigen Processing and Presentation With a Focus on the MHC Class II Pathway

Professional APCs such as DCs employ several means of acquiring antigen. Aside from macropinocytosis, clathrin-mediated endocytosis and phagocytosis (which comprises clathrin-mediated and -independent uptake of material), autophagy constitutes an important set of pathways that contribute as source for antigens in APCs (Roche and Furuta, 2015). The first compelling evidence for the existence of an endogenous MHC class II pathway came from a study on describing how the endogenous measles virus matrix and nucleocapsid protein-derived antigens could be presented to $CD4^+$ T cells via MHC class II (Jacobson *et*

al., 1989). Only one year later, Nuchtern et al. confirmed these findings for yet another viral antigen by reporting the efficient loading of influenza A matrix protein-derived peptides onto MHC class II (Nuchtern *et al.*, 1990). Further proof for the existence of endogenous MHC class II loading pathways was obtained through the direct analysis of peptides bound to MHC class II molecules. In fact, around 20-30% of natural ligands eluted from MHC class II molecules from B cells and DCs were found to be derived from endogenous protein sources (Adamopoulou *et al.*, 2013; Rammensee *et al.*, 1999). In a next step, MA was newly identified as a pathway that delivers endogenous antigenic constituents into endosomal MHC class II-containing compartments (MIICs) for subsequent recognition by $CD4^+$ T cells (Nimmerjahn *et al.*, 2003; Paludan *et al.*, 2005; Schmid *et al.*, 2007). The ability to deliver endogenous antigens to MHC class II seems to be differentially relevant depending on the APC (Brazil *et al.*, 1997).

MA is constitutively active in a variety of MHC class II positive APCs like DCs and B cells (Dengjel *et al.*, 2005; Nimmerjahn *et al.*, 2003; Paludan *et al.*, 2005) and can be induced following immune stimulation of these cells through germline-encoded pattern-recognition receptors such as Toll-like receptors (TLRs) or inflammatory cytokines (Delgado *et al.*, 2008; H. K. Lee *et al.*, 2007; Xu *et al.*, 2007). Colocalization studies indicate that in professional APCs, autophagosomes frequently fuse with MIICs, and that experimental delivery of antigens to autophagosomes by targeting the autophagosomal membrane through fusion with LC3 results in robust recognition by antigen-specific $CD4^+$ T cells (Dengjel *et al.*, 2005; Schmid *et al.*, 2007). Additionally, not only haematopoietic APCs but also thymic epithelial cells expend MA to generate endogenously derived MHC class II-bound peptides for positive and negative selection of $CD4^+$ T cells (Aichinger *et al.*, 2013; Nedjic *et al.*, 2008). Furthermore, macroautophagy has been implicated in generation and MHC class II-presentation of peptidylarginine deiminase-citrullinanted peptides (a group of peptides against which antibody responses are frequently found in autoimmune disorders such as rheumatoid arthritis) in DCs and macrophages (Ireland and Unanue, 2011).

Aside from macroautophagy also the non-canonical autophagy pathway LAP has been implicated in antigen presentation via MHC class II. Although the functional benefit of coupling lipidated LC3 to a phagosome is still not completely understood some have argued that the coating of the phagosome with LC3-II allows the vesicle to travel faster along microtubules which results in faster fusion with the lysosomal compartment (Ma *et al.*, 2014; Martinez *et al.*, 2011; Sanjuan *et al.*, 2007). However, studies that report more rapid cargo degradation were predominantly obtained using murine macrophages. Human studies on the other hand show that in prototypical APCs such as dendritic cells, LAP seems to retain antigenic cargo for sustained MHC class II antigen presentation rather than promoting its degradation (Romao *et al.*, 2013). Antigenic containment and stabilization in combination with low levels of lysosomal proteases has been speculated to be a crucial mechanism by which DCs maintain efficient and prolonged antigen presentation (Delamarre *et al.*, 2005; Romao and Münz, 2014; Romao *et al.*, 2013). Lee and colleagues reported that in murine DCs, TLR-dependent phagocytosed HSV-2 can be found in $LC3^+$ single-membraned vesicles reminiscent of LAPosomes. In absence of LAP-essential protein ATG5 subsequent HSV-2-specific $CD4^+$ T cell responses were markedly reduced, arguing for inefficient MHC class II-dependent presentation of LAP-deficient DC towards cognate T cells (H. K. Lee *et al.*, 2010). Interestingly, pharmacological induction of canonical MA via TORC1 inhibitor rapamycin did not lead to enhanced MHC class II presentation of phagocytosed antigens arguing for a non-MA pathway linking phagocytosis and MHC class II presentation (H. K. Lee *et al.*, 2010).

A recent study extended the role of non-canonical autophagy pathways during antigen presentation to the MHC class I pathway. It was shown, that absence of ATG5 in $CD11c^+$ DCs entailed impaired internalization of MHC class I molecules from the plasma membrane. The defect was mainly based on reduced recruitment of adaptor-associated kinase 1 (AAK1) to cell surface bound MHC class I. Furthermore, this stabilization of MHC class I molecules on the surface of APCs lead to enhanced $CD8^+$ T cell responses upon influenza and LCMV infections *in vivo* (Loi *et al.*, 2016).

1.4.1.2 Experimental Autoimmune Encephalomyelitis: *In Vivo* Model for $CD4^+$ T Cell-Mediated Autoimmunity

The emergence, activation and expansion of autoreactive T cells are considered crucial events in the development and progression of MS and encephalitogenic $CD4^+$ T cells are the main driving forces in the rodent animal model of multiple sclerosis (MS), experimental autoimmune encephalomyelitis (EAE) (Nylander and Hafler, 2012; A. P. Robinson *et al.*, 2014; Sospedra and Martin, 2005; Terry *et al.*, 2014). MS is a chronic immune-mediated disease of the CNS that develops in young adults with a complex predisposing genetic trait (Dendrou *et al.*, 2015). Similar to other autoimmune diseases, HLA-DR and -DQ alleles within the HLA class II region on chromosome 6p21 are by far the strongest risk-conferring genes and are thought to account for 10-60% of the genetic risk of MS (International Multiple Sclerosis Genetics Consortium (IMSGC) *et al.*, 2013; International Multiple Sclerosis Genetics Consortium *et al.*, 2011). Although it is generally accepted that MHC class II molecules influence autoimmune disease risk by cognate interactions with autoreactive $CD4^+$ T lymphocytes, our knowledge of how MHC class II-mediated antigen presentation confers risk for autoimmune diseases and regulates $CD4^+$ T cell autoreactivity at the molecular level is still very sketchy.

EAE, in which disease is induced by immunization of susceptible mice with myelin antigen together with adjuvant or by peripheral introduction of pre-activated myelin-specific $CD4^+$ T cells to naïve mice, represents a well established and suitable model to study $CD4^+$ T cell-mediated autoimmunity (Krishnamoorthy and Wekerle, 2009). Advances in technologies of genetic ablation and transgenesis in mice of C57BL/6 background and the development of myelin-oligodendrocyte glycoprotein (MOG)-induced EAE in C57BL/6 mice contributed substantially to our understanding of cellular and molecular pathways in MS pathogenesis as well as to the development of therapeutic agents (Friese *et al.*, 2006; Krishnamoorthy and Wekerle, 2009; A. P. Robinson *et al.*, 2014; Terry *et al.*, 2014).

Before infiltrating the CNS, autoreactive $CD4^+$ T cells are primed in the peripheral immune system. Priming can be targeted to skin draining lymph

nodes after subcutaneous immunization with myelin antigen and complete Freund's adjuvant (CFA) during active EAE induction. In MS, the site where autoreactive T cells are primed is not known, but the human disease is usually not elicited by vaccinations and persists in the absence of any systemic inflammatory challenges. Local reactivation and sustained expansion of autoreactive T cells within the CNS are considered instrumental in both MS and EAE. This effector phase can be modeled by adoptive transfer of primed myelin-specific $CD4^+$ T cells into naïve mice (adoptive transfer EAE, AT-EAE) and depends on the presence of $CD11c^+$ antigen-presenting cells (APCs) (Greter *et al.*, 2005; Paterka *et al.*, 2016). How autoreactive $CD4^+$ T cells become activated and cause autoimmune tissue damage during the course of MS and EAE are, however, incompletely understood, partly because the detailed antigen processing route of how myelin self-antigens are processed and presented towards $CD4^+$ T cells has not been fully elucidated.

1.4.2 CD1d Antigen Presenting Pathway

1.4.2.1 CD1d Assembly and Trafficking

The CD1 family is comprised of five isoforms that can be partitioned in two groups. Group 1 consists of CD1a, CD1b, CD1c and CD1e and group 2 only includes CD1d. While all isoforms can be found in humans, only CD1d is expressed in mice (Van Kaer *et al.*, 2016). DCs constitutively express CD1d and may activate invariant natural killer T (iNKT) cells by presenting antigenic glycolipids. CD1d is a highly conserved non-polymorphic MHC class I like transmembrane molecule and is regulated by cytokines or through engagement of innate receptors (Sköld *et al.*, 2005). Similar to MHC class I molecules CD1d is a heterodimer that is non-covalently coupled to β2-microglobulin. Many hematopoietic and non-hematopoietic cell types express CD1d constitutively on their surface or upregulate it upon activation (Balk *et al.*, 1994; Blumberg *et al.*, 1991; Busshoff *et al.*, 2001; Canchis *et al.*, 1993; de Lalla *et al.*, 2004). However, in mice, constitutively CD1d-expressing dendritic cells (DCs) appear to be the most potent presenter of exogenous antigenic glycolipids (Arora *et al.*, 2014; Fujii *et al.*, 2002; 2004). Similar to MHC class I molecules, CD1d molecules are synthesized, folded and equipped with β2-microglobulin in the ER (H. S. Kim *et*

al., 1999). Analogous to the placeholder function of the pseudopeptide CLIP in MHC class II, CD1d most likely leaves the ER with a spacer lipid in its antigen-binding groove in order to maintain stability. The biochemical nature of these lipids and the exact mechanisms underlying these transfer processes are not fully elucidated yet. However, the ER chaperone protein microsomal triglyceride transfer protein (MTP) has been suggested to load phospholipids onto nascent CD1d (Dougan *et al.*, 2005). The pharmacological inhibition of MTP lead to significantly reduced CD1d-presentation of the prototypical experimental glycolipid antigen α-galactosylceramide (αGalCer) while leaving MHC class II presentation of ovalbumin (OVA) unperturbed (Dougan *et al.*, 2005). CD1d, after having passed several protein quality control checkpoints, follows the secretory pathway and is being guided to the Golgi apparatus and subsequently reaches the cell surface (Kang and Cresswell, 2002b; H. S. Kim *et al.*, 1999). From there, CD1d is being internalized by its cytoplasmic tyrosine-based sorting motif in an adaptor protein complex 2 (AP2)-dependent manner and delivered to several endosomal compartments. Importantly, a fraction of CD1d molecules also associates with MHC class II molecules in these endosomal compartments (Jayawardena-Wolf *et al.*, 2001; Kang and Cresswell, 2002a). Interaction of CD1d with AP3 mediates sorting into lysosomes (Cernadas *et al.*, 2003; Elewaut *et al.*, 2003; Vartabedian *et al.*, 2016). Lipid antigens destined for CD1d-presentation can be derived from most subcellular compartments but usually encounter loading onto CD1d only in the endosomal/lysosomal system, where exogenous antigens face enzymatic processing and where endogenous antigens are recycled to (**Figure 1.5**). CD1d molecules survey and sample different endosomal compartments via a targeting motif in its cytoplasmic tail (Chiu *et al.*, 2002; Jayawardena-Wolf *et al.*, 2001). Deletion of the cytoplasmic tail does not influence CD1d surface expression, but abrogates the presentation of endogenous and exogenous lipids (Chiu *et al.*, 2002). CD1d also associates with the MHC class II chaperone Ii (Jayawardena-Wolf *et al.*, 2001). In an independent pathway, that appears to be especially important for the presentation of *Mycobacterium tuberculosis*-derived lipid-antigens, Ii diverts CD1d directly towards the lysosome (Sillé *et al.*, 2011).

1.4.2.2. Lipid Loading on CD1d

CD1d itself is unable to extract and acquire lipids from membranes and therefore is in need of lipid transfer proteins (LTPs) which, in analogy to the MHC class II/H2-DM interaction, facilitate loading of antigens within the endosomal/lysosomal compartment. Low molecular weight proteins called saposins (A, B, C, and D), GM2 ganglioside activator (GM2A) and the Niemann-Pick type C1 and C2 proteins (NPC1 and NPC2, respectively) have so far been identified to mediate the loading of lipids on CD1d molecules (Kang and Cresswell, 2004; Sagiv *et al.*, 2006; Schrantz *et al.*, 2007; Zhou *et al.*, 2004). Additionally, in the cases of saposins and GM2A, it was reported that these molecules also aid in the unloading of lipids from the CD1d antigen binding groove (Vartabedian *et al.*, 2016). However, the detailed mechanisms that govern these loading/unloading processes and determine how loaded CD1d is sent to the plasma membrane, whereas unloaded CD1d dwells in the endosomal/lysosomal compartment, as well as the relevance of the autophagy machinery in lipid antigen loading within endosomal compartments, remains to be addressed.

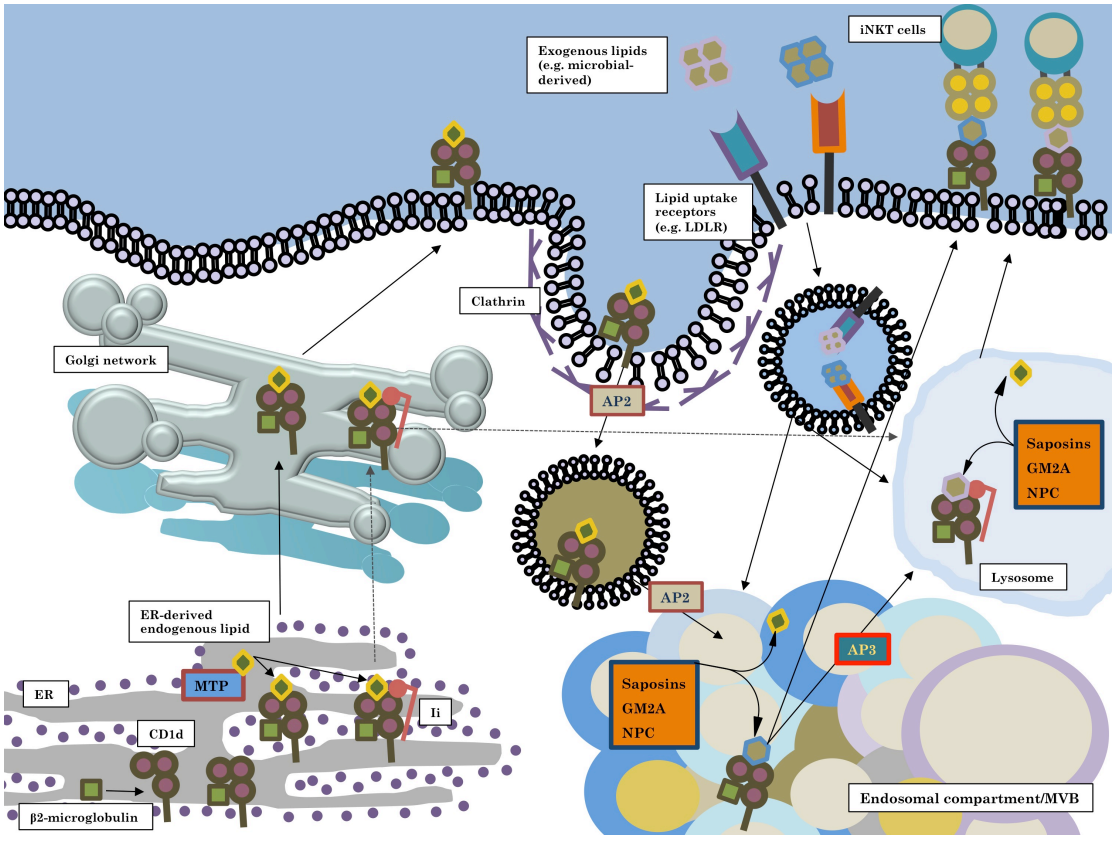

Figure 1.5. CD1d antigen presentation.
CD1d molecules are synthesized in the ER where they associate with β2-microglobulin. Microsomal triglyceride transfer protein (MTP) facilitates loading of ER-derived endogenous spacer lipids onto CD1d in order to stabilize the molecule for further transport. In an independent pathway, some CD1d molecules associate in the ER with invariant chain (Ii). The Ii/CD1d complexes, after travelling through the *trans*-Golgi network, are directly guided to the lysosome. The non-Ii associated CD1d molecules also pass the *trans*-Golgi network on their way to the plasma membrane. From there, CD1d is internalized by clathrin-mediated endocytosis and guided towards endosomal compartments where saposins, GM2 ganglioside activator (GM2A) and Niemann-Pick type C1 and C2 proteins (NPC1, NPC2) help exchanging spacer lipids with exogenous or other endogenous lipids. Loaded CD1d may either be transported to the lysosome in an adaptor protein 3 (AP3) dependent manner, or directly transported to the plasma membrane in order to interact with invariant natural killer T cells (iNKT).

1.4.2.3. Invariant Natural Killer T Cells

NKT cells belong to the group of innate-like T lymphocytes, and represent an important link between innate and adaptive immune responses. They recognize CD1-presented lipid antigens, can be activated in both antigen-dependent and independent manners, secrete large amounts of cytokines upon activation and exhibit remarkable functional plasticity with both proinflammatory and immunoregulatory characteristics (Godfrey *et al.*, 2015; Salio, Silk, *et al.*, 2014). Depending on their T cell receptor (TCR) variability, CD1d-restricted NKT cells can be subdivided into type I or invariant NKT (iNKT) cells and type II or diverse NKT (dNKT) cells. Type I NKT cells are characterized by the expression of a semi-invariant T cell receptor (iTCR) (Vα14Jα18/Vβ8.1/Vβ8.2/Vβ8.3/Vβ7/Vβ2 in mice and Vα24Jα18/Vβ11 in humans) (Brennan *et al.*, 2013; Macho-Fernandez and Brigl, 2015). The Vα14 TCR is exclusively used by iNKT cells but not by conventional T cells (Taniguchi *et al.*, 2015). Furthermore, iNKT cell subsets bear molecules on their surface that were believed to be characteristic for natural killer (NK) cells like NKG2D (Kuylenstierna *et al.*, 2011), KLRG (Shimizu *et al.*, 2014), IL-12 receptor (Brigl *et al.*, 2011) or NK1.1 (CD161) (Benlagha *et al.*, 2000; Godfrey *et al.*, 2004; Kawano *et al.*, 1997; Matsuda *et al.*, 2000), hence their name. However, although this feature may characterize some NKT subsets, other subsets do not show expression of NK cell markers at all and the more stable prerequisite for belonging to the iNKT cell compartment therefore appears to be CD1d-restriction (Godfrey *et al.*, 2015). Unlike conventional $CD4^+$ or $CD8^+$ T cells, iNKT cells recognize antigenic glycolipids which are presented via the monomorphic MHC class I-like molecule CD1d (Bendelac *et al.*, 1995; 2007). Invariant NKT cell responses have proven to be highly conserved between

humans and mice. They enhance activation of innate immune cells such as dendritic cells (DCs) or NK cells and shape immune responses in concert with other lymphocytes such as B cells, thereby acting not only as an amplification relay but also as a shunter at the interface of innate and adaptive immunity (Brossay *et al.*, 1998; Carnaud *et al.*, 1999; P.-P. Chang *et al.*, 2012; Hammond and Kronenberg, 2003)

Invariant NKT cells can be activated via interaction of the iTCR:CD1d:glycolipid tri-molecular complex or in an iTCR-independent manner (e.g. via cytokines) (Brigl *et al.*, 2011; Kawano *et al.*, 1997). Upon activation, iNKT cells readily expand and undergo significant remodeling of their surface expression patterns with regards to several markers such as NK1.1 and the iTCR (Wilson *et al.*, 2003). Although iNKT cells have adaptive characteristics, they exist in a preactivated memory T cell-like effector state ready to release copious amounts of immunomodulatory cytokines (such as IFNγ, IL-4, IL-13, IL-17, GM-CSF and TNF-α) not only upon engagement of their iTCR but also in response to innate signals (Brigl *et al.*, 2011). One of their key features is cytokine-mediated transactivation of other innate and innate-like immune subsets thereby amplifying initial responses (Carnaud *et al.*, 1999; Paget *et al.*, 2009; Schneiders *et al.*, 2012; Smyth *et al.*, 2002; 2005). However, iNKT cells may also provide both antigen-specific cognate and non-cognate help for B cells (P.-P. Chang *et al.*, 2012; King *et al.*, 2012; Leadbetter *et al.*, 2008) and in turn can be activated by B cells (Bialecki *et al.*, 2009; Zietara *et al.*, 2011). Interestingly, unlike non-cognate B cell help, antigen-specific B cell help induces a discontinuous germinal center B cell expansion, rapid initial IL-10-producing B cell expansion but fails to induce humoral memory, all in line with a more innate-biased response (Vomhof-Dekrey *et al.*, 2015).

A key difference between iNKT cells and conventional T cells is the onset of the response to a certain stimulus, which occurs in case of iNKT cells already a few hours after engagement, as opposed to several days in the case of conventional T cells (Crowe *et al.*, 2003; Godfrey *et al.*, 2015).

1.4.2.4 Invariant Natural Killer T Cell Activation by Dendritic Cells

The interaction between iNKT cells and DCs is not unidirectional but characterized by reciprocal feedback loops depending on the biochemical

structure of the CD1d ligand as well as the nature of the APC (Arora *et al.*, 2014; Brennan *et al.*, 2013). Until recently, it remained a conundrum as of how iNKT cells can be activated in a pathological setting in absence of an appropriate lipid agonist. It is now evident that DCs are able to transduce innate signals towards iNKT cell responses. Activation of iNKT cells can often be a combination of recognition of cognate lipid antigen and iTCR-independent signals. DCs will CD1d-present endogenous glycolipids in response to pathogen- and danger-associated molecular patterns (PAMPS/DAMPS) (Paget *et al.*, 2007). iNKT cells constitutively express IL-12 receptor and primitive pattern recognition receptor (PPRR)-mediated secretion of IL-12 by DCs leads to phosphorylation of STAT4 and consecutive IFNγ release by iNKT cells (Brigl *et al.*, 2011; Kitamura *et al.*, 1999). Furthermore, direct cellular contact between DCs and iNKT cells in a CD40:CD40L-dependent manner leads to a feed-forward signal, resulting in additional IL-12 production by DCs and consecutive further upreguation of IL-12 receptor on iNKT cells. CD40/CD40L as well as CD28:CD80/CD86 interactions are required for subsequent iNKT cell mediated-IFNγ secretion whereas IL-4-secretion was described to be solely dependent on CD28:CD80/CD86 interaction (Hayakawa *et al.*, 2001; Kitamura *et al.*, 1999). Coadministration of the iNKT cell agonist αGalCer and OVA in $CD40^{-/-}$ and $CD40L^{-/-}$ mice leads to abrogation of $CD4^+$ and $CD8^+$ T cell responses, while DCs were not affected in their ability to present antigen on MHC class I or II, and are capable of upregulating CD80/86 (Fujii *et al.*, 2004). Recent reports show that acellular artificial APCs loaded with iNKT cell agonists can activate and expand human iNKT cells *in vitro* as potently as autologous immature DCs. Engineering artificial APCs with differential association to costimulatory factors therefore may help to obtain valuable insights into the crosstalk between iNKT cells and DCs and will foster our understanding of how to harness their therapeutic potential (East *et al.*, 2012; Shiratsuchi *et al.*, 2009; W. Sun *et al.*, 2012)

1.4.2.5 Invariant Natural Killer T cell-Mediated Maturation and Licensing of Dendritic Cells

As a feed-back loop, αGalCer activated iNKT cells contribute rapidly to maturation of DCs *in vivo* resulting in upregulation of surface MHC class II, costimulatory molecules CD40, CD80, CD86 and endocytic receptor Dec-205, as

well as increased IFNγ secretion. Invariant NKT cell matured DCs elicit specific $CD4^+$ and $CD8^+$ T cell responses against a coadministered peptide. The observed DC maturation is highly dependent on iNKT cells since administration of αGalCer into iNKT-lacking Jα281 mice fails to induce DC maturation (Fujii *et al.*, 2003). Challenge with OVA-expressing tumors leads to significant tumor resistance in animals that had been challenged with OVA in combination with iNKT cells agonist αGalCer (Hermans *et al.*, 2003).

1.4.2.6 Modifications of Invariant Natural Killer T Cell Responses: Implications for Human Health and Disease

Their ability to mature DCs and to transactivate both cytotoxic T lymphocytes and NK cells for tumor cell eradication (Fujii *et al.*, 2013; Pardoll, 2012) reflect the potential of iNKT cells in improving cancer immunotherapy. However, in contrast to promising studies performed in experimental models (Harada *et al.*, 2005), clinical trials using direct administration of soluble αGalCer in cancer patients so far failed to show promising results (Giaccone *et al.*, 2002). Aside from high interindividual variability in iNKT cell frequencies and inefficient targeting of particular subsets of lipid antigen presenting cells, direct administration of antigenic glycolipids was shown to induce PD1:PDL1-dependent long term anergy (Parekh *et al.*, 2005; 2009; Sullivan and Kronenberg, 2005) or induction of regulatory IL-10 producing iNKT cells (Lynch *et al.*, 2015; Sag *et al.*, 2014) which negatively affect anti-tumor responses (Sag *et al.*, 2014). As an alternative to αGalCer administration, DCs can be glycolipid-pulsed *ex vivo* followed by re-infusion. This strategy has proven to induce prolonged activation of iNKT cells rather than a regulatory/anergic phenotype, inhibits metastasis in an experimental melanoma model and can expand human iNKT cells *in vivo* (Fujii *et al.*, 2002; Toura *et al.*, 1999; van der Vliet *et al.*, 2003). Additionally, adoptive transfer of αGalCer-pulsed matured DCs expands iNKT cells in advanced stage cancer patients (D. H. Chang *et al.*, 2005). A clinical phase I study in a limited number of individuals with metastatic malignancies reported that transfer of immature monocyte-derived DCs loaded with αGalCer is associated with a stronger recall-response (Nieda *et al.*, 2004). The use of *in vitro* matured DCs as compared to immature DCs significantly increases the observed beneficial effects (D. H. Chang *et al.*, 2005; Nieda *et al.*, 2004). Another phase I trial, during which

patients with head and neck squamous cell carcinoma (HNSCC) were treated via singular coadministration of autologous *in vitro* expanded iNKT cells (intraarterial) and submucosal application of αGalCer-loaded APCs, showed partial clinical response (Kunii *et al.*, 2009). In a small phase II clinical study in HNSCC patients using the same treatment regiment, 50% of the patients depicted tumor regression while 50% showed stable disease (Yamasaki *et al.*, 2011). Promising results were reported from a phase I-II study in non-small cell lung cancer patients: sequential intravenous administration of αGalCer-pulsed PBMCs increased the frequencies of IFNγ-producing cells in a majority of patients. This iNKT cell-mediated T_H1 skewing in responders was associated with significantly prolonged median survival time (Motohashi *et al.*, 2009). In a follow-up study, two candidate genes, *LTB4DH* and *DPYSL3*, were proposed to predict responsiveness to above mentioned treatment regimen (Okita *et al.*, 2010). Late stage cancer patients often are immune suppressed and retrieving enough APCs from these individuals for autologous transfer might prove difficult. Therefore, novel artificial APC constructs might help to circumvent lack of appropriate autologous APC numbers (East *et al.*, 2012; Shiratsuchi *et al.*, 2009; W. Sun *et al.*, 2012). Moreover, novel glycolipid-antigen delivery systems that systematically target relevant APC populations are currently being investigated. Some of these nanovector systems already show promising results. αGalCer-containing silica microspheres, poly(lactic-co-glycolic acid) (PLGA) polymers and modified liposomes have already been reported to efficiently elicit iNKT cell responses (Barral *et al.*, 2010; Macho-Fernandez *et al.*, 2012; Nakamura *et al.*, 2013). In order to initiate *in situ* responses of DCs, artificial adjuvant vector cell systems have been recently introduced. Herein, allogeneic CD1d-expressing NIH3T3 fibroblasts loaded with αGalCer were transfected with target-antigen mRNA. Injection of NIH3T3 fibroblasts leads to activation of iNKT cells, consecutive maturation of DCs and activation of NK cells and antigen-specific CTLs. Animals immunized with adjuvant vector cells showed potent immunity against antigen-bearing tumors. Memory cytotoxic T lymphocyte (CTL) responses could still be detected 12 months after initial single injection (Fujii *et al.*, 2009; 2013).

Humans, as compared to inbred mice, show high interindividual variability in iNKT cell frequencies. Patients with low steady state numbers of iNKT cells

might not profit from autologous transfer of lipid-pulsed APCs. Mouse embryonic fibroblast-derived induced pluripotent stem cells (iPSCs) can readily differentiate into functional iNKT cells. These iPSC-derived NKT cells are able to produce IFNγ and mediate anti-neoplastic effects *in vivo* (Watarai *et al.*, 2010). Therefore, patients with low iNKT cell frequencies may be reconstituted with iPSC-derived iNKT cells as an efficient means to fully harness their immunomodulatory potential (Fujii *et al.*, 2013).

First attempts in using engineered iNKT cells with chimeric antigen receptors (CARs) show promising results. CAR-bearing iNKT cells home to designated tumor sites, eradicate tumor cells and effectively execute cytotoxicity against tumor associated macrophages (TAMs) without inducing graft-versus-host disease (GvHD) (Heczey *et al.*, 2014). Additionally, $CD62L^+$ CD19-specific CAR-bearing iNKT cells show potent immunotherapeutic efficacy in a B cell lymphoma model (G. Tian *et al.*, 2016).

In conclusion, murine studies and clinical trials performed to date demonstrate that therapeutic strategies that harness the biology of iNKT cells are generally well tolerated and, in some cases, effective in inducing tumor regression and prolonged survival. All of the tested and currently investigated strategies harness both the powerful cytolytic and adjuvant activity of iNKT cells in order to enhance protective anti-tumor immune responses. In order to fully harness their therapeutic potential it will not only be key to elucidate the differential effector functions and modes of activation of the distinct iNKT cell subsets but also the immunological contexts and transcriptional programs that direct iNKT cell progenitors into development towards a specific subpopulation as well as determinants that gear specific iNKT cell subsets to distinct anatomical sites (Benlagha *et al.*, 2005; Gapin, 2016; Y. J. Lee *et al.*, 2015). Profound mechanistic insight into understanding how DCs activate and instruct iNKT cells and which factors regulate iNKT cell response is a prerequisite for improving the efficacy of iNKT cell-targeting therapies. In addition, clinical trials will be instrumental in identifying the optimal ligand and APC population to induce anti-tumor iNKT cell activation and in determining the routes and intervals of administration to achieve sustained immune responses.

1.5 Hypothesis

Autophagy pathways converge in the endosomal/lysosomal compartment, where antigen loading onto MHC class II and the non-classical MHC class I CD1d molecule takes place. We therefore hypothesized that absence of the essential autophagy protein ATG5 impairs antigen loading and restrains $CD4^+$ T cell and iNKT cell responses. To this end, we investigated mice with conditional deletion of ATG5 in $CD11c^+$ APCs in *in vivo* models for i) $CD4^+$ T cell-driven autoimmunity, i.e. EAE, and ii) for iNKT-cell-mediated protection from infectious pathogens, i.e. *Sphingomonas paucimobilis* infection.

2. Results

2.1 ATG5 in DCs Drives CD4$^+$ T Cell-Mediated CNS Autoimmunity

2.1.1 Phenotypic Analysis of DC-*Atg5*$^{+/+}$ and DC-*Atg5*$^{-/-}$ Mice

In order to assess the role of autophagy during DC-mediated antigen presentation we made use of a Cre/loxP-based conditional knockout targeting the autophagy protein ATG5 in professional antigen presenting cells. To this end, conditional knockout mice (C57BL/6) for disruption of *Atg5*, an essential component of both the canonical pathway of macroautophagy and LC3-associated phagocytosis (LAP), in CD11c$^+$ antigen presenting cells (*Atg5*$^{flox/flox}$ × CD11c-Cre-GFP, designated DC-*Atg5*$^{-/-}$) were generated. Targeted deletion of *Atg5* was confined to the CD11c$^+$ immune compartment represented by distinct increase in the GFP-signal in CD11c$^+$/MHC class II$^+$ splenic DCs in DC-*Atg5*$^{-/-}$ mice as compared to *Atg5*$^{flox/flox}$ control littermates (designated DC-*Atg5*$^{+/+}$) (**Figure 2.1.1 A, B**). By contrast, Ly-6C$^+$/CD11b$^+$/CD11c^{neg} splenic monocytes, splenic CD19$^+$/MHC class II$^+$ B cells and splenic CD4$^+$ T cells did not express GFP indicating cell type specific deletion of *Atg5* within the CD11c$^+$ DC subset (**Figure 2.1.1 A**). Furthermore, knockout of *Atg5* was also confirmed on protein level, using CD11c$^+$ BMDCs (**Figure 2.1.1 C**). DC-*Atg5*$^{-/-}$-derived CD11c$^+$ BMDCs were devoid of ATG5-ATG12-complex, showed a marked accumulation of LC3-I but levels of the lipidated form of LC3 (LC3-II) could not be detected in these cells (**Figure 2.1.1 C**). Having confirmed that ablation of ATG5 was indeed confined to the CD11c$^+$ compartment, we next investigated if tissue-specific knockout of an essential autophagy gene would lead to alterations with regard to the frequency of our target cells. When comparing DC-*Atg5*$^{-/-}$ *vs.* DC-*Atg5*$^{+/+}$ mice, no difference in frequencies of splenic CD11$^+$/MHC class II$^+$ cDCs were detected (**Figure 2.1.1 D**). Moreover, surface levels of MHC class II and costimulatory molecules CD40 and CD86 remained unchanged in DC-*Atg5*$^{-/-}$ mice (**Figure 2.1.1 E**).

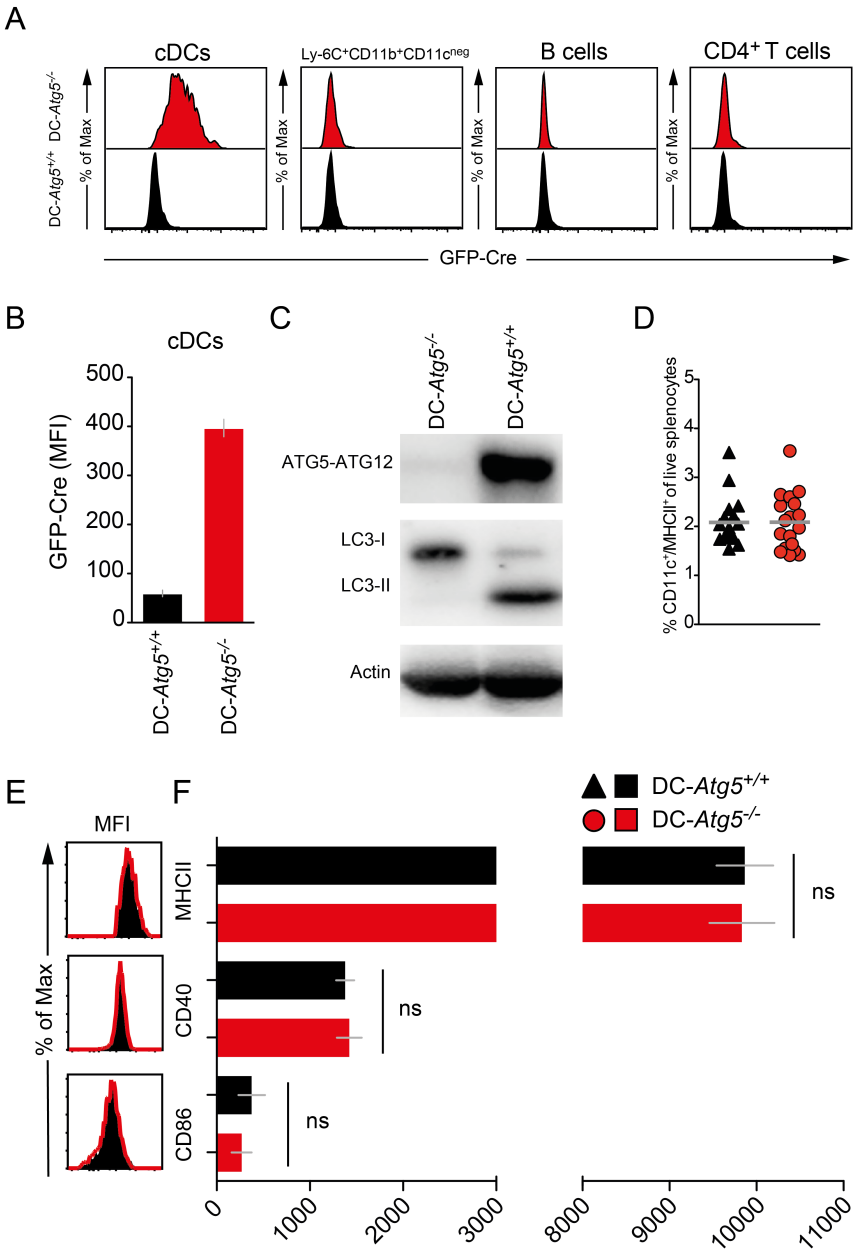

Figure 2.1.1 Characterization of DC-*Atg5*$^{-/-}$ *vs.* DC-*Atg5*$^{+/+}$ mice
(A) Representative histograms depicting GFP-Cre-expression of either CD11c^{+}/MHC class II (MHCII)$^{+}$ splenic conventional DCs (cDCs), Ly-6C^{+}/CD11b^{+}/CD11c^{-} monocytes, B cells CD4^{+} T cells in DC-*Atg5*$^{+/+}$ (black triangles) or DC-*Atg5*$^{-/-}$ (red circles) mice in steady state. **(B)** Quantification of GFP-Cre median fluorescence intensity (n: DC-*Atg5*$^{+/+}$ = 7; DC-*Atg5*$^{-/-}$ = 9). **(C)** Western blot analysis for protein expression of ATG5-ATG12-complex, LC3-I and LC3-II in CD11c^{+} BMDCs derived from DC-*Atg5*$^{+/+}$ or DC-*Atg5*$^{-/-}$ mice. Actin served as a loading control. One representative of 2 experiments is shown. **(D)** Quantified frequencies of splenic CD11c^{+}/MHC class II^{+} DCs in naïve DC-*Atg5*$^{+/+}$ and DC-*Atg5*$^{-/-}$ mice. **(E)** Representative histograms and **(F)** quantification of median fluorescence intensity (MFI) for MHC class II (upper panel), CD40 (middle panel) and CD86 (lower panel) on CD11c^{+}/MHC class II^{+} splenic DCs. Pooled data of 3 independent experiments is shown. Each dot represents one individual animal. Statistical analysis: unpaired two-tailed student t test, mean ± s.e.m., ns = not significant, *P< 0.05, **P< 0.01 and ***P< 0.001.

2.1.2 Absence of ATG5 in CD11c$^+$ Cells Protects Mice from Adoptive Transfer EAE

Next, we wanted to address whether autophagic activity in CD11$^+$ antigen presenting cells regulates the onset and/or severity of autoimmune-mediated neuroinflammation. For this purpose, we made use of EAE, a commonly used animal model of MS. Since we were particularly interested in the role of DC-inherent autophagy during CNS reactivation of encephalitogenic CD4$^+$ T cells, we chose to apply the adoptive transfer model of EAE (AT-EAE), during which preactivated myelin-specific CD4$^+$ T cells are injected into naïve recipients. We found that absence of *Atg5* in CD11c$^+$ cells leads to complete protection from developing AT-EAE upon transfer of T cell receptor-transgenic (TCR-tg) MOG_{35-55}-specific CD4$^+$ T cells derived from 2D2/TCR^{MOG} animals (**Figure 2.1.2 A, left and middle panel**). Furthermore, as opposed to DC-*Atg5*$^{+/+}$ control littermates, DC-*Atg5*$^{-/-}$ mice did not show any signs of weight loss after transfer of preactivated effector cells (**Figure 2.1.2 A, right panel**). These results were confirmed using non-TCR-tg polyclonal encephalitogenic CD4$^+$ T cells obtained from MOG_{35-55} immunized C57BL/6 wild type mice (**Figure 2.1.2 B**). To ensure that the observed protective effect was not due to Cre-recombinase, which is present in DC-*Atg5*$^{-/-}$ mice but absent in DC-*Atg5*$^{+/+}$ control littermates, CD11c-Cre mice were used as recipients for AT-EAE. In contrast to DC-*Atg5*$^{-/-}$ mice, CD11c-Cre mice were fully susceptible to developing AT-EAE and showed a similar disease onset, severity and weight loss pattern as C57BL/6 wild type mice (**Figure 2.1.2 C**).

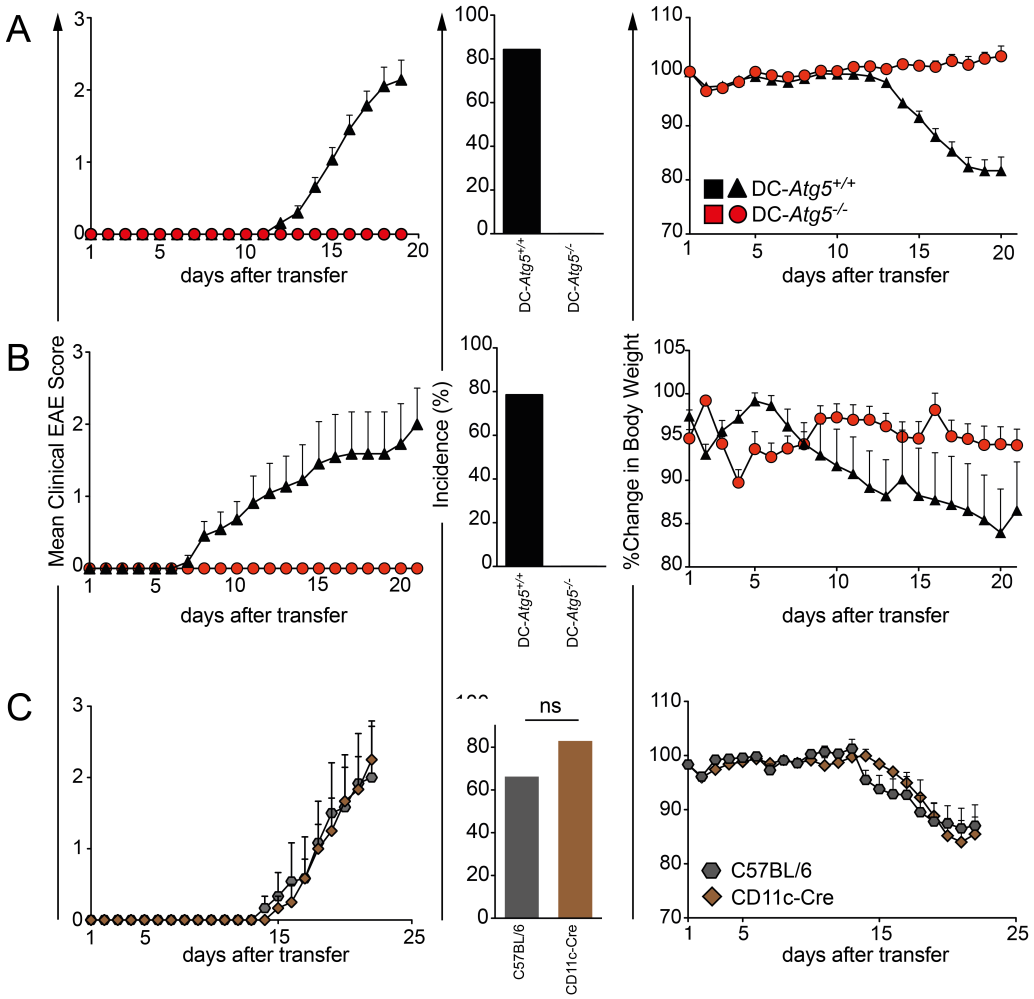

Figure 2.1.2 Preactivated, encephalitogenic CD4⁺ T cells require ATG5 expression by CD11c⁺ cells to induce AT-EAE.
(A) EAE was induced via adoptively transferring 2D2/TCR^{MOG}-derived encephalitogenic CD4⁺ T cells into DC-*Atg5*$^{+/+}$ (black triangles) or DC-*Atg5*$^{-/-}$ mice (red circles). Development of clinical EAE scores is depicted. Each data point represents the mean of animals from 4 independent experiments (n: DC-*Atg5*$^{+/+}$ = 32; DC-*Atg5*$^{-/-}$ = 35) (left panel). Quantification of disease incidence is shown (middle panel). Development of body weight is depicted. Each data point represents the mean of animals from 4 independent experiments (n: DC-*Atg5*$^{+/+}$ = 32; DC-*Atg5*$^{-/-}$ = 35) (right panel). Pooled data of 4 independent experiments is shown. **(B)** EAE was induced via adoptively transferring C57BL/6 wild type-derived encephalitogenic CD4⁺ T cells into DC-*Atg5*$^{+/+}$ (black triangles) or DC-*Atg5*$^{-/-}$ mice (red circles). Development of clinical EAE scores is depicted. Each data point represents the mean of 7 animals (left panel). Quantification of disease incidence is shown (middle panel). Development of body weight is depicted. Each data point represents the mean of 7 animals (right panel). One representative of two independent experiments is shown. **(C)** EAE was induced via adoptively transferring 2D2/TCR^{MOG}-derived encephalitogenic CD4⁺ T cells into C57BL/6 wild type mice (grey hexagons) or CD11c-Cre-GFP mice (brown diamonds). Development of clinical EAE scores is depicted. Each data point represents the mean of 6 animals. (left panel). Quantification of disease incidence is shown (middle panel). Development of body weight is depicted. Each data point represents the mean of 6 animals (right panel). One representative of two independent experiments is shown.

When sacrificing animals at peak of disease (day 19), DC-*Atg5*$^{+/+}$ animals depicted significantly smaller spleens (reflected by total weight and

spleen:body weight ratio) as compared to DC-*Atg5*$^{-/-}$ mice (**Figure 2.1.3 A-C**) which is in line with a previous study that showed atrophy of primary and secondary lymphoid organs during models of progressive EAE (Tsunoda *et al.*, 2005)

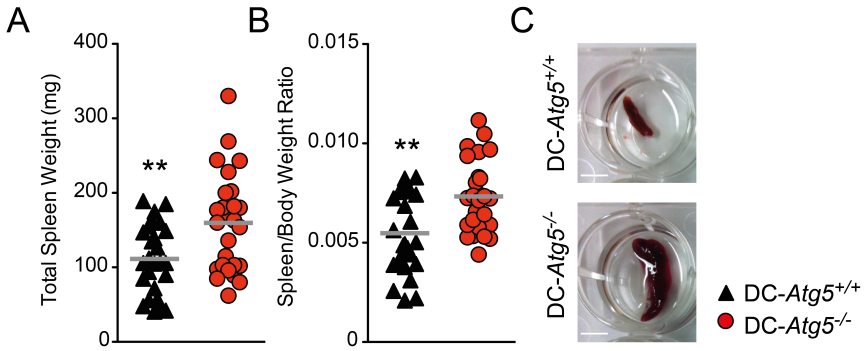

Figure 2.1.3 DC-*Atg5*$^{-/-}$ do not show splenic atrophy at peak of disease.
(A) Total spleen weight in mg and **(B)** spleen/bodyweight ratio on day of sacrifice upon AT-EAE. Each dot represents one individual animal. Pooled data of 3 independent experiments is shown. Scale bar: 0.5 cm Statistics: unpaired two-tailed student t test. * P< 0.05, ** P< 0.01, *** P< 0.001.

2.1.3 Characterization of CD11c-Expressing DCs in the CNS of DC-*Atg5*$^{-/-}$ and DC-*Atg5*$^{+/+}$ Mice at Steady State

Based on the finding that absence of ATG5 in the CD11c^{+} compartment alone sufficed to prevent onset of AT-EAE, we next investigated whether a CD11c^{+} cell population was present in the CNS at steady state, if this subset expressed markers in keeping with a classical DC expression profile and if it is subject to Cre-mediated deletion of ATG5. Indeed, a small subpopulation of CD11b^{+} myeloid cells in the CNS coexpressed CD11c and MHC class II (**Figure 2.1.4 A**). The frequency of this subpopulation (defined as % of CD45^{hi}/CD11b^{+} or % of CD11b^{+}) was unchanged in DC-*Atg5*$^{-/-}$ as compared to DC-*Atg5*$^{+/+}$ mice (**Figure 2.1.4 B**). This CD11c^{+} subset was efficiently targeted by Cre-recombination as indicated by strong GFP-expression, which was confined to the CD11c^{+} compartment and not detectable in DC-*Atg5*$^{+/+}$ mice (**Figure 2.1.4 C**). Additionally, this CNS resident CD11c^{+} population (henceforth CNS DCs) expressed the surface molecules indicative of professional antigen presenting properties such as MHC class II, CD86 and CD40. When comparing the two genotypes, ATG5-deficient CNS DCs did not differ in their expression profile from DC-*Atg5*$^{+/+}$-derived CNS DCs (**Figure 2.1.4 D**).

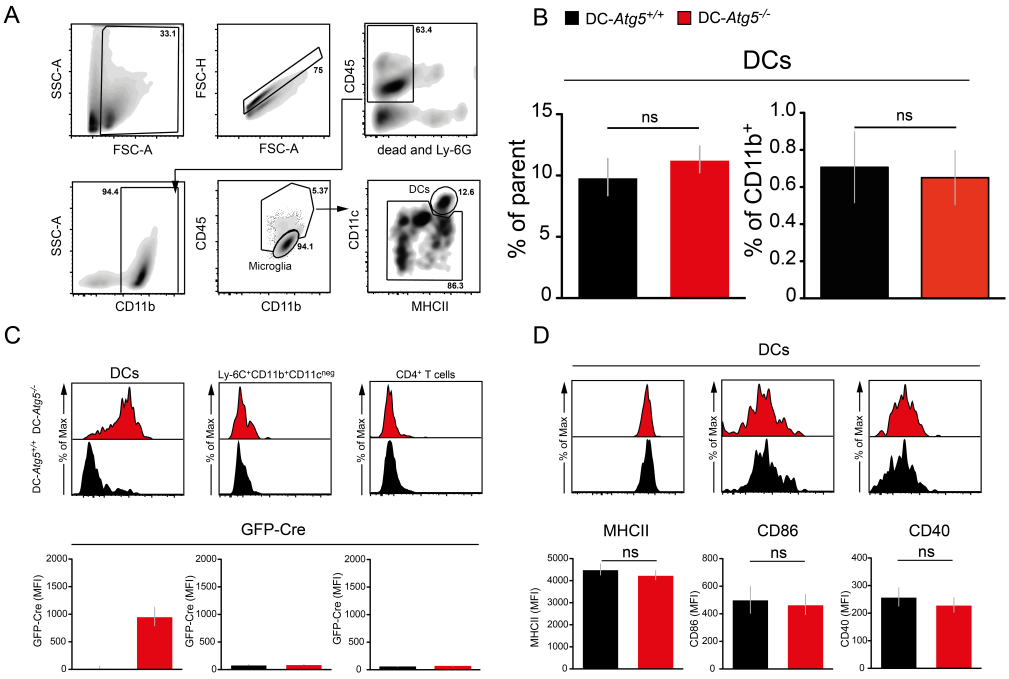

Figure 2.1.4 Phenotypic characterisation of CD11c⁺ CNS DCs at steady state. **(A)** Gating strategy for flow cytometry analysis in the CNS of naïve DC-*Atg5*$^{+/+}$ and DC-*Atg5*$^{-/-}$ mice. First, single leukocytes were defined by applying the respective gates (leukocytes: SSC-A *vs.* FSC-A; single cells: FSC-H *vs.* FSC-A). Next, it was gated on CD45^{+} cells while excluding Ly-6G^{+} neutrophils and dead cells. After gating on CD11b^{+} myeloid cells, microglia were defined as CD45^{lo}/CD11b^{+}. Inside the CD45^{hi}/CD11b^{+} cell gate, it was further gated on CD11c^{+}/MHC class II (MHCII)$^{+}$ cells (CNS DCs). Within the remainder of the cells it was subgated on Ly-6C^{+}/CD11b^{+}/CD11c^{-} monocytes (not shown). **(B)** Quantified frequencies (of parent, left panel and of total CD11b^{+}, right panel) of CNS resident CD11c^{+}/MHCII^{+} DCs in naïve DC-*Atg5*$^{+/+}$ and DC-*Atg5*$^{-/-}$ mice. **(C)** Representative histograms (upper panels) depicting GFP-Cre-expression of either CNS resident CD11c^{+}/MHCII^{+} DCs (left panel) or Ly-6C^{+}/CD11b^{+}/CD11c^{-} monocytes (middle panel) in naïve mice. Representative histogram depicting GFP-Cre-expression in CNS-infiltrating CD4^{+} T cells on peak of disease (right panel). Quantification of GFP-Cre median fluorescence intensity is depicted in the respective lower panels. **(D)** Representative histograms (upper panels) depicting either MHCII (left panel), CD86 (middle panel) or CD40 (right panel) median fluorescence intensity (MFI) of CNS resident CD11c^{+}/MHCII^{+} DCs. Quantification of the respective surface molecules is shown in the lower panels. Pooled data of 2 independent experiments is shown (n: DC-*Atg5*$^{+/+}$ = 5; DC-*Atg5*$^{-/-}$ = 5 for naïve myeloid compartments and n: DC-*Atg5*$^{+/+}$ = 10; DC-*Atg5*$^{-/-}$ = 12 for peak of disease CD4^{+} T cell analysis). Statistical analysis: unpaired two-tailed student t test, mean ± s.e.m., ns = not significant, *P< 0.05, **P< 0.01 and ***P< 0.001.

2.1.4 Characterization of Microglia in DC-*Atg5*$^{-/-}$ and DC-*Atg5*$^{+/+}$ Mice at Steady State

The major population of CD45^{+} CD11b^{+} cells in the CNS of a naïve mouse is comprised of microglial cells (Greter *et al.*, 2015). Albeit not expressing CD11c or MHC class II constitutively, these CD45^{lo} microglia have been described to upregulate surface levels of these molecules upon activation (Greter *et al.*,

2015; Ponomarev *et al.*, 2005; Reichmann *et al.*, 2002; Remington *et al.*, 2007). We analyzed the CD45^{lo}/CD11b^{+} microglial compartment in DC-*Atg5*$^{-/-}$ and DC-*Atg5*$^{+/+}$ mice at steady state, and found their frequencies to be similar (**Figure 2.1.5 A**). Moreover, neither DC-*Atg5*$^{-/-}$- nor DC-*Atg5*$^{+/+}$-derived microglia expressed CD11c to the extent of CNS DCs (**Figure 2.1.5 B, left panel**) and DC-*Atg5*$^{-/-}$-derived microglia did not express GFP indicating that despite low-level CD11c expression, the promotor activity does not support CD11c driven GFP-Cre-recombinase expression. This suggests that microglial cells do not delete Atg5 in DC-*Atg5*$^{-/-}$ mice (**Figure 2.1.5 B, right panel**). The surface levels of costimulatory molecules CD40 and CD86 on microglia were unchanged in DC-*Atg5*$^{-/-}$ mice and the overall expression of MHC class II was low (**Figure 2.1.5 C**).

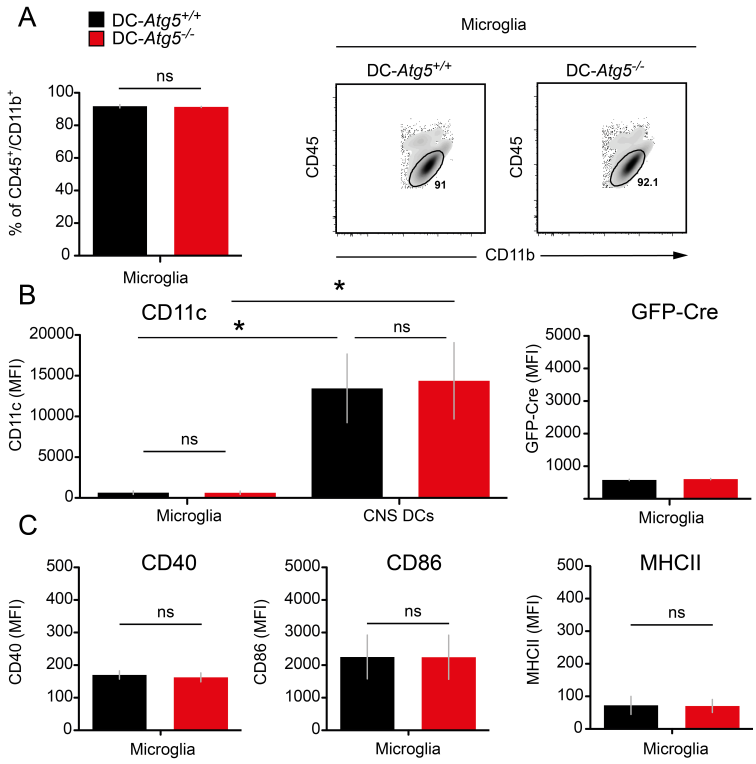

Figure 2.1.5 Characterization of microglial compartment in DC-*Atg5*$^{-/-}$ and DC-*Atg5*$^{+/+}$ mice at steady state.
(A) Frequencies of CD45$^{lo/int}$CD11b^{+} microglial cells are unchanged in DC-*Atg5*$^{-/-}$ mice. **(B)** CD45$^{lo/int}$CD11b^{+} microglial cells do not express CD11c to a substantial level at steady state compared to CD11c^{+}/MHC class II (MHCII)$^{+}$ CNS DCs (left panel). There is no increased GFP-Cre signal in microglia derived from DC-*Atg5*$^{-/-}$ mice as compared to DC-*Atg5*$^{+/+}$ mice (right panel) **(C)** Surface expression levels of CD40, CD86 and MHCII are similar on microglia when comparing DC-*Atg5*$^{+/+}$ and DC-*Atg5*$^{-/-}$ mice. Pooled data of 2 independent experiments is shown (n: DC-*Atg5*$^{+/+}$ = 5; DC-*Atg5*$^{-/-}$ = 5) Statistical analysis: unpaired two-tailed student t test, mean ± s.e.m., ns = not significant, *P< 0.05, **P< 0.01 and ***P< 0.001.

Taken together, we identified a subpopulation of CD11c$^+$/MHC class II$^+$ DCs within the non-diseased CNS that is specifically and exclusively targeted by Cre-mediated *Atg5* deletion in DC-*Atg5*$^{-/-}$ mice. Loss of ATG5 in the CD11c$^+$ compartment does not disturb frequency or expression levels of MHC class II and costimulatory molecules in this subset but completely protects conditional knockout animals from developing AT-EAE.

2.1.5 Lack of ATG5 in CD11c$^+$ DCs Limits Expansion of Encephalitogenic CD4$^+$ T Cells Within the CNS

Next, we analyzed frequencies and effector functions of CNS-infiltrating T cells in DC-*Atg5*$^{-/-}$ and DC-*Atg5*$^{+/+}$ mice upon induction of AT-EAE. For this purpose, animals were sacrificed when DC-*Atg5*$^{+/+}$ animals reached their peak of disease. In accordance with the complete absence of a clinical phenotype in these animals, DC-*Atg5*$^{-/-}$ mice depicted significantly smaller proportions of CNS infiltrating CD45$^+$ cells as compared to DC-*Atg5*$^{+/+}$ mice (**Figure 2.1.6 A**). Moreover, a significantly higher frequency of CD4$^+$ T cells was present in the CNS of *Atg5*$^{+/+}$ mice whereas the frequencies of CD8$^+$ T cells was similar (**Figure 2.1.6 B**). The frequencies of total CD45$^+$ and CD4$^+$ but not CD8$^+$ T cells positively correlated with the severity of EAE in DC-*Atg5*$^{+/+}$ animals which is in accordance with the crucial role of CD4$^+$ T cells in the pathogenesis of EAE (Ben-Nun, Wekerle and Cohen, 1981a; Krishnamoorthy and Wekerle, 2009) (**Figure 2.1.6 C**). Also, the frequencies of activated CNS CD44^{hi} T cells were markedly reduced in DC-*Atg5*$^{-/-}$ mice (**Figure 2.1.6 D**) and the few CD4$^+$ T cells present in the CNS of DC-*Atg5*$^{-/-}$ mice showed a mostly naïve phenotype reflected by a higher frequency of CD62L$^+$/CD44^{neg} cells (**Figure 2.1.6 E**).

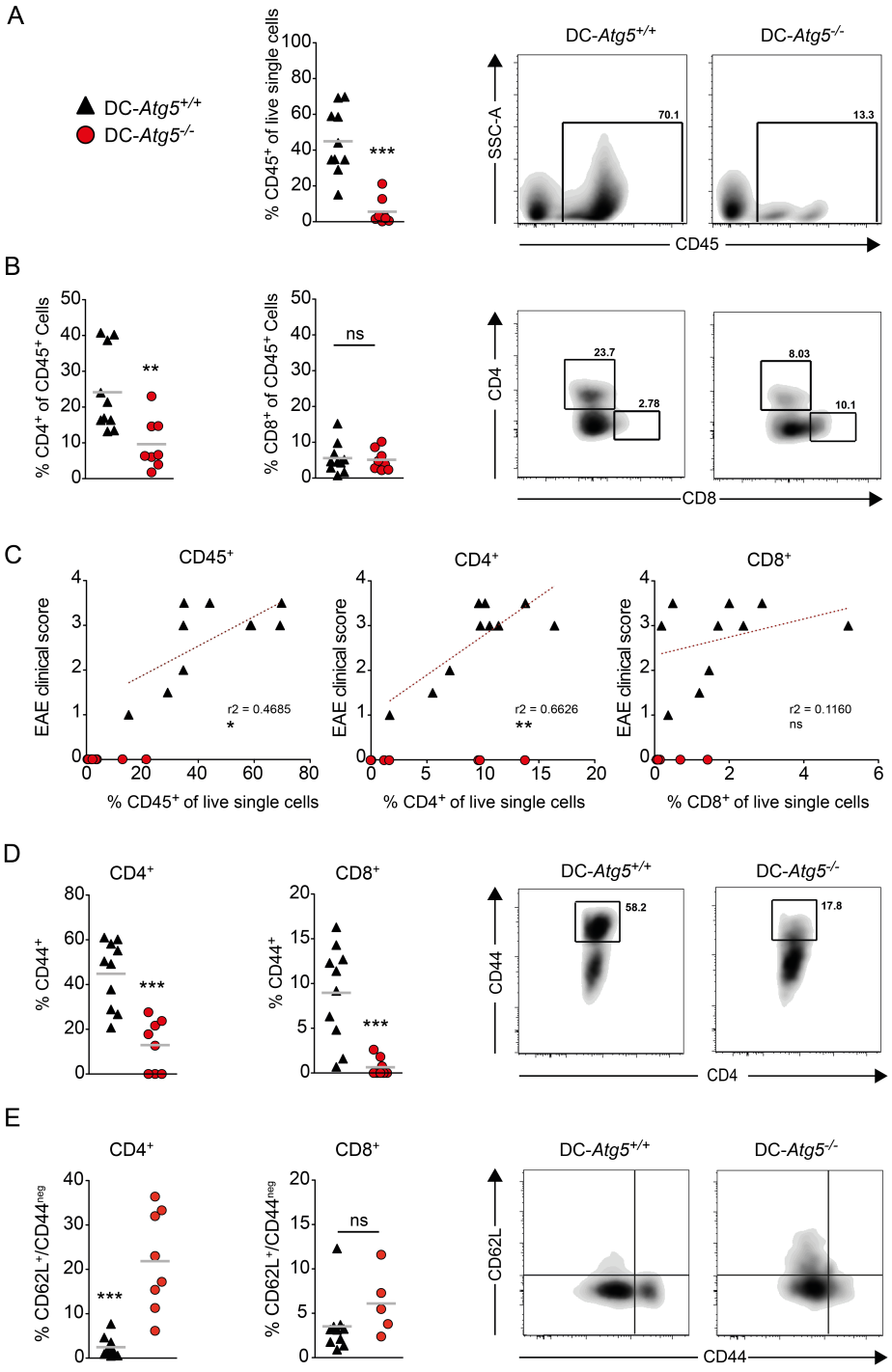

Figure 2.1.6 Characterization of CNS-infiltrating T cells upon induction of adoptive transfer EAE in DC-*Atg5*$^{-/-}$ and DC-*Atg5*$^{+/+}$ mice.
(A) On day of sacrifice after adoptive transfer EAE induction, DC-Atg5$^{-/-}$ mice exhibit significantly fewer CD45^{+} infiltrates in the CNS. **(B)** Furthermore, quantification of immune cell subsets shows significantly lower proportions of CD4^{+} T cells in DC-*Atg5*$^{-/-}$ as compared to DC-*Atg5*$^{+/+}$ mice on peak of disease in the CNS, whereas no difference is observed in the CD8^{+} T cell compartment. **(C)** Correlation analyses of total CD45^{+} cells (left panel), CD4^{+} T cells (middle panel) or CD8^{+} T cells (right panel) within live single cells with EAE disease severity. **(D)** On peak of disease, DC-*Atg5*$^{-/-}$ mice exhibit significantly lower frequencies of activated CD44^{+}/CD4^{+} and CD8^{+} T cells in the CNS. **(E)** The CD4^{+} but not the CD8^{+} T cell compartment in DC-*Atg5*$^{-/-}$-derived CNS contains more CD62L^{+}/CD44^{neg} cells as

compared to DC-*Atg5*$^{+/+}$-derived CNS. Each dot represents one individual animal Pooled data of 2 independent experiments is shown. Statistical analysis: unpaired two-tailed student t test and two-tailed Pearson correlation test. ns = not significant, * P< 0.05, ** P< 0.01, *** P< 0.001.

2.1.6 Analysis of CNS Regulatory T Cells at AT-EAE Peak of Disease

Although the overall frequencies of CD45$^+$ cells, and amongst those, the proportion of conventional CD4$^+$ T cells, were lower in the CNS of DC-*Atg5*$^{-/-}$ animals, the frequencies of CD4$^+$/CD25$^+$/FOXP3$^+$ T regulatory cells (TREGs) were increased in the CNS of DC-*Atg5*$^{-/-}$ animals (**Figure 2.1.7 A**). Both, DC-*Atg5*$^{-/-}$- and DC-*Atg5*$^{+/+}$-derived CNS TREGs expressed similar amounts of CD103, a marker for effector/memory-like phenotype of murine TREGs (Huehn *et al.*, 2004) (**Figure 2.1.7 B**).

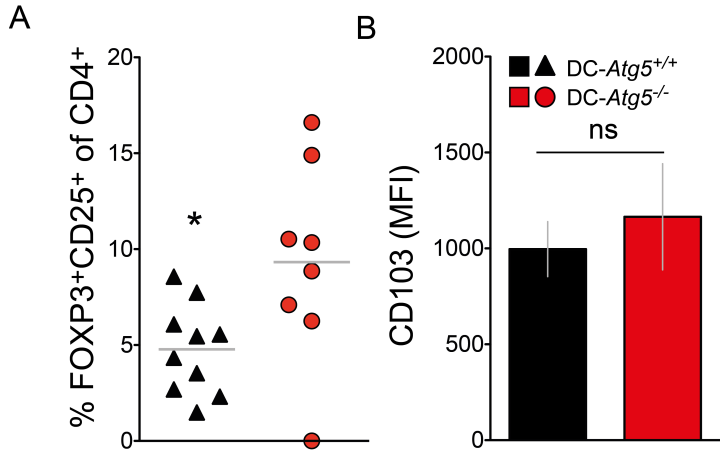

Figure 2.1.7 Analysis of CD4$^+$/CD25$^+$/FOXP3$^+$ TREGs in the CNS of DC-*Atg5*$^{-/-}$ and DC-*Atg5*$^{+/+}$ mice upon induction of AT-EAE.
(A) Quantified frequencies of CD4$^+$/CD25$^+$/FOXP3$^+$ TREGs on day of sacrifice and **(B)** quantification of median fluorescence intensity (MFI) of CD103 on CD4$^+$/CD25$^+$/FOXP3$^+$ TREGs. Each dot represents one individual animal. Pooled data of 2 independent experiments is shown. Statistical analysis: unpaired two-tailed student t test, mean ± s.e.m., ns = not significant, * P< 0.05, ** P< 0.01, *** P< 0.001.

These data indicate that protection from AT-EAE development in DC-*Atg5*$^{-/-}$ mice is associated with reduced activation and accumulation of encephalitogenic CD4$^+$ T cells within the CNS.

2.1.7 CNS-Infiltrating CD4⁺ T Cells in DC-*Atg5*$^{-/-}$ Mice Maintain their Capacity to Produce Effector Cytokines

In a next step, we investigated whether frequencies and/or effector functions of CNS-infiltrating T cells differ between DC-*Atg5*$^{+/+}$ and DC-*Atg5*$^{-/-}$ mice during AT-EAE. We found that the overall frequencies of CNS-infiltrating leukocytes producing the proinflammatory cytokines IFNγ, IL-17A and GM-CSF, upon *ex vivo* restimulation with MOG_{35-55} peptide was significantly diminished in DC-*Atg5*$^{-/-}$ compared to DC-*Atg5*$^{+/+}$ mice at peak of disease (**Figure 2.1.8 A**). Restimulation with MOG_{35-55} lead to a significantly higher production of proinflammatory cytokines than restimulation with an irrelevant peptide derived from ovalbumin ($OVA_{323-339}$) (**Figure 2.1.8 B, C**). Cytokine production was generally preserved in DC-*Atg5*$^{-/-}$ mice as, despite being largely reduced in numbers, the few CNS infiltrating T cells found in these mice showed similar production of IFNγ, IL-17A and GM-CSF upon MOG_{35-55} restimulation (**Figure 2.1.8 B, C**).

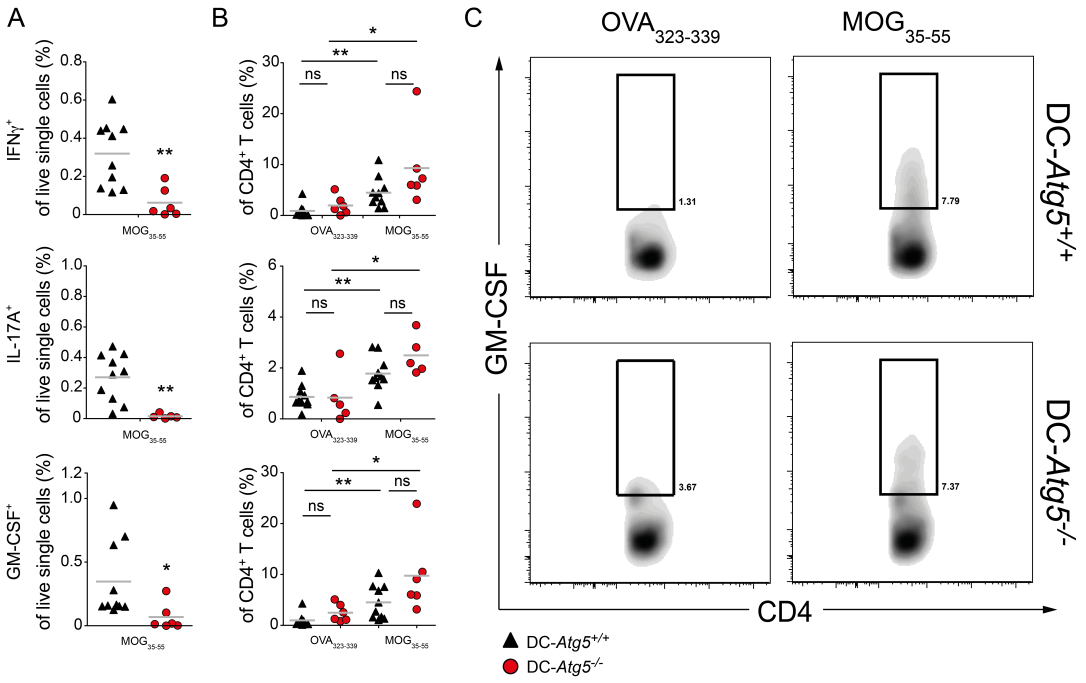

Figure 2.1.8 *Ex vivo* restimulation of CNS-derived infiltrating immune cells and quantification of their effector cytokines.
(A) DC-*Atg5*$^{+/+}$-mice contain significantly more (% of live single cells) cytokine-producing MOG_{35-55}-specific CD4⁺ T cells in the CNS than DC-*Atg5*$^{-/-}$ mice upon AT-EAE induction. **(B)** Both, DC-*Atg5*$^{-/-}$ and DC-*Atg5*$^{+/+}$-derived CD4⁺ T cells are capable of secreting cytokines (IFNγ, IL-17A and GM-CSF) upon restimulation with MOG_{35-55} (but not with $OVA_{323-339}$) to similar degrees. **(C)** Representative contour plot for GM-CSF⁺ CD4⁺ T cells in CNS of DC-*Atg5*$^{-/-}$ or DC-*Atg5*$^{+/+}$ mice on peak of disease. Each dot represents one individual animal. Pooled data of 2 independent

experiments. Statistics: unpaired two-tailed student t test. ns = not significant, * P< 0.05, ** P< 0.01, *** P< 0.001.

Conversely, neither restimulation with MOG_{35-55} nor $OVA_{323-339}$ led to the production of IFNγ, IL-17A or GM-CSF by spleen-derived $CD4^+$ cells, indicating that at the time point of analysis the majority of encephalitogenic effector T cells had already homed to their target organ (**Figure 2.1.9 A, B**).

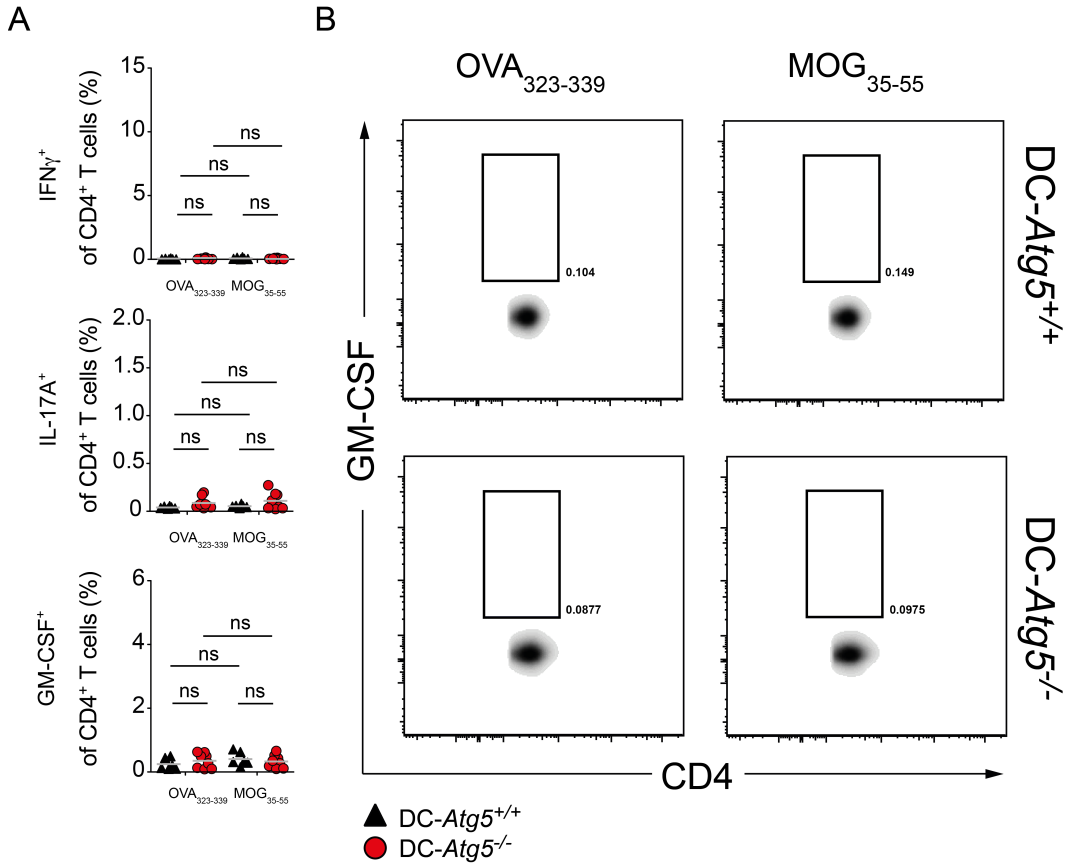

Figure 2.1.9 *Ex vivo* restimulation of spleen-derived $CD4^+$ T cells and quantification of their effector cytokines.
(A) Splenic $CD4^+$ T cells on day of sacrifice upon AT-EAE do not produce significant amounts of proinflammatory cytokines IFNγ, IL-17A and GM-CSF after *ex vivo* restimulation with MOG_{35-55} as compared to restimulation with $OVA_{323-339}$. **(B)** Representative density plot for GM-CSF^+ $CD4^+$ cells spleens of DC-*Atg5*$^{-/-}$ or DC-*Atg5*$^{+/+}$ mice on peak of disease. Each dot represents one individual animal. Pooled data of 2 independent experiments. Statistics: unpaired two-tailed student t test. ns = not significant, * P< 0.05, ** P< 0.01, *** P< 0.001.

These findings suggest that loss of ATG5 in $CD11c^+$ APCs does not modify the encephalitogenic capacity of CNS-infiltrating $CD4^+$ T cells to produce and release effector cytokines per se, but rather restrains their *in situ* reactivation and expansion.

2.1.8 Analysis of CNS Myeloid Cells at AT-EAE Peak of Disease

We additionally profiled the CNS-infiltrating myeloid compartment following induction of AT-EAE. Frequencies of Ly-6G$^+$ neutrophils and Ly-6C$^+$/CD11b$^+$/MHC class II^{neg} monocytes and CD11b$^+$/MHC class II$^+$ inflammatory DCs (iDCs) were significantly lower in the CNS of DC-*Atg5*$^{-/-}$ animals (**Figure 2.1.10 A-C**). Within the iDC compartment the proportion of CD11c$^+$/Ly-6C$^+$ APCs was significantly higher in *Atg5*$^{+/+}$ animals (**Figure 2.1.10 D**).

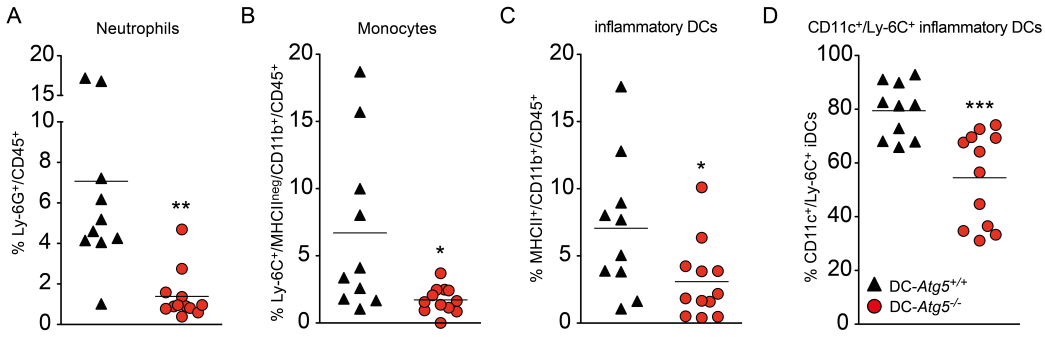

Figure 2.1.10 Characterization of CNS-infiltrating myeloid subsets upon induction of adoptive transfer EAE in DC-*Atg5*$^{-/-}$ and DC-*Atg5*$^{+/+}$ mice.
Quantified CNS frequencies of **(A)** Ly-6G$^+$ neutrophils (depicted as % of live single CD45$^+$ cells), **(B)** Ly-6C$^+$/MHC class II (MHCII)$^+$/CD11b$^+$ monocytes, **(C)** MHCII$^+$/CD11b$^+$ inflammatory DCs (iDCs) and **(D)** CD11c$^+$/Ly-6C$^+$ iDCs on day of sacrifice (**B-D** depicted as % of live single CD11b$^+$/CD45^{hi} cells) . Each dot represents one individual animal. Pooled data of 2 independent experiments is shown. Statistical analysis: unpaired two-tailed student t test. ns = not significant, * P< 0.05, ** P< 0.01, *** P< 0.001.

2.1.9 Analysis of Microglia at AT-EAE Peak of Disease

Furthermore, frequency and MHC class II expression levels of microglia were determined. Similar to steady state analysis, the overall frequency of this CNS resident subset was similar at peak of disease in both genotypes (**Figure 2.1.11 A**). However, following induction of AT-EAE, MHC class II surface expression, which was generally low and similar between DC-*Atg5*$^{-/-}$- and DC-*Atg5*$^{+/+}$-derived microglia at steady state **(Figure 2.1.5 C)**, was markedly upregulated only on microglia of DC-*Atg5*$^{+/+}$ mice (**Figure 2.1.11 B, C**).

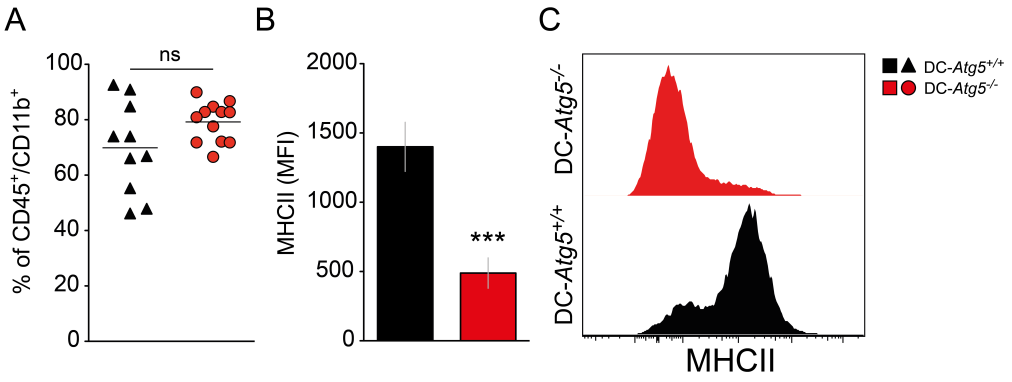

Figure 2.1.11 Characterization of microglial compartment in DC-*Atg5*$^{-/-}$ and DC-*Atg5*$^{+/+}$ mice upon induction of AT-EAE.
(A) Quantified frequencies of CD45$^{lo/int}$/CD11b^{+} microglial cells in DC-*Atg5*$^{-/-}$ and DC-*Atg5*$^{+/+}$ mice on day of sacrifice upon AT-EAE induction. **(B)** Surface expression levels (median fluorescence intesity [MFI]) of MHC class II (MHCII) on microglia. **(C)** Representative histograms of MHCII surface expression on microglia. Each dot represents one individual animal. Pooled data of 2 independent experiments is shown. Statistical analysis: unpaired two-tailed student t test, mean ± s.e.m. ns = not significant, *P< 0.05, **P< 0.01 and ***P< 0.001.

2.1.10 Endogenous Myelin Presentation by CD11c^{+} DCs is Abrogated in Absence of ATG5

It has previously been reported that canonical macroautophagy can deliver intracellular antigens for MHC class II presentation thereby modifying subsequent CD4^{+} T cell responses (Schmid *et al.*, 2007). EAE development is driven by an antigen that is not known to be intrinsically expressed by professional CD11c^{+} APCs and hence requires endocytosis, followed by myelin antigen processing and presentation. ATG proteins contribute to extracellular antigen processing through phagosome maturation, regulated through cytosolic recruitment and binding of LC3 during an autophagy pathway termed LC3-associated phagocytosis (LAP) (Martinez *et al.*, 2015).

We previously showed that both, DC-*Atg5*$^{-/-}$- and DC-*Atg5*$^{+/+}$-derived CD11c^{+} BMDCs phagocytosed similar numbers of either naked polystyrene beads or beads that had been decorated with MOG$_{1\text{-}124}$ full length protein, suggesting that the general capacity of ATG5-deficient DCs to phagocytose extracellular material is not compromised (data Christina Sina).

ATG-dependent phagocytosis of extracellular material via LAP requires pathway-specific triggering through receptor-mediated antigen uptake such as Ptd-L-Ser recognizing receptors, PAMP receptors (Toll-like receptor [TLR]1/2, TLR2/6, TLR4, TLR9 and Dectin), or Fc receptors recognizing DNA

immune complexes (Henault *et al.*, 2012; Ma *et al.*, 2012; Martinez *et al.*, 2011; 2016; Sanjuan *et al.*, 2007). The phospholipid Ptd-L-Ser can be exposed on membrane debris derived from compromised cells or specifically translocated to the cell surface during apoptosis (Nagata *et al.*, 2016). Oligodendrocyte injury and concomitant focal demyelination constitute unique pathological hallmarks of MS lesions and during EAE development (Frohman *et al.*, 2006; Lucchinetti *et al.*, 1999) and can even precede the formation of inflammatory infiltrates (Barnett and Prineas, 2004; Prineas and Parratt, 2012; Traka *et al.*, 2016). We therefore hypothesized that uptake of damaged Ptd-L-Ser-exposing oligodendroglial cells by $CD11c^+$ DCs may trigger myelin-specific T cell activation in an ATG5-dependent manner. In order to test this hypothesis, we established a sequential coculture system using UVB-irradiated Ptd-L-Ser^{hi} compared to non-irradiated Ptd-L-Ser^{lo} MOG-expressing oligodendroglial cells (ODCs) (**Figure 2.1.12 A-C**), which were coincubated with $CD11c^+$ splenic DCs. Subsequently these ODC-pulsed $CD11c^+$ APCs were cocultured with 2D2/TCR^{MOG}-derived $CD4^+$ T cells.

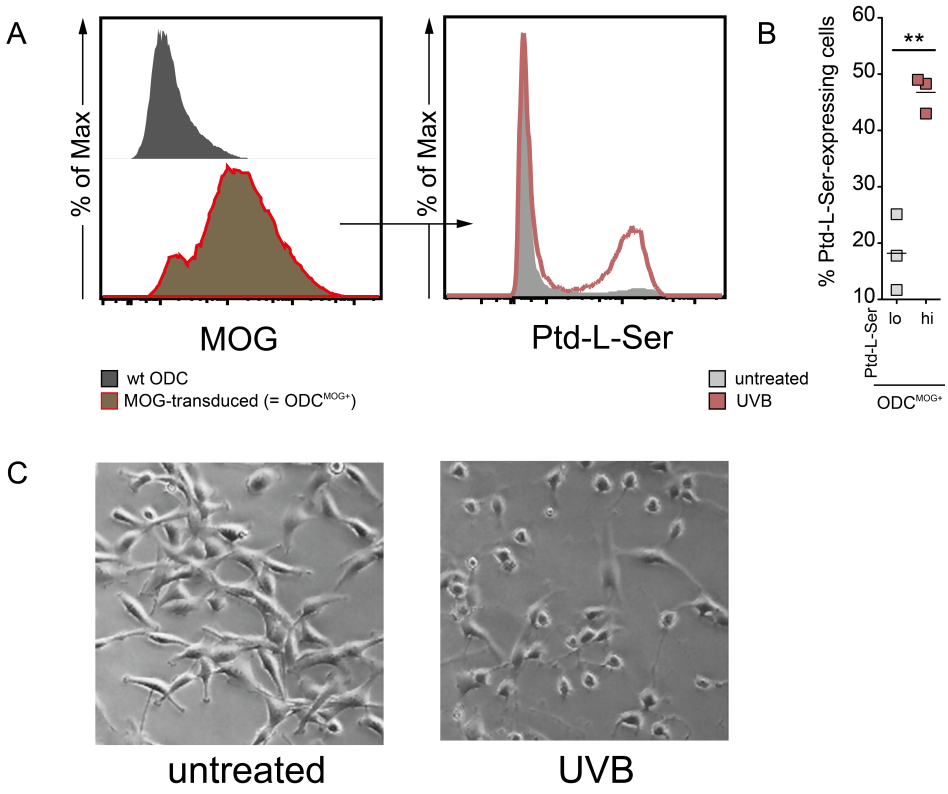

Figure 2.1.12 UVB-irradiation and subsequent Ptd-L-Ser-exposure of MOG-expressing oligodendroglial MO3.13 cells.
(A) Representative histogram comparing MOG-transduced oligodendroglial cell line MO3.13 (ODC^{MOG+}) with wild type MO3.13 cells (wt ODC) for surface MOG-expression. ODC^{MOG+} were either UVB irradiated (870 mJ/cm²) or left untreated, which resulted in Ptd-L-Ser^{hi}- and Ptd-L-Ser^{lo}-expressing ODC^{MOG+} **(A)**, quantified via annexin V staining **(B)**. **(C)** Representative light microscopy pictures of UVB irradiated or untreated ODC^{MOG+} cells. Pooled data of 3 independent experiments are shown. Statistics: unpaired two-tailed student t test. ns = not significant, * P< 0.05, ** P< 0.01, *** P< 0.001.

The sequential coculture system was first set up in C57BL/6 wild type mice. Endogenous myelin peptide presentation and subsequent cognate T cell activation was assessed by IFNγ production via cocultured MOG_{35-55}-specific $CD4^+$ T cells. Only coculture of $CD11c^+$ DCs with Ptd-L-Ser^{hi} ODCs lead to noticable activation of and concomitant IFNγ secretion by MOG-specific $CD4^+$ T cells (**Figure 2.1.13 A**). In a next step, DC-*Atg5*$^{-/-}$- and DC-*Atg5*$^{+/+}$-derived $CD11c^+$ splenic DCs were used as APCs (**Figure 2.1.13 B**). Here, T cell IFNγ production upon presentation of endogenous myelin antigen derived from Ptd-L-Ser^{hi} oligodendroglial cells was abrogated in ATG5-deficient DCs (**Figure 2.1.13 B**).

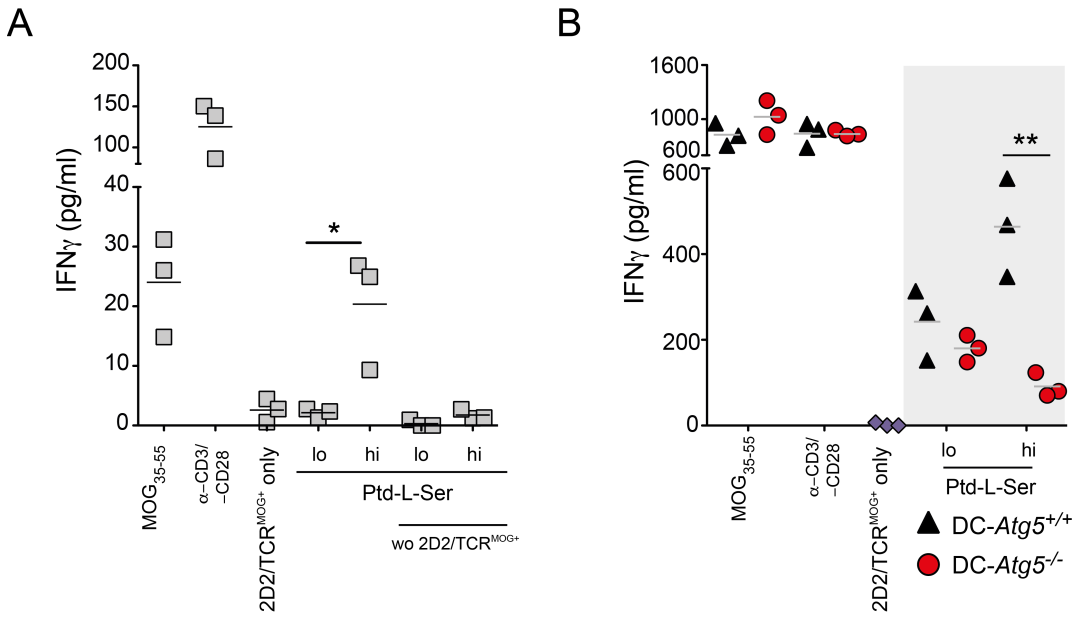

Figure 2.1.13 Coculture analyses for the assessment of ATG5-dependent processing of antigenic material and subsequent presentation to CD4⁺ T cells.
(A) Coculture of MOG-specific 2D2/TCR^{MOG}-derived CD4⁺ T cells with C57BL/6 wild type-derived splenic CD11c⁺ dendritic cells (DCs) that had previously been pulsed with either Ptd-L-Ser^{hi}- or Ptd-L-Ser^{lo}-exposing ODC^{MOG+}. CD4⁺ T cell response (IFNγ secretion) is augmented upon coculture with Ptd-L-Ser^{hi}- ODC^{MOG+}-pulsed DCs. (B) Absence of ATG5 in DCs abrogates CD4⁺ T cell response upon coculture with Ptd-L-Ser^{hi}-exposing ODC^{MOG+}-pulsed DCs. One representative of >3 independent experiments are shown. Statistics: unpaired two-tailed student t test. ns = not significant, * P< 0.05, ** P< 0.01, *** P< 0.001.

Taken together, these data indicate that LAP is an endocytic autophagy pathway that facilitates transport of antigenic material for MHC class II presentation to CD4⁺ T cells. Recognition and engulfment of injured oligodendroglial cells by CD11c⁺ DCs induces myelin peptide presentation on MHC class II molecules and subsequent activation of primed myelin-specific CD4⁺ T cells through this ATG5-regulated phagocytosis pathway.

2.2 The Role of DC-Inherent ATG5 During Presentation of Exogenous Lipid Antigens to Natural Killer T Cells

2.2.1 Colocalization Analysis Between CD1d and LC3 in RAW 264.7 Cells and Splenic CD11c$^+$ DCs

Previous studies have shown that the MHC class I-like antigen presenting molecule CD1d associates with MHC class II molecules in DCs and in B cells (Kang and Cresswell, 2002a). CD1d binds to MHC class II-Ii complexes in the ER, and the CD1d–MHC class II association is maintained in late endosomal/lysosomal MIICs (Kang and Cresswell, 2002a). Macroautophagy delivers antigens to late endosomes/lysosomes for loading on MHC class II molecules and CD4$^+$ T cell recognition (Nedjic *et al.*, 2008; Paludan *et al.*, 2005; Schmid *et al.*, 2007). To determine whether autophagosomes colocalize with CD1d$^+$ loading compartments, we initially performed laser confocal microscopy-based analyzes in RAW 264.7 cells (mouse leukaemic monocyte/macrophage cell line) investigating colocalization of CD1d protein with LC3 which is present on both autophagosomes and LC3-associated phagosomes (Martinez *et al.*, 2015; Romao *et al.*, 2013). We found that both molecules colocalized in RAW 264.7 cells upon inhibition of lysosomal acidification via chloroquine and TLR receptor ligation by TLR agonists LPS, imiquimod, poly(I:C) and Pam_3CSK_4 as determined by Pearson correlation coefficient analysis (**Figure 2.2.1 A-D**). Of all the TLR ligands applied, only Pam_3CSK_4 did not show a significant increase in colocalization compared to the untreated control. However, upon inhibition of lysosomal acidification, also the TLR1/2 ligand Pam_3CSK_4 significantly increased colocalization of CD1d and LC3 (**Figure 2.2.1 D**).

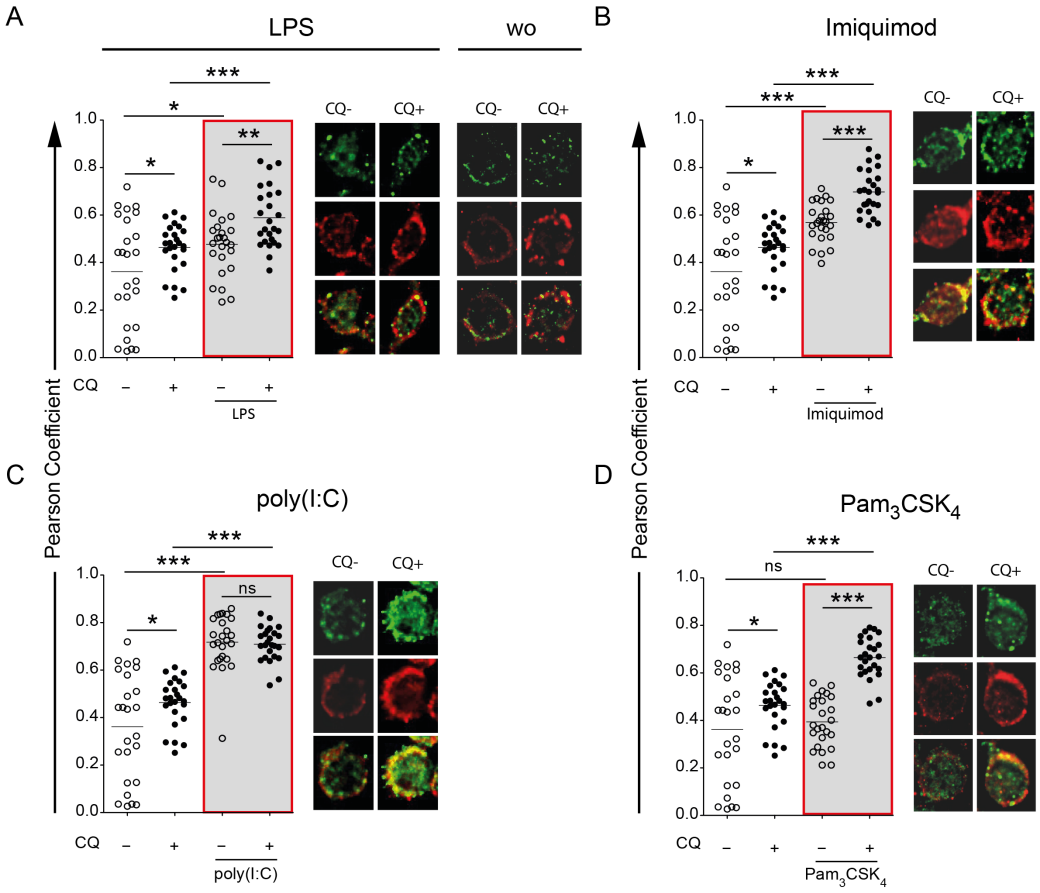

Figure 2.2.1 Colocalization analysis of LC3 and CD1d in RAW 264.7 cells.
RAW 264.7 cells were incubated with either **(A)** LPS (500 ng/ml), **(B)** Imiquimod (10 µg/ml), **(C)** poly(I:C) (25 µg/ml), **(D)** Pam_3CSK_4 (1 µg/ml) for 4 h, or left untreated. Chloroquine (CQ, 50 µM) was added during the last hour of incubation. Scatter dot plot representation and quantification of colocalization between CD1d and LC3 (Pearson coefficient analysis) is depicted in the respective left panels. Each symbol represents one cell. Pooled data of 2 independent experiments are shown. Representative pictures are depicted in the right panel. Statistics: two-tailed Mann-Whitney U Test, *** $P \leq 0.001$,** $P \leq 0.01$,* ≤ 0.05, ns $P > 0.05$.

We proceeded with analyzing colocalization of LC3 and CD1d in sorted $CD11c^+$ splenic DCs derived from C57BL/6 wild type mice. Since high susceptibility to induction of cell death precluded treatment of with chloroquine, cells were only treated with TLR agonists. As observed in RAW 264.7 cells, LC3 and CD1d colocalized in steady state reflected by a Pearson coefficient >0.5. Treatment with TLR agonist CpG ODN and poly(I:C) further increased colocalization (**Figure 2.2.2 A, B**).

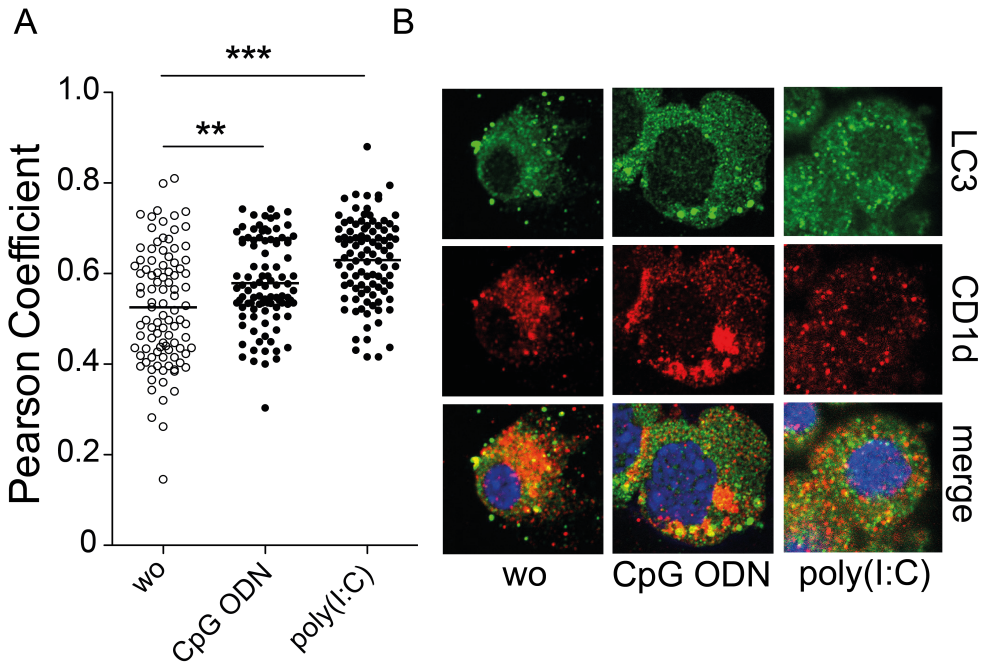

Figure 2.2.2 Colocalization analysis of LC3 and CD1d in splenic CD11c⁺ DCs.
C57BL/6 wild type-derived splenic DCs were either incubated with CpG (2 µg/ml), poly(I:C) (25 µg/ml) for 4 h, or left untreated. **(A)** Scatter dot plot representation and quantification of colocalization between CD1d and LC3 (Pearson coefficient analysis). Each symbol represents one cell. Pooled data of 3 independent experiments are shown. **(B)** representative pictures are depicted. Original magnification with 63×, 1.4 NA oil immersion lens. Statistics: two-tailed Mann-Whitney U Test, *** $P \leq 0.001$,** $P \leq 0.01$,* ≤ 0.05, ns $P > 0.05$.

2.2.2 Absence of ATG5 Increases the NKT Cell Stimulatory Capacity of APCs *In Vitro*

In order to investigate whether absence of the essential macroautophagy gene *Atg5* in CD11c⁺ DCs inhibits CD1d antigen presentation similar to MHC class II presentation (H. K. Lee *et al.*, 2010; Ma *et al.*, 2012; Romao *et al.*, 2013), we again made use of mice harboring a conditional knockout of *Atg5* in CD11c⁺ DCs (**Figure 2.1.1 A-E**). In order to assess if autophagy is implicated in DC mediated glycolipid antigen presentation via CD1d to iNKT cells, FAC-sorted splenic CD11c⁺ DCs, isolated from DC-*Atg5*$^{-/-}$ and DC-*Atg5*$^{+/+}$ mice, were pulsed with increasing amounts (0-10 µg/ml) of the prototypic iNKT agonist αGalCer and the response of iNKT cell hybridomas A.407 and FF13 was assessed. Contrary to what was expected, DC-*Atg5*$^{-/-}$-derived DCs were significantly more potent in eliciting IL-2 production from both iNKT cell lines (**Figure 2.2.3 A, B**). Induction of the autophagy machinery in wild type DCs by noncytotoxic concentrations of the mTOR inhibitor rapamycin reduced IL-2 production by iNKT cells (**Figure 2.2.3 C, D**). To further confirm these findings, we made use of an immortalized macrophage-like cell line generated

from DC-*Atg5*$^{+/+}$-derived bone marrow cells. Induction of recombination by treatment with TAT-cre lead to substantial decrease in ATG5-ATG12-complex as well as LC3-II protein levels (**Figure 2.2.3 E**). In line with our previous results, immortalized macrophage-like cells with reduced ATG5 levels (MΘ-*Atg5*$^{-/-}$) were compared to the ATG5 competent control cell line (MΘ-*Atg5*$^{+/+}$), superior in activating the iNKT cell hybridomas A.407 and FF13 (**Figure 2.2.3 F, G**).

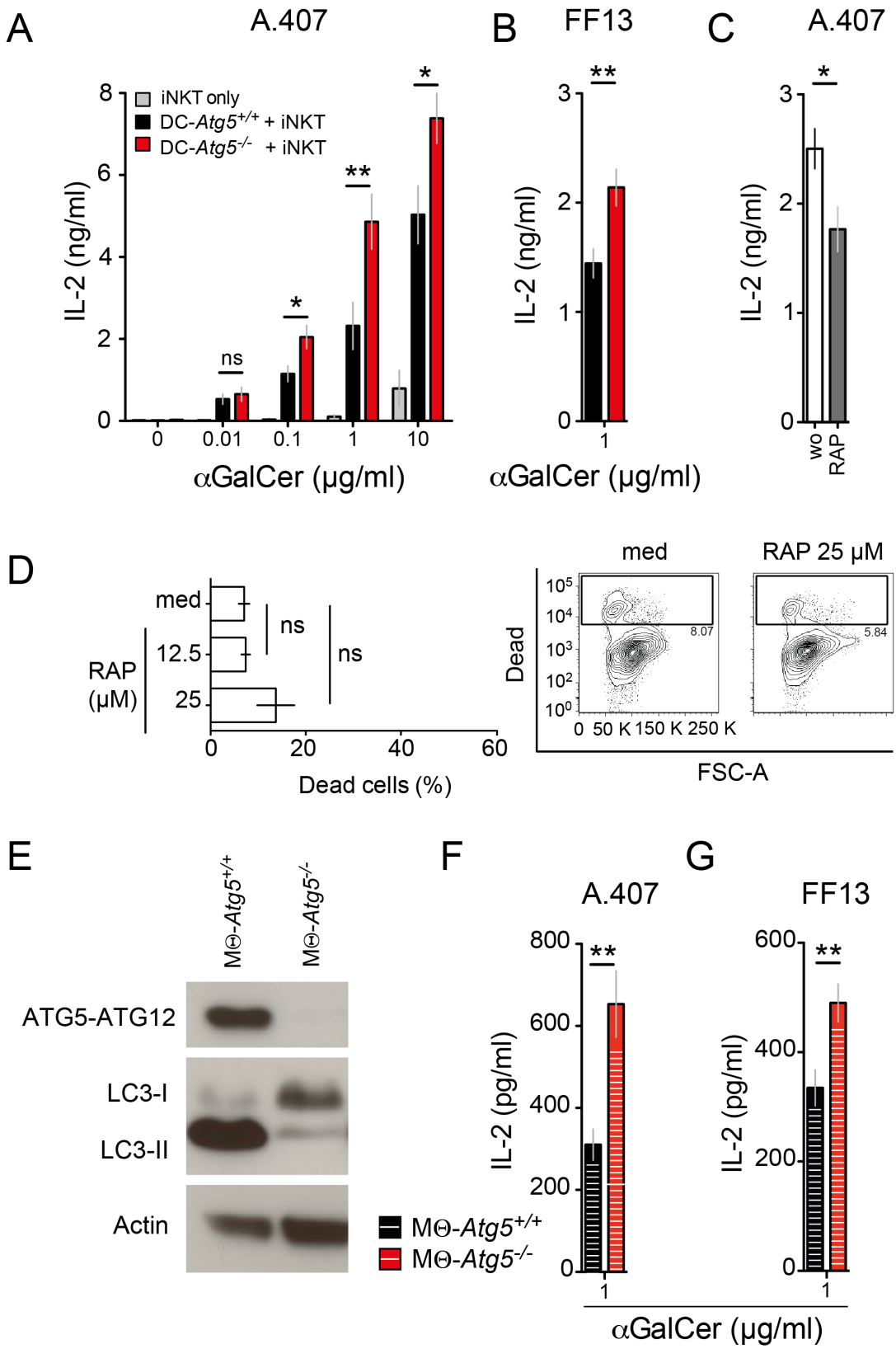

Figure 2.2.3 Coculture of glycolipid-pulsed ATG5-deficient APCs with iNKT cell hybridoma cell lines.
(A) FAC-sorted CD11c$^+$/MHC class II$^+$ splenic DCs derived from DC-*Atg5*$^{-/-}$ and DC-*Atg5*$^{+/+}$ animals were pulsed with increasing concentrations of αGalCer or left untreated and subsequently cocultured with the iNKT hybridoma cell line A.407 or **(B)** FF13 for 24 h (αGalCer: 1 µg/ml). IL-2 concentration in cell culture supernatants

was measured via ELISA. Mean ± s.e.m. of pooled data from >3 independent experiments are shown. Each experiment contained at least 3 animals per group. **(C)** C57BL/6 wild type-derived purified splenic DCs were treated with rapamycin (RAP; 12.5 µM; 4 h), subsequently pulsed with αGalCer (1 µg/ml; 4 h) and cocultured with iNKT hybridoma cell line A.407 (24 h). IL-2 concentration in cell culture supernatants was measured via ELISA. Mean ± s.e.m. of pooled data from 3 independent experiments are shown. Each experiment contained at least 3 animals per group. **(D)** Quantification of cell death upon rapamycin treatment. C57BL/6 wild type-derived purified splenic DCs were treated with or without RAP (12.5, 25 µM; 4 h) and subsequently analyzed for cell death via flow cytometry. Pooled data of 2 independent experiments are shown. **(E)** Western blot analysis for protein expression of ATG5-ATG12-complex, LC3-I and LC3-II in MΘ-*Atg5*$^{-/-}$ and MΘ-*Atg5*$^{+/+}$ cells. Actin served as a loading control. One representative of >3 experiments is shown. **(F)** MΘ-*Atg5*$^{-/-}$ and MΘ-*Atg5*$^{+/+}$ cells were pulsed with αGalCer or left untreated and subsequently cocultured with the iNKT hybridoma cell line A.407 or **(G)** FF13 for 24 h (αGalCer: 1 µg/ml). IL-2 concentration in cell culture supernatants was measured via ELISA. Mean ± s.e.m. of pooled data from 3 independent experiments are shown. Statistics: unpaired two-tailed student t test**.** *** $P \leq 0.001$,** $P \leq 0.01$,* ≤ 0.05, ns $P > 0.05$.

The observed iNKT hybridoma cell line response was dependent on the presence of glycolipid-pulsed APCs as titrating down APC numbers incrementally abolished iNKT hybridoma cell responses (**Figure 2.2.4**).

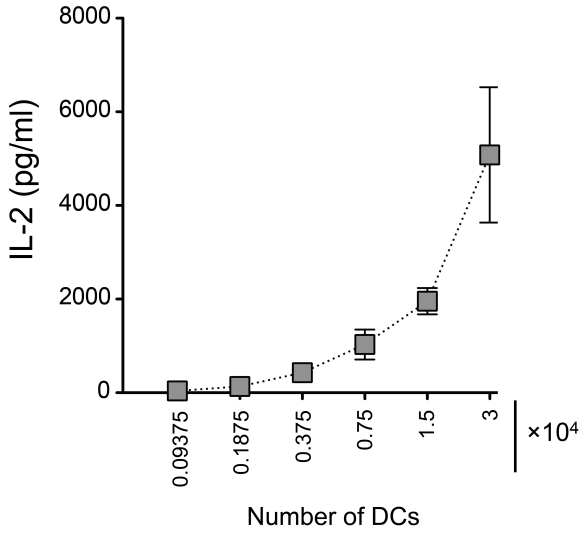

Figure 2.2.4 Titration of glycolipid-pulsed CD11c^{+} splenic DCs in coculture with iNKT cell hybridoma.
Coculture assay as described in **Figure 16 A** using decreasing amounts of sorted splenic DCs derived from C57BL/6 wild type mice. IL-2 concentration in cell culture supernatants was measured via ELISA. Mean ± s.e.m. of one representative of 2 independent experiments are shown.

2.2.3 Increased Capacity of ATG5-Deficient APCs to Stimulate NKT Cells is Independent of Lipid Uptake Receptor Pathway

To analyze if enhanced iNKT cell activation in absence of DC-inherent ATG5 is dependent on distinct lipid uptake pathways we carried out coculture experiments using GalαGalCer (low density lipoprotein receptor [LDLR]-dependent uptake) and GSL-1 (scavenger receptor A[SRA]-dependent uptake) in adition to αGalCer (LDLR/SRA-dependent uptake). We found that, regardless of which receptor uptake pathway was targeted, DC-specific deficiency in ATG5 yielded amplified iNKT hybridoma cell responses (**Figure 2.2.5 A-C**)

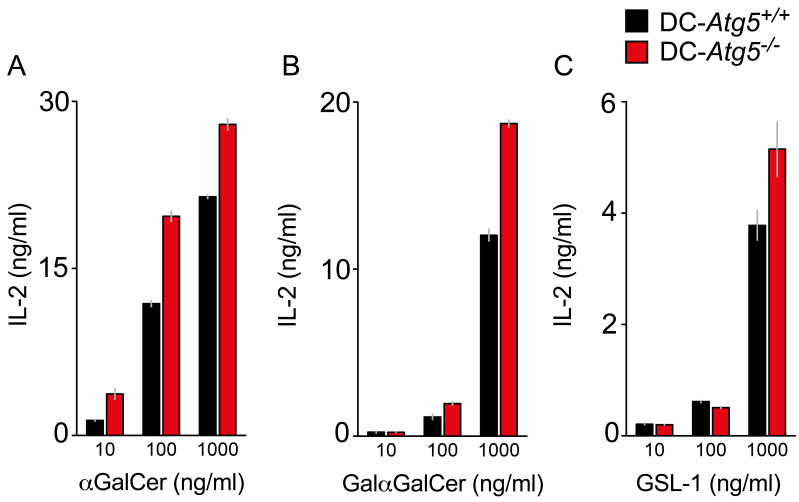

Figure 2.2.5 Receptor-mediated uptake of glycolipid antigens is unchanged in DC-*Atg5*$^{-/-}$-derived splenic DCs.
Receptor-mediated uptake of glycolipid antigens and costimulatory properties remain unchanged in DC-*Atg5*$^{-/-}$-derived DCs. CD1d-presentation of indicated iNKT cell agonists (**(A)** αGalCer **(B)** GalαGalCer **(C)** GSL-1) by primary splenic DCs was assessed using activation of the iNKT hybridoma A.407 as in **Figure 16 A**. Mean ± s.e.m. of triplicate cultures are shown.

2.2.4 Analysis of CD1d-Restricted Presentation of αGalCer in Absence of ATG5 in GM-CSF BMDCs

We additionally generated BMDCs from *Atg5*-deficient mice and observed that coculture with glycolipid-pulsed *Atg5*-deficient BMDCs leads to IL-2 production by iNKT cells to the same level as BMDCs generated from DC-*Atg5*$^{+/+}$ mice (**Figure 2.2.6**).

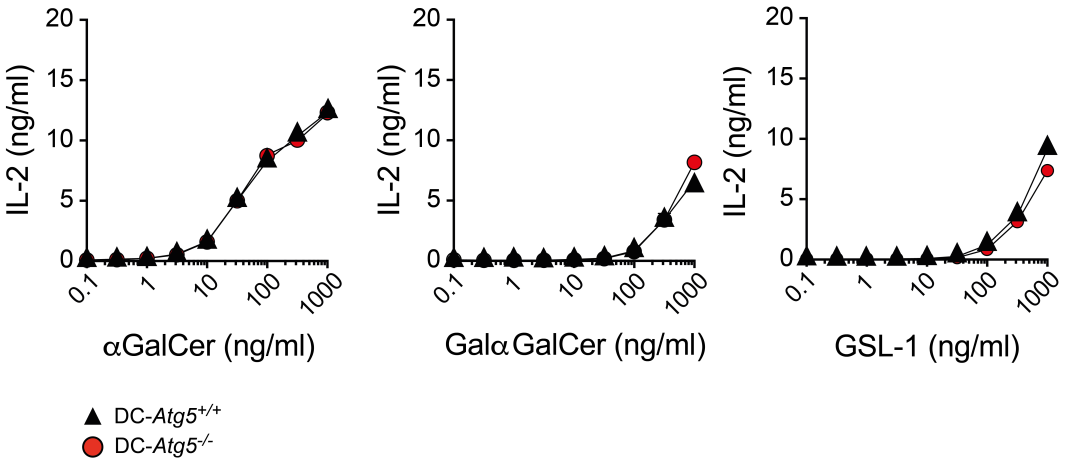

Figure 2.2.6 Coculture of glycolipid-pulsed ATG5-deficient mixed BMDCs with iNKT cell hybridoma cells.
CD1d presentation of the indicated iNKT cell agonists by *in vitro*-GM-CSF-derived BMDCs was assessed using activation of the iNKT hybridoma A.407 as in **Figure 2.2.3 A**. Data are representative of triplicate cultures from 1 of 2 independent experiments.

Since *in vitro*-derived BMDC cultures contain heterogeneous populations including cells most closely resembling macrophages, DCs and neutrophils (Helft *et al.*, 2015; Inaba *et al.*, 1992), we additionally FACS-purified *in vitro* generated BMDCs for CD11c$^+$/MHC class II$^+$ cells, which were subsequently loaded with increasing concentrations of αGalCer and coincubated with iNKT cells. Increased IL-2 production by iNKT cells was observed only in DC-*Atg5*$^{-/-}$-derived CD11c$^+$/MHC class II$^+$ BMDC cultures loaded with high αGalCer concentrations (10 µg/ml) (**Figure 2.2.7**).

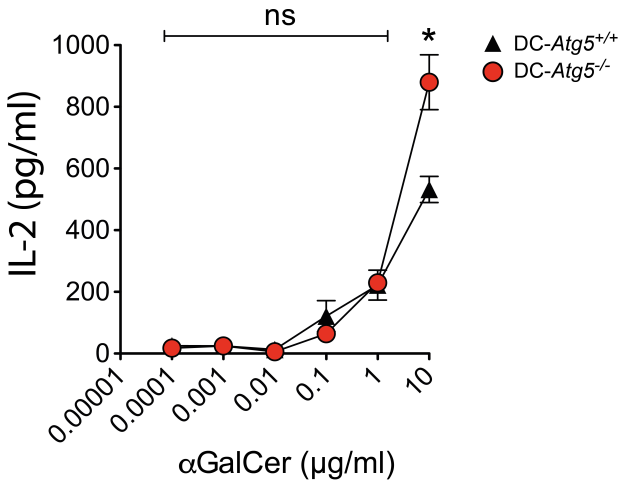

Figure 2.2.7 Coculture of glycolipid-pulsed ATG5-deficient FAC-sorted CD11$^+$/MHC class II$^+$ BMDCs with iNKT cell hybridoma cells
CD1d presentation of αGalCer by enriched *in vitro* GM-CSF-derived BMDCs to the iNKT hybridoma A.407. Both, DC-*Atg5*$^{+/+}$- and DC-*Atg5*$^{-/-}$-derived BMDCs were

FACS-purified for CD11c$^+$/MHC class II$^+$ cells. DC-*Atg5*$^{-/-}$-derived BMDCs were further enriched for GFP-Cre$^+$ cells. Mean ± s.e.m. of pooled data from 2 independent experiments are shown. Statistics: Unpaired two-tailed student t test. *** $P \leq 0.001$,** $P \leq 0.01$,* ≤ 0.05, ns $P > 0.05$.

2.2.5 Analysis of Costimulatory Properties for NKT:DC Crosstalk in DC-*Atg5*$^{-/-}$- and DC-*Atg5*$^{+/+}$-Derived DCs

Next, we determined whether *Atg5*-deficient DCs differed from their *Atg5*-competent counterparts in providing costimulatory signals required for iNKT cell activation, *i.e.* CD40 expression and production of IL-12. αGalCer-mediated activation of and subsequent cytokine secretion by iNKT cells requires DC-derived IL-12 and formation of an immunological synapse through CD40/CD40L (Kitamura *et al.*, 1999). DC-*Atg5*$^{-/-}$-derived DCs exhibited similar CD40 levels as DC-*Atg5*$^{+/+}$-DCs (**Figure 2.2.8 A, Figure 2.1.1 E**). Moreover, *Atg5*-deficiency did not affect the frequency of IL-12-producing DCs or the total amount of IL-12 secreted by DCs in response to CD40 ligation (**Figure 2.2.8 B, C**).

Taken together, these data indicate that autophagy proteins in APCs may regulate iNKT cell responses independent of glycolipid uptake pathways and most costimulatory properties.

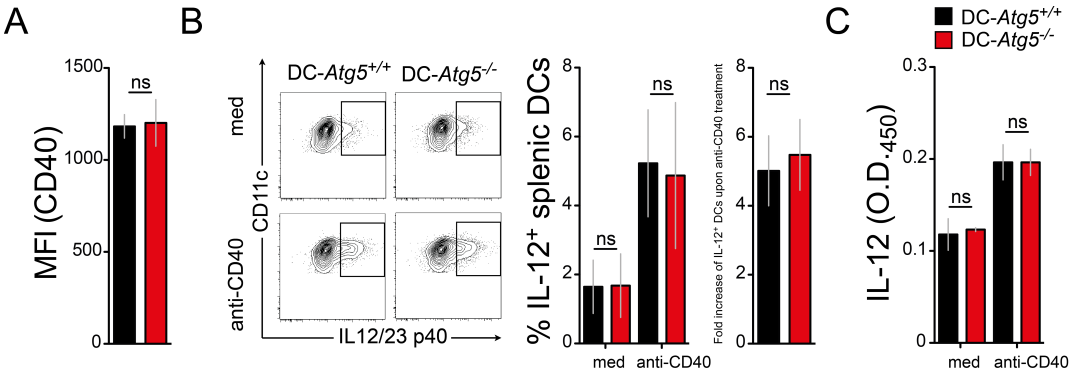

Figure 2.2.8 Analysis of costimulatory properties of DC-*Atg5*$^{-/-}$- and DC-*Atg5*$^{+/+}$-derived DCs.
(A) Splenic DCs derived from either DC-*Atg5*$^{-/-}$ or DC-*Atg5*$^{+/+}$ animals were stained for CD40 surface expression. **(B)** Frequency of IL-12-producing splenic DCs upon CD40 ligation. Purified splenic DCs were either incubated with anti-CD40 overnight or left untreated. IL-12 production was measured via intracellular cytokine staining and by **(C)** ELISA. Mean ± s.e.m. of pooled data from 3 independent experiments are shown. Each experiment contained at least 3 animals per group. Statistics: Unpaired two-tailed student t test. *** $P \leq 0.001$,** $P \leq 0.01$,* ≤ 0.05, ns $P > 0.05$. MFI, mean fluorescence intensity.

2.2.6 Analysis of CD1d-surface Expression on DC-*Atg5*$^{-/-}$- and DC-*Atg5*$^{+/+}$-Derived APCs and on a Macrophage-Like Cell Line

In order to assess by which means other than costimulatory properties ATG5-deficient splenic DCs elicited superior iNKT cell responses *in vitro*, we analyzed CD1d surface expression in purified splenic CD11c^{+}/MHC class II^{+} DCs and CD19^{+}/MHC class II^{+} B cells from DC-*Atg5*$^{-/-}$ and DC-*Atg5*$^{+/+}$ mice. Surface expression of CD1d was significantly elevated in Atg5-deficient splenic DCs (**Figure 2.2.9 A, B**). Splenic B cells derived from DC-*Atg5*$^{-/-}$ mice have normal levels of ATG5, indicated by the absence of GFP-Cre expression in this cellular subset (**Figure 2.1.1 A**) and did not differ in their CD1d surface expression from DC-*Atg5*$^{+/+}$-derived splenic B cells (**Figure 2.2.9 B**). Furthermore, also immortalized ATG5-deficient macrophage-like cells depicted increased surface levels of CD1d as compared to ATG5-competent control cells (**Figure 2.2.9 B**). To determine whether loss of *Atg5* regulates CD1d expression *in vivo*, DC-*Atg5*$^{-/-}$ and DC-*Atg5*$^{+/+}$ mice were injected with αGalCer and CD1d presentation was quantified using the monoclonal antibody L363 that specifically detects CD1d:αGalCer-complexes, but does not bind to CD1d molecules loaded with other antigens (K. O. A. Yu *et al.*, 2007). Compared to autophagy-competent DCs, *Atg5*-deficient DCs showed increased expression levels of CD1d-glycolipid complexes (**Figure 2.2.9 C**). Levels of stimulatory CD1d-antigen complexes were similar for B cells in DC-*Atg5*$^{-/-}$ mice (**Figure 2.2.9 C**). In contrast to CD1d, the expression levels of CD11c and MHC class II remained unchanged in DC-*Atg5*$^{-/-}$-derived DCs (**Figure 2.2.9 D**).

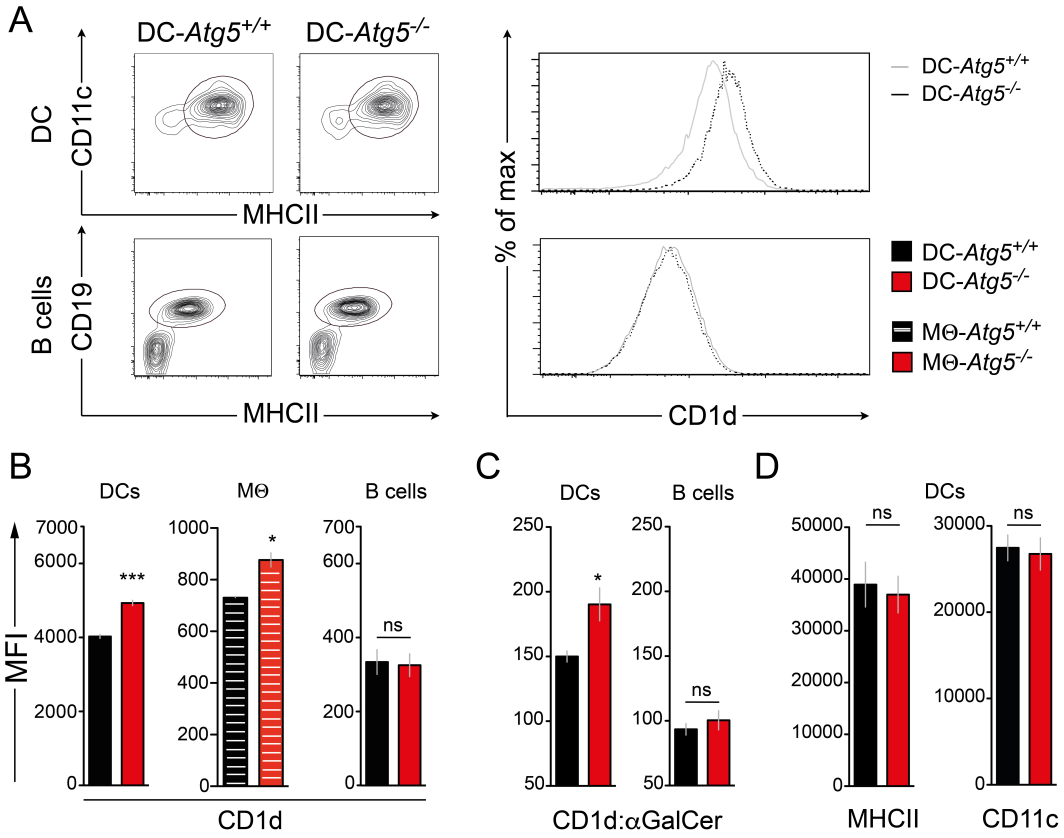

Figure 2.2.9 Analysis of CD1d-surface expression on DC-*Atg5*$^{-/-}$- and DC-*Atg5*$^{+/+}$-derived APCs and on a macrophage-like cell line.
(A) Flow cytometric analysis of CD1d surface levels on splenic DCs. Representative contour plots of splenic DCs or B cells and histograms showing CD1d surface expression. **(B)** Quantification of CD1d surface expression on splenic DCs, immortalized macrophage-like cell line and B cells. Mean ± s.e.m. of pooled data from >3 independent experiments are shown. Each experiment contained at least 2 animals per group. **(C)** CD1d:αGalCer-complex staining (L363 clone) in splenic DCs or B cells 4 h after i.p. application of either αGalCer or PBS. Mean ± s.e.m. of pooled data from 2 independent experiments are shown. **(D)** DC surface expression of CD11c or MHC class II (MHCII). Mean ± s.e.m. of pooled data from >3 independent experiments are shown. Each experiment contained at least 2 animals per group. Statistics: Unpaired two-tailed t test. *** $P \leq 0.001$,** $P \leq 0.01$,* $P \leq 0.05$, ns $P > 0.05$. MFI, mean fluorescence intensity.

2.2.7 Analysis of CD1d Turnover

CD1d expression levels at the cell surface are largely determined by the rates of CD1d internalization and recycling through endosomal and lysosomal compartments (Jayawardena-Wolf *et al.*, 2001; Sugita *et al.*, 2004). Therefore, we analyzed the rates of CD1d internalization and CD1d recycling to the cell surface in *Atg5*-deficient and *Atg5*-competent splenic CD11c^{+} DCs. To evaluate the kinetics of CD1d internalization, the remainder of CD1d molecules previously labeled with biotinylated anti-CD1d was detected after given time points. To assess CD1d recycling rates, we quantified newly resurfaced CD1d molecules after the cell surface CD1d had been previously

blocked with unconjugated anti-CD1d antibodies (**Figure 2.2.10**).

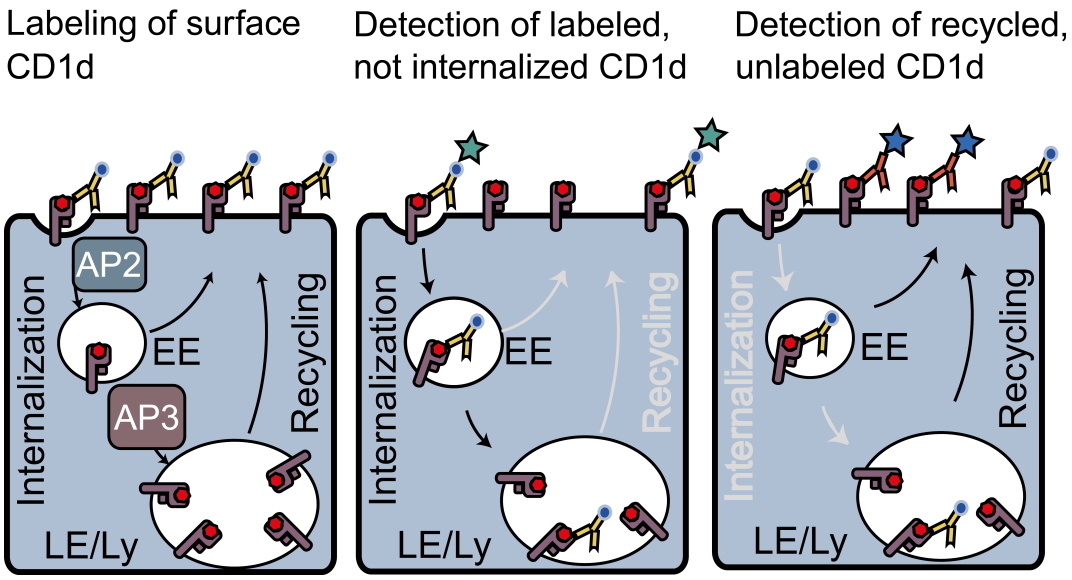

Figure 2.2.10 Scheme illustrating the flow cytometry-based assays used to quantify internalization and recycling of CD1d in *Atg5*-deficient and *Atg5*-competent cells.
CD1d surface levels are determined by the rates of CD1d internalization and recycling through endosomal and lysosomal compartments. EE, early endosomes; LE, late endosomes; Ly, lysosomes.

We found that CD1d internalization from the cell surface is significantly hampered in absence of ATG5 in CD11$^+$/MHC class II$^+$ splenic DCs (**Figure 2.2.11 A, left panel**), whereas internalization of CD1d in ATG5-competent CD19$^+$/MHC class II$^+$ splenic B cells derived from either DC-*Atg5*$^{-/-}$ or DC-*Atg5*$^{+/+}$ mice remained unaffected (**Figure 2.2.11 A, right panel**). Additionally, recycling kinetics of CD1d in absence of ATG5 were similar between ATG5-deficient and -competent splenic DCs (**Figure 2.2.11 B, left panel**) as well in ATG5-competent splenic B cells derived from both genotypes (**Figure 2.2.11 B, right panel**).

From these observations we conclude that absence of *Atg5* in splenic DCs impedes CD1d internalization, resulting in increased CD1d surface expression levels and therefore enhanced capacity of *Atg5*-deficient DCs to activate iNKT cells.

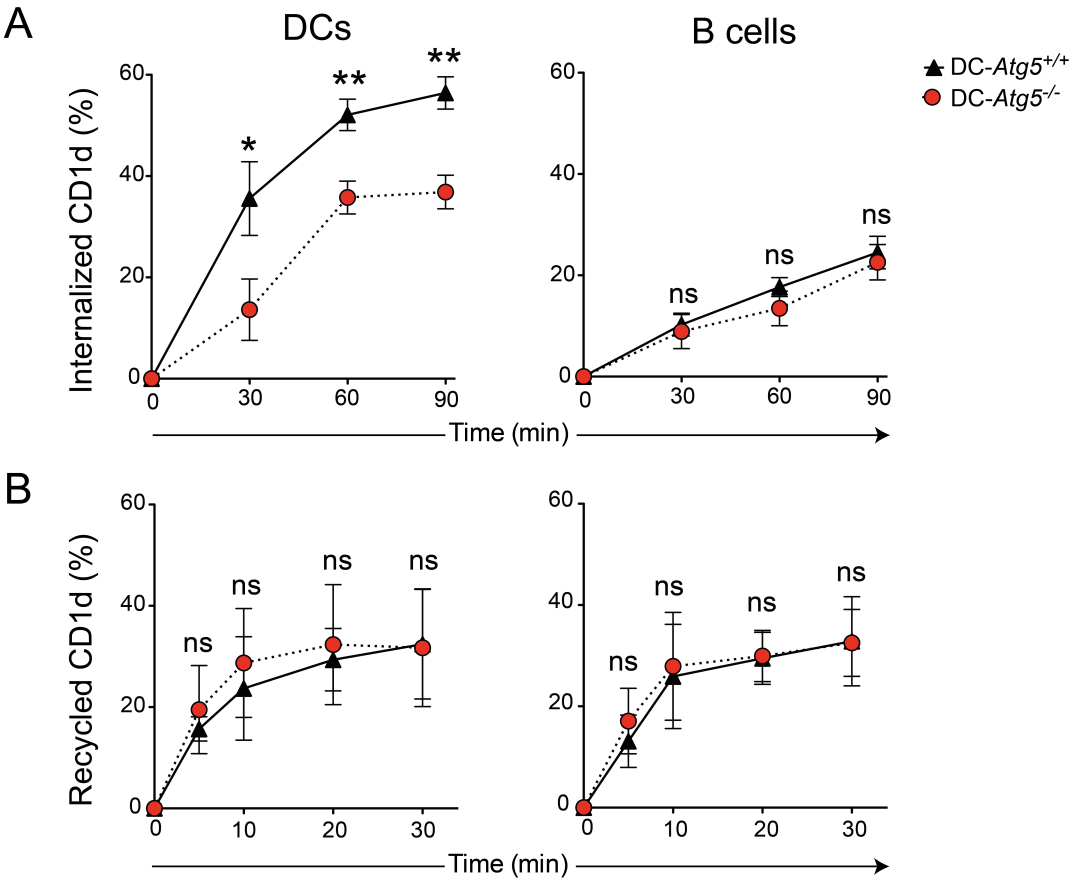

Figure 2.2.11 Quantification of CD1d internalization and recycling in splenic DCs and B cells.
(A) Internalization of surface CD1d on splenic DCs or splenic B cells was analyzed using a biotin-based flow cytometric endocytosis assay. Mean ± s.e.m. of pooled data from at least 3 independent experiments are shown. Each experiment contained at least 2 animals per group. **(B)** CD1d recycling in splenic DCs or splenic B cells was analyzed using a flow cytometry based recycling assay. Mean ± s.e.m. of pooled data from at least 3 independent experiments are shown. Each experiment contained at least 2 animals per group. Statistics: Two-tailed unpaired student t test. *** $P \leq 0.001$,** $P \leq 0.01$,* $P \leq 0.05$, ns $P > 0.05$.

2.2.8 Recruitment of CD1d and its Adaptor Protein AP2 to Endosomal Compartments is Reduced in *Atg5*-Deficient CD11c$^+$ DCs

To determine whether loss of autophagy proteins impairs trafficking of AP2 and CD1d to endosomal compartments in primary splenic DCs, we investigated colocalization of both molecules with EEA1 (early endosomal antigen 1) by confocal microscopy (**Figure 2.2.12 A**). Colocalization of AP2 and CD1d with EEA1 was significantly reduced in *Atg5*-deficient DCs as compared to DC-*Atg5*$^{+/+}$-derived DCs (**Figure 2.2.12 B**). These data suggest that autophagy proteins assist in the recruitment of CD1d molecules into endosomal compartments and provide a mechanistic explanation as to how loss of autophagy proteins stabilizes the cell surface expression of CD1d-glycolipid complexes on DCs.

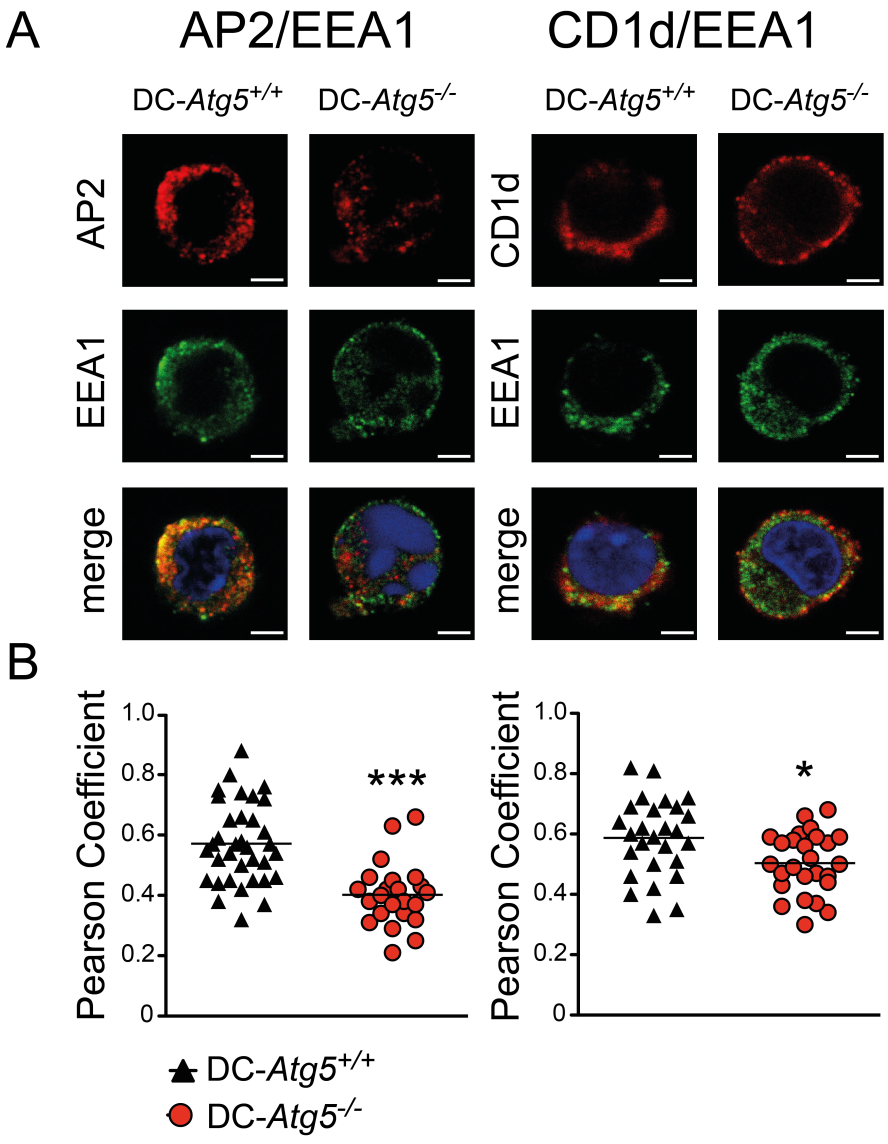

Figure 2.2.12 Reduced endosomal recruitment of CD1d and its adaptor protein AP2 in *Atg5*-deficient primary DCs. (C).
Colocalization study of AP2 and EEA1, as well as CD1d and EEA1 via confocal microscopy. Original magnification with 63×, 1.4 NA oil immersion lens. **(A)** Representative photographs from 2 independent experiments per colocalization study are shown. Scale bar: 2.5 µm. **(B)** Scatter dot plot representation and quantification of colocalization between AP2 and EEA1 and between CD1d and EEA1 via the Pearson coefficient. Each symbol represents one cell. Pooled data of 2 independent experiments per colocalization study are shown. Statistics: Unpaired two-tailed student t test. *** $P \leq 0.001$,** $P \leq 0.01$,* ≤ 0.05, ns $P > 0.05$.

2.2.9 Analysis of Organspecific NKT Cell and Splenic B Cell Frequencies at Steady State in DC-*Atg5*$^{-/-}$ and DC-*Atg5*$^{+/+}$ Mice

We next addressed if absence of *Atg5* alters iNKT cell activation and DC maturation following αGalCer application *in vivo*. Organ-specific numbers of iNKT cells were quantified by staining with αGalCer-loaded CD1d tetramer (Benlagha *et al.*, 2000; Matsuda *et al.*, 2000) (**Figure 2.2.13**).

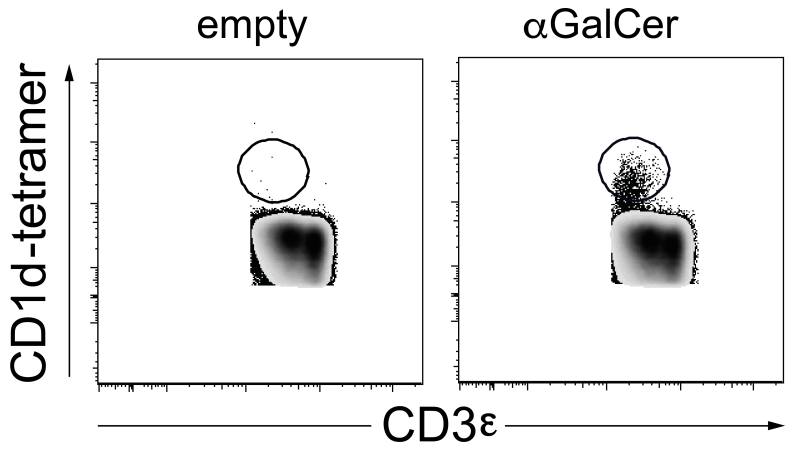

Figure 2.2.13 Visualization of iNKT cells via staining with glycolipid-loaded or empty CD1d-tetramer in C57BL/6 wild type mice-derived splenocytes.

Frequencies of splenic, thymic, and liver iNKT cells (**Figure 2.2.14 A-C**), splenic B cells (**Figure 2.2.14 D**) and splenic DCs (**Figure 2.1.1 D**) were similar in DC-*Atg5*$^{-/-}$ and DC-*Atg5*$^{+/+}$ mice at steady state.

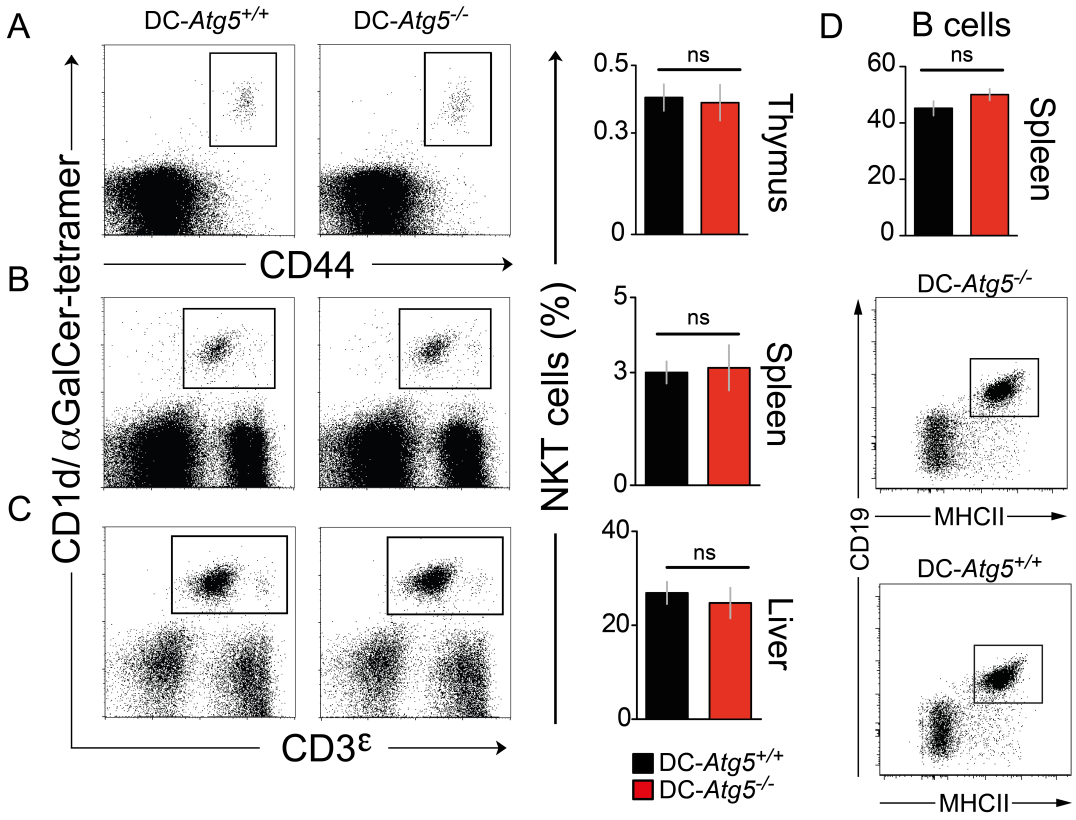

Figure 2.2.14 Organspecific frequencies of iNKT cells and splenic B cells at steady state in DC-*Atg5*$^{-/-}$ and DC-*Atg5*$^{+/+}$ mice.
Frequencies of iNKT cells (**(A)** thymus, **(B)** spleen and **(C)** liver) and **(D)** splenic B cells from naïve DC-*Atg5*$^{-/-}$ and DC-*Atg5*$^{+/+}$ mice were quantified. Representative bar graphs (mean ± s.e.m.) from at least 2 independent experiments are shown. Statistics: Unpaired two-tailed student t test. *** $P \leq 0.001$,** $P \leq 0.01$,* ≤ 0.05, ns $P > 0.05$.

2.2.10 Serum Cytokine Quantification Upon αGalCer *In Vivo* Challenge in DC-*Atg5*$^{-/-}$ and DC-*Atg5*$^{+/+}$ Mice

Antigen presentation to iNKT cells by DCs leads to activation of and cytokine secretion by iNKT cells which in turn aids further activation and maturation of DCs. In order to address this reciprocal crosstalk between iNKT cells and DCs, we first determined IFNγ and IL-4 serum levels after glycolipid challenge *in vivo*. We found that following αGalCer injection, DC-*Atg5*$^{-/-}$ mice showed substantially higher IL-4 levels after 4 h and IFNγ levels after 12 h, as compared to DC-*Atg5*$^{+/+}$ mice (**Figure 2.2.15 A, B**).

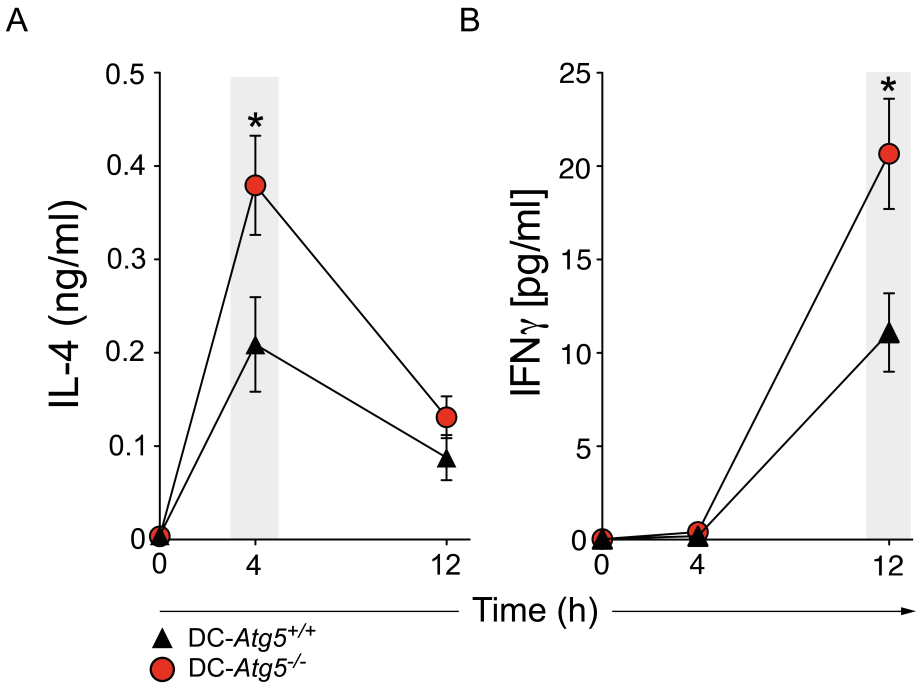

Figure 2.2.15 Serum cytokine kinetics upon αGalCer injection into DC-*Atg5*$^{-/-}$ and DC-*Atg5*$^{+/+}$ mice.
Serum concentration kinetics of **(A)** IL-4 and **(B)** IFNγ upon glycolipid challenge *in vivo* measured via ELISA. Pooled data (mean ± s.e.m.) from 2 independent experiments are shown. Statistics: Unpaired two-tailed student t test. *** $P \leq 0.001$,** $P \leq 0.01$,* ≤ 0.05, ns $P > 0.05$.

2.2.11 DC Phenotypisation Upon αGalCer *In Vivo* Challenge in DC-*Atg5*$^{-/-}$ and DC-*Atg5*$^{+/+}$ Mice

The increased and prolonged iNKT cell activation observed in DC-*Atg5*$^{-/-}$ mice, as reflected by enhanced serum cytokine levels upon glycolipid injection (**Figure 2.2.15 A, B**), was associated with enhanced phenotypic DC maturation as indicated by higher expression levels of CD86 and CD40 12 h after αGalCer challenge. Costimulatory molecule expression by B cells remained low and was comparable in αGalCer-treated DC-*Atg5*$^{-/-}$ and DC-*Atg5*$^{+/+}$ animals (**Figure 2.2.16 A, B**).

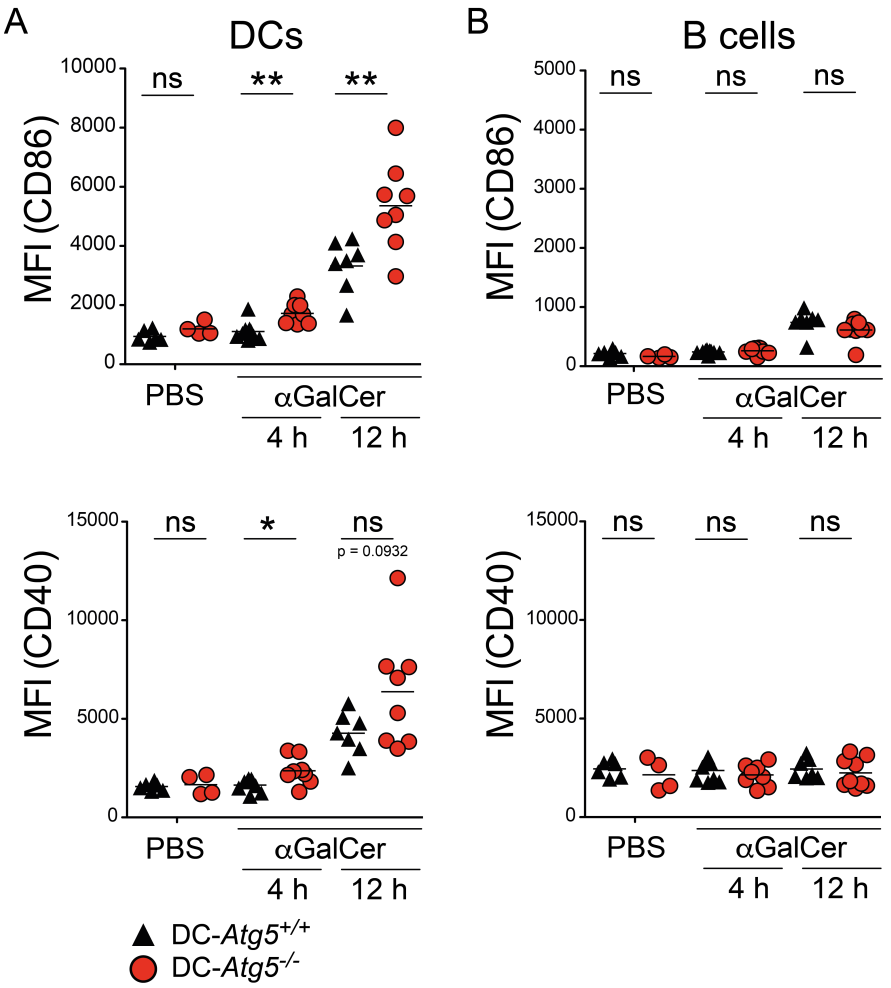

Figure 2.2.16 Surface expression kinetics of CD86 and CD40 on splenic DCs and B cells upon αGalCer injection into DC-*Atg5*$^{-/-}$ and DC-*Atg5*$^{+/+}$ mice.
Surface expression kinetics of CD86 and CD40 on **(A)** splenic DCs and **(B)** splenic B cells. Each symbol represents one animal. Pooled data of at least 2 independent experiments are shown. Statistics: Unpaired two-tailed student t test. Statistics: Unpaired two-tailed student t test. *** $P \leq 0.001$,** $P \leq 0.01$,* ≤ 0.05, ns $P > 0.05$

2.2.12 *Sphingomonas paucimobilis In Vivo* challenge in DC-*Atg5*$^{-/-}$ and DC-*Atg5*$^{+/+}$ Mice

Members of the genus *Sphingomonas* have been the first microorganisms identified to express natural ligands for iNKT cells in their LPS-free bacterial envelope and it has been reported that iNKT cells are essential in controlling both septic shock reaction and bacterial clearance in *Sphingomonas* infected mice (Kinjo *et al.*, 2005; Mattner *et al.*, 2005; Sriram *et al.*, 2005). The gram-negative, lipopolysaccharide-free bacterium *Sphingomonas paucimobilis (S. paucimobilis)* is associated with opportunistic and nosocomial infections in immunocompromised patients (Ryan and Adley, 2010) and contains glycosphingolipids that stimulate iNKT cells through their TCR in a CD1d-

specific manner (Holzapfel *et al.*, 2014; Kinjo *et al.*, 2005; Mattner *et al.*, 2005; Sriram *et al.*, 2005). We therefore investigated whether iNKT cells activated by *Atg5*-deficient DCs conferred superior protection against infection with the pathologically relevant microorganism *S. paucimobilis*. The stimulatory potential of *S. paucimobilis*-derived glycosphingolipids is lower as compared to αGalCer, however iNKT cell recognition of these natural microbial-derived glycolipids induces potent proinflammatory cytokine production *in vitro* and *in vivo* (Holzapfel *et al.*, 2014; Kinjo *et al.*, 2005; Mattner *et al.*, 2005). Upon infection with *S. paucimobilis*, DC-*Atg5*$^{-/-}$ mice exhibited significantly lower pathogen loads in spleens and lungs as compared to their DC-*Atg5*$^{+/+}$ littermate controls (**Figure 2.2.17 A, B**). Reduced pathogen loads were associated with increased serum levels of proinflammatory cytokines such as IP-10 and TNF-α (**Figure 2.2.17 C, D**). Production of IFNγ tended to be higher in DC-*Atg5*$^{-/-}$ mice, whereas IL-17 production was unchanged (**Figure 2.2.17 E, F**).

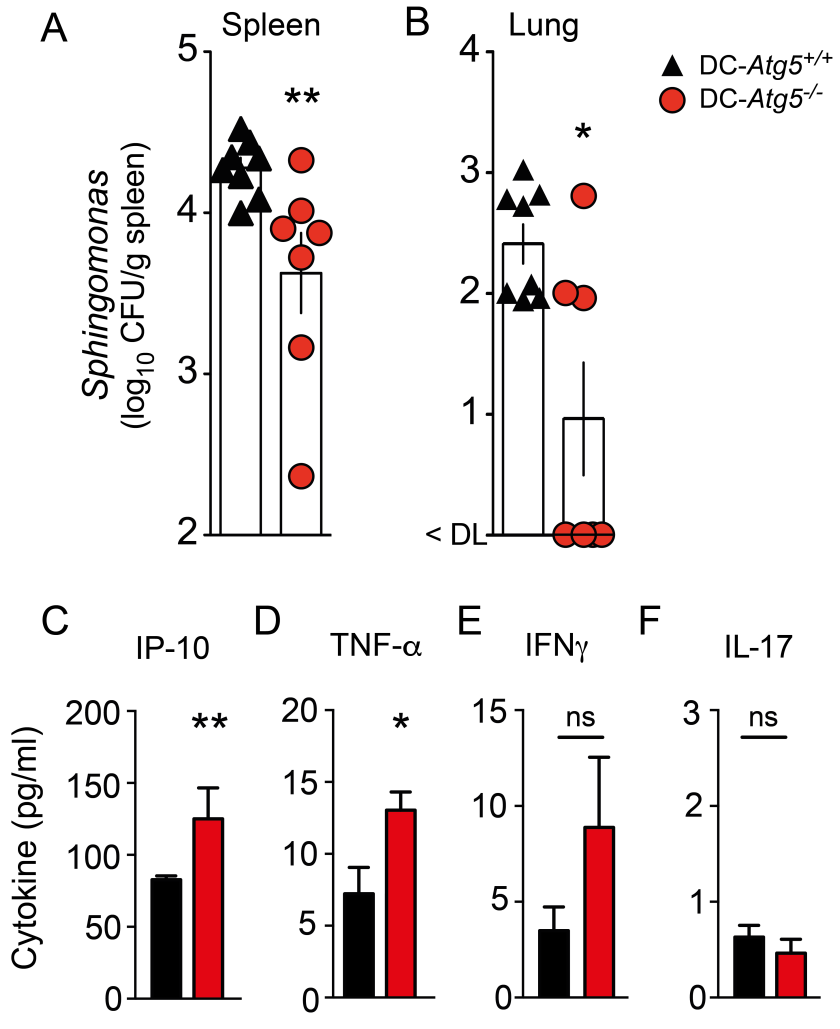

Figure 2.2.17 *In vivo* challenge of DC-*Atg5*$^{-/-}$ and DC-*Atg5*$^{+/+}$ mice with *Sphingomonas paucimobilis*.
(A) Quantification of bacterial titers (CFU/g tissue) in spleen and lung after *in vivo* infection of mice with *S. paucimobilis*. Each symbol represents one animal. One representative of 2 experiments is shown. Quantification of serum cytokines upon *in vivo* infection with *S. paucimobilis*. One representative of 2 experiments is shown. Statistics: two-tailed Mann-Whitney U Test **(D)**. *** $P \leq 0.001$,** $P \leq 0.01$,* ≤ 0.05, ns $P > 0.05$.

In conclusion, autophagy proteins in DCs regulate surface expression of CD1d-glycolipid complexes and thereby modify iNKT cell activation and the resultant DC maturation in response to exogenous glycolipid antigen αGalCer and natural microbial glycolipids *in vivo*.

3. Discussion

3.1 Prelude

In this study, I investigated non-canonical use of the essential autophagy protein ATG5 in the context of two different antigen presenting pathways. Lack of ATG5 in CD11c$^+$ APCs conferred protection from development of adoptively transferred EAE and restrained CD4$^+$ T cell reactivation within the CNS. On the contrary, CD11c$^+$-conditional deletion in ATG5 resulted in prolonged CD1d-restricted exogenous glycolipid presentation, enhanced iNKT cell activation and improved clearance from *Sphingomonas spp.* infection. These data indicate that ATG5 supports loading of endocytosed antigen onto MHC class II molecules for augmented CD4$^+$ T cell recognition while restraining iNKT cell activation through CD1d internalization.

3.2 ATG5-Dependent Autophagy During Autoimmune CNS Inflammation

MS is a chronic neuroinflammatory condition during which autoaggressive leukocytes invade across a compromised blood brain barrier (BBB) into the CNS. On site, the infiltrated immune cells, in concert with CNS-resident cells mediate progressive axonal demyelination and engender spatio-temporally disseminated lesions within the CNS which entails diffuse cytodegeneration in grey and white matter areas of the CNS (Mahad *et al.*, 2015). Although the complex pathoaetiology of MS prompts relevant involvement of other cellular and humoral immune components such as cytotoxic CD8$^+$ T cells, B cells and autoantibodies ('t Hart *et al.*, 2015; 'tHart *et al.*, 2016; Hohlfeld *et al.*, 2016; Martin *et al.*, 2016), CD4$^+$ T cells are considered to be the pivot of the underlying disease mechanism (Hohlfeld *et al.*, 2015). Genome-wide association studies revealed that HLA class II haplotypes, in particular HLA-DRB1*1501/HLA-DRB5*0101, are the strongest genetic risk factors for MS development (International Multiple Sclerosis Genetics Consortium (IMSGC) *et al.*, 2013; International Multiple Sclerosis Genetics Consortium *et al.*, 2011) and albeit frequencies of myelin protein specific CD4$^+$ T cells in the blood have been reported to be similar in MS patients compared to healthy individuals, *ex vivo* treatment of blood and cerebrospinal fluid (CSF)-derived T cells with recombinant IL-2 lead to significant proliferation of encephalitogenic CD4$^+$ T

cells in MS patient-derived specimens as compared to those derived from healthy individuals (Zhang *et al.*, 1994). Promiscuous restriction, means the ability of some TCRs to use different HLA restriction elements. One study found that two out of five *in vivo*-expanded MS patient-derived and CSF-infiltrating $CD4^+$ T cell clones were able to use different HLA class II molecules for antigen recognition. One of the two $CD4^+$ T cell clones recognized identical peptides in the context of all MS-associated HLA class II molecules coexpressed in the HLA-DR2 haplotype (DRB1*1501, DRB5*0101, and DQB1*0602) arguing for a pathomechanistic role of this overlapping antigen presentation to $CD4^+$ T cells during MS (Sospedra *et al.*, 2006).

EAE is a commonly used animal model of MS in which disease is induced by immunization with myelin-derived antigenic peptides together with adjuvant or by adoptively transferring pre-activated myelin-specific $CD4^+$ T cells in naïve recipients (Ben-Nun, Wekerle and Cohen, 1981a; 1981b; Stromnes and Goverman, 2006). This model is predominantly $CD4^+$ T cell-driven (Ben-Nun, Wekerle and Cohen, 1981b; Zamvil *et al.*, 1986) and a pathomechanistic prerequisite for CNS damage is the local reactivation of $CD4^+$ T cells specific for myelin-derived antigens (Greter *et al.*, 2005). Reactivated $CD4^+$ T cells together with activated myeloid cells initiate a cascade of proinflammatory events, which is believed to perpetuate CNS tissue damage leading to the development of clinical EAE symptoms (Becher *et al.*, 2000; Huitinga *et al.*, 1990; Schreiner *et al.*, 2009).

How and by which antigen-presenting cell subset pathogenic $CD4^+$ T cells are locally reactivated and cause tissue damage during the course of MS and EAE is, however, incompletely understood. This is in part due to the fact that the detailed route of how myelin self-antigens are processed and presented towards $CD4^+$ T cells has not been fully elucidated.

The autophagic machinery delivers cytoplasmic constituents and substrates to endosomal/lysosomal compartments including MIICs for subsequent MHC class II presentation (Schmid *et al.*, 2007). Additionally, autophagy proteins regulate degradation of extracellular material via the non-canonical use of ATGs during LAP (Florey *et al.*, 2011; Henault *et al.*, 2012; J.-Y. Kim *et al.*, 2013; H. K. Lee *et al.*, 2010; Martinez *et al.*, 2011; 2015; 2016; Sanjuan *et al.*, 2007).

In order to investigate the role of ATG5 during EAE, we made use of a conditional knockout mouse in which CD11c$^+$ cells do not express ATG5 and are therefore incapable of carrying out macroautophagy or LAP. Cre/loxP-mediated deletion of *Atg5* in these mice was confined to the CD11c$^+$ compartment, did not perturb steady state frequencies of splenic CD11$^+$/MHC class II$^+$ DCs and did not alter surface expression of distinctive DC markers. These results are in line with a previous report using the identical CD11c-Cre and *Atg5*$^{flox/flox}$-strains and showing that *Atg5*-deficient DCs have intact migratory capacities, normal phagocytic activity, similar expression levels of MHC class II, CD40, CD86 in both steady state and upon immune activation along with similar secretion levels of IL-12p40, IL-6, and TNF-α (H. K. Lee *et al.*, 2010). Furthermore Lee and colleagues reported that in murine DCs, TLR-dependent phagocytosed HSV-2 can be found in LC3$^+$ single-membraned vesicles reminiscent of LAPosomes. In absence of ATG5, CD4$^+$ T cell responses against phagocytosed protein-derived peptides were markedly reduced, arguing for inefficient MHC class II-dependent processing and presentation (H. K. Lee *et al.*, 2010). Interestingly, pharmacological induction of canonical macroautophagy via TORC1 inhibitor rapamycin did not lead to enhanced MHC class II presentation of phagocytosed material arguing for the non-canonical LAP pathway linking phagocytosis and MHC class II presentation (H. K. Lee *et al.*, 2010).

We therefore hypothesized that lack of ATG5 in professional antigen presenting cells like DCs would alter the onset and/or course of disease during EAE, where the presentation of myelin-derived antigens activate CD4$^+$ T cells which engender disease. Potentially both, the macroautophagy pathway and LAP are ATG5-dependent degradation pathways, which facilitate MHC class II presentation of self-antigens. Nevertheless, myelin-derived candidate antigens are not expressed in professional APCs such as CD11c$^+$ DCs thus an intracellular loading of these peptides onto MHC class II molecules in the context of CNS autoimmunity appears counterintuitive. LAP couples phagocytosis of extracellular solid cargo to key members of the autophagy machinery (including ATG5) (Martinez *et al.*, 2015; Münz, 2015). A prerequisite for triggering LAP activity is the engagement of germline encoded pattern recognition receptors or Ptd-L-Ser receptors via phagocytosed material. The role of TLR signaling in the context of EAE has partly been investigated. TLR9 and, to some extend, TLR2 signaling mediates the pathogenicity of EAE, both receptors that have been

implicated in triggering LAP (Sanjuan *et al.*, 2007), whereas TLR1 and 6-deficiency in mice did not have an impact on the development of active EAE (Miranda-Hernandez *et al.*, 2011; M. Prinz *et al.*, 2006). Importantly, also adoptive transfer EAE-induction was dependent on TLR2 signaling, discarding the assumption that microbial-derived constituents in the adjuvant preparation during active EAE serve as ligands (Miranda-Hernandez *et al.*, 2011). Additionally, both studies showed that deficiency of the downstream TLR signaling molecule myeloid differentiation primary response gene 88 (MyD88) abrogates disease (Miranda-Hernandez *et al.*, 2011; M. Prinz *et al.*, 2006).

There are various protocols for induction of EAE available, differing in parameters such as mouse genetic background, antigenic myelin peptide and mode of disease induction. The two most commonly used induced EAE models are "active EAE", where animals are subcutaneously immunzed with an emulsion of myelin protein/peptide (commonly MOG_{35-55} or proteolipid protein $[PLP]_{139-155}$) and complete Freund's adjuvant (CFA) and the "adoptive transfer EAE" model, where activated encephalitogenic $CD4^+$ T cells are isolated from spleen and draining lymph nodes of actively immunized animals and, after *in vitro* restimulation for 2 days, are injected into naïve recipient animals. While active EAE models the induction and effector stages of the disease, adoptive transfer EAE models only the effector phase (Miller and Karpus, 2007). During EAE, CNS-infiltrating $CD4^+$ T cells require local reactivation by myelin-antigen presenting cells to efficiently induce sustained inflammatory demyelination (Greter *et al.*, 2005; Kawakami *et al.*, 2004; Kivisäkk *et al.*, 2009). $CD11c^+$ cells within the CNS alone, i.e. in the absence of secondary lymphoid tissues, are sufficient to present antigen *in vivo* to primed myelin-reactive T cells in order to mediate CNS inflammation and clinical disease development (Greter *et al.*, 2005; Paterka *et al.*, 2016). We found that mice with a CD11c-conditional deletion of *Atg5* are completely protected from clinically developing EAE upon adoptive transfer of encephalitogenic T cells. Studies that employed inducible ablation of cDCs through CD11c promoter-driven human diphtheria toxin (DT) receptor (DTR) expression demonstrated that DT-treated mice remain susceptible to disease development after active EAE induction with myelin antigen emulsified in CFA. Isaksson et al. (Isaksson *et al.*, 2012) reported that DT-treated mice still develop EAE after active immunization indicating that a population of APCs other than $CD11c^+$ DCs executed initial priming of encephalitogenic T cells.

However, DT treatment did not ablate $CD11c^+$ APCs in the CNS during peak of disease and $CD11c^+$ APCs present in the CNS still could present myelin to invading encephalitogenic T cells (Isaksson *et al.*, 2012). Yogev et al. (Yogev *et al.*, 2012) also used CD11c-DTR mice to deplete $CD11c^+$ DCs including dermal $CD103^+/CD207^+$ DCs and found that mice lacking these DC populations are even hypersusceptible to EAE induction, supporting the concept that DCs maintain peripheral tolerance. However, they demonstrated that after T cell priming and during T cell expansion within the CNS (effector phase), DC-depleted mice showed reduced clinical scores as compared with control mice. In line with these findings, Paterka and colleagues recently reported that adoptive transfer of primed, encephalitogenic $CD4^+$ T cells into $CD11c^+$-depleted recipients lead to reduced disease incidence and scores (Paterka *et al.*, 2016). Thus, while the aforementioned studies reflect the complex roles of professional APCs during T cell priming and indicate that, after active EAE induction, priming synapses can be formed between non-DC-APC populations, they do not contradict but support the concept that $CD11c^+$ DCs are the most efficient APCs in driving the re-activation of transferred myelin-specific $CD4^+$ T cells within the CNS during the effector phase of EAE (Becher and Greter, 2012). In the case of DC-depleted mice that remain to be susceptible for developing actively induced EAE it has yet to be defined which APC subset primes $CD4^+$ T cells. Two candidate APCs would be macrophages and B cells and both populations have been found to take up fluorescent microbeads that had been coadministered with CFA. After phagocytosis B cells and macrophages both migrated to the draining lymphnodes where they could potentially prime T cells. However, depletion of $CD20^+$ B cells did lead to enhanced disease (Yogev *et al.*, 2012). Previous attempts to efficiently deplete macrophages via the expression of thymidine kinase of herpes simplex virus (HSVTK) driven by the CD11b promotor have proven unfeasible, since this procedure entails fatal aplastic anemia (Heppner *et al.*, 2005). It is therefore conceiveable that certain macrophage populations, in absence of DCs, take over in priming encephalitogenic T cell in secondary lymphoid organs during the onset of active EAE. Additionally, also neutrophils may serve under certain circumstances as professional APCs and might be capable of priming T cells, however experimental evidence for this scenario is still lacking (Abi Abdallah *et al.*, 2011; Kalyan and Kabelitz, 2014; Maletto *et al.*, 2006).

At steady state, CD11c$^+$/MHC class II$^+$ DCs within the CNS are enriched in the choroid plexus (McMenamin, 1999; Prodinger *et al.*, 2011) which, together with the meningeal vasculature, is an active site for immune trafficking into and out of the CNS (Mohammad *et al.*, 2014; Ransohoff *et al.*, 2003; Schläger *et al.*, 2016) and a first port of entry for pathogenic T cells during EAE (Reboldi *et al.*, 2009). Choroid plexus DCs resemble splenic CD11c$^+$/MHC class II$^+$ DCs in morphology, gene expression profile, antigen-presenting function and their shared intrinsic requirement for Fms-related tyrosine kinase 3 (Flt3) ligand (Anandasabapathy *et al.*, 2011). In line with the aforementioned studies, we identified a small population of CD11c$^+$/MHC class II$^+$ DCs that are specifically targeted by Cre-mediated recombination within the non-diseased CNS. Targeted deletion of the essential autophagy protein ATG5 in this population abrogated CD4$^+$ T cell reactivation as well as CNS accumulation and completely prevented clinical disease development of adoptive transfer EAE. Interestingly, we found higher frequencies of CD25$^+$/FOXP3$^+$ TREGS within the CNS CD4$^+$ T cell compartment in DC-*Atg5*$^{-/-}$ animals at peak of disease. A previous report showed that supplementation of TREGs via adoptive transfer prior to inducing EAE, both actively or by adoptive transfer significantly reduced disease severity by biasing the immune response into the direction of T_H2 (Kohm *et al.*, 2002). Splenic TREG counts are unchanged in naïve DC-*Atg5*$^{-/-}$ animals (data Christina Sina) and we obtained no evidence that loss of ATG5 in DCs directly lead to an increase of TREGs in the CNS in DC-*Atg5*$^{-/-}$ animals. It is rather conceivable that the incremental accumulation of encephalitogenic CD4$^+$ cells in the CNS of DC-*Atg5*$^{+/+}$ animals strongly diluted the TREG population in these animals. We additionally found several myeloid subsets to be enriched in the CNS of diseased *Atg5*$^{+/+}$ animals at peak of disease whereas these subsets where much less abundant in DC-*Atg5*$^{-/-}$ animals. Also, while in steady state microglia frequencies and surface expression of CD40, CD86 and MHC class II were similar, upon adoptive transfer EAE, microglia in *Atg5*$^{+/+}$animals strongly upregulated MHC class II. CD4$^+$ T cells specific to CNS antigens constitute the only immune cell subset capable of conferring EAE when transferred into immunocompetent syngeneic recipient animals (Ben-Nun, Wekerle and Cohen, 1981a; Pettinelli and McFarlin, 1981). A yet to be defined myeloid subset (most likely resident) is probable to acquire disease relevant antigen on site and subsequently presents it to patroling encephalitogenic T cells, which may set off a self-perpetuating

sequence of proinflammatory events. Therefore, local reactivation of $CD4^+$ T cells during EAE is considered to occur upstream of stepwise further accumulation of peripherall myeloid cells. Consequently, the reduced ingress of myeloid populations into the CNS of DC-*Atg5*$^{-/-}$ animals and the lack of microglial activation are likely to be in the wake of an inefficient local restimulation of $CD4^+$ cells.

Conditional targeting of ATG7 in $CD11c^+$ DCs was reported to attenuate the disease course and lowered EAE incidence initiated by active immunization with myelin antigen/CFA (Bhattacharya *et al.*, 2014). Given the negligible function of cDCs during the priming phase of EAE (Isaksson *et al.*, 2012; Yogev *et al.*, 2012) we investigated whether the autophagic machinery in DCs is important for local T cell reactivation. The data presented here thus supports the concept of CNS DCs as indispensible in initiating the effector phase of EAE and demonstrate the essential requirement of ATG5 in DCs for myelin-reactive T cells to face their antigen *in vivo* before mediating inflammatory demyelination.

Absence of LAP in myeloid cells by means of lysozyme M-Cre-mediated gene deletion, which targets macrophages, monocytes, some neutrophils and $CD11^+$ DCs to varying degrees, was recently shown to drive development of a systemic autoinflammatory syndrome in aged mice (52 weeks) with increased expression of IFN signature genes, occurrence of anti-double-stranded DNA and -nuclear antibodies, and signs of kidney damage, commonly associated with systemic lupus erythematosus (SLE) (Martinez *et al.*, 2016). The aforementioned study showed that macrophages deficient in ATG7 or Rubicon, both reported to be required for LAP (Martinez *et al.*, 2015), did engulf, but not effectively clear, dying cells and produced proinflammatory cytokines, including IL-1β and IL-6, upon challenge with apoptotic cell material (Martinez *et al.*, 2016). An increased propensity of ATG7$^{-/-}$ macrophages to produce proinflammatory cytokines after engulfment of apoptotic cells has also been described *in vitro* (Martinez *et al.*, 2011) indicating that defective LAP in macrophages results in a failure to process engulfed dying cells, leading to elevated inflammatory cytokine production and the development of a SLE-like syndrome. It should be noted that macrophages and DCs significantly differ in their employment of lysosomal degradation. While macrophages harbor large amounts of lysosomal proteases and swiftly degrade phagocytosed material, DCs have much lower levels of these enzymes, degrade engulfed cargo rather slowly and seem to favor antigen rentention which

promotes efficient presentation (Delamarre *et al.*, 2005). The crosstalk between non-canonical autophagy and MHC class II-dependent antigen presentation therefore is likely to be different inbetween these two myeloid lineages. This differential usage of phagocytosis-associated components is also illustrated in the case of the NADPH oxidase NOX2, another essential component of the non-canonical autophagy pathway LAP. Its predominant and initially alloted function, generation of reactive oxygen species (ROS), has been linked to killing of intraphagosomal pathogens by providing the adequate environment for protease function. In professional APCs such as DCs, whose principal function is to take up, process and present antigens in order to initiate and shape adaptive immune responses rather than pathogen killing or clearance of cell debris as in the case of macrophages, NOX2 expression was shown to regulate antigen presentation due to its ability to control the level of antigen degradation via altering phagosomal pH levels (Savina *et al.*, 2006). Indeed, DCs lacking NOX2 show enhanced phagosomal acidification and increased antigen degradation, resulting in impaired cross presentation (Savina *et al.*, 2006). In addition to cell type dependent tuning of phagosomal acidification, NOX2 has recently also been implicated in regulating serine and cysteine proteases (cathepsins B, L, and S) within phagosomes (Rybicka *et al.*, 2012) and it has been suggested that increased hydrolysis of critical regions within the encephalitogenic $MOG_{35–55}$ antigen by cysteine cathepsins in the early phagosome contribute to the reduced incidence and delayed onset of EAE reported in NOX2-deficient mice (Allan *et al.*, 2014). It is conceivable that NOX2 as essential component of the non-canonical autophagy pathway LAP not only affects levels of phagosomal proteolysis as previously shown, but facilitates the execution of an alternative pathway for antigen loading onto MHC class II molecules, thereby contributing to $CD4^+$ T cell-mediated augmentation of autoimmune CNS inflammation.

In our study, DC-*Atg5*$^{-/-}$ mice were protected from the development of a $CD4^+$ T cell-mediated autoimmune disease and ATG5 was required for DCs to efficiently present antigen derived from Ptd-L-Ser-exposing oligodendroglial cells to myelin-specific $CD4^+$ T cells. These data are in line with *in vitro* studies that identified LAP in professional APCs to support downstream $CD4^+$ T cell responses by promoting sustained MHC class II antigen presentation (Ma *et al.*, 2012; Romao *et al.*, 2013). LAP was shown to be essential for retinoid recycling by phagocytic retinal pigment epithelial cells, which contributes to maintaining vision in mice

(J.-Y. Kim *et al.*, 2013), to occur on macropinosomes (Florey *et al.*, 2011), and at the ruffled border in osteoclasts (DeSelm *et al.*, 2011) suggesting that this pathway contributes significantly to physiology in multiple contexts (Bandyopadhyay and Overholtzer, 2016). During $CD4^+$ T cell-driven CNS inflammation, non-canonical autophagy in DCs may use ATG5 for enhanced presentation of endocytosed cargo derived from damaged oligodendrocytes on MHC class II molecules, thus linking oligodendrocyte injury with myelin antigen processing and T cell-pathogenicity. The cellular architecture of MS lesions is dynamic in its neuropathological features including leukocyte composition (Lassmann and van Horssen, 2011). Commonly, T cell infiltration occurs in two distinct waves (A. P. D. Henderson *et al.*, 2009; Marik *et al.*, 2007). Initially MS lesions are characterized by oligodendrocyte damage and commencing demyelination accompanied by microglia that show an activated phenotype. However, in these initial lesions lymphocytes are scarce. Thereupon progressive demyelination occurs, and myelin constituents are phagocytosed by microglia and other myeloid cells which ensues a dramatic T cell influx (Barnett and Prineas, 2004). Widespread oligodendrocyte injury and concomitant focal demyelination with deterioration of axonal conduction in the CNS constitutes a unique pathological hallmark of MS lesions and protection of oligodendrocytes against injury leads to protection against the development of EAE (Butzkueven *et al.*, 2002; Frohman *et al.*, 2006; A. P. D. Henderson *et al.*, 2009; Hisahara *et al.*, 2000; Lucchinetti *et al.*, 1999; Mi *et al.*, 2007). Importantly, primary myelin loss, can precede the formation of inflammatory infiltrates (Barnett and Prineas, 2004; Prineas and Parratt, 2012; Traka *et al.*, 2016) and, detected by virtue of discreet changes in white matter areas, can be visualized several months prior to blazing lesions in MS patients (Fazekas *et al.*, 2002). Furthermore, genome-wide epigenetic differences in the DNA methylation status have been reported between normal appearing white matter derived from MS patients and non-diseased control brains (Huynh *et al.*, 2014). The observed hypermethylation and subsequent diminished expression of loci in MS affected brains included genes that control oligodendrocyte survival (*BCL2L2* and *NDRG1*), compatible with the concept that oligodendrocyte injury might trigger or augment myelin protein processing if professional APCs are present and suggesting that augmented susceptibility to injury precedes inflammatory infiltration.

Importantly, a recent study showed that oligodendrocyte death is sufficient to induce encephalitogenic T cell responses and subsequent neuroinflammation *in vivo* (Traka *et al.*, 2016). In line with this, an increasing number of recent reports support the role of primary myelin-forming oligodendrocyte injury and cell death pathoetiologically upstream of inflammatory ingress by encephalitogenic lymphocytes to the CNS (Frohman *et al.*, 2006; Furlan *et al.*, 1999; Hisahara *et al.*, 2000; 2001; Lucchinetti *et al.*, 1999; Pender *et al.*, 1991). *In vivo* multi-spectral two-photon analyses during EAE and high resolution confocal imaging of actively demyelinating MS foci revealed a centripetal trajectory of oligodendrocyte damage, originating at protruding structures called myelinosomes. The vast majority of the investigated myelinosomes were located in the direct vicinity of non-microglial phagocytes (Romanelli *et al.*, 2016). It is therefore conceivable that primary death of oligodendrocytes of yet unknown cause leads to subsequent uptake of myelin-derived antigenic debris by CNS-resident APCs and the following mounting of a myelin specific adaptive response (Stys *et al.*, 2012).

There are several limitations to this study. ATG5 is not restricted to LAP but is also essential for canonical macroautophagy. Due to the fact that proteins that give rise to disease relevant antigenic peptides during EAE are not known to be intrinsically expressed in CNS resident professional APCs and there is no evidence that oligodendrocytes serve as antigen presenting cells in this context, it appears unlikely that our documented results can be attributed to canonical macroautophagy. Nevertheless, this remains to be experimentally addressed. Possible experiments include the conditional targeting of genes that encode for proteins essential for LAP but not canonical macroautophagy, e.g. *cybb* (encoding NOX2). Complementary, experiments using conditional knockouts of macroautophagy essential proteins that are dispensible for LAP (e.g. FIP200) would help to resolve this issue. Furthermore, it remains to be shown that ATG5-deficient CNS APCs fail to reactivate encephalitogenic T cells *in vivo/ex vivo*. This will be more difficult to address, since the small numbers of target cells that can be obtained from the CNS of non-diseased DC-*Atg5*$^{-/-}$ animals partly preclude the performance of large well-controlled *ex vivo* cocultures.

We conclude from our data that ATG-dependent processing of phagocytosed injured oligodendrocytes for antigen presentation is required for encephalitogenic T cells to recognize the CNS as their target organ and to induce inflammatory

demyelination. ATG-regulated phagocytosis in CNS DCs might also be relevant for the perpetuation of neuroinflammation in patients with MS and, therefore, an attractive therapeutic target to limit inflammatory CNS damage.

3.3 ATG5-Mediated Stabilization of Surface CD1d Expression in DCs

Both, canonical macroautophagy and LAP support loading of vesicular antigens onto MHC class II molecules, leading to increased and more efficient $CD4^+$ T cell responses. CD1d, another antigen presenting molecule, exhibits glycolipid antigens to innate-like iNKT cells. iNKT cell-targeted responses and iNKT cell agonists are used and currently being evaluated as adjuvants to enhance the efficacy of anti-tumor immunotherapy. Presentation of exogenous glycolipid antigens for iNKT cell activation *in vivo* is predominantly mediated by DCs (Arora *et al.*, 2014) and previous studies have shown that a proportion of CD1d molecules in APCs spatially associates with MHC class II molecules which are sorted into late endosomal MIICs before trafficking to the cell surface (Jayawardena-Wolf *et al.*, 2001; Kang and Cresswell, 2002a).

We found that already in steady state, CD1d partly colocalized with LC3 in APCs and this colocalization was further increased using several different TLR agonists. The respective contribution of different TLRs in the activation of CD1d-restricted iNKT cells by DCs remains still unclear. It has been reported that DCs stimulated with the TLR9 agonist CpG ODN activate CD1d-restricted iNKT cells to produce IFNγ hereby conferring protection in mice against B16F10-induced melanoma metastases (Paget *et al.*, 2007). Intratracheal administration of the prototypic glycolipid antigen αGalCer in combination with the TLR3 agonist poly(I:C) has been reported to upregulate IL-17A production by CD1d-restricted iNKT subsets rendering mice more susceptible to airway hyperreactivity (AHR) (Vultaggio *et al.*, 2012). We therefore focused on these two TLR agonists for the colocalization analyses in primary splenic DCs and found that treatment with both increased colocalization of CD1d and LC3.

Depending on the biochemical structure of the antigenic glycolipid, the elicited iNKT cell responses will be skewed more towards a T_H1, T_H2 or mixed phenotype. Unlike T_H2-biasing agonists, which have been shown to directly load into CD1d molecules on the cell surface, thereby circumventing uptake and subsequent processing, T_H1-biasing agonists (including αGalCer) require loading onto CD1d

molecules in endocytic compartments to be subsequently trafficked to the plasma membrane (Arora *et al.*, 2011; Im *et al.*, 2009). Given the supportive role autophagy pathways occupy during MHC class II-dependent antigen processing and presentation, we initially hypothesized a similar contribution during CD1d dependent presentation of glycolipids to iNKT cells. Surprisingly, in contrast to the auxiliary activity on MHC class II presentation, we found that the essential autophagy protein ATG5 negatively regulates the presentation of exogenous lipid antigens by CD1d.

One candidate mechanism that we initially investigated was the use of differential uptake pathways for glycolipids with various biochemical properties. Metabolic requirements pressure cells into continuously taking up lipids which traffic through the circulation complexed with apolipoproteins. Amongst others, low density lipoprotein receptor (LDLR), scavenger receptor A (SR-A) and -BI, lectin-type oxidized lDl receptor 1 (LOX1; also known as OlR1) and CD36 have been implicated in uptake of antigenic glycolipids (Freigang *et al.*, 2012; Greaves and Gordon, 2005). However, our detailed knowledge in transport and uptake pathways that target glycolipid antigens for CD1d presentation in APCs remains largely obscure. The biochemical composition of glycolipid antigen head groups has proven to be a key determinant for their respective receptor uptake pathway. While the prototypic iNKT cell agonist αGalCer facilitates uptake via both, LDLR and SRA, Digalactosylceramides (e.g. GalαGalCer), bearing a second galactose moiety in their head group, are strongly biased towards uptake via the LDLR pathway. Whereas glucuronylceramides (e.g. the *Sphingomonas*-derived GSL-1) carrying a carboxyl moiety on their head group, favor uptake by the SRA pathway (Freigang *et al.*, 2012). Recently, it was reported that macrophages deficient in the essential macroautophagy gene *Atg7*, depict increased expression of two class A scavenger (SRA) receptors (Bonilla *et al.*, 2013). However, we did not find any evidence for a role of ATG5 in either LDLR- or SRA-mediated glycolipid uptake.

Our results obtained by using primary $CD11c^+$ DCs were unexpected and appeared to be in contrast with a recent study in which *Atg7*-deficient GM-CSF-differentiated bone marrow-derived DCs (BMDCs) did not differ from *Atg7*-competent BMDCs in eliciting cytokine production by iNKT cells (Salio, Puleston, *et al.*, 2014). To address this discrepancy we generated BMDCs from *Atg5*-

deficient mice and, in line with Salio et al., observed that coculture with glycolipid-pulsed *Atg5*-deficient BMDCs leads to IL-2 production by iNKT cells to the same level as BMDCs generated from DC-*Atg5*$^{+/+}$ mice. A recent study characterized the composition of *in vitro*-derived BMDC cultures and found them to contain heterogeneous populations including cells most closely resembling macrophages, DCs and neutrophils (Helft *et al.*, 2015; Inaba *et al.*, 1992). Helft and colleagues did specifically report heterogenicity *within* the CD11c^{+}/MHC class II^{+} population of BMDCs (Helft *et al.*, 2015). CD11c^{+}/MHC class II^{+} BMDCs contained subsets that significantly differed in their expression of surface molecules such as CD115 and CD135 but also in their capability to release inflammatory mediators in response to microbial challenge (Helft *et al.*, 2015). These subsets include also common monocyte precursor-derived macrophages which are inferior to common DC precursor antigen presenting cells in their T cell priming and stimulatory capacity (Guilliams and Malissen, 2015; Helft *et al.*, 2015). Furthermore, processes related to antigen presentation have been described to significantly differ in their requirement of the autophagic machinery dependening on the APC subset (Mintern *et al.*, 2015). It is therefore conceivable, that the CD11c^{+}/MHC class II^{+} population of BMDCs comprise a melange of APCs that may differentially make use (or not) of the autophagy machinery. Additionally, these subsets might fundamentally differ in their capacity to present CD1d ligands to begin with. We therefore continued to study DC-mediated iNKT cell activation using FAC-sorted CD11c^{+} splenic DCs.

Loss of *Atg5* in CD11c^{+} DCs significantly impaired CD1d internalization, therefore leading to increased expression of stimulatory CD1d-glycolipid complexes, prolonged iNKT cell responses and helped in clearing *Sphingomonas paucimobilis* infection *in vivo*.

The turnover of CD1d molecules is largely determined by their internalization and recycling. Data in reference not only to CD1d but also other CD1 isotypes suggest that *de novo* synthesized CD1d molecules are guided via signal sequences into the ER (Sugita *et al.*, 1997), where self-lipids are likely to be loaded upon CD1d (De Silva *et al.*, 2002; Park *et al.*, 2004) which may function either as self-antigen or stabilizing chaperones ensuring structural integrity during trafficking through the secretory pathway towards the cell surface (Batuwangala *et al.*, 2004; Bauer *et al.*, 1997; Brutkiewicz *et al.*, 1995; Garcia-

Alles *et al.*, 2006; Sugita *et al.*, 1997). In an independent CD1d-trafficking pathway however, CD1d associates with the invariant chain (Ii), which governs CD1d/Ii-complexes prior from reaching the plasma membrane from the *trans*-Golgi network into lysosomal compartments (Jayawardena-Wolf *et al.*, 2001; Kang and Cresswell, 2002a). Conversely, professional APCs, deficient in Ii expression, show significantly increased levels of CD1d on the surface (Jayawardena-Wolf *et al.*, 2001) over Ii-competent APCs while control proteins such as the transferrin receptor were unaffected. Interestingly, Chervonsky and colleagues suggested before that Ii which is not associated with MHC class II molecules might be directed to endosomal/lysosomal compartments via the autophagic pathway (Chervonsky and Sant, 1995).

Internalization of CD1d, which contains a tyrosine-based endosomal-targeting motif in its cytoplasmic tail, follows a clathrin-dependent pathway that allows binding of CD1d to adaptor protein complexes (AP) and is essential for their ability to sample antigens in the endocytic system (Chiu *et al.*, 2002; Sugita *et al.*, 1999). CD1d molecules can bind both AP2, which mediates CD1d internalization from the plasma membrane, and AP3, which targets internalized CD1d molecules from the early recycling pathway to late endosomes and lysosomes (Elewaut *et al.*, 2003; Lawton *et al.*, 2005; Sugita *et al.*, 2002). During macroautophagy, LC3-conjugation to the autophagosomal membrane promotes the recruitment of specific substrates into autophagosomes via LC3-binding anchor proteins which function as selective autophagy receptors. A structural prerequisite for these anchor proteins to interact with LC3 is the presence of so-called LC3-interacting regions (LIRs) (Noda *et al.*, 2010). A representative of these motifs could first be identified in p62/sequestosome (SQSTM)1 (Pankiv *et al.*, 2007). Later, the functional sequence crucial for the protein-protein interaction with 2 hydrophobic pockets in LC3 was narrowed down to a tetrapeptide with the consensus sequence of W/Y/F-X-X-I/L (Ichimura *et al.*, 2008; Noda *et al.*, 2008). Using LC3 affinity purification and mass spectrometry analysis, immunoprecipitation, as well as live imaging analysis, Tian et al. (Y. Tian *et al.*, 2013) recently identified AP2 as binding protein of LC3. Mutation of the identified LIR sequence "WKQL" to alanine repeats abrogated LC3 coimmunoprecipitation with AP2 (Y. Tian *et al.*, 2013). AP2 is a heterotetrameric protein complex consisting of the subunits α, β, μ, and σ (AP2A1, AP2B1, AP2M1,

AP2S1) (Keen, 1987). While the α subunit was shown to facilitate binding to target membranes (Hirst and M. S. Robinson, 1998; Kirchhausen, 1999) and the β subunit recruits clathrin via a clathrin box (Brodsky *et al.*, 2001), the μ subunit mediates cargo recognition with its phosphoinositide-binding site (Bonifacino and Traub, 2003; Nakatsu and Ohno, 2003). Apart from sterically stabilizing the AP2 complex, the precise function of the small subunit σ has not been elucidated (Collins *et al.*, 2002).

Investigating the effects of ATG5-mediated internalization of CD1d *in vivo*, we first did not observe evidence for increased iNKT cell activation upon glycolipid application. Unlike conventional T cells, iNKT cells rapidly release copious amounts of cytokines upon engagement of their invariant TCR and amongst others, IFNγ and IL-4 are prototypical cytokines secreted by iNKT cells upon activation (Bendelac *et al.*, 2007). One of the characteristics of this innate T cell subset however is the immediate downregulation of numerous surface receptors including their TCR (Wilson *et al.*, 2003) which initially led to the misinterpretation that iNKT cells would undergo dramatic cell death upon ligand recognition (Eberl and MacDonald, 1998; Leite-de-Moraes *et al.*, 2000). Since the gold standard for detection of iNKT cells is staining with lipid-loaded CD1d-multimers (Benlagha *et al.*, 2000; Matsuda *et al.*, 2000) and therefore requires surface expression of their TCR, glycolipid-binding-induced TCR downregulation precluded a robust evaluation of iNKT cell frequencies and phenotypes by lipid-loaded CD1d-multimers after αGalCer challenge *in vivo* at early time points.

The physiological consequence of facilitated internalization of CD1d by autophagy might be an increased colocalization of CD1d with antigens that require intracellular loading, for example lipid antigens released by bacteria during lysosomal degradation. Autophagy is currently being explored for its efficacy to enhance MHC class II presentation of potential *vaccine* antigens in order to establish long-lasting T cell memory and to support antigen-specific $CD8^+$ T cell function (Berner *et al.*, 2007; Jagannath *et al.*, 2009; Marzo *et al.*, 2000; Ravindran *et al.*, 2014) Our data suggest that ATG5 is an essential component of a non-canonical autophagy pathway which exerts a tuning function in lipid antigen presentation. Depending on the targets of intervention and depending on which other components besides ATG5 are shared between canonical and this non-canonical pathway, targeting macroautophagy for

improved $CD4^+$ T cell immunity might limit the efficacy of vaccination strategies that include NKT cell ligands as adjuvants.

Similar to the MHC class I-like molecule CD1d, a recent study found that surface levels of classical MHC class I molecules are elevated due to decreased endocytosis and degradation in ATG5-deficient DCs (Loi *et al.*, 2016). However, AP2 components were not significantly reduced in immunoprecipitates of classical MHC class I molecules derived from *Atg5*-deficient cells compared to controls. Instead, *Atg5*-deficiency compromised MHC class I-association with AAK1 which is known to support AP2-independent, but clathrin-dependent endocytosis pathways (Gupta-Rossi *et al.*, 2011; D. M. Henderson and Conner, 2007; Loi *et al.*, 2016). Furthermore, LIR motifs have also been described in clathrin itself (Rogov *et al.*, 2014). Thus, autophagy proteins appear to affect different clathrin-dependent pathways for the internalization and degradation of classical and non-classical MHC class I molecules, respectively.

Loss of autophagy proteins has recently been reported to exert a T cell-intrinsic role in regulating iNKT cell development (Pei *et al.*, 2015; Salio, Puleston, *et al.*, 2014). Mice with T lymphocyte-specific deletion of *Atg5* or *Atg7* show reduced progression of thymic iNKT cells through the cell cycle and lower frequencies of both thymic and peripheral iNKT cell populations due to increased apoptosis and impaired survival (Pei *et al.*, 2015; Salio, Puleston, *et al.*, 2014). Frequencies of thymic and peripheral iNKT cells were unchanged in DC-*Atg5*$^{-/-}$ mice supporting the notion that the reported deficit in iNKT cell differentiation is cell-autonomous. Our data show that while autophagy proteins regulate iNKT cell development via T cell-intrinsic effects, they attenuate peripheral iNKT activation through their function in DC-mediated antigen processing and presentation.

Collectively, these data indicate that absence of the autophagy machinery protein ATG5 leads to increased CD1d-mediated lipid presentation due to stabilization of CD1d on the cell surface by interfering with AP2-mediated internalization.

3.4 Concluding Remarks

Our findings identified ATG5 in $CD11c^+$ DCs as a key regulator for both conventional and unconventional T cells and broaden the concept of ATG-mediated antigen presentation beyond canonical macroautophagy. ATG5-regulated phagocytosis supports $CD4^+$ T cell immunity through mediating the loading and processing of extracellular antigen onto MHC class II molecules while ATG5-controlled internalization of CD1d restrains iNKT cell responses. The use and function of ATG5 is, therefore, context-dependent and a clear and comprehensive concept of how the autophagy machinery couples to antigen-presentation and lymphocyte activation appears to be required to predict the outcome of therapeutic interventions in this pathway to boost adaptive immunity.

4. Materials and Methods

4.1 Materials

4.1.1 Machines

Machine	Company
autoMACS Pro Separator	Miltenyi Biotech (Bergisch Gladbach, Germany)
BD FACSCanto-II	BD Biosciences (San Jose, USA)
BD LSR Fortessa	BD Biosciences (San Jose, USA)
C1000 Thermal Cycler	Bio-Rad (Hercules, USA)
CLSM Leica SP5 Mid UV-VIS	Leica Microsystems (Heerbrugg, Switzerland)
Eppendorf Thermomixer 21516-170	Eppendorf (Hamburg, Germany)
Fusion FX Detector	Vilber-Lourmat (Eberhardzell, Germany)
Leica DM IL LED Microscope	Leica Microsystems (Heerbrugg, Switzerland)
Microplate Reader Infinite M1000 Pro	Tecan (Männedorf, Switzerland)
Multipurpose Centrifuge 5810 R	Eppendorf (Hamburg, Germany)
SDS-PAGE Chamber Set Up	Bio-Rad (Hercules, USA)
Sorvall Legend RT Plus Centrifuge	Thermo Scientific (Rockford, USA)
Sorvall RC 6 Plus Superspeed Centrifuge	Thermo Scientific (Rockford, USA)
Tissue Lyzer	Qiagen Instruments (Hombrechtikon, Switzerland)

Waldmann UV 181 BL Irradiation Unit	Waldmann Group (Villingen-Schwenningen, Germany)

4.1.2 Antibodies, Flow Cytometry and Cellular Assays

Antigen	Fluorochrome	Clone	Dilution/ Concentration	Company
CD103	APC	2E7	1:50	Biolegend (San Diego, USA)
CD11b	APC-Cy7	M1/70	1:200	Biolegend (San Diego, USA)
CD11c	APC	N418	1:200	Biolegend (San Diego, USA)
CD11c	PE-Cy7	N418	1:400	Biolegend (San Diego, USA)
CD16/32	unconjugated	2.4G2	22.4 µg/ml	Bio X Cell (West Lebanon, USA)
CD19	Alexa Fluor 700	eBio1D3	1:200	eBioscience (San Diego, USA)
CD19	Pacific Blue	6D5	1:400	Biolegend (San Diego, USA)
CD1d	PE	1B1	1:50	eBioscience (San Diego, USA)
CD1d	unconjugated	1B1	1:50	Biolegend (San Diego, USA)

CD1d	biotinylated	1B1	1:50	Biolegend (San Diego, USA)
CD25	Brilliant Violet 605	PC61	1:200	Biolegend (San Diego, USA)
CD4	Alexa Fluor 700	GK1.5	1:200	eBioscience (San Diego, USA)
CD4	Pacific Blue	GK1.5	1:400	Biolegend (San Diego, USA)
CD40	unconjugated	FGK4.5/ FGK45)	1:200	Bio X Cell (West Lebanon, USA)
CD40	PE	3/23	1:50	Biolegend (San Diego, USA)
CD40	PE-Cy	3/23	1:50	Biolegend (San Diego, USA)
CD44	PerCP-Cy5.5	IM7	1:100	eBioscience (San Diego, USA)
CD45	APC-Cy7	30-F11	1:400	BD Biosciences (San Jose, USA)
CD45.2	Pacific Blue	104	1:400	Biolegend (San Diego, USA)
CD62L	PE-CF594	MEL-14	1:100	BD Biosciences (San Jose, USA)
CD86	Brilliant Violet	GL-1	1:200	Biolegend (San Diego,

	650			USA)
CD8α	PE-CF594	53-6.7	1:400	BD Biosciences (San Jose, USA)
CD8α	Brilliant Violet 510	53-6.7	1:200	Biolegend (San Diego, USA)
CD8α	FITC	53-6.7	1:400	eBioscience (San Diego, USA)
CD8α	Brilliant Violet 785	53-6.7	1:100	Biolegend (San Diego, USA)
CD8α	PerCP-Cy5.5-	53-6.7	1:100	eBioscience (San Diego, USA)
FOXP3	PerCP-Cy5.5	FJK-16s	1:100	eBioscience (San Diego, USA)
GM-CSF	PE	MP1-22E9	1:250	BD Biosciences (San Jose, USA)
I-A^b	Pacific Blue	M5/114.15.2	1:200	Biolegend (San Diego, USA)
I-A^b	APC	M5/114.15.2	1:800	Biolegend (San Diego, USA)
IFNγ	FITC	XMG1.2	1:400	Biolegend (San Diego, USA)
IL-12/IL-23 p40	PE	C17.8	1:100	eBioscience (San Diego, USA)

IL-17A	PE-Cy7	TC11/18 H10	1:200	Biolegend (San Diego, USA)
Ly-6C	PerCP-Cy5.5	HK1.4	1:200	Biolegend (San Diego, USA)
Ly-6G	Alexa Fluor 700	1A8	1:200	Biolegend (San Diego, USA)
TCRβ	APC	H57-597	1:50	eBioscience (San Diego, USA)
Vβ11 TCR	PE	RR3-15	1:300	BD Biosciences (San Jose, USA)
αGalCer:CD1d-complex	PE	L363	1:50	eBioscience (San Diego, USA)

4.1.3 Miscellaneous

Isotype /Streptavidin/etc.	**Fluorochrome**	**Clone**	**Dilution**	**Company**
Annexin V	FITC	---	1:20	BD Biosciences (San Jose, USA)
anti-MOG	unconjugated	8-18C5	1:200	In-house production (Isaak Quast)
IgG2bκ	PE	eB149/ 10H5	1:50	eBioscience (San Diego, USA)
Streptavidin	PE	---	1:400	Biolegend (San Diego, USA)

4.1.4 Primary and Secondary Antibodies for Immunocytochemistry

Conjugate	Reactivity	Isotype	Dilution	Company
Alexa Fluor488	donkey anti-goat	IgG (H+L)	1:500	Life Technologies (Zug, Switzerland)
Alexa Fluor488	goat anti-rabbit	IgG (H+L)	1:500	Life Technologies (Zug, Switzerland)
Alexa Fluor555	rabbit anti-mouse	IgG (H+L)	1:500	Life Technologies (Zug, Switzerland)
Alexa Fluor555	goat anti-rat	IgG (H+L)	1:500	Life Technologies (Zug, Switzerland)
AP2	mouse anti-mouse	IgG (H+L)	1:250	BD Biosciences (San Jose, USA)
EEA1, unconjugated	goat anti-mouse	polyclonal	1:250	Antibodies-online
LC3, unconjugated	rabbit anti-mouse	polyclonal	1:250	MBL (Woburn, USA)

4.1.5 Tetramer

Tetramer	Fluorochrome	Dilution	Company
Non-ligand carrier-loaded murine CD1d tetramer (negative control)	PE	1:100	ProImmune (Oxford, UK)
αGalCer-loaded murine CD1d tetramer	PE	1:100	ProImmune (Oxford, UK)

4.1.6 MACS Beads

Product	Company
Anti-murine CD11c MicroBeads	Miltenyi Biotech (Bergisch Gladbach, Germany)
Anti-murine CD4 (L3T4) MicroBeads	Miltenyi Biotech (Bergisch Gladbach, Germany)

4.1.7 General Material

Product	Company
"Rapid"-Filtermax 250 Filters	TPP Techno Plastic Products AG (Trasadingen, Switzerland)
1 ml Syringe Luer-Lok™ Tip	BD Medical (Le Pont de Claix Cedex, France)
1.8 ml Cryo Pure Tubes	Sarstedt (Nümbrecht, Germany)
17 ml Tube, Thinwall, Ultra-clear™, 16 × 102 mm Tubes (for ultracentrifuge rotors)	Beckmann Coulter (Brea, USA)
25G × 25 mm Needles	BD Microlance (Heidelberg, Germany)
30G × 12 mm Needles	BD Microlance (Heidelberg, Germany)
8-Well Glass Chamber Slides	Lab-Tek/Nunc (Rochester, USA)
Butterfly™ Winged Infusion Set, 21G × 19 mm	Hospira (Warwickshire, UK)
C-Chip Neubauer Improved DHC-N01, Disposable Hemocytometer	Digital-Bio (Seoul, South Korea)
Carbon Steel Surgical Blades	Swann-Morton (Sheffield, UK)
Cell Freezing Container	Thermo Scientific (Rockford, USA)

Cell Scraper (13 mm)	SPL Life Sciences (Pocheon, South Korea)
Eppendorf Safe Lock Tubes	Sarstedt (Nümbrecht, Germany)
FACS Tubes, 5 ml, Polystyrene Round Bottom	BD Falcon / Bioswisstech (Schaffhausen, Switzerland)
FACS Tubes, 5 ml, Polystyrene Round Bottom (with cell strainer cap)	BD Falcon / Bioswisstech (Schaffhausen, Switzerland)
Microtainer Tubes K2E	BD Biosciences (San Jose, USA)
Microtainer Tubes SST	BD Biosciences (San Jose, USA)
Non-Tissue Culture Treated Round Petri Dishes, ⦸ 90 mm	Thermo Fisher Scientific AG (Reinach, Switzerland)
PVDF Membrane	GE Healthcare (Little Chalfont, UK)
Reusable Hemocytometer	Hecht-Assistant (Sondheim v.d. Rhön, Germany)
Sealing Tape for ELISA Plates	Nunc / Thermo Fisher Scientific AG (Reinach, Switzerland)
Syringes (2, 5, 10, 20, 50 ml)	Braun (Melsungen, Germany)
Tissue Culture Treated Round Dishes, ⦸ 100 mm	Sigma-Aldrich (St. Louis, USA)
U-100 Insulin Syringe (29G × 12.7 mm)	BD Medical (Le Pont de Claix Cedex, France)
Whatman Blotting Paper 3 mm CHR	VWR international (Radnor, USA)

4.1.8 NKT Cell Agonists

Product	Company
NKT cell agonist variants	GSL-1 and GalαGalCer were kindly provided by Paul B. Savage, BYU, Provo, UT, USA.

α-Galactosylceramide (αGalCer)	Adipogen AG (Liestal, Switzerland)

4.1.9 General Reagents

Product	Company
4',6-Diamidino-2-Phenylindole, Dihydrochloride	Life Technologies (Zug, Switzerland)
ACK Lysing Buffer	Life Technologies (Zug, Switzerland)
Acrylamide/Bis-acrylamide, 30% Solution	Bio-Rad (Hercules, USA)
Agarose, LE, Analytical Grade	Promega (Dübendorf, Switzerland)
Ammonium Persulfate (APS)	Sigma-Aldrich (St. Louis, USA)
Bovine Serum Albumin	Amresco (Solon, USA)
Bovine Serum Albumin Solution, 30%	Sigma-Aldrich (St. Louis, USA)
Brefeldin A	Sigma-Aldrich (St. Louis, USA)
Carboxyfluorescein Succinimidyl Ester	eBioscience (San Diego, USA)
Chloroquine	InvivoGen (San Diego, USA)
Collagenase D	Roche (Rotkreuz, Switzerland)
Complete Freund's Adjuvant	Difco / BD Biosciences (San Jose, USA)
cOmplete Protease Inhibitor Cocktail Tablets	Roche (Rotkreuz, Switzerland)
CpG ODN 1826	InvivoGen (San Diego, USA)

Cycloheximide	Sigma-Aldrich (St. Louis, USA)
DMSO	Sigma-Aldrich (St. Louis, USA)
DNA Loading Dye, 6×	Fermentas / Thermo Fisher Scientific AG (Reinach, Switzerland)
DNAse	QIAGEN Instruments AG (Hombrechtikon, Switzerland)
dNTPs, 10 mM	QIAGEN Instruments AG (Hombrechtikon, Switzerland)
Dulbecco's Modified Eagle Medium (4.5 g/L Glucose)	Biochrom AG (Berlin, Germany)
ECL Western Blotting Substrate	Thermo Scientific (Rockford, USA)
EDTA	Sigma-Aldrich (St. Louis, USA)
Ethanol	Sigma-Aldrich (St. Louis, USA)
Fetal Calf Serum	Biochrom AG (Berlin, Germany)
GelRedTM Nucleic Acid Gel Stain, 10000×	Biotium (Hayward, USA)
GeneRuler 100 bp DNA Ladder	Fermentas / Thermo Fisher Scientific AG (Reinach, Switzerland)
Imiquimod	InvivoGen (San Diego, USA)
Ionomycin	Sigma-Aldrich (St. Louis, USA)
Isoflurane	Piramal Healthcare (Mumbai, India)
Isopropanol	Sigma-Aldrich (St. Louis, USA)

L-Glutamine 200 mM 100×	Gibco / Thermo Fisher Scientific AG (Reinach, Switzerland)
Lipopolysaccharide (LPS)	InvivoGen (San Diego, USA)
MEM Non-Essential Amino Acids (NEAA) Solution (100×)	Gibco/Thermo Fisher Scientific AG (Reinach, Switzerland)
Methanol	Sigma-Aldrich (St. Louis, USA)
Muller-Hinton Agar	Sigma-Aldrich (St. Louis, USA)
Mycobacterium Tuberculosis H37 Ra (Desiccated)	Difco / BD Biosciences (San Jose, USA)
NaN_3	Sigma-Aldrich (St. Louis, USA)
Normal Goat Serum	Sigma-Aldrich (St. Louis, USA)
NP-40	Sigma-Aldrich (St. Louis, USA)
OneComp eBeads	eBioscience (San Diego, USA)
Pam_3CSK_4	InvivoGen (San Diego, USA)
Paraformaldehyde	Santa Cruz Biotechnology Inc. (Dallas, USA)
PCR Reaction Buffer with Mg^{2+}	Roche (Rotkreuz, Switzerland)
Penicillin	Biochrom AG (Berlin, Germany)
Percoll	GE Healthcare (Little Chalfont, UK)
Pertussis Toxin from *B. pertussis* (in Glycerol)	List Biological Laboratories, Inc (Campbell, USA)
Phorbol 12-Myristate 13-Acetate (PMA)	Sigma-Aldrich (St. Louis, USA)

Phosphate Buffered Saline (PBS)	Cantonal Pharmacy (Zurich, Switzerland)
Pipet Tips with Microcapillary for Gel-Loading	VWR (Radnor, USA)
Poly-L-lysine	Sigma-Aldrich (St. Louis, USA)
Poly(I:C)	InvivoGen (San Diego, USA)
Precision Plus Protein Dual Color Standards	Bio-Rad (Hercules, USA)
ProLong Gold Antifade Reagent	Life Technologies (Zug, Switzerland)
Proteinase K	Roche (Rotkreuz, Switzerland)
Rapamycin	Sigma-Aldrich (St. Louis, USA)
ReBlot Plus Strong Antibody Stripping Solution, 10×	Merck / Millipore (Schaffhausen, Switzerland)
Recombinant Murine GM-CSF	Life Technologies (Zug, Switzerland)
Recombinant Murine IL-2	R&D Systems (Minneapolis, USA)
Recombinant Murine IL-23	eBioscience (San Diego, USA)
Roswell Park Memorial Institute-1640 Medium (RPMI-1640)	Biochrom AG (Berlin, Germany)
Saponin	Sigma-Aldrich (St. Louis, USA)
Sodium Dodecyl Sulfate (SDS)	Sigma-Aldrich (St. Louis, USA)
SDS, 20% solution	Fluka / Sigma-Aldrich (St. Louis, USA)
Streptomycin	Biochrom AG (Berlin, Germany)

Taq DNA Polymerase	Roche (Rotkreuz, Switzerland)
TEMED	Bio-Rad (Hercules, USA)
Triton X-100	Sigma-Aldrich (St. Louis, USA)
Trypan Blue	Gibco / Thermo Fisher Scientific AG (Reinach, Switzerland)
Trypsin-EDTA 0.25%	Gibco / Thermo Fisher Scientific AG (Reinach, Switzerland)
Tween 20	Sigma-Aldrich (St. Louis, USA)
β-Mercaptoethanol	Gibco/Thermo Fisher Scientific AG (Reinach, Switzerland)

4.1.10 Kits

Product	**Company**
Cytofix/Cytoperm Fixation/Permeabilization Solution Kit	BD Biosciences (San Jose, USA)
FOXP3 Staining Buffer Set	eBioscience (San Diego, USA)
LIVE/DEAD Fixable Aqua Dead Cell Stain Kit	Life Technologies (Zug, Switzerland)
LIVE/DEAD Fixable Near-IR Dead Cell Stain Kit	Life Technologies (Zug, Switzerland)
Mouse IFNγ Instant ELISA Kit	eBioscience (San Diego, USA)
Mouse IL-12/-23 (p40) ELISA Development Kit	Mabtech AB (Nacka Strand, Sweden)
Mouse IL-2 Ready-SET-GO ELISA Reagent Kit	eBioscience (San Diego, USA)
Mouse IL-4 Instant ELISA Kit	eBioscience (San Diego, USA)
Permeabilization Solution Kit	BD Biosciences

	(San Jose, USA)
Pierce BCA Protein Assay Kit	Thermo Scientific (Rockford, USA)

4.1.11 MOG Protein and Peptide

Product	Company
MOG_{35-55} Peptide (MEVGWYRSPFSRVVHLYRNGK)	GenScript (Piscataway, USA)
Recombinant MOG_{1-124} Protein	In-house production (Christina Sina/Isaak Quast)

4.1.12 OVA Peptide

Product	Company
$OVA_{323-339}$ Peptide *(ISQAVHAAHAEINEAGR)*	InvivoGen (San Diego, USA)

4.1.13 Antibodies for T Cell Stimulation During Coculture Assays

Antigen	Clone	Final concentration	Company
CD28	37.51	5 µg/ml	BD Biosciences (San Jose, USA)
CD3	145-2C11	5 µg/ml	BD Biosciences (San Jose, USA)

4.1.14 Antibodies (1° and 2°) for Western Blot

Antigen	Dilution	Company
ATG5-ATG12 complex	1:400	Biomol (Hamburg, Germany)
HRP-conjugated goat anti-mouse IgG	1:10000	Bio-Rad (Hercules, USA)
HRP-conjugated β-Actin	1:50000	Abcam (Cambridge, UK)
LC3	1:1000	Biomol (Hamburg, Germany)

4.1.15 Plastic Supplies

Plastic supplies such as multiwell plates, disposable plastic pipettes and plastic reaction tubes were obtained from Becton Dickinson Labware (FALCON), VWR International, Costar and Nunc.

4.1.16 Cell Lines and Bacteria

Specimen	Kindly provided by/Bought from
A.407 iNKT Cell Hybridoma Cell Line (murine, C57BL/6 background)	Stefan Freigang, Institute of Pathology, Department of Experimental Pathology, University of Bern, Bern, Switzerland
FF13 iNKT cell Hybridoma Cell Line (murine, C57BL/6 background))	Gennaro DeLibero, Singapore Immunology Network, Agency for Science, Technology and Research (A*STAR), Singapore, Singapore and Department of Biomedicine, Laboratory of Experimental Immunology, University Hospital Basel, University of Basel, Basel, Switzerland

Immortilized *Atg5*-deficient macrophage cell line + respective *Atg5*-competent control cell line (designated MΘ-*Atg5*$^{-/-}$ and MΘ-*Atg5*$^{+/+}$) (murine, C57BL/6 background)	Eicke Latz, Institute of Innate Immunity Biomedical Center, University Hospitals / University of Bonn, Bonn, Germany
MO3.13 Glial (Oligodendrocytic) hybrid cell line (MOG-transduced and wild type cell lines)	Fabienne Brilot-Turville, *Brain Autoimmunity Group* *Institute for Neuroscience and Muscle Research (INMR)* *The Kids Research Institute at the Children's Hospital at Westmead* University of Sydney, Australia
RAW 264.7 Leukaemic monocyte macrophage cell line (murine, BALB/c background)	ATCC (Wesel, Germany)
Sphingomonas paucimobilis	ATCC (Wesel, Germany)

4.1.16.1 NKT Cell Hybridoma Lines

The Vα14^{+}/Vβ8^{+} iNKT cell hybridoma A.407 was generated by fusion of *ex vivo* CD1d tetramer-sorted NKT cells with the murine thymoma BW5147 (S.F. unpublished data). The FF13 hybridoma was generated by fusion of Vα14i NKT cells sorted from αGalCer-treated C57BL/6 mice with mouse BW5147 thymic lymphoma cells (Schümann *et al.*, 2007).

4.1.16.2 *Atg5*-Deficient Immortalized Macrophage-Like Cell Line

The *Atg5*-deficient immortalized macrophage cell line was kindly provided by Eicke Latz (Institute of Innate Immunity Biomedical Center, Bonn Germany). Immortilized cell lines were generated from DC-*Atg5*$^{-/-}$ mice using a J2 recombinant retrovirus carrying v-myc and v-raf(mil) oncogenes as previously described (Peitz *et al.*, 2002; Roberson and Walker, 1988). For functional disruption of macroautophagy in DC-*Atg5*$^{-/-}$-derived macrophages through

conditional mutagenesis using TAT-Cre transduction, a cell-permeable Cre recombinase was titrated onto the cells, which resulted in deletion of floxed target genes upon recombination.

4.1.17 PCR Primers

Primer name	Primer Target	Primer sequence (5'- 3')
CS003	*Atg5*$^{flox/flox}$	GAATATGAAGGCACACCCCTGAAATG
CS004	*Atg5*$^{flox/flox}$	GTACTGCATAATGGTTTAACTCTTGC
CS005	*Atg5*$^{flox/flox}$	ACAACGTCGAGCACAGCTGCGCAAGG
CS006	*Atg5*$^{flox/flox}$	CAGGGAATGGTGTCTCCCAC
CS007	CD11c-Cre-GFP	GCGGTCTGGCAGTAAAAACTATC
CS008	CD11c-Cre-GFP	GTGAAACAGCATTGCTGTCACTT
CS009	CD11c-Cre-GFP (positive control)	CTAGGCCACAGAATTGAAAGATCT
CS010	CD11c-Cre-GFP (positive control)	GTAGGTGGAAATTCTAGCATCATCC

4.1.18 Cell Culture Media

All media were filter-sterilized with 0.2 µm filters prior to use and stored at 4 °C.

Medium	Ingredients
D10	DMEM Medium (high glucose)
	10% Heat Inactivated FCS
	1% Penicillin/Streptomycin
R10	RPMI-1640 Medium
	10% Heat Inactivated FCS
	1% Penicillin/Streptomycin
BMDC Medium	RPMI-1640 Medium
	20% Heat Inactivated FCS
	1% Penicillin/Streptomycin
	50 µM β-Mercaptoethanol
	2.5 ng/ml GM-CSF (carrier-free)

Restimulation Medium (adoptive transfer)	RPMI-1640 Medium 10% Heat Inactivated FCS 1% Penicillin/Streptomycin IL-23 (20 ng/ml) MOG_{35-55} (20 µg/ml)
Freezing Medium	Heat Inactivated FCS 10% DMSO
Hybridoma Media for A.407 and FF13 iNKT Cell Lines	RPMI-1640 Medium 10% Heat inactivated FCS 1% Penicillin/Streptomycin 2mM L-Glutamin 1% Non-Essential Amino Acid Solution

4.1.19 General Buffers

Buffer	**Ingredients**
PBS (1×) pH 7.4	137 mM NaCl 2.7 mM KCl 10 mM Na_2HPO_4 1.8 mM KH_2PO_4 Adjust pH to 7.4 with HCl and add H_2O to 1 L
Tail Lysis Buffer (1×; stored at RT)	100 mM Tris, pH 8.0 100 mM NaCl 10 mM EDTA, pH 8.0 0.2% SDS 0.2 mg/ml Proteinase K (added freshly for each digestion)
Cell Lysing Buffer (for protein quantification; prepared freshly each time)	PBS 1% NP-40 1× Protease Inhibitor Cocktail
Tissue Digestion Buffer (for spleen; prepared freshly each time)	PBS 0.4 mg/ml Collagenase D 20 µg/ml DNase

Tissue Digestion Buffer (for CNS; prepared freshly each time)	RPMI-1640 0.2 mg/ml Collagenase D 20 µg/ml DNase
FACS Buffer (stored at 4 °C)	PBS 0.5% Bovine Serum Albumin (BSA) 0.01% NaN_3
Sorting Buffer	PBS 2% BSA
MACS Buffer (stored at 4 °C)	PBS 2 mM EDTA 0.5% BSA
Annexin V Staining Buffer (stored at 4 °C)	10 mM Hepes/NaOH; pH 7.4 140 mM NaCl 2.5 mM $CaCl_2$
TBE (5×; stored at RT)	44.5 mM Tris Base; pH 8.5 44.5 mM Boric Acid 2 mM EDTA
Laemmli Buffer (stored at −20 °C)	60 mM Tris-Cl, pH 6.8 2% SDS 10% Glycerol 5% β-Mercaptoethanol 0.01% Bromophenol Blue

4.1.20 Buffers Immunocytochemistry

Buffer	Ingredients
Blocking Buffer	PBS 10% Normal Goat Serum (NGS) 1% BSA
Dilution Buffer	PBS 10% NGS 1% BSA 0.1% Saponin
Fixation Buffer	PBS 4% PFA

Permeabilization Buffer	PBS
	0.1% Triton X-100
Washing Buffer	PBS
	0.01% Saponin

4.1.21 Buffer for SDS-PAGE and Western Blot

Buffer	Ingredients
PBS-T	PBS
	0.1% Tween 20
Running Buffer 10×, pH 8.3, 1L	30.3 g Tris base
	144 g Glycine
	10 g SDS
	H_2O
1.5 M Tris, pH 8.8 (150 ml)	27.23 Tris Base
	H_2O
1.5 M Tris pH 6.8 (100 ml)	18.17 g Tris Base
	H_2O
Transfer buffer 1×	25 mM Tris Base
	192 mM Glycine
	20% Methanol

4.1.22 ELISA Buffer

Buffer	Ingredients
ELISA Wash buffer	PBS
	0.05% Tween 20

4.1.23 Recipes for SDS-PAGE Gels (0.75 mm)

Components	12% Resolving gel (2 gels)	Stacking gel (2 gels)
Acrylamide/Bis-acrylamide, 30% Solution [ml]	4.8	1.5
0.5M Tris pH 6.8 [ml]	---	1.2
2M Tris pH 8.8 [ml]	2.5	---

20% SDS [µl]	60	45
H_2O	4.5	6.3
TEMED	24	12
APS	96	80

4.1.24 Percoll Solutions

4.1.24.1 Leukocyte Isolation from Mouse Liver

Solution	Ingredients
90% Percoll Solution (50 ml)	45 ml Percoll
	5 ml PBS (10×)
70% Percoll Solution (50 ml)	38,9 ml 90% Percoll Solution
	11.1 ml PBS (1×)
40% Percoll Solution (45 ml)	20 ml 70% Percoll Solution
	15 ml PBS (1×)

4.1.24.2 Leukocyte Isolation from Mouse CNS

Solution	Ingredients
30% Percoll Solution (15 ml; for one CNS)	10.5 ml PBS (1×)
	4.5 ml Percoll

4.1.25 Optical Configurations of Flow Cytometers Used

4.1.25.1 BD SLR Fortessa

Laser [wave length]	Mirror	Filter	Applicable Dyes
Violet [405 nm]	735 LP	800/50	Qdot800, BV785
	685 LP	710/50	Qdot705, BV711
	640 LP	670/30	Qdot 655, eFluor650nc, BV650,
	600 LP	610/20	Qdot605, eFluor 605nc, BV605
	505 LP	525/50	AmCyan, Aqua L/D stain, Pacific
		450/50	Orange, BV510
			Pacific Blue, V450, BV421, Cell Trace

			Violet
Blue [488]	635 LP	690/50	PerCP, PerCP-Cy5.5
	505 LP	525/50	FITC, Alexa 488, GFP
		488/10	SSC
Yellow/Green	750 LP	780/60	PE-Cy7
[561]	685 LP	710/50	PE-Cy5.5
	635 LP	670/30	PE-Cy5, 7AAD
	600 LP	610/20	PE-Texas Red, mCherry
		582/15	PE, DsRED, PKH26
Red [640]	750 LP	780/60	APC-Cy7, APC-H7, APC-Alexa750,
	685 LP	730/45	Near IR-L/D stain
		670/30	AlexaFluor 700
			APC, Alexa 647, TO-PRO-3

4.1.25.2 BD FACSCanto-II

Laser [wave length]	**Mirror**	**Filter**	**Applicable Dyes**
Violet [405 nm]	502 LP	510/50	AmCyan, Aqua L/D stain
		450/50	Pacific Blue, V450, BV421, Cell Trace Violet
Blue [488]	735 LP	780/60	PE-Cy7
	655 LP	670 LP	PerCP, PerCP-Cy5.5, 7AAD
	556 LP	585/42	PE, DsRED, PKH26
	502 LP	530/30	FITC, Alexa 488, GFP
		488/10	SSC
Red [640]	750 LP	780/60	APC-Cy7, APC-H7, APC-Alexa750,
	685 LP	660/20	Near IR-L/D stain
			APC, Alexa 647, TO-PRO-3

4.2 Methods

4.2.1 Mice

8 to 12 weeks old C57BL/6 mice (female and male) were purchased from Janvier Labs. C57BL/6J-Tg(Itgax-cre,-EGFP)4097Ach/J mice (designated CD11c-Cre Tg)

were purchased from Charles River. Atg5$^{flox/flox}$ mice (Hara *et al.*, 2006), were a kind gift of Noboru Mizushima (University of Tokyo, Japan). MOG-specific TCR transgenic mice C57BL/6-Tg(Tcra2D2,Tcrb2D2)1Kuch/J (designated 2D2/TCR^{MOG}) were a kind gift from Vijay K. Kuchroo (Harvard Institutes of Medicine, USA) / Burkhard Becher (University of Zurich, Switzerland). All animals were bred and housed in the University of Zurich animal facility in individually ventilated cages on a 12 h light/dark cycle with food and water available *ad libitum* according to institutional guidelines and Swiss animal laws. Atg5$^{flox/flox}$ mice were crossed to CD11c-Cre Tg mice to obtain CD11c Cre-Atg5$^{-/-}$ (designated DC-*Atg5*$^{-/-}$) on a C57BL/6 background. CD11c Cre^{neg}-Atg5$^{fl/fl}$ (designated DC-*Atg5*$^{+/+}$) were used as littermate controls. All animal protocols were approved by and conducted in accordance with the cantonal veterinary office of the canton of Zurich, Switzerland (protocols 25706-ZH209/2014 and ZH210/2014) and the canton of Bern, Switzerland (protocols BE46/14, BE73/14).

4.2.2 Mouse Organ Processing

Mice were euthanized by CO_2 inhalation. Depending on the organ of interest, different leukocyte isolation protocols were applied.

4.2.2.1 Leukocyte Isolation from Spleen, Thymus and Lymph Nodes

Spleens, thymus or lymph nodes were removed, collected in 15 ml tubes containing cold PBS, dissected into small pieces and digested for 30 min at 37 °C and 5% CO_2 with collagenase D (0.4 mg/ml) and DNAse (20 µg/ml) in PBS (3 ml/organ). Digest was stopped by adding 0.5 M EDTA at a 1:50 ratio for the final 5 min at 37 °C and 5% CO_2. The digested tissue was passed through a 70 µm cell strainer to obtain single cell solutions. After a washing step with cold PBS, red blood cell lysis (2 min, RT) was performed using 1 ml ACK lysis buffer per spleen followed by washing with cold PBS. Cell concentration was determined using Neubauer counting chambers and trypan blue staining for the exclusion of dead cells. Samples were kept on ice until further processing.

4.2.2.2 Leukocyte Isolation from Liver

The liver was removed, collected in 50 ml tubes containing cold PBS, dissected into small pieces and digested for 45 min at 37°C and 5% CO_2 with collagenase D

(0.4 mg/ml) and DNAse (20 µg/ml) in PBS (4 ml/organ). The digest was stopped by the addition of EDTA to a final concentration of 10 mM for the last 5 min at 37 °C and 5% CO_2. The digested tissue was passed through a 70 µm cell strainer to obtain a single cell solution. Tubes were spun down at 400 × g and 4 °C for 5 min. The supernatant was discarded and the resulting cell pellet was suspended in 1 ml of a 40% percoll solution. Another 3 ml of 40% percoll solution was added followed by carefully overlaying onto a 4 ml layer of 70% percoll solution in a 15 ml tube. The 40% percoll layer was then overlayed with 2 ml RPMI. The tubes were spun down at 1450 × g and 4°C for 30 min. Acceleration and deceleration speed was set to 4 and 1 (with 9 being maximal speed), respectively. After centrifugation, the top layer was removed and discarded and the visible leukocyte ring was carefully transferred into a new 50 ml tube containing cold PBS. Tubes were centrifuged at 400 × g and 4 °C for 5 min. The supernatant was discarded, cell pellets were resuspended in 1 ml of PBS, cells were counted according to **4.2.25** and afterwards kept on ice until further processing.

4.2.2.3 Leukocyte Isolation from CNS

In order to remove all non-parenchymatic leukocytes from the CNS, the mice were perfused using 50 ml of ice cold PBS by carefully incising the right atrium before a 50 ml syringe with a 21G × 19 mm butterfly needle was inserted into the left ventricle by means of which the circulatory system was flushed. The mouse was decapitated and the cerebrum, cerebellum and the brain stem were carefully removed from the scull and transferred into a 15 ml tube containing 5 ml of ice cold PBS. The spinal cord was exposed as followes: the animal's decapitated body was fixated and the lower extremities were carefully cut off just above the hips in order to expose a caudal access to the spinal canal. A 10 ml syringe with a 25G × 25 mm needle was inserted in the caudal end of the spinal canal and the needle was fixed using a surgical clamp. The spinal canal was quickly flushed with cold PBS in order for the spinal cord to be released intact from the cranial end of the exposed spinal canal. The spinal cord was then carefully removed from the spine and transferred into a 15 ml tube containing 5 ml of ice cold PBS. For each animal, brain and spinal cord were pooled, cut into small pieces using surgical scissors and CNS tissues were suspended in freshly prepared CNS digest buffer (4 ml/CNS) and incubated for 40 min at 37 °C and 5% CO_2. The

digest was terminated by adding 0.5 M EDTA to a final concentration of 10 mM during the last 5 min of the incubation. The following steps were all carried out on ice. Firstly, using a 2 ml syringe punch, the digested tissue was meshed through a 70 µm nylon mesh into a 50 ml tube already containing 5 ml of cold PBS. The tube was filled up with cold PBS and centrifuged at 400 × g and 4 °C for 5 min. The supernatant was discarded and the pellet was suspended in 30% percoll solution. The cell suspension was then transferred into 16 ml ultracentrifuge tubes, positioned in a fixed angle rotor ultracentrifuge and spun down at 10800 rpm for 30 min at 4 °C. Acceleration and deceleration were set to 9 and 1 respectively. The resulting lipid layer was carefully sucked off with a vacuum pump and discarded, the remaining cell layer but the pelleted red blood cells at the bottom of the tube, was transferred into a 50 ml tube which was filled up with cold PBS. The tubes were centrifuged at 400 × g and 4 °C for 5 min. The supernatant was discarded and the remaining cell pellet was suspended in 1 ml of ice cold PBS. Cells were counted according to **4.2.25** and left on ice until further processing.

4.2.3 Bleeding of Mice

Mice were positioned under a heat lamp for 5 min in order for the tail veins to warm up and dilate. Animals were then carefully transferred to a restraining tube device and a lateral vein was incised using sterile blades. Blood samples were collected in K2E Microtainer tubes and blood flow was stopped by applying pressure on the sampling site for approximately 45 sec before the animal was returned to its cage. Blood samples (approximately 50 µl/animal) were quickly spun down at 2000 × g for 10 min at 4 °C, the resulting plasma was transferred into a new 1.5 ml Eppendorff tube, snap frozen using liquid nitrogen and stored at −80 °C until further processing of the sample.

4.2.4 Generation of BMDCs

In order to obtain bone marrow derived DCs, mice were painlessly euthanized with CO_2. Fur, skin and muscles were carefully dissected from lower extremities of the animal (including tibia, femur, hips) until the bare bones were exposed. The femur was detached from tibia and hip without opening up any bones. Individual bones were then cut open distally and a syringe with a 30G × 12 mm

needle was introduced into the bone marrow canal to flush out the bone marrow with sterile cold PBS. The obtained cell solution was collected on a 70 µm cell strainer and passed into a 50 ml tube already containing 5 ml of cold PBS. The tube was filled up with cold PBS, centrifuged at 400 × g for 10 min at 4 °C. After the supernatant was discarded, a red blood cell lysis (2 min, RT) was performed using 1 ml ACK lysis buffer per bone marrow equivalent to one mouse followed by washing with cold PBS. Single cell solutions were kept on ice until further processing. 2.5 - 5 × 10^6 bone marrow cells were plated out in a non-tissue culture treated petri dish in 10 ml of BMDC culture medium (see table 4.1.18 for medium composition). A complete medium change was performed every second day: supernatants including non-adherent bone marrow cells were carefully collected from each dish and centrifuged at 400 × g for 5 min at 4 °C. The resulting pellet was resuspended in 10 ml of fresh BMDC culture medium and the cell suspension was pipetted back into the respective culture dish. Between days 9 - 11 cells were harvested from the culture dishes, counted and stored on ice until further analysis and processing.

4.2.5 Genotyping

Animal genotype was either confirmed by flow cytometry (2D2/TCR^{MOG} mice) or PCR analysis on DNA from tail or ear biopsies (all other strains).

4.2.5.1 Tissue Digestion and DNA Isolation

Tail or ear biopsies (0.3 - 0.6 cm) were obtained from mice, transferred to 1.5 ml Eppendorf safe-lock tubes and either stored at −20 °C or immediately immersed in 100 µl of tail lysis buffer. For each lysis preparation tail lysis buffer was freshly supplemented with proteinase K at a dilution of 1:50. Tissue biopsies were digested between 4 - 12 h at 56 °C at 550 rpm in a thermoshaker. Following the tissue digest, 300 µl of ddH_2O was added to each sample and tubes were centrifuged in order to pellet the tissue debris (12 000 rpm/10 min). Supernatants were transferred to freshly prepared 1.5 ml Eppendorf tubes containing 500 µl isopropanol. The tubes were vortexed followed by another centrifugation step (12000 rpm/10 min). Supernatants were carefully discarted and 200 µl of ice-cold (−20 °C) 70%-EtOH was added to the pelleted DNA followed by another centrifugation step (12000 rpm/10 min). Supernatants were

discarted and the remaining droplets were carefully removed using a vacuum pump. The precipitated DNA was air dried in 1.5 ml centrifuge tubes with open lids for a maximum amount of 15 min. DNA was resuspended in 50 µl of ddH_2O and stored at 4 °C until further processing for genotyping.

4.2.5.2 *Atg5*$^{flox/flox}$ Genotyping

In order to genotype the *Atg5*$^{flox/flox}$ allele the FIREPol® 5× Mix 7.5 mM *Ready to Load* system was used.

The anticipated PCR products were 650 bp for the *Atg5* floxed allele and 350 bp for the *Atg5* wt allele.

4.2.5.3 Master Mix Components and PCR Program

FIREPol® Master Mix (1×)

Reagent	**Volume (µl)**
DNA	2.0
5× FIREPol® mix	4.0
Primer CS 003, 10 µM	0.5
Primer CS 004, 10 µM	0.5
Primer CS 005, 10 µM	0.5
Primer CS 006, 10 µM	0.5
H_2O	12.00
Total Volume	**20.0**

PCR program

Temperature	**Time**	
95 °C	10 min	
95 °C	30 sec	×35
60 °C	30 sec	
72 °C	1 min	
72 °C	10 min	
12 °C	∞	

4.2.5.4 CD11c-Cre Genotyping

In order to genotype the Cre allele the FIREPol® 5× Mix 7.5 mM *Ready to Load* system was used.

The anticipated PCR products were 100 bp for the Cre transgene and 324 bp for the internal positive control.

4.2.5.5 Master Mix Components and PCR Program

FIREPol® Master Mix (1×)

Reagent	**Volume (µl)**
DNA	2.0
5× FIREPol® mix	4.0
Primer CS 007, 10 µM	0.5
Primer CS 008, 10 µM	0.5
Primer CS 009, 10 µM	0.5
Primer CS 010, 10 µM	0.5
H_2O	12.00
Total Volume	**20.0**

PCR program

Temperature	**Time**	
94 °C	3 min	
94 °C	30 sec	×35
63 °C	1 min	
72 °C	1 min	
72 °C	5 min	
12 °C	∞	

4.2.5.6 2D2/TCR^{MOG} Genotyping

2D2/TCR^{MOG} transgenic mice carry the Vα3.2 Jα18 and Vβ11DJβ1.1 region of a the MOG-specific murine T cell clone 2D2 (Bettelli *et al.*, 2003).

In virtue of their transgenic MOG-specific TCR expressed within the CD4$^+$ T cell compartment, 2D2/TCR^{MOG} transgenic mice were genotyped via flow cytometry using Vα3.2 and Vβ11 specific antibodies and transgenic animals were identified

due to the overrepresentation of these TCR α and β chains in their CD4 T cell repertoire (Bettelli et al., 2003). Therefore, animals were painlessly bled from the tail vein according to Swiss animal laws and institutional guidelines. The collected blood was mixed with an appropriate amount of heparin in order to avoid clotting. 30-50 µl of the blood:heparin mix were transferred to FACS tubes and supplemented with 1 ml of ACK lysing buffer. After incubation with the lysing buffer for 3 min at RT, FACS tubes were filled up with PBS and centrifuged at 400 × g for 5 min. Supernatants were discarded and the cell pellets were resuspended in 50 µl of antibody mix. Samples were stained on ice for 20 min, followed by another washing step with PBS as described above. Finally, cell pellet was resuspended in 50 µl of FACS buffer and samples were immediately aquired on a FACSCanto-II (BD) (see **4.1.25.2** for optical configuration) using FACSDiva software v6.1.3 (BD Biosciences) and analyzed with FlowJo software v9.3.1 (Tree Star Inc).

4.2.6 Flow Cytometry

For surface and intracellular expression analysis of CD40, CD1d, CD11c and I-A^b, DC-*Atg5*$^{+/+}$- and DC-*Atg5*$^{-/-}$-derived splenocytes were purified for $CD11c^+$ cells using magnetic microbeads according to the manufacturer's recommendation. After Fc receptor block (22.4 µg/ml, 20 min, 4 °C) and a subsequent washing step, CD11c-enriched fractions were stained for 20 min with *LIVE/DEAD fixable Aqua Dead Stain Kit* in PBS at 4 °C in the dark. The CD11c-depleted fractions were used for CD1d surface staining of B cells (gated on CD19/MHC class II double positive cells). Samples were washed twice in cold PBS followed by incubation with respective fluorochrome-labeled antibodies in FACS buffer (1% BSA/0.1% NaN_3 in PBS) for 25 min at 4 °C in the dark. For intracellular CD1d staining, the incubation with fluorochrome-labeled antibodies was preceded by permeabilization of cells in 0.5% saponin for 10 min at RT. After 2 washing steps with cold PBS, samples were resuspended in 50 µl FACS buffer prior to sample acquisition using FACSDiva software v6.1.3 (BD Biosciences) on FACSCanto-II (BD) and analysis with FlowJo software v9.3.1 (Tree Star Inc). For IL-12 intracellular cytokine staining (ICS) using BD's *Fixation/Permeabilization Solution Kit*, CD11c-enriched fractions were plated out at 5×10^5 cells/well in 48-well tissue culture plates and incubated for 12 hours in R10 either supplemented

with 15 µg/ml anti-CD40 or not at 37 °C and 5% CO_2. For flow cytometry analysis of IL-12$^+$ cells, samples were additionally treated with Brefeldin A (10 µg/ml) during the last 5 hours of the incubation time to block IL-12 secretion. Cells were washed twice with PBS and stained for live cells and the surface molecules CD11c and MHC class II (see above). Fixation and permeabilization for subsequent ICS was carried out according to the manufacturers recommendations (*Fixation/Permeabilization Solution Kit*). Samples were acquired with a FACSCanto-II (BD) using FACSDiva software v6.1.3 (BD Biosciences) and all data were analyzed using FlowJo software v9.3.1 (Tree Star). The same set up as the ICS experiments was carried out omitting the addition of Brefeldin A. In these instances, cell culture supernatants were collected after 12 hours for analysis of secreted IL-12 via ELISA.

4.2.7 Magnetic Activated Cell Sorting (MACS)

All magnetic activated cell sorting procedures were carried out using magnetic MicroBeads from Miltenyi (anti-CD11c and anti-CD4), the autoMACS Separator (Miltenyi) and in accordance with the provider's protocol recommendations. Generally, single cell suspensions derived from organ isolates (spleen, liver, brain, bone marrow, blood) were incubated with 100 µl of MicroBead solution / 1 × 10^8 cells in 400 µl of MACS buffer (CD11c$^+$ purification) or 10 µl of MicroBead solution / 1 × 10^7 cells in 90 µl of MACS buffer (CD4$^+$ purification) for 15 min at 4 °C in 15 ml tubes. Tubes were then filled up with cold MACS buffer and centrifuged at 400 × g for 10 min. The supernatant was aspirated and the pellet was resuspended in 500 µl of cold MACS buffer / 1 × 10^8 cells (CD11c$^+$ and CD4$^+$ purification). Before automatic separation, cell suspensions were passed through a 70 µm cell strainer in order to avoid cell clumps. Cell suspensions were kept on ice throughout the entire preparation procedure. Cell suspensions were installed into the autoMACS machine in pre-cooled racks and an appropriate separation program was chosen (*possel"d"* and *possel* for CD11c$^+$ and CD4$^+$ purification, respectively).

4.2.8 UVB Irradiation

ODC^{MOG+} were UVB-irradiated at 870 mJ/cm^2 using a Waldmann UV 181 BL irradiation unit. On day 0, cells were detached, washed in PBS and plated in tissue culture dishes and cultured in serum free DMEM supplemented with 1%

P/S overnight at 37 °C, 5% CO_2 (1 × 10^5 cells/dish, 2 ml volume). On day 1, medium was removed and 2 ml of PBS were added to each dish. Cells were UVB irradiated and, after irradiation, PBS was substituted with fresh serum free medium. Cells were again incubated overnight at 37 °C, 5% CO_2. Surface Ptd-L-Ser^+ of irradiated (Ptd-L-Ser^{hi} ODC^{MOG+}) and non-irradiated MO3.13 cells (Ptd-L-Ser^{lo} ODC^{MOG+}) were quantified one day after irradiation by flow cytometry analysis using annexin V staining.

4.2.9 Quantification of Ptd-L-Ser$^+$ Cells

Single ODC^{MOG+} cell suspension was washed twice with cold PBS and pellet was resuspended in 1× annexin V binding buffer at a concentration of 1 × 10^6 cells/ml. FITC-conjugated annexin V (1:20) was added, cells were gently mixed and incubated for 15 min at RT in the dark. Suspensions were then washed and resuspended in 400 µl of annexin V staining buffer. Samples were acquired on a FACSCanto-II (BD) within 1 hour using FACSDiva v6.1.3 (BD Biosciences) software and analyzed with FlowJo software V9.3.1 (Tree Star Inc.).

4.2.10 Ptd-L-Ser-Expressing Cell Phagocytosis and Coculture Assay

ODC^{MOG+} were either UVB irradiated (870 mJ/cm^2) or left untreated. DC-*Atg5*$^{-/-}$- and DC-*Atg5*$^{+/+}$-derived splenocytes were isolated and frequency of $CD11c^+$/MHC class II^+ DCs was determined via flow cytometry using a small aliquot of the splenocyte suspension. Bulk splenocytes from DC-*Atg5*$^{-/-}$- and DC-*Atg5*$^{+/+}$ mice where then cocultured overnight (37 °C, 5% CO_2) in cell culture dishes with either Ptd-L-Ser^{hi} or Ptd-L-Ser^{lo} ODC^{MOG+} (10:1 ratio of ODC^{MOG+} to $CD11c^+$/MHC class II^+ DCs based on their frequencies within splenocyte suspension determined earlier) in R10 medium + 1% P/S. On the next day, $CD11c^+$/MHC class II^+ DCs were MACS-purified from all conditions (DC-*Atg5*$^{-/-}$ + Ptd-L-Ser^{lo} ODC^{MOG+}; DC-*Atg5*$^{-/-}$ + Ptd-L-Ser^{hi} ODC^{MOG+}; DC-*Atg5*$^{+/+}$ + Ptd-L-Ser^{lo} ODC^{MOG+}; DC-*Atg5*$^{+/+}$ + Ptd-L-Ser^{hi} ODC^{MOG+}) CD11c-enriched fractions were further cocultured at 1:5 ratio (DC:T cell) in a 96-well plate U bottom overnight (37 °C, 5% CO_2) with 2D2/TCR^{MOG}-derived MACS-purified $CD4^+$ T cells in a total volume of 200 µl of R10 supplemented with 1% P/S and IL-2 (10 ng/ml). Wells containing 2D2/TCR^{MOG} $CD4^+$ T cells only and, MOG_{35-55} peptide (20 µg/mL), anti-CD3 and anti-CD28 antibodies (5 µg/ml each) were also included. All conditions

were performed in triplicates. After 24 h of incubation, cell culture supernatants were collected for analysis of IFNγ concentrations by ELISA.

4.2.11 Fluorescent Activated Cell Sorting

In some experimental settings (DC:iNKT cell cocultures, 2.2.2), MACS-derived $CD11c^+$-enriched populations were further purified using fluorescent activated cell sorting with a BD FACS Aria III. Briefly, post-MACS $CD11c^+$-enriched cell suspensions were stained with fluorochrome-labeled antibodies (anti-CD11c and anti-I-A^b) and a dead cell marker for 20 min on ice and in the dark. $CD11c^{hi}$/I-$A^{b\text{-}hi}$ double positive cells were determined as target population and either bulk sorted into 15 ml tubes or 96-well round bottom plates, both already containing the appropriate culture medium.

4.2.12 Immunocytochemistry and Colocalization Assays

For assessing colocalization between LC3 and CD1d in splenic DCs, C57BL/6-derived splenocytes were MACS-sorted via magnetic CD11c microbeads according to the manufacturer's recommendation using an autoMACS Pro Separator (Miltenyi). 8-well glass chamber slides were coated with 0.01% poly-l-lysine in ddH_2O and extensively washed with PBS before MACS-purified $CD11c^+$ cells were plated at a density of 1×10^5 per chamber. $CD11c^+$ splenocytes were either kept in R10 (RPMI-1640 + 10% FCS + 50 U/ml P/S) only or R10 supplemented with 2 µg/ml of the B-class murine TLR9 agonist CpG ODN 1826 for 5 hours at 37 °C and 5% CO_2. A cytospin was performed (3 min, 300 × g), supernatants were carefully aspired and chambers were washed twice (200 µl/chamber) with cold PBS. Cells were fixed for 15 min at RT in 3% PFA in PBS followed by 2 washing steps with PBS (200 µl/chamber). For CD1d and EEA1 colocalization studies, cells were incubated with Fc blocking antibody, labeled for CD1d 30 min at 4 °C, then incubated at 37 °C for an additional hour in R10, before fixation. Cells were permeabilized for 5 min at RT in 200 µl of 0.1% Triton X-100 in PBS followed by 30 min of blocking with 100 µl of 1% BSA, 10% NGS in PBS at RT. Cells were permeabilized for 5 min at RT in 200 µl of 0.1% Triton X-100 in PBS followed by 30 min of blocking with 100 µl of 1% BSA/10% NGS in PBS at RT. Afterwards cells were incubated with primary antibodies (rabbit anti-LC3, rat anti-CD1d, anti-EEA1 and anti-AP2) in 0.1% saponin/10% NGS in

PBS for 1 hour at RT. Chambers were carefully washed twice with 0.1% saponin in PBS (200 µl/chamber) followed by a 45 min incubation with secondary antibodies in 0.1% saponin/10% NGS in PBS (Alexa Fluor488-conjugated or Alexa Fluor555-conjugated anti-rabbit, anti-rat, anti-goat and anti-mouse). Cells were washed twice with PBS (200 µl/chamber), followed by incubation with DAPI for 2 min at RT. Washing steps as above were performed and slides were mounted with ProLong Gold antifade reagent, let sit for 24 hours at RT in the dark and transferred to 4 °C in the dark until further analysis. Pictures were acquired using a 63×, 1.4 NA oil immersion lens with an inverted confocal laser scanning microscope (SP5-UV). To determine colocalization, Pearson's correlation coefficient values were calculated using JACoP (Just Another Colocalization Plugin) in ImageJ software. A Pearson score >0.5 indicates a statistically relevant colocalization of the signals.

4.2.13 Coculture Assays with Splenic DCs and NKT Cell Hybridoma

CD1d-mediated presentation of lipid antigens was measured using the murine $V\alpha14^+/V\beta8^+$ NKT cell hybridomas A.407 and FF13. NKT cell hybridomas were cultured in hybridoma culture medium (RPMI-1640 supplemented with 10% FCS, 50 U/ml P/S, 2 mM L-glutamine and non-essential amino acids) at 37 °C and 5% CO_2. For coculture assays DC-*Atg5*$^{+/+}$- and DC-*Atg5*$^{-/-}$-derived splenocytes were purified for $CD11c^+$ cells using magnetic microbeads according to the manufacturer's recommendation. CD11c-enriched fractions were further purified through FAC-sorting using an ARIA III FCF (BD) (gated on live CD11c/I-A^b double positive cells). Purified splenic DCs were directly sorted in round-bottom 96-well tissue culture plates at 3×10^4 cells/well and kept in R10 at 37 °C and 5% CO_2 for 45 min in order to settle. Afterwards, wells were either supplemented with increasing amounts of the glycolipid antigen αGalCer (0.01 – 10 µg/ml) or left untreated for 4 hours. Each condition was applied in triplicates. Wells were carefully washed 3× with PBS (200 µl/well) and 5×10^4 NKT hybridoma cells (A.407 or FF13) in hybridoma culture medium were added to a final volume of 200 µl/well. Control wells containing APC- and NKT hybridoma cells-only (with or without addition of αGalCer) were included. Wells were incubated at 37 °C and 5% CO_2. After 24 hours, cell culture supernatants were collected for analysis of IL-2 concentrations via ELISA. In some experiments, titrated concentrations

of indicated glycolipid antigens were used instead of αGalCer (Freigang *et al.*, 2012). In some experiments (2.2.2) instead of purified splenic DCs, an ATG5-defiecent (and the ATG5-competent counterpart) macrophage-like cell line was used (MΘ-*Atg5*$^{-/-}$ and MΘ-*Atg5*$^{+/+}$).

4.2.14 CD1d Antigen Presentation Assays

BMDCs were generated by culturing the bone marrow of DC-*Atg5*$^{+/+}$ or DC-*Atg5*$^{-/-}$ mice in presence of 2 ng/ml recombinant GM-CSF *in vitro*. After 7 days, differentiated BMDCs were harvested, purified over a 14.5% Histodenz gradient and pulsed with titrated amounts of lipid antigens for 4 hours at 37 °C and 5% CO_2. Thereafter, cells were washed and 1×10^4 BMDCs were used to stimulate 5×10^4 A.407 NKT hybridoma cells in triplicate cultures in 96-well tissue culture plates. IL-2 concentrations in 24 hours cell culture supernatant were determined by ELISA. In some experiments (**2.2.4**) BMDCs were further FACS-purified for CD11c/MHC class II double positive cells using ARIA III FCF (BD).

4.2.15 NKT Cell Detection

NKT cells were detected using αGalCer-loaded CD1d tetramers. Single-cell suspensions from spleens, livers, and thymi were pre-treated with Fc block and 0.5 mg/ml avidin in FACS buffer for 10 min. After 2 washes, cells were incubated with CD1d/αGalCer tetramers at RT for 15 min before addition of anti–CD3ε and further staining for 30 min. Washed cells were depleted of erythrocytes, fixed and acquired on a LSR Fortessa system (BD) using FACSDiva software v6.1.3 (BD Biosciences). Analysis was performed using the FlowJo software v9.3.1 (Tree Star Inc.).

4.2.16 Determination of Cytokine Concentration

The IL-2 concentrations in coculture supernatants was measured using the eBioscience *Mouse IL-2 Ready-SET-GO Reagent Kit*. IL-12 concentrations in cell culture supernatants were measured using the Mabtech *Mouse IL-12/-23 (p40) ELISA Development Kit*. Serum concentrations of IFNγ and IL-4 were measured using the eBioscience *Mouse IFNγ* or *Mouse IL-4 Instant ELISA Kit*. All measurements were carried out according to the respective manufacturer's recommendation.

4.2.17 CD1d Internalization Assay

For assessing internalization of surface CD1d in splenic DCs and B cells respectively, DC-*Atg5*$^{+/+}$- and DC-*Atg5*$^{-/-}$-derived splenocytes were purified for CD11c^{+} cells using magnetic microbeads according to the manufacturer's recommendation. After Fc receptor block (22.4 µg/ml, 20 min, 4 °C) and subsequent washing step, the CD11c-enriched fraction was incubated for 30 min on ice with a biotinylated-CD1d antibody. After extensive washing with ice cold PBS cells were fractionated into the following groups (1 × 10^5/group): 90 min on ice, 90, 60 and 30 min at 37 °C, 5% CO_2. To assess CD1d internalization in B cells, the negative fraction from the MACS purification was processed accordingly in parallel. After respective incubation time, cells were washed with ice cold PBS and incubated with PE-labeled streptavidin, anti-CD11c (CD11c-enriched fraction for DC analysis) or anti-CD19 (CD11c-depleted fraction for B cell analysis), anti-I-A^b and *LIVE/DEAD fixable Aqua Dead Stain Kit* for 20 min on ice in the dark. Samples were fixed with 3% PFA in PBS and acquired with a FACSCanto-II (BD) using FACSDiva software v6.1.3 (BD Biosciences). Analysis was performed using the FlowJo software v9.3.1 (Tree Star Inc.). To obtain *% internalized CD1d* values, the following equation was employed:

$$\%\ \text{internalized CD1d} = 100 - \left[\left(\frac{\text{MFI}_{\text{sample}}}{\text{MFI}_{\text{90 min ice}}}\right) \times 100\right]$$

4.2.18 CD1d Recycling Assay

CD11c-enriched or -depleted fractions of DC-*Atg5*$^{+/+}$- and DC-*Atg5*$^{-/-}$-derived splenocytes (see internalization assay for details) were incubated with protein synthesis inhibitor cycloheximide (1 µg/ml) supplemented R10 (60 min at 37 °C, 5% CO_2). After extensive washing with ice cold PBS, cells were either incubated with unconjugated anti-CD1d antibody for 30 min (pre-blocked) or left untreated (non-blocked) on ice. After washing step, cells were divided into the following groups (1 × 10^5/group): 30 min on ice (pre-blocked), 30 min on ice (non-blocked), 30, 20, 10, 5 min at 37 °C, 5% CO_2. After respective incubation times, cells were washed with ice cold PBS and incubated with PE-labeled anti-CD1d antibody (of

the same clone used for pre-blocking), anti-CD11c (CD11c-enriched fraction for DC analysis) or anti-CD19 (CD11c-depleted fraction for B cell analysis), anti-I-A^b and *LIVE/DEAD fixable Aqua Dead Stain Kit* for 20 min on ice in the dark. A non-blocked sample was stained with PE-labeled isotype control instead of the PE-labeled anti-CD1d antibody. Samples were fixed with 3% PFA in PBS and acquired with a FACSCanto-II (BD) using FACSDiva software v6.1.3 (BD Biosciences). Analysis was performed using the FlowJo software v9.3.1 (Tree Star Inc.). To obtain *% recycled CD1d* values, the following equation was employed:

$$\%\ \text{recycled CD1d} = \left[\frac{(\text{MFI sample} - \text{MFI preblocked})}{(\text{MFI unblocked AB} - \text{MFI unblocked isotype})}\right] \times 100$$

4.2.19 Lipid *In Vivo* Chase

DC-*Atg5*$^{+/+}$ and DC-*Atg5*$^{-/-}$ mice were either injected i.p. with 200 µl PBS or αGalCer (1 µg). Injection time points were chosen as such that animals could be sacrificed at the same time point. Blood for serum cytokine analysis was collected via cardiac puncture. Blood was utilized for serum cytokine analysis (IFNγ, IL-4). Spleens were processed as described above (see mouse organ processing). MFI of costimulatory molecules was analyzed on either Cre^+ (DC-*Atg5*$^{-/-}$) or Cre^- (DC-*Atg5*$^{+/+}$) CD11c/MHC class II double positive splenocytes.

4.2.20 Infection with *S. paucimobilis*

Mice were intravenously (i.v.) infected with 10^7 colony forming units (CFU) *S. paucimobilis* and organs were harvested and weighed at 24 hours post infection. After homogenizing the organs in sterile H_2O using a tissue lyzer, tenfold serial dilutions were plated onto Muller-Hinton agar containing 200 µg/ml streptomycin and incubated for 48 hours at 30 °C. Colonies were then counted and bacterial titers calculated as CFU per g tissue.

4.2.21 Adoptively Transferred EAE

For induction of adoptively transferred EAE, 8 to 12 weeks old C57BL/6 or 2D2/TCR^{MOG} transgenic mice were used as donor mice. On day 0, donor mice (either C57BL/6 or 2D2/TCR^{MOG} transgenic mice) were anaesthetized with

isoflurane and subsequently injected s.c. with 100 µl of a MOG_{35-55}/CFA emulsion in each flank using a 24G needle attached to a 1 ml syringe. Additionally, each mouse was i.p. injected with 100 µl containing 200 ng Pertussis toxin in PBS using a 29G × 12.7 mm insulin syringe. The MOG_{35-55}/CFA emulsion was prepared as followes: MOG_{35-55} peptide (MEVGWYRSPFSRVVHLYRNGK) at a stock concentration of 5 mg/ml was diluted in PBS to obtain a final concentration 0.5 mg/ml. An equal volume of CFA additionally supplemented with desiccated inactivated *Mycobacterium tuberculosis* (at 3.333 mg per 1 ml of CFA) was added to obtain 200 µl of a 1:1 ratio of the MOG_{35-55}/CFA emulsion per mouse (100 µl per flank). An excess volume of 20% was prepared in addition to account for partial loss of the viscous emulsion within the syringes. The MOG_{35-55}/CFA emulsion was thoroughly mixed via quick repetitive transfer in between two syringes connected by a luer-lock interconnector device for 20 min at RT. On day 7 after immunization with MOG_{35-55}/CFA, donor mice were euthanized with CO_2 (in none of the experiments carried out did any of the donor mice develop clinical signs of EAE within these first 7 days upon immunization). Spleen and draining lymph nodes (dLN) were harvested and leukocytes were purified according to **4.2.2**. Bulk leukocytes were counted and re-plated at 1-2 × 10^7 cells/ml restimulation medium in 10 cm tissue-culture-treated round dishes (10 ml/dish). The restimulation medium contained IL-23 (10 ng/ml) and MOG_{35-55} (10 µg/ml). Cells were incubated for 48 hours at 37 °C and 5% CO_2. Afterwards cells were collected, washed with sterile cold PBS twice and adjusted to a density of 5 × 10^6 cells/100 µl PBS. 200 µl of this cell suspension was i.p. injected into each recipient mouse which had been sublethally irradiated with 550 rad (using a cesium source irradiator) one day prior to cell transfer. After the induction of EAE (either by active immunization with MOG_{35-55} peptide as applied to the donor mice or by adoptively transferring donor splenocytes into recipient mice), mice were observed daily for well-being and accessibility of food and water. Furthermore, clinical manifestations of EAE and weight loss were monitored and documented daily using a stringent scoring procedure including a grid test and manual examination:

Disease score	Clinical manifestation
0	No detectable signs of EAE
0.5	Distal limp tail
1	Complete limp tail
1.5	Limp tail and hint limp weakness
2	Unilateral partial hind limb paralysis
2.5	Bilateral partial hind limb paralysis
3	Complete bilateral hind limb paralysis
3.5	Complete bilateral hind limb paralysis and partial fore limb paralysis
4	Moribund (animal unable to move due to paralysis)
5	Animal found dead

In the following instances animals were immediately euthanized with CO_2 upon evaluation: Disease score of 3 for more than 7 days, disease score of 3.5 for more than 3 days, reaching disease score of 4 or loss of more than 30% of the animal's maximum body weight.

4.2.22 Detection of Regulatory T Cells Via Intranuclear FOXP3 Staining

The detection of $FOXP3^+$ regulatory T cells (Tregs) in CNS-derived and splenic lymphocytes was carried out using eBioscience's *FOXP3 Staining Buffer Set* according to the manufacturer's recommendations. In brief, Samples were initially stained for surface molecules (including at least CD4, CD8 and CD25) and with a fixable live cell marker according to standard surface staining procedures for flow cytometry analyses (**4.2.6**). Next, *Fixation/Permeabilization Working Solution* was prepared freshly by diluting *Fixation/Permeabilization Concentrate* (1 part) in *Fixation/Permeabilization Diluent* (3 parts). After surface staining, the cell pellet was suspended in 500 µl of *Fixation/Permeabilization Working Solution*/sample for fixation. Samples were incubated at 4 °C for 30 min in the dark. Samples were washed twice with 1 ml of *1× Permeabilization Buffer* (10× stock solution diluted in H_2O) followed by centrifugation at 400 × g and 4 °C for 5 min. Each sample was stained with 10 µl of a 1:100 dilution of a fluorescently labeled anti-mouse FOXP3 antibody in *1× permeabilization buffer*

and incubated at 4 °C for 30 min in the dark. Cells were washed once with *1× permeabilization buffer,* followed by centrifugation step at 400 × g and 4 °C for 5 min. Supernatant was discarded and cell pellet was resuspended in FACS buffer and samples were immediately recorded with a LSR Fortessa system (BD) using FACSDiva software v6.1.3 (BD Biosciences). Analysis was performed using the FlowJo software v9.3.1 (Tree Star Inc.).

4.2.23 Detection of the Intracellular Cytokines IFNγ, IL-17 and GM-CSF

During some EAE peak of disease experiments intracellular cytokines were determined in CNS-derived and splenic $CD4^+$ T cells upon restimulation with either MOG_{35-55} peptide, $OVA_{323-339}$ peptide (negative control) or PMA/Ionomycin (positive control). Leukocytes were isolated and purified from the respective organs according to **4.2.2**. For each sample/animal the organ-specific (CNS or spleen) cell suspension was divided in three groups determined by the restimulation agent (MOG_{35-55} peptide, $OVA_{323-339}$ peptide, or PMA/Ionomycin). Brefeldin A was added to inhibit cytokine secretion by induction of retrograde transport from the Golgi apparatus back to the ER (Sciaky *et al.*, 1997). Each sample was resuspended in 500 µl of the respective restimulation medium:

Restimulation medium	**Ingredients**
I	$OVA_{323-339}$ peptide + Brefeldin A in R10 + P/S
II	MOG_{35-55} peptide + Brefeldin A in R10 + P/S
III	PMA/Ionomycin + Brefeldin A in R10 + P/S

Concentrations of restimulation agents

	$OVA_{323-339}$ peptide	**MOG_{35-55} peptide**	**PMA**	**Ionomycin**	**Brefeldin A**
Stock	5 mg/ml	5 mg/ml	1 mg/ml	1 mM	10 mg/ml
Dilution	1:250	1:250	1:50000	1:747	1:1000

Samples were incubated in restimulation media at 37 °C and 5% CO_2 for 4 hours, then washed twice in cold PBS followed by centrifugation at 400 × g and 4 °C for

5 min. Supernatants were discarded and each cell pellet was resuspended in 50 µl of staining solution containing the antibodies against the respective surface antigens and a fixable live cell marker according to standard surface staining procedures for flow cytometry analyses (**4.2.6**). In order to detect intracellular cytokines, BD's *Cytofix/Cytoperm Fixation/Permeabilization Solution Kit* was used according to the manufacturer's recommendation. Briefly, cell pellets were resuspended in 200 µl of *Cytofix/Cytoperm Buffer* and incubated for 30 min at 4 °C in the dark. Next, 1 ml of 1× *Permeabilization/Wash Buffer* was added to each sample followed by a centrifugation step at 400 × g and 4 °C for 5 min. Supernatants were discarded and each cell pellet was resuspended in 50 µl staining solution containing the appropriate dilutions of antibodies against murine IFNγ, IL-17A and GM-CSF in 1× *Permeabilization/Wash Buffer*. Samples were incubated in the dark at 4 °C for 20 min. Samples were washed in 1 ml of 1× *Permeabilization/Wash Buffer*, centrifuged at 400 × g and 4 °C for 5 min and supernatants were discarded. Cell pellets were resuspended in PBS and immediately recorded using LSR Fortessa (BD) with FACSDiva software v6.1.3 (BD Biosciences). Analysis was performed using the FlowJo software v9.3.1 (Tree Star Inc.).

4.2.24 Cell Culture

In general, all cell lines and murine primary cells were maintained and cultured at 37°C, 5% CO_2. All materials used during cell culture were sterile. Cell culture work was only performed under sterile conditions using a biological safety hood.

4.2.25 Cell Count

Regularly, the number of cells in a given suspension had to be determined. Depending on the expected cell density within the suspension an appropriate pre-dilution was chosen. In order to distinguish live from dead cells, cell suspension was further diluted with trypan blue staining solution at a 1:1 ratio. 10 µl of this dilution was pipetted into a hemocytometer (Neubauer-counting chamber). Live (trypan blue^{neg} cells) were counted in 4 quadrants using an inverted laboratory light microscope and cell concentration was calculated.

4.2.26 Freezing Cells

Cell line-derived cells and murine BMDCs were frozen down using freezing medium (10% DMSO in FCS). In doing so cells were carefully and slowly resuspended in freezing medium and transferred into 1.8 ml cryo tubes. Cryo tubes were positioned into a isopropanol containing freezing container that allowed for an optimal 1 °C/min cooling rate. The freezing container was stored at −80 °C overnight. Afterwards cryo tubes were stored in liquid nitrogen until further useage.

For thawing, cryo tubes were quickly transferred from liquid nitrogen into a 37 °C water bath just until only a small amount of cell suspension was still frozen. Cryo tubes were removed from water bath, sprayed with 70%-EtOH. The cell suspension was slowly pipetted up and down in order to thaw the remainder suspension. The thawed content of the cryo tubes was transferred into a 50 ml tube. The tube was filled up with cold sterile PBS and centrifuged at 400 × g and 4 °C for 5 min. Supernatant was discarded and cell pellet was resuspended in fresh culture medium dependend on the nature of the cells.

4.2.27 Cell Lysis for Protein Quantification

The culture medium of the cell population of interest was removed and cells were washed twice with cold PBS. Adherent cells were removed from culture plate by trypsinization or mechanical detachment using a cell scraper. The obtained cell suspension was transferred in a 15 ml tube. The tube was filled up with cold PBS and centrifuged at 400 × g and 4 °C for 5 min. From this step on, samples were meticulously kept on ice at all times. Supernatant was discarded and the cell pellet was resuspended with 1 ml of cold PBS. The cell suspension was transferred in 1.5 ml tubes and centrifuged at 400 × g and 4 °C for 5 min. Supernatant was discarded and cell pellet was resuspended in an appropriate amount of freshly prepared cold lysis buffer (50 µl/ 1×10^6 cells). Cell suspension was forcefully pipetted up and down in order to mechanically benefit the lysis. Samples were incubated in lysis buffer for 30 min on ice and centrifuged at >20000 × g and 4 °C for 10 min. The supernatant was carefully transferred into a fresh 1.5 ml tube. At this stage, a small amount of each sample was set aside to use for determination of protein concentration. The remainder of each sample was stored at −80 °C until further use.

4.2.28 BCA/Protein Quantification

For determination of the protein concentration in whole cell lysates the *Pierce BCA Protein Assay Kit* was used according to the manufacturer's recommendation. In brief, for each measurement a fresh BSA in PBS serial dilution ranging from 25 - 2000 µg/ml was prepared. To obtain the *BCA Working Reagent* (200 µl required per sample/standard singlet), reagent A was mixed with reagent B at a 50:1 ratio. 10 µl of each standard and sample were pipetted into a flat bottom 96-well plate in duplicates (of note: in this particular sample-saving microplate set-up the working range of the assay was limited to 125 - 2000 µg/ml). Usually, samples were pre-diluted (1:10, 1:50). Then, 200 µl of *BCA Working Reagent* was added per well. The 96-well plate was put on a rocking plate shaker for 30 sec in order to thoroughly mix the substances. Thereafter, the plate was covered with multi well sealing film and incubated at 37 °C for 30 min. After equilibration to RT, absorbance at 540 nm was measured.

4.2.29 SDS-PAGE and Western Blot

Protein samples (which had been prepared for subsequent SDS-PAGE as described in (**4.2.27, 4.2.28**) were diluted with 5× Laemmli Buffer and boiled for 5 min at 95 °C. The 0.75 mm gels had either been prepared one day in advance, wrapped in moist paper towels and stored at 4 °C or were prepared freshly according to the recipes in **4.1.23**. The gels were assembled in a Bio-Rad stacking system and protein samples including a protein ladder were carefully loaded into the gel pockets using Corning gel-loading pipet tips. Gel was run at 70V until samples had entered the resolving gel when the voltage was increased to 100V until the protein front had almost reached the bottom of the gel. When the SDS-PAGE was done, the gel was gently removed from inbetween the glass plates. A polyvinylidenefluoride (PVDF) membrane was activated in 100% methanol for 2 min. Appropriatly tailored Whatman filter papers, PVDF membrane and gel were soaked in 1× transfer buffer for equilibration for 10 min. Proteins were transferred via a semi-dry transfer system at 10V for 1 hour. The membrane was removed and blocked for 1 hour at RT in 4% skimmed milk in PBS-T buffer (blocking solution) followed by incubation with primary antibody diluted in blocking solution overnight at 4 °C on a shaker. After washing for at least 5 min with PBS-T, the membrane was incubated for 1 hour at RT with secondary antibody (HRP labeled anti-goat, -mouse, -rat or -rabbit IgG) diluted in blocking

solution on a shaker. Membrane was again washed three times for at least 5 min with PBS-T and finally once with PBS for 5 min. Pierce ECL Western Blotting Subrate was used to develop the membrane. Protein bands were visualized with a Fusion FX detector (Vilber-Lourmat). In some instances stripping of the PVDF membrane was required. In doing so, the membrane was washed twice in PBS-T and twice in H_2O for at least 5 min. Afterwards the membrane was incubated rocking with 5 ml of 1× *ReBlot System Strong Solution* for 30 min at RT. The membrane was washed twice in H_2O followed by two washes in PBS-T for 5 min each. Henceforth, the protocol regarding blocking, incubation with primary and secondary antibodies and detection corresponded to the procedures mentioned above.

4.2.30 Statistics

Statistical tests applied are indicated in the respective figure legends. Unpaired, two-tailed student t test, Mann-Whitney U test and Pearson correlation coefficient were performed/calculated. A P-value <0.05 was considered statistically significant. The asterisks depicted in the figures translate into the following grouping: * $P<0.05$, ** $P<0.01$,*** $P<0.001$. All quantitative analyses were performed with GraphPad Prism v5.0a for Mac OSX (GraphPad Software, Inc).

5. References

't Hart BA, van Kooyk Y, Geurts JJG, Gran B. The primate autoimmune encephalomyelitis model; a bridge between mouse and man. Ann Clin Transl Neurol 2015; 2: 581–593.

'tHart BA, Kap YS, Morandi E, Laman JD, Gran B. EBV Infection and Multiple Sclerosis: Lessons from a Marmoset Model. Trends Mol Med 2016; 22: 1012–1024.

Abi Abdallah DS, Egan CE, Butcher BA, Denkers EY. Mouse neutrophils are professional antigen-presenting cells programmed to instruct Th1 and Th17 T-cell differentiation. Int. Immunol. 2011; 23: 317–326.

Adamopoulou E, Tenzer S, Hillen N, Klug P, Rota IA, Tietz S, et al. Exploring the MHC-peptide matrix of central tolerance in the human thymus. Nature Communications 2013; 4: 2039.

Aichinger M, Wu C, Nedjic J, Klein L. Macroautophagy substrates are loaded onto MHC class II of medullary thymic epithelial cells for central tolerance. J. Exp. Med. 2013; 210: 287–300.

Allan ERO, Tailor P, Balce DR, Pirzadeh P, McKenna NT, Renaux B, et al. NADPH oxidase modifies patterns of MHC class II-restricted epitopic repertoires through redox control of antigen processing. J. Immunol. 2014; 192: 4989–5001.

Anandasabapathy N, Victora GD, Meredith M, Feder R, Dong B, Kluger C, et al. Flt3L controls the development of radiosensitive dendritic cells in the meninges and choroid plexus of the steady-state mouse brain. J. Exp. Med 2011; 208: 1695–1705.

Araki Y, Ku W-C, Akioka M, May AI, Hayashi Y, Arisaka F, et al. Atg38 is required for autophagy-specific phosphatidylinositol 3-kinase complex integrity. J Cell Biol 2013; 203: 299–313.

Arora P, Baena A, Yu KOA, Saini NK, Kharkwal SS, Goldberg MF, et al. A Single Subset of Dendritic Cells Controls the Cytokine Bias of Natural Killer T Cell Responses to Diverse Glycolipid Antigens. Immunity 2014; 40: 105–116.

Arora P, Venkataswamy MM, Baena A, Bricard G, Li Q, Veerapen N, et al. A rapid fluorescence-based assay for classification of iNKT cell activating glycolipids. J. Am. Chem. Soc. 2011; 133: 5198–5201.

Axe EL, Walker SA, Manifava M, Chandra P, Roderick HL, Habermann A, et al. Autophagosome formation from membrane compartments enriched in phosphatidylinositol 3-phosphate and dynamically connected to the endoplasmic reticulum. J Cell Biol 2008; 182: 685–701.

Balk SP, Burke S, Polischuk JE, Frantz ME, Yang L, Porcelli S, et al. Beta 2-microglobulin-independent MHC class Ib molecule expressed by human intestinal epithelium. Science 1994; 265: 259–262.

Bandyopadhyay U, Overholtzer M. LAP: the protector against autoimmunity. Cell Res. 2016; 26: 865–866.

Barnett MH, Prineas JW. Relapsing and remitting multiple sclerosis: pathology of the newly forming lesion. Ann. Neurol. 2004; 55: 458–468.

Barral P, Polzella P, Bruckbauer A, van Rooijen N, Besra GS, Cerundolo V, et al. CD169(+) macrophages present lipid antigens to mediate early activation of iNKT cells in lymph nodes. Nat. Immunol. 2010; 11: 303–312.

Batuwangala T, Shepherd D, Gadola SD, Gibson KJC, Zaccai NR, Fersht AR, et al. The crystal structure of human CD1b with a bound bacterial glycolipid. J. Immunol. 2004; 172: 2382–2388.

Bauer A, Hüttinger R, Staffler G, Hansmann C, Schmidt W, Majdic O, et al. Analysis of the requirement for beta 2-microglobulin for expression and formation of human CD1 antigens. Eur. J. Immunol. 1997; 27: 1366–1373.

Becher B, Greter M. Acquitting an APC: DCs found 'not guilty' after trial by ablation. Eur. J. Immunol. 2012; 42: 2551–2554.

Becher B, Prat A, Antel JP. Brain-immune connection: immuno-regulatory properties of CNS-resident cells. Glia 2000; 29: 293–304.

Ben-Nun A, Wekerle H, Cohen IR. The rapid isolation of clonable antigen-specific T lymphocyte lines capable of mediating autoimmune encephalomyelitis. Eur. J. Immunol. 1981a; 11: 195–199.

Ben-Nun A, Wekerle H, Cohen IR. Vaccination against autoimmune encephalomyelitis with T-lymphocyte line cells reactive against myelin basic protein. Nature 1981b; 292: 60–61.

Bendelac A, Lantz O, Quimby ME, Yewdell JW, Bennink JR, Brutkiewicz RR. CD1 recognition by mouse NK1+ T lymphocytes. Science 1995; 268: 863–865.

Bendelac A, Savage PB, Teyton L. The biology of NKT cells. Annu. Rev. Immunol. 2007; 25: 297–336.

Benlagha K, Wei DG, Veiga J, Teyton L, Bendelac A. Characterization of the early stages of thymic NKT cell development. J. Exp. Med. 2005; 202: 485–492.

Benlagha K, Weiss A, Beavis A, Teyton L, Bendelac A. In vivo identification of glycolipid antigen-specific T cells using fluorescent CD1d tetramers. J. Exp. Med. 2000; 191: 1895–1903.

Berner V, Liu H, Zhou Q, Alderson KL, Sun K, Weiss JM, et al. IFN-gamma mediates CD4+ T-cell loss and impairs secondary antitumor responses after successful initial immunotherapy. Nat Med 2007; 13: 354–360.

Bettelli E, Pagany M, Weiner HL, Linington C, Sobel RA, Kuchroo VK. Myelin oligodendrocyte glycoprotein-specific T cell receptor transgenic mice develop spontaneous autoimmune optic neuritis. J. Exp. Med. 2003; 197: 1073–1081.

Bhattacharya A, Parillon X, Zeng S, Han S, Eissa NT. Deficiency of Autophagy in Dendritic Cells Protects against Experimental Autoimmune Encephalomyelitis. J. Biol. Chem. 2014; 289: 26525–26532.

Bialecki E, Paget C, Fontaine J, Capron M, Trottein F, Faveeuw C. Role of marginal zone B lymphocytes in invariant NKT cell activation. J. Immunol. 2009; 182: 6105–6113.

Blum JS, Wearsch PA, Cresswell P. Pathways of antigen processing. Annu. Rev. Immunol. 2013; 31: 443–473.

Blumberg RS, Terhorst C, Bleicher P, McDermott FV, Allan CH, Landau SB, et al. Expression of a nonpolymorphic MHC class I-like molecule, CD1D, by human intestinal epithelial cells. J. Immunol. 1991; 147: 2518–2524.

Bonifacino JS, Traub LM. Signals for sorting of transmembrane proteins to endosomes and lysosomes. Annu. Rev. Biochem. 2003; 72: 395–447.

Bonilla DL, Bhattacharya A, Sha Y, Xu Y, Xiang Q, Kan A, et al. Autophagy regulates phagocytosis by modulating the expression of scavenger receptors. Immunity 2013; 39: 537–547.

Brazil MI, Weiss S, Stockinger B. Excessive degradation of intracellular protein in macrophages prevents presentation in the context of major histocompatibility complex class II molecules. Eur. J. Immunol. 1997; 27: 1506–1514.

Brennan PJ, Brigl M, Brenner MB. Invariant natural killer T cells: an innate activation scheme linked to diverse effector functions. Nat. Rev. Immunol. 2013; 13: 101–117.

Brigl M, Tatituri RVV, Watts GFM, Bhowruth V, Leadbetter EA, Barton N, et al. Innate and cytokine-driven signals, rather than microbial antigens, dominate in natural killer T cell activation during microbial infection. J. Exp. Med. 2011; 208: 1163–1177.

Brodsky FM, Chen CY, Knuehl C, Towler MC, Wakeham DE. Biological basket weaving: formation and function of clathrin-coated vesicles. Annu. Rev. Cell Dev. Biol. 2001; 17: 517–568.

Brossay L, Chioda M, Burdin N, Koezuka Y, Casorati G, Dellabona P, et al. CD1d-mediated recognition of an alpha-galactosylceramide by natural killer T cells is highly conserved through mammalian evolution. J. Exp. Med. 1998; 188: 1521–1528.

Brutkiewicz RR, Bennink JR, Yewdell JW, Bendelac A. TAP-independent, beta 2-microglobulin-dependent surface expression of functional mouse CD1.1. J. Exp. Med. 1995; 182: 1913–1919.

Busshoff U, Hein A, Iglesias A, Dörries R, Régnier-Vigouroux A. CD1 expression is differentially regulated by microglia, macrophages and T cells in the central nervous system upon inflammation and demyelination. J. Neuroimmunol. 2001; 113: 220–230.

Butzkueven H, Zhang J-G, Soilu-Hanninen M, Hochrein H, Chionh F, Shipham KA, et al. LIF receptor signaling limits immune-mediated demyelination by enhancing oligodendrocyte survival. Nat Med 2002; 8: 613–619.

Cadwell K. Crosstalk between autophagy and inflammatory signalling pathways: balancing defence and homeostasis. Nat. Rev. Immunol. 2016; 16: 661–675.

Canchis PW, Bhan AK, Landau SB, Yang L, Balk SP, Blumberg RS. Tissue distribution of the non-polymorphic major histocompatibility complex class I-like molecule, CD1d. Immunology 1993; 80: 561–565.

Carnaud C, Lee D, Donnars O, Park SH, Beavis A, Koezuka Y, et al. Cutting edge: Cross-talk between cells of the innate immune system: NKT cells rapidly activate NK cells. J. Immunol. 1999; 163: 4647–4650.

Cernadas M, Sugita M, van der Wel N, Cao X, Gumperz JE, Maltsev S, et al. Lysosomal localization of murine CD1d mediated by AP-3 is necessary for NK T cell development. J. Immunol. 2003; 171: 4149–4155.

Chan EYW, Kir S, Tooze SA. siRNA screening of the kinome identifies ULK1 as a multidomain modulator of autophagy. J. Biol. Chem. 2007; 282: 25464–25474.

Chang DH, Osman K, Connolly J, Kukreja A, Krasovsky J, Pack M, et al. Sustained expansion of NKT cells and antigen-specific T cells after injection of alpha-galactosyl-ceramide loaded mature dendritic cells in cancer patients. J. Exp. Med. 2005; 201: 1503–1517.

Chang P-P, Barral P, Fitch J, Pratama A, Ma CS, Kallies A, et al. Identification of Bcl-6-dependent follicular helper NKT cells that provide cognate help for B cell responses. Nat. Immunol. 2012; 13: 35–43.

Chang Y-Y, Neufeld TP. An Atg1/Atg13 complex with multiple roles in TOR-mediated autophagy regulation. Mol. Biol. Cell 2009; 20: 2004–2014.

Chervonsky A, Sant AJ. In the absence of major histocompatibility complex class II molecules, invariant chain is translocated to late endocytic compartments by autophagy. Eur. J. Immunol. 1995; 25: 911–918.

Chiu Y-H, Park S-H, Benlagha K, Forestier C, Jayawardena-Wolf J, Savage PB, et al. Multiple defects in antigen presentation and T cell development by mice expressing cytoplasmic tail-truncated CD1d. Nat. Immunol. 2002; 3: 55–60.

Codogno P, Mehrpour M, Proikas-Cezanne T. Canonical and non-canonical autophagy: variations on a common theme of self-eating? Nat. Rev. Mol. Cell Biol. 2011; 13: 7–12.

Collins BM, McCoy AJ, Kent HM, Evans PR, Owen DJ. Molecular architecture and functional model of the endocytic AP2 complex. Cell 2002; 109: 523–535.

Crowe NY, Uldrich AP, Kyparissoudis K, Hammond KJL, Hayakawa Y, Sidobre S, et al. Glycolipid

antigen drives rapid expansion and sustained cytokine production by NK T cells. J. Immunol. 2003; 171: 4020–4027.

de Lalla C, Galli G, Aldrighetti L, Romeo R, Mariani M, Monno A, et al. Production of profibrotic cytokines by invariant NKT cells characterizes cirrhosis progression in chronic viral hepatitis. J. Immunol. 2004; 173: 1417–1425.

De Silva AD, Park J-J, Matsuki N, Stanic AK, Brutkiewicz RR, Medof ME, et al. Lipid protein interactions: the assembly of CD1d1 with cellular phospholipids occurs in the endoplasmic reticulum. J. Immunol. 2002; 168: 723–733.

Delamarre L, Pack M, Chang H, Mellman I, Trombetta ES. Differential lysosomal proteolysis in antigen-presenting cells determines antigen fate. Science 2005; 307: 1630–1634.

Delgado MA, Elmaoued RA, Davis AS, Kyei G, Deretic V. Toll-like receptors control autophagy. EMBO J. 2008; 27: 1110–1121.

Dendrou CA, Fugger L, Friese MA. Immunopathology of multiple sclerosis. Nat. Rev. Immunol. 2015; 15: 545–558.

Dengjel J, Schoor O, Fischer R, Reich M, Kraus M, Müller M, et al. Autophagy promotes MHC class II presentation of peptides from intracellular source proteins. Proc. Natl. Acad. Sci. U.S.A. 2005; 102: 7922–7927.

Denton D, Nicolson S, Kumar S. Cell death by autophagy: facts and apparent artefacts. Cell Death Differ. 2012; 19: 87–95.

Denzin LK, Cresswell P. HLA-DM induces CLIP dissociation from MHC class II alpha beta dimers and facilitates peptide loading. Cell 1995; 82: 155–165.

Denzin LK, Sant'Angelo DB, Hammond C, Surman MJ, Cresswell P. Negative regulation by HLA-DO of MHC class II-restricted antigen processing. Science 1997; 278: 106–109.

Deretic V. Autophagy in leukocytes and other cells: mechanisms, subsystem organization, selectivity, and links to innate immunity. J. Leukoc. Biol. 2016; 100: 969–978.

DeSelm CJ, Miller BC, Zou W, Beatty WL, van Meel E, Takahata Y, et al. Autophagy proteins regulate the secretory component of osteoclastic bone resorption. Dev. Cell 2011; 21: 966–974.

Deter RL, Baudhuin P, De Duve C. Participation of lysosomes in cellular autophagy induced in rat liver by glucagon. J Cell Biol 1967; 35: C11–6.

Deter RL, De Duve C. Influence of glucagon, an inducer of cellular autophagy, on some physical properties of rat liver lysosomes. J Cell Biol 1967; 33: 437–449.

Dooley HC, Razi M, Polson HEJ, Girardin SE, Wilson MI, Tooze SA. WIPI2 links LC3 conjugation with PI3P, autophagosome formation, and pathogen clearance by recruiting Atg12-5-16L1. Mol. Cell 2014; 55: 238–252.

Dougan SK, Salas A, Rava P, Agyemang A, Kaser A, Morrison J, et al. Microsomal triglyceride transfer protein lipidation and control of CD1d on antigen-presenting cells. J. Exp. Med. 2005; 202: 529–539.

Dugast M, Toussaint H, Dousset C, Benaroch P. AP2 clathrin adaptor complex, but not AP1, controls the access of the major histocompatibility complex (MHC) class II to endosomes. J. Biol. Chem. 2005; 280: 19656–19664.

East JE, Sun W, Webb TJ. Artificial antigen presenting cell (aAPC) mediated activation and expansion of natural killer T cells. J Vis Exp 2012: e4333–e4333.

Eberl G, MacDonald HR. Rapid death and regeneration of NKT cells in anti-CD3epsilon- or IL-12-treated mice: a major role for bone marrow in NKT cell homeostasis. Immunity 1998; 9: 345–353.

Efeyan A, Comb WC, Sabatini DM. Nutrient-sensing mechanisms and pathways. Nature 2015; 517: 302–310.

Egan DF, Shackelford DB, Mihaylova MM, Gelino S, Kohnz RA, Mair W, et al. Phosphorylation of ULK1 (hATG1) by AMP-activated protein kinase connects energy sensing to mitophagy. Science 2011; 331: 456–461.

Elewaut D, Lawton AP, Nagarajan NA, Maverakis E, Khurana A, Honing S, et al. The Adaptor Protein AP-3 Is Required for CD1d-Mediated Antigen Presentation of Glycosphingolipids and Development of V 14i NKT Cells. J. Exp. Med. 2003; 198: 1133–1146.

Fass E, Shvets E, Degani I, Hirschberg K, Elazar Z. Microtubules support production of starvation-induced autophagosomes but not their targeting and fusion with lysosomes. J. Biol. Chem. 2006; 281: 36303–36316.

Fazekas F, Ropele S, Enzinger C, Seifert T, Strasser-Fuchs S. Quantitative magnetization transfer imaging of pre-lesional white-matter changes in multiple sclerosis. Mult. Scler. 2002; 8: 479–484.

Feng Y, He D, Yao Z, Klionsky DJ. The machinery of macroautophagy. Cell Res. 2014; 24: 24–41.

Florey O, Kim SE, Sandoval CP, Haynes CM, Overholtzer M. Autophagy machinery mediates macroendocytic processing and entotic cell death by targeting single membranes. Nature Cell Biology 2011; 13: 1335–1343.

Freigang S, Landais E, Zadorozhny V, Kain L, Yoshida K, Liu Y, et al. Scavenger receptors target glycolipids for natural killer T cell activation. J. Clin. Invest. 2012; 122: 3943–3954.

Friese MA, Montalban X, Willcox N, Bell JI, Martin R, Fugger L. The value of animal models for drug development in multiple sclerosis. Brain 2006; 129: 1940–1952.

Frohman EM, Racke MK, Raine CS. Multiple sclerosis--the plaque and its pathogenesis. N Engl J Med 2006; 354: 942–955.

Fujii S-I, Goto A, Shimizu K. Antigen mRNA-transfected, allogeneic fibroblasts loaded with NKT-cell ligand confer antitumor immunity. Blood 2009; 113: 4262–4272.

Fujii S-I, Liu K, Smith C, Bonito AJ, Steinman RM. The linkage of innate to adaptive immunity via maturing dendritic cells in vivo requires CD40 ligation in addition to antigen presentation and CD80/86 costimulation. J. Exp. Med. 2004; 199: 1607–1618.

Fujii S-I, Shimizu K, Kronenberg M, Steinman RM. Prolonged IFN-gamma-producing NKT response induced with alpha-galactosylceramide-loaded DCs. Nat. Immunol. 2002; 3: 867–874.

Fujii S-I, Shimizu K, Okamoto Y, Kunii N, Nakayama T, Motohashi S, et al. NKT cells as an ideal anti-tumor immunotherapeutic. Front Immunol 2013; 4: 409.

Fujii S-I, Shimizu K, Smith C, Bonifaz L, Steinman RM. Activation of natural killer T cells by alpha-galactosylceramide rapidly induces the full maturation of dendritic cells in vivo and thereby acts as an adjuvant for combined CD4 and CD8 T cell immunity to a coadministered protein. J. Exp. Med. 2003; 198: 267–279.

Fujita N, Hayashi-Nishino M, Fukumoto H, Omori H, Yamamoto A, Noda T, et al. An Atg4B mutant hampers the lipidation of LC3 paralogues and causes defects in autophagosome closure. Mol. Biol. Cell 2008; 19: 4651–4659.

Fujita N, Itoh T, Omori H, Fukuda M, Noda T, Yoshimori T. The Atg16L complex specifies the site of LC3 lipidation for membrane biogenesis in autophagy. Mol. Biol. Cell 2008; 19: 2092–2100.

Furlan R, Martino G, Galbiati F, Poliani PL, Smiroldo S, Bergami A, et al. Caspase-1 regulates the inflammatory process leading to autoimmune demyelination. J. Immunol. 1999; 163: 2403–2409.

Gammoh N, Florey O, Overholtzer M, Jiang X. Interaction between FIP200 and ATG16L1

distinguishes ULK1 complex-dependent and -independent autophagy. Nat. Struct. Mol. Biol. 2013; 20: 144–149.

Ganley IG, Lam DH, Wang J, Ding X, Chen S, Jiang X. ULK1.ATG13.FIP200 complex mediates mTOR signaling and is essential for autophagy. J. Biol. Chem. 2009; 284: 12297–12305.

Ganley IG. Autophagosome maturation and lysosomal fusion. Essays Biochem. 2013; 55: 65–78.

Gapin L. Development of invariant natural killer T cells. Curr. Opin. Immunol. 2016; 39: 68–74.

Garcia-Alles LF, Versluis K, Maveyraud L, Vallina AT, Sansano S, Bello NF, et al. Endogenous phosphatidylcholine and a long spacer ligand stabilize the lipid-binding groove of CD1b. EMBO J. 2006; 25: 3684–3692.

Ge L, Melville D, Zhang M, Schekman R. The ER-Golgi intermediate compartment is a key membrane source for the LC3 lipidation step of autophagosome biogenesis. Elife 2013; 2: e00947.

Ge L, Zhang M, Schekman R. Phosphatidylinositol 3-kinase and COPII generate LC3 lipidation vesicles from the ER-Golgi intermediate compartment. Elife 2014; 3: e04135.

Geng J, Klionsky DJ. The Atg8 and Atg12 ubiquitin-like conjugation systems in macroautophagy. 'Protein modifications: beyond the usual suspects' review series. EMBO Rep. 2008; 9: 859–864.

Ghosh P, Amaya M, Mellins E, Wiley DC. The structure of an intermediate in class II MHC maturation: CLIP bound to HLA-DR3. Nature 1995; 378: 457–462.

Giaccone G, Punt CJA, Ando Y, Ruijter R, Nishi N, Peters M, et al. A phase I study of the natural killer T-cell ligand alpha-galactosylceramide (KRN7000) in patients with solid tumors. Clinical Cancer Research 2002; 8: 3702–3709.

Godfrey DI, Macdonald HR, Kronenberg M, Smyth MJ, Van Kaer L. NKT cells: what's in a name? Nat. Rev. Immunol. 2004; 4: 231–237.

Godfrey DI, Uldrich AP, McCluskey J, Rossjohn J, Moody DB. The burgeoning family of unconventional T cells. Nat. Immunol. 2015; 16: 1114–1123.

Gray M, Botelho RJ. Phagocytosis: Hungry, Hungry Cells. Methods Mol. Biol. 2017; 1519: 1–16.

Greaves DR, Gordon S. Thematic review series: the immune system and atherogenesis. Recent insights into the biology of macrophage scavenger receptors. J. Lipid Res. 2005; 46: 11–20.

Greter M, Heppner FL, Lemos MP, Odermatt BM, Goebels N, Laufer T, et al. Dendritic cells permit immune invasion of the CNS in an animal model of multiple sclerosis. Nat Med 2005; 11: 328–334.

Greter M, Lelios I, Croxford AL. Microglia Versus Myeloid Cell Nomenclature during Brain Inflammation. Front Immunol 2015; 6: 249.

Guilliams M, Malissen B. A Death Notice for In-Vitro-Generated GM-CSF Dendritic Cells? Immunity 2015; 42: 988–990.

Guo Y, Chang C, Huang R, Liu B, Bao L, Liu W. AP1 is essential for generation of autophagosomes from the trans-Golgi network. J. Cell. Sci. 2012; 125: 1706–1715.

Gupta-Rossi N, Ortica S, Meas-Yedid V, Heuss S, Moretti J, Olivo-Marin J-C, et al. The adaptor-associated kinase 1, AAK1, is a positive regulator of the Notch pathway. J. Biol. Chem. 2011; 286: 18720–18730.

Hailey DW, Rambold AS, Satpute-Krishnan P, Mitra K, Sougrat R, Kim PK, et al. Mitochondria supply membranes for autophagosome biogenesis during starvation. Cell 2010; 141: 656–667.

Hamasaki M, Furuta N, Matsuda A, Nezu A, Yamamoto A, Fujita N, et al. Autophagosomes form

at ER-mitochondria contact sites. Nature 2013; 495: 389–393.

Hammond KJL, Kronenberg M. Natural killer T cells: natural or unnatural regulators of autoimmunity? Curr. Opin. Immunol. 2003; 15: 683–689.

Hara T, Mizushima N. Role of ULK-FIP200 complex in mammalian autophagy: FIP200, a counterpart of yeast Atg17? Autophagy 2009; 5: 85–87.

Hara T, Nakamura K, Matsui M, Yamamoto A, Nakahara Y, Suzuki-Migishima R, et al. Suppression of basal autophagy in neural cells causes neurodegenerative disease in mice. Nature 2006; 441: 885–889.

Hara T, Takamura A, Kishi C, Iemura S-I, Natsume T, Guan J-L, et al. FIP200, a ULK-interacting protein, is required for autophagosome formation in mammalian cells. J Cell Biol 2008; 181: 497–510.

Harada Y, Imataki O, Heike Y, Kawai H, Shimosaka A, Mori S-I, et al. Expansion of alpha-galactosylceramide-stimulated Valpha24+ NKT cells cultured in the absence of animal materials. J. Immunother. 2005; 28: 314–321.

Hayakawa Y, Takeda K, Yagita H, Van Kaer L, Saiki I, Okumura K. Differential regulation of Th1 and Th2 functions of NKT cells by CD28 and CD40 costimulatory pathways. J. Immunol. 2001; 166: 6012–6018.

Hayashi-Nishino M, Fujita N, Noda T, Yamaguchi A, Yoshimori T, Yamamoto A. A subdomain of the endoplasmic reticulum forms a cradle for autophagosome formation. Nature Cell Biology 2009; 11: 1433–1437.

Heczey A, Liu D, Tian G, Courtney AN, Wei J, Marinova E, et al. Invariant NKT cells with chimeric antigen receptor provide a novel platform for safe and effective cancer immunotherapy. Blood 2014; 124: 2824–2833.

Helft J, Böttcher J, Chakravarty P, Zelenay S, Huotari J, Schraml BU, et al. GM-CSF Mouse Bone Marrow Cultures Comprise a Heterogeneous Population of CD11c(+)MHCII(+) Macrophages and Dendritic Cells. Immunity 2015; 42: 1197–1211.

Hemelaar J, Lelyveld VS, Kessler BM, Ploegh HL. A single protease, Apg4B, is specific for the autophagy-related ubiquitin-like proteins GATE-16, MAP1-LC3, GABARAP, and Apg8L. J. Biol. Chem. 2003; 278: 51841–51850.

Henault J, Martinez J, Riggs JM, Tian J, Mehta P, Clarke L, et al. Noncanonical autophagy is required for type I interferon secretion in response to DNA-immune complexes. Immunity 2012; 37: 986–997.

Henderson APD, Barnett MH, Parratt JDE, Prineas JW. Multiple sclerosis: distribution of inflammatory cells in newly forming lesions. Ann. Neurol. 2009; 66: 739–753.

Henderson DM, Conner SD. A novel AAK1 splice variant functions at multiple steps of the endocytic pathway. Mol. Biol. Cell 2007; 18: 2698–2706.

Heppner FL, Greter M, Marino D, Falsig J, Raivich G, Hövelmeyer N, et al. Experimental autoimmune encephalomyelitis repressed by microglial paralysis. Nat Med 2005; 11: 146–152.

Hermans IF, Silk JD, Gileadi U, Salio M, Mathew B, Ritter G, et al. NKT cells enhance CD4+ and CD8+ T cell responses to soluble antigen in vivo through direct interaction with dendritic cells. J. Immunol. 2003; 171: 5140–5147.

Hiltbold EM, Roche PA. Trafficking of MHC class II molecules in the late secretory pathway. Curr. Opin. Immunol. 2002; 14: 30–35.

Hirst J, Robinson MS. Clathrin and adaptors. Biochim. Biophys. Acta 1998; 1404: 173–193.

Hisahara S, Araki T, Sugiyama F, Yagami KI, Suzuki M, Abe K, et al. Targeted expression of baculovirus p35 caspase inhibitor in oligodendrocytes protects mice against autoimmune-mediated demyelination. EMBO J. 2000; 19: 341–348.

Hisahara S, Yuan J, Momoi T, Okano H, Miura M. Caspase-11 mediates oligodendrocyte cell death and pathogenesis of autoimmune-mediated demyelination. J. Exp. Med. 2001; 193: 111–122.

Hohlfeld R, Dornmair K, Meinl E, Wekerle H. The search for the target antigens of multiple sclerosis, part 1: autoreactive CD4+ T lymphocytes as pathogenic effectors and therapeutic targets. Lancet Neurol 2015; 15: 198–209.

Hohlfeld R, Dornmair K, Meinl E, Wekerle H. The search for the target antigens of multiple sclerosis, part 2: CD8+ T cells, B cells, and antibodies in the focus of reverse-translational research. Lancet Neurol 2016; 15: 317–331.

Hohlfeld R, Engel AG. Induction of HLA-DR expression on human myoblasts with interferon-gamma. Am. J. Pathol. 1990; 136: 503–508.

Hohlfeld R, Engel AG. HLA expression in myoblasts. Neurology 1991; 41: 2015.

Holzapfel KL, Tyznik AJ, Kronenberg M, Hogquist KA. Antigen-dependent versus -independent activation of invariant NKT cells during infection. J. Immunol. 2014; 192: 5490–5498.

Hosokawa N, Hara T, Kaizuka T, Kishi C, Takamura A, Miura Y, et al. Nutrient-dependent mTORC1 association with the ULK1-Atg13-FIP200 complex required for autophagy. Mol. Biol. Cell 2009; 20: 1981–1991.

Hosokawa N, Sasaki T, Iemura S-I, Natsume T, Hara T, Mizushima N. Atg101, a novel mammalian autophagy protein interacting with Atg13. Autophagy 2009; 5: 973–979.

Huehn J, Siegmund K, Lehmann JCU, Siewert C, Haubold U, Feuerer M, et al. Developmental stage, phenotype, and migration distinguish naive- and effector/memory-like CD4+ regulatory T cells. J. Exp. Med. 2004; 199: 303–313.

Huitinga I, van Rooijen N, de Groot CJ, Uitdehaag BM, Dijkstra CD. Suppression of experimental allergic encephalomyelitis in Lewis rats after elimination of macrophages. J. Exp. Med. 1990; 172: 1025–1033.

Huynh JL, Garg P, Thin TH, Yoo S, Dutta R, Trapp BD, et al. Epigenome-wide differences in pathology-free regions of multiple sclerosis-affected brains. Nature Neuroscience 2014; 17: 121–130.

Ichimura Y, Kirisako T, Takao T, Satomi Y, Shimonishi Y, Ishihara N, et al. A ubiquitin-like system mediates protein lipidation. Nature 2000; 408: 488–492.

Ichimura Y, Kumanomidou T, Sou Y-S, Mizushima T, Ezaki J, Ueno T, et al. Structural basis for sorting mechanism of p62 in selective autophagy. J. Biol. Chem. 2008; 283: 22847–22857.

Im JS, Arora P, Bricard G, Molano A, Venkataswamy MM, Baine I, et al. Kinetics and cellular site of glycolipid loading control the outcome of natural killer T cell activation. Immunity 2009; 30: 888–898.

Inaba K, Inaba M, Romani N, Aya H, Deguchi M, Ikehara S, et al. Generation of large numbers of dendritic cells from mouse bone marrow cultures supplemented with granulocyte/macrophage colony-stimulating factor. J. Exp. Med. 1992; 176: 1693–1702.

International Multiple Sclerosis Genetics Consortium (IMSGC), Beecham AH, Patsopoulos NA, Xifara DK, Davis MF, Kemppinen A, et al. Analysis of immune-related loci identifies 48 new susceptibility variants for multiple sclerosis. Nat. Genet. 2013; 45: 1353–1360.

International Multiple Sclerosis Genetics Consortium, Wellcome Trust Case Control Consortium 2, Sawcer S, Hellenthal G, Pirinen M, Spencer CCA, et al. Genetic risk and a primary role for cell-

mediated immune mechanisms in multiple sclerosis. Nature 2011; 476: 214–219.

Ireland JM, Unanue ER. Autophagy in antigen-presenting cells results in presentation of citrullinated peptides to CD4 T cells. J. Exp. Med. 2011; 208: 2625–2632.

Isaksson M, Lundgren BA, Ahlgren KM, Kämpe O, Lobell A. Conditional DC depletion does not affect priming of encephalitogenic Th cells in EAE. Eur. J. Immunol. 2012; 42: 2555–2563.

Itakura E, Kishi C, Inoue K, Mizushima N. Beclin 1 forms two distinct phosphatidylinositol 3-kinase complexes with mammalian Atg14 and UVRAG. Mol. Biol. Cell 2008; 19: 5360–5372.

Itakura E, Mizushima N. Characterization of autophagosome formation site by a hierarchical analysis of mammalian Atg proteins. Autophagy 2010; 6: 764–776.

Jacobson S, Sekaly RP, Jacobson CL, McFarland HF, Long EO. HLA class II-restricted presentation of cytoplasmic measles virus antigens to cytotoxic T cells. J. Virol. 1989; 63: 1756–1762.

Jagannath C, Lindsey DR, Dhandayuthapani S, Xu Y, Hunter RL, Eissa NT. Autophagy enhances the efficacy of BCG vaccine by increasing peptide presentation in mouse dendritic cells. Nat Med 2009; 15: 267–276.

Janeway C. Immunobiology. Taylor & Francis Group; 1996.

Jayawardena-Wolf J, Benlagha K, Chiu YH, Mehr R, Bendelac A. CD1d endosomal trafficking is independently regulated by an intrinsic CD1d-encoded tyrosine motif and by the invariant chain. Immunity 2001; 15: 897–908.

Johansen T, Lamark T. Selective autophagy mediated by autophagic adapter proteins. Autophagy 2011; 7: 279–296.

Kabeya Y, Mizushima N, Ueno T, Yamamoto A, Kirisako T, Noda T, et al. LC3, a mammalian homologue of yeast Apg8p, is localized in autophagosome membranes after processing. EMBO J. 2000; 19: 5720–5728.

Kabeya Y, Mizushima N, Yamamoto A, Oshitani-Okamoto S, Ohsumi Y, Yoshimori T. LC3, GABARAP and GATE16 localize to autophagosomal membrane depending on form-II formation. J. Cell. Sci. 2004; 117: 2805–2812.

Kalyan S, Kabelitz D. When neutrophils meet T cells: beginnings of a tumultuous relationship with underappreciated potential. Eur. J. Immunol. 2014; 44: 627–633.

Kambayashi T, Laufer TM. Atypical MHC class II-expressing antigen-presenting cells: can anything replace a dendritic cell? Nat. Rev. Immunol. 2014; 14: 719–730.

Kang S-J, Cresswell P. Regulation of intracellular trafficking of human CD1d by association with MHC class II molecules. EMBO J. 2002a; 21: 1650–1660.

Kang S-J, Cresswell P. Calnexin, calreticulin, and ERp57 cooperate in disulfide bond formation in human CD1d heavy chain. J. Biol. Chem. 2002b; 277: 44838–44844.

Kang S-J, Cresswell P. Saposins facilitate CD1d-restricted presentation of an exogenous lipid antigen to T cells. Nat. Immunol. 2004; 5: 175–181.

Karanasios E, Walker SA, Okkenhaug H, Manifava M, Hummel E, Zimmermann H, et al. Autophagy initiation by ULK complex assembly on ER tubulovesicular regions marked by ATG9 vesicles. Nature Communications 2016; 7: 12420.

Kawakami N, Lassmann S, Li Z, Odoardi F, Ritter T, Ziemssen T, et al. The activation status of neuroantigen-specific T cells in the target organ determines the clinical outcome of autoimmune encephalomyelitis. J. Exp. Med. 2004; 199: 185–197.

Kawano T, Cui J, Koezuka Y, Toura I, Kaneko Y, Motoki K, et al. CD1d-restricted and TCR-mediated activation of valpha14 NKT cells by glycosylceramides. Science 1997; 278: 1626–1629.

Kazansky DB. MHC restriction and allogeneic immune responses. J Immunotoxicol 2008; 5: 369–384.

Keen JH. Clathrin assembly proteins: affinity purification and a model for coat assembly. J Cell Biol 1987; 105: 1989–1998.

Kim HS, Garcia J, Exley M, Johnson KW, Balk SP, Blumberg RS. Biochemical characterization of CD1d expression in the absence of beta2-microglobulin. J. Biol. Chem. 1999; 274: 9289–9295.

Kim J, Kundu M, Viollet B, Guan K-L. AMPK and mTOR regulate autophagy through direct phosphorylation of Ulk1. Nature Cell Biology 2011; 13: 132–141.

Kim J-Y, Zhao H, Martinez J, Doggett TA, Kolesnikov AV, Tang PH, et al. Noncanonical autophagy promotes the visual cycle. Cell 2013; 154: 365–376.

Kimmey JM, Huynh JP, Weiss LA, Park S, Kambal A, Debnath J, et al. Unique role for ATG5 in neutrophil-mediated immunopathology during M. tuberculosis infection. Nature 2015; 528: 565–569.

Kimura S, Noda T, Yoshimori T. Dissection of the autophagosome maturation process by a novel reporter protein, tandem fluorescent-tagged LC3. Autophagy 2007; 3: 452–460.

Kimura S, Noda T, Yoshimori T. Dynein-dependent movement of autophagosomes mediates efficient encounters with lysosomes. Cell Struct. Funct. 2008; 33: 109–122.

King IL, Fortier A, Tighe M, Dibble J, Watts GFM, Veerapen N, et al. Invariant natural killer T cells direct B cell responses to cognate lipid antigen in an IL-21-dependent manner. Nat. Immunol. 2012; 13: 44–50.

Kinjo Y, Wu D, Kim G, Xing G-W, Poles MA, Ho DD, et al. Recognition of bacterial glycosphingolipids by natural killer T cells. Nature 2005; 434: 520–525.

Kirchhausen T. Adaptors for clathrin-mediated traffic. Annu. Rev. Cell Dev. Biol. 1999; 15: 705–732.

Kitamura H, Iwakabe K, Yahata T, Nishimura S, Ohta A, Ohmi Y, et al. The natural killer T (NKT) cell ligand alpha-galactosylceramide demonstrates its immunopotentiating effect by inducing interleukin (IL)-12 production by dendritic cells and IL-12 receptor expression on NKT cells. J. Exp. Med. 1999; 189: 1121–1128.

Kivisäkk P, Imitola J, Rasmussen S, Elyaman W, Zhu B, Ransohoff RM, et al. Localizing central nervous system immune surveillance: meningeal antigen-presenting cells activate T cells during experimental autoimmune encephalomyelitis. Ann. Neurol. 2009; 65: 457–469.

Klionsky DJ, Cuervo AM, Dunn WA, Levine B, van der Klei I, Seglen PO. How shall I eat thee? Autophagy 2007; 3: 413–416.

Kohm AP, Carpentier PA, Anger HA, Miller SD. Cutting edge: CD4+CD25+ regulatory T cells suppress antigen-specific autoreactive immune responses and central nervous system inflammation during active experimental autoimmune encephalomyelitis. J. Immunol. 2002; 169: 4712–4716.

Komatsu M, Waguri S, Chiba T, Murata S, Iwata J-I, Tanida I, et al. Loss of autophagy in the central nervous system causes neurodegeneration in mice. Nature 2006; 441: 880–884.

Korolchuk VI, Saiki S, Lichtenberg M, Siddiqi FH, Roberts EA, Imarisio S, et al. Lysosomal positioning coordinates cellular nutrient responses. Nature Cell Biology 2011; 13: 453–460.

Köchl R, Hu XW, Chan EYW, Tooze SA. Microtubules facilitate autophagosome formation and

fusion of autophagosomes with endosomes. Traffic 2006; 7: 129–145.

Krishnamoorthy G, Wekerle H. EAE: an immunologist's magic eye. Eur. J. Immunol. 2009; 39: 2031–2035.

Kroemer G, Levine B. Autophagic cell death: the story of a misnomer. Nat. Rev. Mol. Cell Biol. 2008; 9: 1004–1010.

Kunii N, Horiguchi S, Motohashi S, Yamamoto H, Ueno N, Yamamoto S, et al. Combination therapy of in vitro-expanded natural killer T cells and alpha-galactosylceramide-pulsed antigen-presenting cells in patients with recurrent head and neck carcinoma. Cancer Sci. 2009; 100: 1092–1098.

Kuylenstierna C, Björkström NK, Andersson SK, Sahlström P, Bosnjak L, Paquin-Proulx D, et al. NKG2D performs two functions in invariant NKT cells: direct TCR-independent activation of NK-like cytolysis and co-stimulation of activation by CD1d. Eur. J. Immunol. 2011; 41: 1913–1923.

Lam GY, Cemma M, Muise AM, Higgins DE, Brumell JH. Host and bacterial factors that regulate LC3 recruitment to Listeria monocytogenes during the early stages of macrophage infection. Autophagy 2013; 9: 985–995.

Lassmann H, van Horssen J. The molecular basis of neurodegeneration in multiple sclerosis. FEBS Lett 2011; 585: 3715–3723.

Lawton AP, Prigozy TI, Brossay L, Pei B, Khurana A, Martin D, et al. The mouse CD1d cytoplasmic tail mediates CD1d trafficking and antigen presentation by adaptor protein 3-dependent and -independent mechanisms. J. Immunol. 2005; 174: 3179–3186.

Leadbetter EA, Brigl M, Illarionov P, Cohen N, Luteran MC, Pillai S, et al. NK T cells provide lipid antigen-specific cognate help for B cells. Proc. Natl. Acad. Sci. U.S.A. 2008; 105: 8339–8344.

Lee HK, Lund JM, Ramanathan B, Mizushima N, Iwasaki A. Autophagy-dependent viral recognition by plasmacytoid dendritic cells. Science 2007; 315: 1398–1401.

Lee HK, Mattei LM, Steinberg BE, Alberts P, Lee YH, Chervonsky A, et al. In vivo requirement for Atg5 in antigen presentation by dendritic cells. Immunity 2010; 32: 227–239.

Lee YJ, Wang H, Starrett GJ, Phuong V, Jameson SC, Hogquist KA. Tissue-Specific Distribution of iNKT Cells Impacts Their Cytokine Response. Immunity 2015; 43: 566–578.

Leite-de-Moraes MC, Herbelin A, Gouarin C, Koezuka Y, Schneider E, Dy M. Fas/Fas ligand interactions promote activation-induced cell death of NK T lymphocytes. J. Immunol. 2000; 165: 4367–4371.

Levine B, Mizushima N, Virgin HW. Autophagy in immunity and inflammation. Nature 2011; 469: 323–335.

Liljedahl M, Kuwana T, Fung-Leung WP, Jackson MR, Peterson PA, Karlsson L. HLA-DO is a lysosomal resident which requires association with HLA-DM for efficient intracellular transport. EMBO J. 1996; 15: 4817–4824.

Loi M, Müller A, Steinbach K, Niven J, Barreira da Silva R, Paul P, et al. Macroautophagy Proteins Control MHC Class I Levels on Dendritic Cells and Shape Anti-viral CD8(+) T Cell Responses. Cell Reports 2016; 15: 1076–1087.

Lucchinetti C, Brück W, Parisi J, Scheithauer B, Rodriguez M, Lassmann H. A quantitative analysis of oligodendrocytes in multiple sclerosis lesions. A study of 113 cases. Brain 1999; 122 (Pt 12): 2279–2295.

Lynch L, Michelet X, Zhang S, Brennan PJ, Moseman A, Lester C, et al. Regulatory iNKT cells lack expression of the transcription factor PLZF and control the homeostasis of T(reg) cells and macrophages in adipose tissue. Nat. Immunol. 2015; 16: 85–95.

Ma J, Becker C, Lowell CA, Underhill DM. Dectin-1-triggered recruitment of light chain 3 protein to phagosomes facilitates major histocompatibility complex class II presentation of fungal-derived antigens. J. Biol. Chem. 2012; 287: 34149–34156.

Ma J, Becker C, Reyes C, Underhill DM. Cutting edge: FYCO1 recruitment to dectin-1 phagosomes is accelerated by light chain 3 protein and regulates phagosome maturation and reactive oxygen production. J. Immunol. 2014; 192: 1356–1360.

Macho-Fernandez E, Brigl M. The Extended Family of CD1d-Restricted NKT Cells: Sifting through a Mixed Bag of TCRs, Antigens, and Functions. Front Immunol 2015; 6: 362.

Macho-Fernandez E, Chang J, Fontaine J, Bialecki E, Rodriguez F, Werkmeister E, et al. Activation of invariant Natural Killer T lymphocytes in response to the α-galactosylceramide analogue KRN7000 encapsulated in PLGA-based nanoparticles and microparticles. Int J Pharm 2012; 423: 45–54.

Maday S, Wallace KE, Holzbaur ELF. Autophagosomes initiate distally and mature during transport toward the cell soma in primary neurons. J Cell Biol 2012; 196: 407–417.

Mahad DH, Trapp BD, Lassmann H. Pathological mechanisms in progressive multiple sclerosis. Lancet Neurol 2015; 14: 183–193.

Maletto BA, Ropolo AS, Alignani DO, Liscovsky MV, Ranocchia RP, Moron VG, et al. Presence of neutrophil-bearing antigen in lymphoid organs of immune mice. Blood 2006; 108: 3094–3102.

Mari M, Griffith J, Rieter E, Krishnappa L, Klionsky DJ, Reggiori F. An Atg9-containing compartment that functions in the early steps of autophagosome biogenesis. J Cell Biol 2010; 190: 1005–1022.

Marik C, Felts PA, Bauer J, Lassmann H, Smith KJ. Lesion genesis in a subset of patients with multiple sclerosis: a role for innate immunity? Brain 2007; 130: 2800–2815.

Martin R, Sospedra M, Rosito M, Engelhardt B. Current multiple sclerosis treatments have improved our understanding of MS autoimmune pathogenesis. Eur. J. Immunol. 2016; 46: 2078–2090.

Martinez J, Almendinger J, Oberst A, Ness R, Dillon CP, Fitzgerald P, et al. Microtubule-associated protein 1 light chain 3 alpha (LC3)-associated phagocytosis is required for the efficient clearance of dead cells. Proc. Natl. Acad. Sci. U.S.A. 2011; 108: 17396–17401.

Martinez J, Cunha LD, Park S, Yang M, Lu Q, Orchard R, et al. Noncanonical autophagy inhibits the autoinflammatory, lupus-like response to dying cells. Nature 2016; 533: 115–119.

Martinez J, Malireddi RKS, Lu Q, Cunha LD, Pelletier S, Gingras S, et al. Molecular characterization of LC3-associated phagocytosis reveals distinct roles for Rubicon, NOX2 and autophagy proteins. Nature Cell Biology 2015; 17: 893–906.

Marzo AL, Kinnear BF, Lake RA, Frelinger JJ, Collins EJ, Robinson BW, et al. Tumor-specific CD4+ T cells have a major 'post-licensing' role in CTL mediated anti-tumor immunity. J. Immunol. 2000; 165: 6047–6055.

Matsuda JL, Naidenko OV, Gapin L, Nakayama T, Taniguchi M, Wang CR, et al. Tracking the response of natural killer T cells to a glycolipid antigen using CD1d tetramers. J. Exp. Med. 2000; 192: 741–754.

Matsunaga K, Morita E, Saitoh T, Akira S, Ktistakis NT, Izumi T, et al. Autophagy requires endoplasmic reticulum targeting of the PI3-kinase complex via Atg14L. J Cell Biol 2010; 190: 511–521.

Mattner J, Debord KL, Ismail N, Goff RD, Cantu C, Zhou D, et al. Exogenous and endogenous glycolipid antigens activate NKT cells during microbial infections. Nature 2005; 434: 525–529.

McCormick PJ, Martina JA, Bonifacino JS. Involvement of clathrin and AP-2 in the trafficking of MHC class II molecules to antigen-processing compartments. Proc. Natl. Acad. Sci. U.S.A. 2005; 102: 7910–7915.

McMenamin PG. Distribution and phenotype of dendritic cells and resident tissue macrophages in the dura mater, leptomeninges, and choroid plexus of the rat brain as demonstrated in wholemount preparations. J. Comp. Neurol. 1999; 405: 553–562.

Mercer CA, Kaliappan A, Dennis PB. A novel, human Atg13 binding protein, Atg101, interacts with ULK1 and is essential for macroautophagy. Autophagy 2009; 5: 649–662.

Mi S, Hu B, Hahm K, Luo Y, Kam Hui ES, Yuan Q, et al. LINGO-1 antagonist promotes spinal cord remyelination and axonal integrity in MOG-induced experimental autoimmune encephalomyelitis. Nat Med 2007; 13: 1228–1233.

Miller SD, Karpus WJ. Experimental autoimmune encephalomyelitis in the mouse. Curr Protoc Immunol 2007; Chapter 15: Unit 15.1.

Mintern JD, Macri C, Chin WJ, Panozza SE, Segura E, Patterson NL, et al. Differential use of autophagy by primary dendritic cells specialized in cross-presentation. Autophagy 2015; 11: 906–917.

Miranda-Hernandez S, Gerlach N, Fletcher JM, Biros E, Mack M, Körner H, et al. Role for MyD88, TLR2 and TLR9 but not TLR1, TLR4 or TLR6 in experimental autoimmune encephalomyelitis. J. Immunol. 2011; 187: 791–804.

Mizushima N, Klionsky DJ. Protein turnover via autophagy: implications for metabolism. Annu. Rev. Nutr. 2007; 27: 19–40.

Mizushima N, Komatsu M. Autophagy: renovation of cells and tissues. Cell 2011; 147: 728–741.

Mizushima N, Ohsumi Y, Yoshimori T. Autophagosome formation in mammalian cells. Cell Struct. Funct. 2002; 27: 421–429.

Mizushima N, Yamamoto A, Hatano M, Kobayashi Y, Kabeya Y, Suzuki K, et al. Dissection of autophagosome formation using Apg5-deficient mouse embryonic stem cells. J Cell Biol 2001; 152: 657–668.

Mizushima N, Yoshimori T, Ohsumi Y. The role of Atg proteins in autophagosome formation. Annu. Rev. Cell Dev. Biol. 2011; 27: 107–132.

Mohammad MG, Tsai VWW, Ruitenberg MJ, Hassanpour M, Li H, Hart PH, et al. Immune cell trafficking from the brain maintains CNS immune tolerance. J. Clin. Invest. 2014; 124: 1228–1241.

Motohashi S, Nagato K, Kunii N, Yamamoto H, Yamasaki K, Okita K, et al. A phase I-II study of alpha-galactosylceramide-pulsed IL-2/GM-CSF-cultured peripheral blood mononuclear cells in patients with advanced and recurrent non-small cell lung cancer. J. Immunol. 2009; 182: 2492–2501.

Münz C. Of LAP, CUPS, and DRibbles - Unconventional Use of Autophagy Proteins for MHC Restricted Antigen Presentation. Front Immunol 2015; 6: 200.

Nagata S, Suzuki J, Segawa K, Fujii T. Exposure of phosphatidylserine on the cell surface. Cell Death Differ. 2016; 23: 952–961.

Nair U, Yen W-L, Mari M, Cao Y, Xie Z, Baba M, et al. A role for Atg8-PE deconjugation in autophagosome biogenesis. autophagy 2012; 8: 780–793.

Nakamura T, Yamazaki D, Yamauchi J, Harashima H. The nanoparticulation by octaarginine-modified liposome improves α-galactosylceramide-mediated antitumor therapy via systemic administration. J Control Release 2013; 171: 216–224.

Nakatogawa H, Ichimura Y, Ohsumi Y. Atg8, a ubiquitin-like protein required for autophagosome formation, mediates membrane tethering and hemifusion. Cell 2007; 130: 165–178.

Nakatsu F, Ohno H. Adaptor protein complexes as the key regulators of protein sorting in the post-Golgi network. Cell Struct. Funct. 2003; 28: 419–429.

Nedjic J, Aichinger M, Emmerich J, Mizushima N, Klein L. Autophagy in thymic epithelium shapes the T-cell repertoire and is essential for tolerance. Nature 2008; 455: 396–400.

Nieda M, Okai M, Tazbirkova A, Lin H, Yamaura A, Ide K, et al. Therapeutic activation of Valpha24+Vbeta11+ NKT cells in human subjects results in highly coordinated secondary activation of acquired and innate immunity. Blood 2004; 103: 383–389.

Nimmerjahn F, Milosevic S, Behrends U, Jaffee EM, Pardoll DM, Bornkamm GW, et al. Major histocompatibility complex class II-restricted presentation of a cytosolic antigen by autophagy. Eur. J. Immunol. 2003; 33: 1250–1259.

Nishimura T, Kaizuka T, Cadwell K, Sahani MH, Saitoh T, Akira S, et al. FIP200 regulates targeting of Atg16L1 to the isolation membrane. EMBO Rep. 2013; 14: 284–291.

Noda NN, Kumeta H, Nakatogawa H, Satoo K, Adachi W, Ishii J, et al. Structural basis of target recognition by Atg8/LC3 during selective autophagy. Genes Cells 2008; 13: 1211–1218.

Noda NN, Ohsumi Y, Inagaki F. Atg8-family interacting motif crucial for selective autophagy. FEBS Lett 2010; 584: 1379–1385.

Nuchtern JG, Biddison WE, Klausner RD. Class II MHC molecules can use the endogenous pathway of antigen presentation. Nature 1990; 343: 74–76.

Nylander A, Hafler DA. Multiple sclerosis. J. Clin. Invest. 2012; 122: 1180–1188.

Ohashi Y, Soler N, García Ortegón M, Zhang L, Kirsten ML, Perisic O, et al. Characterization of Atg38 and NRBF2, a fifth subunit of the autophagic Vps34/PIK3C3 complex. Autophagy 2016; 12: 2129–2144.

Okita K, Motohashi S, Shinnakasu R, Nagato K, Yamasaki K, Sato Y, et al. A set of genes associated with the interferon-γ response of lung cancer patients undergoing α-galactosylceramide-pulsed dendritic cell therapy. Cancer Sci. 2010; 101: 2333–2340.

Paget C, Bialecki E, Fontaine J, Vendeville C, Mallevaey T, Faveeuw C, et al. Role of invariant NK T lymphocytes in immune responses to CpG oligodeoxynucleotides. J. Immunol 2009; 182: 1846–1853.

Paget C, Mallevaey T, Speak AO, Torres D, Fontaine J, Sheehan KCF, et al. Activation of invariant NKT cells by toll-like receptor 9-stimulated dendritic cells requires type I interferon and charged glycosphingolipids. Immunity 2007; 27: 597–609.

Paludan C, Schmid D, Landthaler M, Vockerodt M, Kube D, Tuschl T, et al. Endogenous MHC class II processing of a viral nuclear antigen after autophagy. Science 2005; 307: 593–596.

Pankiv S, Clausen TH, Lamark T, Brech A, Bruun J-A, Outzen H, et al. p62/SQSTM1 binds directly to Atg8/LC3 to facilitate degradation of ubiquitinated protein aggregates by autophagy. J. Biol. Chem. 2007; 282: 24131–24145.

Pardoll DM. The blockade of immune checkpoints in cancer immunotherapy. Nat. Rev. Cancer 2012; 12: 252–264.

Parekh VV, Lalani S, Kim S, Halder R, Azuma M, Yagita H, et al. PD-1/PD-L blockade prevents anergy induction and enhances the anti-tumor activities of glycolipid-activated invariant NKT cells. J. Immunol. 2009; 182: 2816–2826.

Parekh VV, Wilson MT, Olivares-Villagómez D, Singh AK, Wu L, Wang C-R, et al. Glycolipid

antigen induces long-term natural killer T cell anergy in mice. J. Clin Invest. 2005; 115: 2572–2583.

Park J-J, Kang S-J, De Silva AD, Stanic AK, Casorati G, Hachey DL, et al. Lipid-protein interactions: biosynthetic assembly of CD1 with lipids in the endoplasmic reticulum is evolutionarily conserved. Proc. Natl. Acad. Sci. U.S.A. 2004; 101: 1022–1026.

Paterka M, Siffrin V, Voss JO, Werr J, Hoppmann N, Gollan R, et al. Gatekeeper role of brain antigen-presenting CD11c+ cells in neuroinflammation. EMBO J. 2016; 35: 89–101.

Pei B, Zhao M, Miller BC, Véla JL, Bruinsma MW, Virgin HW, et al. Invariant NKT cells require autophagy to coordinate proliferation and survival signals during differentiation. J. Immunol. 2015; 194: 5872–5884.

Peitz M, Pfannkuche K, Rajewsky K, Edenhofer F. Ability of the hydrophobic FGF and basic TAT peptides to promote cellular uptake of recombinant Cre recombinase: a tool for efficient genetic engineering of mammalian genomes. Proc. Natl. Acad. Sci. U.S.A. 2002; 99: 4489–4494.

Pender MP, Nguyen KB, McCombe PA, Kerr JF. Apoptosis in the nervous system in experimental allergic encephalomyelitis. J. Neurol. Sci. 1991; 104: 81–87.

Pettinelli CB, McFarlin DE. Adoptive transfer of experimental allergic encephalomyelitis in SJL/J mice after in vitro activation of lymph node cells by myelin basic protein: requirement for Lyt 1+ 2- T lymphocytes. J. Immunol. 1981; 127: 1420–1423.

Pfeifer U. Inhibition by insulin of the formation of autophagic vacuoles in rat liver. A morphometric approach to the kinetics of intracellular degradation by autophagy. J Cell Biol 1978; 78: 152–167.

Ponomarev ED, Shriver LP, Maresz K, Dittel BN. Microglial cell activation and proliferation precedes the onset of CNS autoimmunity. J. Neurosci. Res. 2005; 81: 374–389.

Prineas JW, Parratt JDE. Oligodendrocytes and the early multiple sclerosis lesion. Ann. Neurol. 2012; 72: 18–31.

Prinz M, Garbe F, Schmidt H, Mildner A, Gutcher I, Wolter K, et al. Innate immunity mediated by TLR9 modulates pathogenicity in an animal model of multiple sclerosis. J. Clin. Invest. 2006; 116: 456–464.

Prodinger C, Bunse J, Krüger M, Schiefenhövel F, Brandt C, Laman JD, et al. CD11c-expressing cells reside in the juxtavascular parenchyma and extend processes into the glia limitans of the mouse nervous system. Acta Neuropathol. 2011; 121: 445–458.

Puri C, Renna M, Bento CF, Moreau K, Rubinsztein DC. Diverse Autophagosome Membrane Sources Coalesce in Recycling Endosomes. Cell 2013; 154: 1285–1299.

Radoshevich L, Murrow L, Chen N, Fernandez E, Roy S, Fung C, et al. ATG12 conjugation to ATG3 regulates mitochondrial homeostasis and cell death. Cell 2010; 142: 590–600.

Rammensee H, Bachmann J, Emmerich NP, Bachor OA, Stevanović S. SYFPEITHI: database for MHC ligands and peptide motifs. Immunogenetics 1999; 50: 213–219.

Randow F, Youle RJ. Self and nonself: how autophagy targets mitochondria and bacteria. Cell Host Microbe 2014; 15: 403–411.

Ransohoff RM, Kivisäkk P, Kidd G. Three or more routes for leukocyte migration into the central nervous system. Nat. Rev. Immunol. 2003; 3: 569–581.

Ravikumar B, Acevedo Arozena A, Imarisio S, Berger Z, Vacher C, O'Kane CJ, et al. Dynein mutations impair autophagic clearance of aggregate-prone proteins. Nat. Genet. 2005; 37: 771–776.

Ravikumar B, Moreau K, Jahreiss L, Puri C, Rubinsztein DC. Plasma membrane contributes to

the formation of pre-autophagosomal structures. Nature Cell Biology 2010; 12: 747–757.

Ravindran R, Khan N, Nakaya HI, Li S, Loebbermann J, Maddur MS, et al. Vaccine activation of the nutrient sensor GCN2 in dendritic cells enhances antigen presentation. Science 2014; 343: 313–317.

Reboldi A, Coisne C, Baumjohann D, Benvenuto F, Bottinelli D, Lira S, et al. C-C chemokine receptor 6-regulated entry of TH-17 cells into the CNS through the choroid plexus is required for the initiation of EAE. Nat. Immunol. 2009; 10: 514–523.

Reichmann G, Schroeter M, Jander S, Fischer H-G. Dendritic cells and dendritic-like microglia in focal cortical ischemia of the mouse brain. J. Neuroimmunol. 2002; 129: 125–132.

Remington LT, Babcock AA, Zehntner SP, Owens T. Microglial recruitment, activation, and proliferation in response to primary demyelination. Am. J. Pathol. 2007; 170: 1713–1724.

Roberson SM, Walker WS. Immortalization of cloned mouse splenic macrophages with a retrovirus containing the v-raf/mil and v-myc oncogenes. Cell. Immunol. 1988; 116: 341–351.

Robinson AP, Harp CT, Noronha A, Miller SD. The experimental autoimmune encephalomyelitis (EAE) model of MS: utility for understanding disease pathophysiology and treatment. Handb Clin Neurol 2014; 122: 173–189.

Roche PA, Cresswell P. Invariant chain association with HLA-DR molecules inhibits immunogenic peptide binding. Nature 1990; 345: 615–618.

Roche PA, Furuta K. The ins and outs of MHC class II-mediated antigen processing and presentation. Nat. Rev. Immunol. 2015; 15: 203–216.

Rogov V, Dötsch V, Johansen T, Kirkin V. Interactions between autophagy receptors and ubiquitin-like proteins form the molecular basis for selective autophagy. Mol. Cell 2014; 53: 167–178.

Romanelli E, Merkler D, Mezydlo A, Weil M-T, Weber MS, Nikić I, et al. Myelinosome formation represents an early stage of oligodendrocyte damage in multiple sclerosis and its animal model. Nature Communications 2016; 7: 13275.

Romao S, Gasser N, Becker AC, Guhl B, Bajagic M, Vanoaica D, et al. Autophagy proteins stabilize pathogen-containing phagosomes for prolonged MHC II antigen processing. J Cell Biol 2013; 203: 757–766.

Romao S, Münz C. LC3-associated phagocytosis. Autophagy 2014; 10: 526–528.

Ryan MP, Adley CC. Sphingomonas paucimobilis: a persistent Gram-negative nosocomial infectious organism. J. Hosp. Infect. 2010; 75: 153–157.

Rybicka JM, Balce DR, Chaudhuri S, Allan ERO, Yates RM. Phagosomal proteolysis in dendritic cells is modulated by NADPH oxidase in a pH-independent manner. EMBO J. 2012; 31: 932–944.

Sag D, Krause P, Hedrick CC, Kronenberg M, Wingender G. IL-10-producing NKT10 cells are a distinct regulatory invariant NKT cell subset. J. Clin. Invest. 2014; 124: 3725–3740.

Sagiv Y, Hudspeth K, Mattner J, Schrantz N, Stern RK, Zhou D, et al. Cutting edge: impaired glycosphingolipid trafficking and NKT cell development in mice lacking Niemann-Pick type C1 protein. J. Immunol. 2006; 177: 26–30.

Saitoh T, Fujita N, Jang MH, Uematsu S, Yang B-G, Satoh T, et al. Loss of the autophagy protein Atg16L1 enhances endotoxin-induced IL-1β production. Nature 2008; 456: 264–268.

Salio M, Puleston DJ, Mathan TSM, Shepherd D, Stranks AJ, Adamopoulou E, et al. Essential role for autophagy during invariant NKT cell development. Proc. Natl. Acad. Sci. U.S.A. 2014; 111: E5678–87.

Salio M, Silk JD, Jones EY, Cerundolo V. Biology of CD1- and MR1-restricted T cells. Annu. Rev. Immunol. 2014; 32: 323–366.

Sanjuan MA, Dillon CP, Tait SWG, Moshiach S, Dorsey F, Connell S, et al. Toll-like receptor signalling in macrophages links the autophagy pathway to phagocytosis. Nature 2007; 450: 1253–1257.

Savina A, Jancic C, Hugues S, Guermonprez P, Vargas P, Moura IC, et al. NOX2 controls phagosomal pH to regulate antigen processing during crosspresentation by dendritic cells. Cell 2006; 126: 205–218.

Schläger C, Körner H, Krueger M, Vidoli S, Haberl M, Mielke D, et al. Effector T-cell trafficking between the leptomeninges and the cerebrospinal fluid. Nature 2016; 530: 349–353.

Schmid D, Pypaert M, Münz C. Antigen-loading compartments for major histocompatibility complex class II molecules continuously receive input from autophagosomes. Immunity 2007; 26: 79–92.

Schneiders FL, de Bruin RCG, Santegoets SJAM, Bonneville M, Scotet E, Scheper RJ, et al. Activated iNKT cells promote Vγ9Vδ2-T cell anti-tumor effector functions through the production of TNF-α. Clin. Immunol. 2012; 142: 194–200.

Schrantz N, Sagiv Y, Liu Y, Savage PB, Bendelac A, Teyton L. The Niemann-Pick type C2 protein loads isoglobotrihexosylceramide onto CD1d molecules and contributes to the thymic selection of NKT cells. J. Exp. Med. 2007; 204: 841–852.

Schreiner B, Heppner FL, Becher B. Modeling multiple sclerosis in laboratory animals. Semin Immunopathol 2009; 31: 479–495.

Schümann J, Facciotti F, Panza L, Michieletti M, Compostella F, Collmann A, et al. Differential alteration of lipid antigen presentation to NKT cells due to imbalances in lipid metabolism. Eur. J. Immunol. 2007; 37: 1431–1441.

Schworer CM, Shiffer KA, Mortimore GE. Quantitative relationship between autophagy and proteolysis during graded amino acid deprivation in perfused rat liver. J. Biol. Chem. 1981; 256: 7652–7658.

Sciaky N, Presley J, Smith C, Zaal KJ, Cole N, Moreira JE, et al. Golgi tubule traffic and the effects of brefeldin A visualized in living cells. J Cell Biol 1997; 139: 1137–1155.

Shiao SL, Kirkiles-Smith NC, Shepherd BR, McNiff JM, Carr EJ, Pober JS. Human effector memory CD4+ T cells directly recognize allogeneic endothelial cells in vitro and in vivo. J. Immunol. 2007; 179: 4397–4404.

Shibutani ST, Yoshimori T. A current perspective of autophagosome biogenesis. Cell Res. 2014; 24: 58–68.

Shimizu K, Sato Y, Shinga J, Watanabe T, Endo T, Asakura M, et al. KLRG+ invariant natural killer T cells are long-lived effectors. Proc. Natl. Acad. Sci. U.S.A. 2014; 111: 12474–12479.

Shiratsuchi T, Schneck J, Kawamura A, Tsuji M. Human CD1 dimeric proteins as indispensable tools for research on CD1-binding lipids and CD1-restricted T cells. J. Immunol. Methods 2009; 345: 49–59.

Sillé FCM, Martin C, Jayaraman P, Rothchild A, Besra GS, Behar SM, et al. Critical role for invariant chain in CD1d-mediated selection and maturation of Vα14-invariant NKT cells. Immunol. Lett. 2011; 139: 33–41.

Singh R, Kaushik S, Wang Y, Xiang Y, Novak I, Komatsu M, et al. Autophagy regulates lipid metabolism. Nature 2009; 458: 1131–1135.

Sköld M, Xiong X, Illarionov PA, Besra GS, Behar SM. Interplay of cytokines and microbial signals

in regulation of CD1d expression and NKT cell activation. J. Immunol. 2005; 175: 3584–3593.

Smyth MJ, Crowe NY, Pellicci DG, Kyparissoudis K, Kelly JM, Takeda K, et al. Sequential production of interferon-gamma by NK1.1(+) T cells and natural killer cells is essential for the antimetastatic effect of alpha-galactosylceramide. Blood 2002; 99: 1259–1266.

Smyth MJ, Wallace ME, Nutt SL, Yagita H, Godfrey DI, Hayakawa Y. Sequential activation of NKT cells and NK cells provides effective innate immunotherapy of cancer. J. Exp. Med. 2005; 201: 1973–1985.

Sospedra M, Martin R. Immunology of multiple sclerosis. Annu. Rev. Immunol. 2005; 23: 683–747.

Sospedra M, Muraro PA, Stefanová I, Zhao Y, Chung K, Li Y, et al. Redundancy in antigen-presenting function of the HLA-DR and -DQ molecules in the multiple sclerosis-associated HLA-DR2 haplotype. J. Immunol. 2006; 176: 1951–1961.

Sou Y-S, Waguri S, Iwata J-I, Ueno T, Fujimura T, Hara T, et al. The Atg8 conjugation system is indispensable for proper development of autophagic isolation membranes in mice. Mol. Biol. Cell 2008; 19: 4762–4775.

Sriram V, Du W, Gervay-Hague J, Brutkiewicz RR. Cell wall glycosphingolipids of Sphingomonas paucimobilis are CD1d-specific ligands for NKT cells. Eur. J. Immunol. 2005; 35: 1692–1701.

Stromnes IM, Goverman JM. Passive induction of experimental allergic encephalomyelitis. Nat Protoc 2006; 1: 1952–1960.

Stys PK, Zamponi GW, van Minnen J, Geurts JJG. Will the real multiple sclerosis please stand up? Nat. Rev. Neurosci. 2012; 13: 507–514.

Subramani S, Malhotra V. Non-autophagic roles of autophagy-related proteins. EMBO Rep. 2013; 14: 143–151.

Sugita M, Cao X, Watts GFM, Rogers RA, Bonifacino JS, Brenner MB. Failure of trafficking and antigen presentation by CD1 in AP-3-deficient cells. Immunity 2002; 16: 697–706.

Sugita M, Cernadas M, Brenner MB. New insights into pathways for CD1-mediated antigen presentation. Curr. Opin. Immunol. 2004; 16: 90–95.

Sugita M, Grant EP, van Donselaar E, Hsu VW, Rogers RA, Peters PJ, et al. Separate pathways for antigen presentation by CD1 molecules. Immunity 1999; 11: 743–752.

Sugita M, Porcelli SA, Brenner MB. Assembly and retention of CD1b heavy chains in the endoplasmic reticulum. J. Immunol. 1997; 159: 2358–2365.

Sullivan BA, Kronenberg M. Activation or anergy: NKT cells are stunned by alpha-galactosylceramide. J. Clin. Invest. 2005; 115: 2328–2329.

Sun Q, Fan W, Chen K, Ding X, Chen S, Zhong Q. Identification of Barkor as a mammalian autophagy-specific factor for Beclin 1 and class III phosphatidylinositol 3-kinase. Proc. Natl. Acad. Sci. U.S.A. 2008; 105: 19211–19216.

Sun W, Subrahmanyam PB, East JE, Webb TJ. Connecting the dots: artificial antigen presenting cell-mediated modulation of natural killer T cells. J. Interferon Cytokine Res. 2012; 32: 505–516.

Suzuki H, Osawa T, Fujioka Y, Noda NN. Structural biology of the core autophagy machinery. Curr. Opin. Struct. Biol. 2016; 43: 10–17.

Tanida I, Sou Y-S, Ezaki J, Minematsu-Ikeguchi N, Ueno T, Kominami E. HsAtg4B/HsApg4B/autophagin-1 cleaves the carboxyl termini of three human Atg8 homologues and delipidates microtubule-associated protein light chain 3- and GABAA receptor-associated protein-phospholipid conjugates. J. Biol. Chem. 2004; 279: 36268–36276.

Taniguchi M, Harada M, Dashtsoodol N, Kojo S. Discovery of NKT cells and development of NKT cell-targeted anti-tumor immunotherapy. Proc. Jpn. Acad., Ser. B, Phys. Biol. Sci. 2015; 91: 292–304.

Terry RL, Ifergan I, Miller SD. Experimental Autoimmune Encephalomyelitis in Mice. In: Shiozawa S, editor(s). Arthritis Research. Totowa, NJ: Humana Press; 2014. p. 1–16.

Thurston TLM, Wandel MP, Muhlinen von N, Foeglein Á, Randow F. Galectin 8 targets damaged vesicles for autophagy to defend cells against bacterial invasion. Nature 2012: 1–6.

Tian G, Courtney AN, Jena B, Heczey A, Liu D, Marinova E, et al. CD62L+ NKT cells have prolonged persistence and antitumor activity in vivo. J. Clin. Invest. 2016; 126: 2341–2355.

Tian Y, Chang JC, Fan EY, Flajolet M, Greengard P. Adaptor complex AP2/PICALM, through interaction with LC3, targets Alzheimer's APP-CTF for terminal degradation via autophagy. Proc. Natl. Acad. Sci. U.S.A. 2013; 110: 17071–17076.

Toura I, Kawano T, Akutsu Y, Nakayama T, Ochiai T, Taniguchi M. Cutting edge: inhibition of experimental tumor metastasis by dendritic cells pulsed with alpha-galactosylceramide. J. Immunol. 1999; 163: 2387–2391.

Traka M, Podojil JR, McCarthy DP, Miller SD, Popko B. Oligodendrocyte death results in immune-mediated CNS demyelination. Nature Neuroscience 2016; 19: 65–74.

Trombetta ES, Mellman I. Cell biology of antigen processing in vitro and in vivo. Annu. Rev. Immunol. 2005; 23: 975–1028.

Tsukada M, Ohsumi Y. Isolation and characterization of autophagy-defective mutants of Saccharomyces cerevisiae. FEBS Lett 1993; 333: 169–174.

Tsunoda I, Libbey JE, Kuang L-Q, Terry EJ, Fujinami RS. Massive apoptosis in lymphoid organs in animal models for primary and secondary progressive multiple sclerosis. Am. J. Pathol. 2005; 167: 1631–1646.

Ueyama T, Nakakita J, Nakamura T, Kobayashi T, Kobayashi T, Son J, et al. Cooperation of p40(phox) with p47(phox) for Nox2-based NADPH oxidase activation during Fcγ receptor (FcγR)-mediated phagocytosis: mechanism for acquisition of p40(phox) phosphatidylinositol 3-phosphate (PI(3)P) binding. J. Biol. Chem. 2011; 286: 40693–40705.

van der Vliet HJJ, Molling JW, Nishi N, Masterson AJ, Kölgen W, Porcelli SA, et al. Polarization of Valpha24+ Vbeta11+ natural killer T cells of healthy volunteers and cancer patients using alpha-galactosylceramide-loaded and environmentally instructed dendritic cells. Cancer Research 2003; 63: 4101–4106.

van Ham SM, Tjin EP, Lillemeier BF, Grüneberg U, van Meijgaarden KE, Pastoors L, et al. HLA-DO is a negative modulator of HLA-DM-mediated MHC class II peptide loading. Curr. Biol. 1997; 7: 950–957.

Van Kaer L, Wu L, Joyce S. Mechanisms and Consequences of Antigen Presentation by CD1. Trends in Immunology 2016; 37: 738–754.

Vartabedian VF, Savage PB, Teyton L. The processing and presentation of lipids and glycolipids to the immune system. Immunol. Rev. 2016; 272: 109–119.

Vermijlen D, Prinz I. Ontogeny of Innate T Lymphocytes - Some Innate Lymphocytes are More Innate than Others. Front Immunol 2014; 5: 486.

Vomhof-Dekrey EE, Yates J, Hägglöf T, Lanthier P, Amiel E, Veerapen N, et al. Cognate interaction with iNKT cells expands IL-10-producing B regulatory cells. Proc. Natl. Acad. Sci. U.S.A. 2015; 112: 12474–12479.

Vultaggio A, Nencini F, Pratesi S, Petroni G, Romagnani S, Maggi E. Poly(I:C) promotes the

production of IL-17A by murine CD1d-driven invariant NKT cells in airway inflammation. Allergy 2012; 67: 1223–1232.

Watarai H, Fujii S-I, Yamada D, Rybouchkin A, Sakata S, Nagata Y, et al. Murine induced pluripotent stem cells can be derived from and differentiate into natural killer T cells. J. Clin. Invest. 2010; 120: 2610–2618.

Weidberg H, Shvets E, Shpilka T, Shimron F, Shinder V, Elazar Z. LC3 and GATE-16/GABARAP subfamilies are both essential yet act differently in autophagosome biogenesis. EMBO J. 2010; 29: 1792–1802.

Wiendl H, Behrens L, Maier S, Johnson MA, Weiss EH, Hohlfeld R. Muscle fibers in inflammatory myopathies and cultured myoblasts express the nonclassical major histocompatibility antigen HLA-G. Ann. Neurol. 2000; 48: 679–684.

Wilson MT, Johansson C, Olivares-Villagómez D, Singh AK, Stanic AK, Wang C-R, et al. The response of natural killer T cells to glycolipid antigens is characterized by surface receptor down-modulation and expansion. Proc. Natl. Acad. Sci. U.S.A. 2003; 100: 10913–10918.

Xu Y, Jagannath C, Liu X-D, Sharafkhaneh A, Kolodziejska KE, Eissa NT. Toll-like receptor 4 is a sensor for autophagy associated with innate immunity. Immunity 2007; 27: 135–144.

Yamasaki K, Horiguchi S, Kurosaki M, Kunii N, Nagato K, Hanaoka H, et al. Induction of NKT cell-specific immune responses in cancer tissues after NKT cell-targeted adoptive immunotherapy. Clin. Immunol. 2011; 138: 255–265.

Ylä-Anttila P, Vihinen H, Jokitalo E, Eskelinen E-L. 3D tomography reveals connections between the phagophore and endoplasmic reticulum. Autophagy 2009; 5: 1180–1185.

Yogev N, Frommer F, Lukas D, Kautz-Neu K, Karram K, Ielo D, et al. Dendritic cells ameliorate autoimmunity in the CNS by controlling the homeostasis of PD-1 receptor(+) regulatory T cells. Immunity 2012; 37: 264–275.

Young LN, Cho K, Lawrence R, Zoncu R, Hurley JH. Dynamics and architecture of the NRBF2-containing phosphatidylinositol 3-kinase complex I of autophagy. Proc. Natl. Acad. Sci. U.S.A. 2016; 113: 8224–8229.

Yu KOA, Im JS, Illarionov PA, Ndonye RM, Howell AR, Besra GS, et al. Production and characterization of monoclonal antibodies against complexes of the NKT cell ligand alpha-galactosylceramide bound to mouse CD1d. J. Immunol. Methods 2007; 323: 11–23.

Yu Z-Q, Ni T, Hong B, Wang H-Y, Jiang F-J, Zou S, et al. Dual roles of Atg8-PE deconjugation by Atg4 in autophagy. Autophagy 2012; 8: 883–892.

Zalckvar E, Berissi H, Eisenstein M, Kimchi A. Phosphorylation of Beclin 1 by DAP-kinase promotes autophagy by weakening its interactions with Bcl-2 and Bcl-XL. Autophagy 2009; 5: 720–722.

Zamvil SS, Mitchell DJ, Moore AC, Kitamura K, Steinman L, Rothbard JB. T-cell epitope of the autoantigen myelin basic protein that induces encephalomyelitis. Nature 1986; 324: 258–260.

Zhang J, Markovic-Plese S, Lacet B, Raus J, Weiner HL, Hafler DA. Increased frequency of interleukin 2-responsive T cells specific for myelin basic protein and proteolipid protein in peripheral blood and cerebrospinal fluid of patients with multiple sclerosis. J. Exp. Med. 1994; 179: 973–984.

Zhao Z, Fux B, Goodwin M, Dunay IR, Strong D, Miller BC, et al. Autophagosome-independent essential function for the autophagy protein Atg5 in cellular immunity to intracellular pathogens. Cell Host Microbe 2008; 4: 458–469.

Zhou D, Cantu C, Sagiv Y, Schrantz N, Kulkarni AB, Qi X, et al. Editing of CD1d-bound lipid antigens by endosomal lipid transfer proteins. Science 2004; 303: 523–527.

Zietara N, Łyszkiewicz M, Krueger A, Weiss S. ICOS-dependent stimulation of NKT cells by marginal zone B cells. Eur. J. Immunol. 2011; 41: 3125–3134.

Zoppino FCM, Militello RD, Slavin I, Alvarez C, Colombo MI. Autophagosome formation depends on the small GTPase Rab1 and functional ER exit sites. Traffic 2010; 11: 1246–1261.

Guidelines for the use and interpretation of assays for monitoring autophagy (3rd edition). Autophagy 2016; 12: 1–222.

6. Abbreviations

AAK1	Adaptor-associated kinase 1
ACK	Ammonium-chloride-potassium
AMPK	AMP-activated protein kinase
AP2	Adaptor protein complex 2
APC	Antigen presenting cell
APS	Ammonium persulfate
Atg	Autophagy-related gene
ATG	Autophagy related protein
BBB	Blood brain barrier
BCA	Bicinchoninic acid
Bcl-2	B-cell lymphoma 2
BMDC	Bone marrow-derived dendritic cells
Bp	Base pairs
BSA	Bovine serum albumin
CAMKK2	Ca^{2+}/calmodulin-dependent protein kinase kinase 2
CAR	Chimeric antigen receptors
CD	Cluster of differentiation
CFA	Complete Freund's adjuvant
CFSE	Carboxyfluorescein succinimidyl ester
CLIP	Class II-associated invariant chain peptide
CMA	Chaperone-mediated autophagy
CNS	Central nervous system
COPII	Coat protein complex II
Cre	Cyclization (or causes) recombination enzyme
CTL	Cytotoxic T lymphocyte
DAPI	4',6-diamidino-2-phenylindole
DAPK	Death-associated protein kinase
DC	Dendritic cell
dLN	Draining lymph node
DMSO	Dimethyl sulfoxide
DNA	Desoxyribnucleic acid
DNAse	Desoxyribonuclease
dNTP	Desoxyribonucleotide
DTR	diphtheria toxin (DT) receptor
EAE	Experimental autoimmune encephalomyelitis
EDTA	Ethylenediaminetetraacetic acid

EE	Early endosome
EEA1	Early endosome antigen 1
EGFP	Enhanced green fluorescent protein
ER	Endoplasmic reticulum
ESCRT	Endosomal sorting complexes required for transport
EtOH	Ethanol
FACS	Fluorescent activated cell sorting
FCS	Fetal calf serum
FIP200	FAK family kinase-interacting protein of 200 kDa
Fl or flox	DNA sequence that is flanked by two loxP sites
Flt3	Fms related tyrosine kinase 3
FOXO3	Forkhead box O3
FOXP3	Forkhead box P3
FSC	Forward scatter
GalαGalCer	Digalactosylceramide
GM-CSF	Granulocyte-macrophage colony-stimulating factor
GM2A	GM2 ganglioside activator
GSL-1	Glucuronylceramide
HLA	Human leukocyte antigen
HRP	Horseradish peroxidase
HSC70	Heat shock cognate protein of 70 kDa
HSVTK	Thymidine kinase of herpes simplex virus
i.p.	Intraperitoneal (injection)
ICS	Intracellular cytokine staining
IFN	Interferon
IgG	Immunoglobulin G
Ii	Invariant chain
IL	Interleukin
iPSC	Induced pluripotent stem cells
IRF7	Interferon regulatory factor 7
kb	Kilobase
kDa	Kilodalton
KFERQ	One-letter code for amino acid sequence Lys-Phe-Glu-Arg-Gln
KO	Knockout
LAMP-2a	Lysosomal membrane-associated protein 2a
LAP	LC3-associated phagocytosis
LC3	Microtubule-associated protein 1A/1B-light chain 3

LDLR	Low density lipoprotein receptor
LE	Late endosome
LIR	LC3-interacting region
LKB1	Liver kinase B1
loxP	Locus of crossover (x) in P1
LPS	Lipopolysaccharide
LTP	Lipid transfer protein
Ly	Lysosome
MA	Macroautophagy
MACS	Magnetic activated cell sorting
MAIT cells	Mucosal-associated invariant T cells
MBP	Myelin basic protein
MHC	Major histocompatibility complex
MI	Microautophagy
MIIC	MHC class II-containing compartments
min	Minutes
moDC	Monocyte-derived DCs
MOG	Myelin oligodendrocyte glycoprotein
mRNA	Messenger RNA
MS	Multiple sclerosis
mTOR	Mammalian target of rapamycin
MTP	Microsomal triglyceride transfer protein
MVB	Multivesicular bodies
MyD88	Myeloid differentiation primary response gene 88
NaCl	Sodium chloride
NEAA	Non-essential amino acids
NGS	Normal goat serum
NK cells	Natural killer cells
NKT cells	Natural killer T cells
NOX2	NADPH oxidase 2
NPC1/2	Niemann-Pick type C1 and C2 proteins
p62 (SQSTM1)	Ubiquitin-binding protein involved in cell signaling
PAGE	Polyacrylamide gel electrophoresis
Pam_3CSK_4	Pam3Cys-Ser-(Lys)4, Synthetic triacylated lipoprotein
PAMPs	Pathogen-associated molecular patterns
PAS	Pre-autophagosomal structure
PBS	Phosphate buffered saline
PCR	Polymerase chain reaction

pDC	Plasmacytoid DC
PE	Phosphatidylethanolamine
PFA	Paraformaldehyde
PI3K	Phosphatidylinositol 3-kinase
PI3P	Phosphatidylinositol 3-phosphate
PMA	Phorbol-12-myristate-13-acetate
PNS	Peripheral nervous system
PRAS40	Proline-rich Akt substrate of 40 kDa
PRR	Pattern recognition receptor
Ptd-L-Ser	Phosphatidylserine
PTx	Pertussis toxin
RA	Rheumatoid arthritis
RAP	Rapamycin
Rheb	Ras homolog enriched in brain
RNA	Ribonucleic acid
ROS	Reactive oxygen species
rpm	Rounds per minute
RT	Room temperature
s.c.	Subcutaneous (injection)
SDS	Sodium dodecyl sulfate
sec	seconds
SLE	Systemic lupus erythematosus
SNARE	SNAP [Soluble NSF Attachment Protein] Receptor
SNP	Single nucleotide polymorphism
SRA	Scavenger receptor A
SSC	Side scatter
ssRNA	Single stranded RNA
T cell	T lymphocyte, matured in the thymus
TAK1	Transforming growth factor beta-activated kinase 1
TAP-1 and 2	Transporter-associated with antigen processing-1 and -2
TBE	Tris-borate-EDTA buffer
TCR	T cell receptor
TEM	Transmission electron microscopy
TEMED	Tetramethylethylenediamine
TGF	Transforming growth factor
T_H cell	T helper cell
TIM4	T cell immunoglobulin mucin-4
TLR	Toll-like receptor

TNF	Tumor necrosis factor
Treg	Regulatory T cell
TSC	Tuberous sclerosis complex
ULK1	Uncoordinated (UNC)-51-like kinase 1
VAMP3	Vesicle-associated membrane protein 3
VPS34	Vacuolar protein sorting protein 34; is a class III PI 3-kinase
WIPI	WD repeat domain phosphoinositide-interacting protein
wt	Wild type
ZNS	Zentrales Nervensystem
αGalCer	α-Galactosyceramide
β2-m	β2-microglobulin

7. Declaration

Herewith I declare that I have written this thesis myself and only used the stated references.

Furthermore,

I declare that I have performed all the experiments myself, with assistance and help from Patrick Weber (genotyping, animal experiments) Giulia Ramelli (DC:ODC coculture assays, genotyping), Stefan Freigang, Svenja Ewert, Romina Theiler (receptor-mediated uptake of glycolipid antigens in DCs/BMDCs, determination of organspecific NKT cell frequencies and *in vivo* infection of DC-*Atg5*$^{-/-}$ and DC-*Atg5*$^{+/+}$ mice with *S. paucimobilis*) and with the exception of AP2:EEA and CD1d:EEA colocalization studies which was performed by Monica Loi and steady state analysis of CNS myeloid cells which was performed by Sarah Mundt.

Zurich, 31.03.2017

Christian Wolfgang Keller, Zurich, Switzerland

Curriculum Vitae

Personal Data:

Name:	KELLER
First names:	Christian Wolfgang
Birthday:	July 14th 1980
Nationality:	German
Address:	Leutholdstrasse 22, 8037 Zurich, Switzerland
Cell phone:	+41 76 816 0444
E-mail:	keller@immunology.uzh.ch

Education:

Since March 2013	Admitted into the Graduate School *Microbiology and Immunology* (MIM), Zurich
Since February 2013	Admitted to the MD/PhD Program Zurich
Since October 2011	Physician scientist, Institute of Experimental Immunology, Department of Neuroinflammation (Prof. Dr. Jan Lünemann), University of Zurich, Switzerland
April 2011 – September 2011	Resident, Department of Neurology (Prof. Dr. M. Bähr), Stroke Unit/Interdisciplinary Emergency Room (IER), University Clinic Göttingen, Germany
November 2010	Final examination/Medical School (*2. Abschnitt der ärztlichen Prüfung*) Georg-August University Göttingen, Germany
February 2006	Intermediate examination/Medical School (*1. Abschnitt der ärztlichen Prüfung*) Georg-August University Göttingen, Germany
2004 – 2010	Medical Studies in Göttingen, Germany; London, UK; Addis Abeba, Ethiopia
1999 – 2001	Highschool leaving exam (*Abitur*), Hans-Furler Highschool Oberkirch, Germany
1998 – 1999	Exchange year, River Ridge Highschool, Lacey, WA, USA
1991 – 1998	Hans-Furler-Highschool Oberkirch, Germany
1987 – 1991	Elementary School Oppenau, Germany

MD Dissertation:

October 2006 – February 201	Titel: *"Pathomechanismen der sporadischen Einschlusskörpermyositis: Molekulare Interaktionen zwischen Autophagie, Zellstress und Akkumulation von β–Amyloid im Skelettmuskel"* Department of Neurology/Department of Clinical and Experimental Neuroimmunology, Georg-August University of Göttingen, Germany Supervisor: Prof. Dr. Jens Schmidt Written dissertation: *magna cum laude* Oral examination: *magna cum laude* Research stay for MD thesis project:
March 2007 – August 2007	Laboratory of Viral Immunobiology (Prof. Dr. Christian Münz), Christopher H. Browne Center for Immunology and Immune Diseases, The Rockefeller University, New York, NY, USA Supervisor: Prof. Dr. Jan Lünemann

Clinical Experience

April 2011 – September 2011	Resident, Department of Neurology (Prof. Dr. Mathias Bähr), Stroke Unit/Interdisciplinary Emergency Room (IER), University Clinic Göttingen, Germany

Fellowships and Awards

March 2015	Travel Grant from the German Society for Immunology (DGfI) in association with attendance to the RIKEN IMS Summer Program 2015, Yokohama, Japan
June 2014	1-year PhD Fellowship by the University of Zurich (*Forschungskredit*)
November 2012	Keystone Symposia Scholarship in association with attendance to the Keystone meeting *Autophagy, Inflammation and Immunity* in Montreal, Canada.
June 2012	3-year Postdoctoral Fellowship, German Research Foundation/DFG Bonn, Germany

May 2007	Scholarship from the University of Göttingen to fund a research stay at the Rockefeller University in New York, USA
January 2007	Travel allowance Scholarship from Boehringer Ingelheim Fonds to fund a research stay at the Rockefeller University in New York, USA

Scientific Organizations

Member of the International Society of Neuroimmunology (ISNI) and the German Society for Immunology (DGfI)

Original Publications

Keller CW, Loi M, Ewert S, Quast I, Theiler R, Gannagé M, Münz C, De Libero G, Freigang S, Lünemann JD. The autophagy machinery restrains iNKT cell activation through CD1d internalization. *Autophagy*, 2017. doi: org/10.1080/15548627.2017.1297907
In press.

Schneider C, Wicki S, Graeter S, Timcheva TM, **Keller CW**, Quast I, Leontyev D, Djoumerska-Alexieva IK, Käsermann F, Jakob SM, Dimitrova PA, Branch DR, Cummings RD, Lu¨nemann JD, Kaufmann T, Simon HU, von Gunten S. IVIG regulates the survival of human but not mouse neutrophils. *Sci Rep*
In press

Keller CW, Sina C, Ramelli G, Mundt S, Quast I, Weber P, Becher B, Münz C, Lünemann JD. Noncanonical autophagy in DCs drives autoimmune $CD4^+$ T cell pathogenicity.
In review

Peschke B, **Keller CW**, Li T, Weber P, Wang LX, Quast I, Lünemann JD. Fc-galactosylation of human IgG isotypes improves C1q binding and enhances complement-dependent cytotoxicity
In review

Schmidt K, Wienken M, **Keller CW**, Balcarek P, Mu¨nz C, Schmidt J. IL-1β-induced accumulation of amyloid: macroautophagy in skeletal muscle depends on ERK. *Mediators Inflamm,* 2017. doi.org/10.1155/2017/5470831

Quast I*, **Keller CW***, Hiepe F, Tackenberg B, Lünemann JD. Terminal complement activation is increased and associated with disease severity in CIDP. *Ann Clin Transl Neurol*, 2016. 3(9):730-5.

Quast I, **Keller CW**, Weber P, Schneider C, von Gunten S, Lünemann JD. Protection from experimental autoimmune encephalomyelitis by polyclonal IgG requires adjuvant-induced inflammation. *J Neuroinflammation*, 2016. 13:42.

Quast I, **Keller CW**, Maurer MA, Giddens JP, Tackenberg B, Wang LX, Münz C, Nimmerjahn F, Dalakas, MC, Lünemann JD. Sialylation of IgG Fc domain impairs complement-dependent cytotoxicity.
J Clin Invest, 2015. 125(11):4160-70.

Keller CW, Schmitz M, Mu¨nz C, Lu¨nemann JD, Schmidt J. TNF-α upregulates macroautophagy of APP/β-amyloid in a muscle cell line from human rhabdomyosarcoma. *J Neurol Sci*, 2012. 325(1-2): 103-7.

Keller CW, Fokken C, Turville SG, Lünemann A, Schmidt J, Münz C, Lünemann JD. TNF-α induces Macroautophagy and regulates MHC Class II expression in human skeletal muscle cells. *J Biol Chem*, 2011. 286(5): 3970-80.

* Equally contributing first authors

Review Articles

Keller CW & Lünemann JD. Autophagy and Autophagy-Related Proteins in CNS Autoimmunity. *Front Immunol,* 2017. 8:165. doi: 10.3389/fimmu.2017.00165

Keller CW, Schmidt J, Lünemann JD. Immune and Myodegenerative Pathomechanisms in Inclusion Body Myositis. *Ann Clin Transl Neurol,* 2017. doi: 10.1002/acn3.419
In press

Keller CW, Freigang S, Lünemann JD. Reciprocal Crosstalk between Dendritic Cells and Natural Killer T cells: Mechanisms and Therapeutic Potential.
In review